



PROGRAMA DE PÓS-GRADUAÇÃO EM BIOTECNOLOGIA

AMANDA EVELYN DA SILVA

**ACUSTOFLUÍDICA COMO INOVAÇÃO TECNOLÓGICA PARA A  
BIOESPECTROSCOPIA APLICADA AO ESTUDO DAS LEISHMANIOSES**

Maceió

2022

AMANDA EVELYN DA SILVA

**ACUSTOFLUÍDICA COMO INOVAÇÃO TECNOLÓGICA PARA A  
BIOESPECTROSCOPIA APLICADA AO ESTUDO DAS LEISHMANIOSES**

Defesa de tese apresentada ao Programa de Pós-Graduação em Biotecnologia como requisito para obtenção do grau de Doutora.

Área de concentração: Biotecnologia em Saúde

Linha de pesquisa: Desenvolvimento de agentes profiláticos, terapêuticos e testes de diagnósticos.

Profa. Orientadora: Dra. Magna Suzana Moreira

Prof. Coorientador: Dr. Glauber José Ferreira Tomaz da Silva

Maceió

2022

**Catálogo na fonte  
Universidade Federal de Alagoas  
Biblioteca Central  
Divisão de Tratamento Técnico**

Bibliotecária: Taciana Sousa dos Santos – CRB-4 – 2062

5586a Silva, Amanda Evelyn da.  
Acustofluidica como inovação tecnológica para a bioespectroscopia aplicada ao estudo das leishmanioses / Amanda Evelyn da Silva. – 2022.  
108 f. : il. color.

Orientadora: Magna Suzana Moreira.  
Coorientador: Glauber José Ferreira Tomaz da Silva.  
Tese (Doutorado em Biotecnologia) – Universidade Federal de Alagoas.  
Instituto de Química e Biotecnologia. RENORBIO. Maceió, 2022.

Bibliografia: f. 102-108.

1. Leishmaniose. 2. Acustofluidica. 3. Bioespectroscopia. I. Título.

CDU: 616.993.161


AMANDA EVELYN DA SILVA

**“Acustofluídica como inovação tecnológica para a bioespectroscopia aplicada ao estudo das leishmanioses.”**

Tese apresentada ao Programa de Pós-Graduação em Biotecnologia da Rede Nordeste de Biotecnologia – RENORBIO, ponto focal Alagoas, Universidade Federal de Alagoas, como requisito para a obtenção do título de Doutora em Biotecnologia, área de concentração: Biotecnologia em Saúde.

Aprovada em: 21/03/2022.

**BANCA EXAMINADORA**

**BANCA EXAMINADORA**  
Documento assinado digitalmente  
 MAGNA SUZANA ALEXANDRE MOREIRA  
Data: 21/03/2022 20:04:24-0300  
Verifique em <https://verificador.itl.br>


---

**Profa. Dra. Magna Suzana Alexandre Moreira**  
Orientadora - Universidade Federal de Alagoas - UFAL

Documento assinado digitalmente  
 GLAUBER JOSE FERREIRA TOMAZ DA SILVA  
Data: 21/03/2022 17:19:02-0300  
Verifique em <https://verificador.itl.br>

---

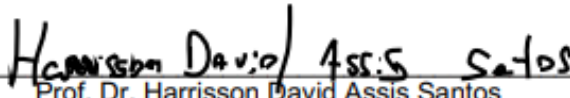
**Prof. Dr. Glauber José Ferreira Tomaz da Silva**  
Coorientador - Universidade Federal de Alagoas - UFAL


Documento assinado digitalmente  
 ALYSSON WAGNER FERNANDES DUARTE  
Data: 21/03/2022 20:28:09-0300  
Verifique em <https://verificador.itl.br>

---

**Prof. Dr. Alysson Wagner Fernandes Duarte**  
Universidade Federal de Alagoas - UFAL


---

  
**Prof. Dr. Harrison David Assis Santos**  
Universidade Estadual da Paraíba - UEPB

Documento assinado digitalmente  
 João Xavier de Araújo Júnior  
Data: 21/03/2022 18:47:21-0300  
Verifique em <https://verificador.itl.br>

---

**Prof. Dr. João Xavier de Araújo Júnior**  
Universidade Federal de Alagoas - UFAL

Documento assinado digitalmente  
 LUIZ HENRIQUE AGRA CAVALCANTE SILVA  
Data: 22/03/2022 09:07:15-0300  
Verifique em <https://verificador.itl.br>

---

**Prof. Dr. Luiz Henrique Agra Cavalcante**  
Faculdades Nova Esperança - FACENE

*Dedico esta tese de doutorado a todas as pessoas que lutam por dias melhores, todos aqueles que buscam na educação um futuro melhor não só para si, mas também para a humanidade. Aquelas que carregam a esperança de uma humanidade pacífica, com qualidade de vida e com oportunidades para todos os habitantes deste planeta.*

## AGRADECIMENTOS

Ao Pai criador de todo o universo, Deus, por ser o meu guia espiritual e o meu fortalecimento.

À minha mãe, **Eliete**, por ser a minha guia em todos os momentos da minha vida, me concedendo fortaleza para continuar a lutar pelos meus sonhos, sendo exemplo de força e determinação. Obrigada por tanto amor e cuidado.

Ao meu pai, **Aluísio**, ao meu irmão, **Anderson**, à minha cunhada, **Nadja** e à minha sobrinha, **Elisa** por estarem sempre me apoiando e me fortalecendo em toda a jornada acadêmica. Em especial, ao meu irmão por sempre me orientar a buscar o melhor para a minha vida e educação. Estes que me incentivaram a continuar e deixam claro o orgulho que sentem por mim. Obrigada por serem o meu alicerce.

A toda a minha família, materna e paterna, incluindo tios, primos, avós e amigos. Sou grata por todo o apoio e todo amor recebido. Obrigada pelos belíssimos momentos vividos e por serem maravilhosos, em especial à minha avó paterna, **Maria Helena**, gratidão por seu um dos meus exemplos de mulher.

À minha avó, **Inês** (*in memoriam*), a qual tive o enorme prazer de ser parcialmente educada por ela. Sua paz e paciência eram únicas, e seus ensinamentos nunca sairão de dentro de mim.

À minha amiga, **Morgana**, ao meu amigo, **João Kaycke**, e à minha amiga, **Karoline**, eu agradeço por sempre me ouvirem. Gratidão pelo incentivo e apoio que tem me dado, e principalmente pela amizade.

Ao meu namorado, **Willams**, obrigada por me apoiar e me incentivar na busca dos meus sonhos e ser companheiro em todas as áreas da minha vida.

Aos amigos da graduação, agradeço por cada apoio, mesmo após a conclusão do curso, estando presente no meu dia a dia, **Bianca**, **Marílya**, **Carol**, **Valcilaine**, **Rafael**, **Ellymaira**, **Mayara**, **Ábner**, **Ceysse**, **Luiz Antônio**, **Rosineide**, **Neto** e **Emanuelle**.

Aos amigos do mestrado na UNESP, **Leandro**, **Letícia**, **Aline**, **Thays**, **Rayanne** e **Mayara**. Obrigada pelo apoio e por permanecerem junto comigo.

Aos amigos, **Tainá, Kamyla, Gabriela, Luciana, Amanda Regina e Cícero**, muito grata pelo apoio e pelo incentivo ao longo desses anos. Vocês foram fundamentais.

À minha prima, **Regina**, a qual dividiu o mesmo lar comigo em diversas fases da vida, obrigada por toda a paciência.

Aos meus amigos que ao longo de toda a carreira acadêmica me apoiaram e alguns estão comigo até hoje nessa jornada.

À minha orientadora do doutorado, **Magna Suzana**, e também da graduação, a qual tenho imensa gratidão por me orientar na vida acadêmica, sendo o meu maior exemplo de pesquisadora e professora. A maneira que você transforma vidas é uma inspiração para todos. Gratidão por todos os ensinamentos, principalmente pessoais que levarei sempre comigo. Obrigada também pela amizade que construímos ao longo do doutorado, por ser justa e parceira. Você é um grande exemplo como pessoa e como mulher forte, batalhadora e determinada.

Aos doutores, **Anderson Brandão e Aline Cavalcanti**, gratidão por todos os ensinamentos. Saibam que vocês são a minha inspiração acadêmica. Obrigada pela sabedoria compartilhada.

Ao meu coorientador, **Glauber Thomaz**, obrigada por tanto aprendizado na área da física, além de me orientar na carreira acadêmica.

À Família LaFI, que por muitos anos (graduação e doutorado), estiveram sempre me apoiando durante toda a jornada. Muita gratidão pelos ensinamentos acadêmicos e pessoais. Em especial aos amigos **João Kaycke, Diogo Brandão, João Flávio, Marcio Thomaz, Karoline Jatobá, Shakira Cavalcante, Lilyanna Albuquerque, Ana Rachel, Joice Fragoso, Gessyca Gouveia, Thiago Goes, Fábio, Éder, José Clementino, Hilda Caroline, Mariana Santos, Suellen Albuquerque**, e muitos outros, de todas as gerações lafianas, que me ajudaram de forma direta ou indireta na produção da minha tese e na minha formação como doutora. Serei eternamente grata a cada um de vocês.

A todos os membros do Grupo de Acústica Física (**GAF**), pelo apoio nos experimentos realizados na física, principalmente ao **Dr. Harisson** por me orientar na realização dos experimentos, nos estudos e agradeço também por nossas

discussões científicas e filosóficas. Também agradeço ao Ms., **Giclênio** por t  
apoio nos experimentos.

Agradeço a todos os profissionais que contribuíram durante o processo de doutoramento. Obrigada a todos os servidores, técnicos de laboratório, serviços gerais, administração e segurança. Gratidão por todo o apoio.



*"A mente que se abre a uma nova ideia jamais voltará ao seu tamanho original. "*

(Albert Einstein)

## RESUMO

As leishmanioses são um grupo de doenças causadas por parasitos do gênero *Leishmania*, da família *Trypanosomatidae*. Estima-se que 350 milhões de pessoas estão em risco de contrair a doença em 102 países de diferentes continentes. As leishmanioses apresentam três formas clínicas: cutânea, mucocutânea e visceral, esta última é a mais severa e apresenta o maior número de óbitos. Apesar do avanço em biotecnologia no último século, o diagnóstico para as leishmanioses baseia-se em métodos diretos, os quais detectam o estágio intracelular do parasito por microscopia óptica. No entanto, estes procedimentos invasivos requerem microscopista experiente e não fornecem diagnóstico assertivo em todos os casos, pois a distribuição dos parasitos nos tecidos afetados não é homogênea. Os exames de sangue são os mais fáceis de realizar, porém há pouquíssimas células parasitadas circulantes. Com o objetivo de desenvolver métodos mais sensíveis e específicos, novas estratégias tecnológicas estão sendo desenvolvidas. Nesse contexto, este estudo visou desenvolver um instrumento para um novo método de diagnóstico baseado na técnica de acustofluídica, a qual combina a tecnologia de microfluídica com forças acústicas para manipulação de células e microrganismos. De maneira inovadora, estamos combinando métodos de espectroscopia óptica e imagens com acustofluídica. Para tanto, foram usados macrófagos da linhagem J774.A1, células hospedeiras da leishmania, foram armadilhados e paralisados através da técnica de acustofluídica utilizando ondas de ultrassom, permitindo que um espectro Raman completo fosse obtido dentro de alguns intervalos de segundos e minutos. Os resultados produzidos confirmam a robustez dos métodos acustofluídicos como uma plataforma capaz de armadilhar células macrofágicas da linhagem J774.A1. promastigotas de *Leishmania amazonensis* e *Leishmania chagasi*, e também, células J774.A1 infectadas com amastigotas de *L. amazonensis*, as quais são alvos de testes de diagnóstico. Também foi demonstrado que o dispositivo acustofluídico desenvolvido pelo grupo de pesquisa foi capaz de armadilhar macrófagos da linhagem J774.A1 para bio-Raman espectroscopia, como demonstrado no artigo derivado desta tese, intitulado, “3D - *Printed Acoustofluidic Devices for Raman Spectroscopy of Cells*”. Por fim, o trabalho desenvolvido pode facilitar e aperfeiçoar o diagnóstico das leishmanioses, utilizando amostras biológicas menos invasivas.

Palavras-chave: Leishmaniose; Acustofluídica; Bioespectroscopia.

## ABSTRACT

The leishmaniasis are a group of diseases caused by protozoan parasites of the genus *Leishmania*, family Trypanosomatidae. Approximately 350 million people are at risk of developing the disease in 102 countries. The leishmaniasis are composed of three main clinical forms, namely cutaneous, mucosal, and visceral, with the last one being the most severe and causing most deaths. Despite the technological advances, routine diagnostics is based on direct methods which detect the intracellular stage of the parasite using microscopy in tissue samples from aspiration of the spleen, liver, bone marrow, and lymph nodes. However, these invasive procedures require an experienced microscopist and do not provide a safe diagnosis in all cases because parasite distribution in affected tissues is not homogenous. Blood tests are the most practical ones to perform, but there are little circulating infected cells. With the aim of developing more sensitive and specific methods, new technological strategies are being developed. Then, this study aimed to develop an instrument for a new diagnostic method based on the acoustofluidic method which combines the technology of microfluidics with acoustic forces to manipulate cells and microorganisms. As an innovation, we are combining optical spectroscopy with acoustofluidics. The obtained results confirm the robustness of acoustofluidic methods as a platform to trap macrophages of the J774.A1 cell line, *Leishmania amazonensis* and *Leishmania chagasi* promastigotes, and J774.A1 cells infected with *L. amazonensis* amastigotes, which are targets of diagnostic methods. It was also demonstrated that the acoustofluidic device developed by our research group was able to trap J774.A1 macrophages for bio-Raman spectroscopy as showed in the paper, obtained from this thesis, which is entitled "3D - Printed Acoustofluidic Devices for Raman Spectroscopy of Cells". Therefore, this study can facilitate and improve leishmaniasis diagnosis using less invasive biological samples.

Keywords: Leishmaniasis, Acoustofluidics, Bioespectroscopy.

## LISTA DE FIGURAS

- Figura 1** – Esquema tridimensional da forma promastigota metacíclica de *L. amazonensis* mostrando as principais estruturas, sendo A - Forma promastigota e B - Forma amastigota..... 17
- Figura 2** – Micrografia da forma amastigota dentro de um vacúolo parasitóforo no interior de um macrófago através de um microscópio eletrônico de varredura..... 18
- Figura 3** – Ciclo de vida de *Leishmania* spp..... 19
- Figura 4** – Esquema do mecanismo imunológico que induz a diferenciação das células T CD4+ nas subpopulações Th1 e Th2..... 21
- Figura 5** – Hepatoesplenomegalia em paciente com leishmaniose visceral..... 22
- Figura 6** – Cães com sinais clínicos da leishmaniose visceral canina, como queda de pelo, feridas na derme e perda de peso..... 23
- Figura 7** – Formas clínicas da LC: A: Leishmaniose cutânea; B: Leishmaniose Cutânea difusa; C: Leishmaniose Mucocutânea..... 24
- Figura 8** – Fêmea de flebotomíneo (*Diptera: Psychodidae*) ingurgitada durante repasto sanguíneo realizado em pele de isca humana..... 25
- Figura 9** – Incidência de leishmaniose cutânea e mucosa no Brasil..... 27
- Figura 10** – Situação epidemiológica das leishmanioses no mundo: A - Distribuição da leishmaniose tegumentar; B - Distribuição da leishmaniose visceral..... 28
- Figura 11** – Esquema representativo de um órgão em um chip (do inglês “organ-on-a-chip”) ..... 37
- Figura 12** – Esquema e foto do dispositivo de separação de células acústicas.... 38

<b>Figura 13</b> – Demonstração do dispositivo acusticofluidica.....	de 44
<b>Figura 14</b> – Instrumentos eletrônicos utilizados no experimento.....	45
<b>Figura 15</b> – Promastigotas de <i>L. amazonensis</i> (A) e <i>L. chagasi</i> (B), estáticas durante o aprisionamento, no aumento de 40x.....	57
<b>Figura 16</b> – Macrófagos infectados com <i>L. amazonensis</i> , estáticos durante o aprisionamento, nos aumentos de 40x (A) e 10x (B).....	

### LISTA DE ABREVIATURAS

<b>C3b</b>	Componente C3b do sistema complemento
<b>C3bi</b>	Componente inativado C3b do sistema complemento
<b>CD4<sup>+</sup></b>	“Grupamento de diferenciação 4 ativado”, do inglês “ <i>Cluster of Differentiation</i> ”
<b>CD8<sup>+</sup></b>	“Grupamento de diferenciação 8 ativado”, do inglês “ <i>Cluster of Differentiation</i> ”
<b>CR1</b>	Receptor do complemento 1
<b>CR2</b>	Receptor do complemento 2
<b>DNA</b>	“Ácido desoxirribonucleico”, do inglês “ <i>Deoxyribonucleic Acid</i> ”
<b>ELISA</b>	Ensaio imunoenzimático
<b>HIV</b>	“Vírus da Imunodeficiência Humana”, do inglês “ <i>Human Immunodeficiency Virus</i> ”
<b>IFAT</b>	Imunofluorescência indireta
<b>IFN-<math>\gamma</math></b>	“Interferon gama”
<b>IL-2</b>	“Interleucina-2”
<b>IL-4</b>	“Interleucina-4”
<b>IL-10</b>	“Interleucina-10”

<b>IL-13</b>	“Interleucina-13”
<b>LC</b>	“Leishmaniose Cutânea”
<b>LCM</b>	“Leishmaniose Mucocutânea”
<b>LV</b>	“Leishmaniose Visceral”
<b>MHC</b>	“Complexo principal de histocompatibilidade “, do inglês “ <i>Major Histocompatibility Complex</i> ”
<b>NO</b>	“Óxido Nítrico”, do inglês “ <i>Nitric Oxide</i> ”
<b>OMS</b>	“Organização Mundial de Saúde”
<b>PCR</b>	“Reação em Cadeia da Polimerase”, do inglês “ <i>Polymerase Chain reaction</i> ”
<b>Sb<sup>III</sup></b>	“Antimônio na forma trivalente “
<b>Sb<sup>V</sup></b>	“Antimônio na forma pentavalente”
<b>Th1</b>	“Resposta T auxiliar do tipo 1”, do inglês “ <i>T helper response type 1</i> ”
<b>Th2</b>	“Resposta T auxiliar do tipo 2”, do inglês “ <i>T helper response type 2</i> ”
<b>TNF<math>\alpha</math></b>	“Fator de Necrose Tumoral $\alpha$ ”, do inglês “ <i>Tumor Necrosis Factor <math>\alpha</math></i> ”
<b>TGF-<math>\beta</math></b>	“Fator de transformação do crescimento beta”, do inglês “ <i>transforming growth factor beta</i> ”

## SUMÁRIO

<b>1. INTRODUÇÃO</b> .....	<b>15</b>
<b>2. REVISÃO DA LITERATURA</b> .....	<b>17</b>
<b>2.1 Agente etiológico e ciclo de vida</b> .....	<b>17</b>
<b>2.2 Imunopatogenia e manifestações clínicas</b> .....	<b>19</b>
2.2.1 Leishmaniose visceral .....	21
2.2.2 Leishmaniose cutânea .....	23
<b>2.3 Vetores e reservatórios</b> .....	<b>24</b>
<b>2.4 Epidemiologia</b> .....	<b>26</b>
<b>2.5 Tratamento</b> .....	<b>29</b>
2.5.1 Antimoniais.....	29
2.5.2 Anfotericina b .....	31
2.5.3 Pentamidina .....	31
2.5.4 Miltefosina .....	32
<b>2.6 Diagnóstico</b> .....	<b>33</b>
<b>2.7 Avanços em biotecnologia</b> .....	<b>35</b>
2.7.1 Microfluídica .....	36
2.7.2 A Técnica de acustofluídica e suas aplicações biotecnológicas .....	37
<b>3. JUSTIFICATIVA</b> .....	<b>40</b>
<b>4. OBJETIVOS</b> .....	<b>41</b>
<b>4.1 Objetivo geral</b> .....	<b>41</b>
<b>4.1 Objetivos específicos</b> .....	<b>41</b>
<b>5. METODOLOGIA</b> .....	<b>42</b>
<b>5.1 Experimentos realizados no LAFL</b> .....	<b>42</b>
5.1.1 Macrófagos murinos J774.A1 .....	42
5.1.2 Promastigotas de <i>Leishmania</i> spp .....	42
5.1.3 Amastigotas de <i>Leishmania amazonensis</i> .....	43
5.1.4 Armadilhamento das células e parasitos .....	43
<b>5.2 Experimentos realizados no GAF</b> .....	<b>43</b>
5.2.1 Fabricação do dispositivo de acustofluídica .....	43
5.2.2 Espectroscopia Raman .....	44
5.2.3 Instrumentação eletrônica .....	45
<b>6. RESULTADOS E DISCUSSÃO</b> .....	<b>46</b>

<b>6.1 Artigo derivado da tese .....</b>	<b>46</b>
<b>7. CONCLUSÃO .....</b>	<b>59</b>
<b>8. MATERIAL SUPLEMENTAR .....</b>	<b>60</b>
<b>REFERÊNCIAS.....</b>	<b>102</b>



## 1. INTRODUÇÃO

As leishmanioses são doenças causadas pelo protozoário parasito que pertence ao gênero *Leishmania*, ordem Kinetoplastida e família *Trypanosomatidae*. A transmissão ocorre durante o repasto sanguíneo de fêmeas de flebotomíneo infectadas com o parasito. Existem 53 espécies de *Leishmania*, sendo 20 delas patogênicas para o homem, diferindo nas manifestações clínicas provocadas no hospedeiro, divididas em três grupos principais, assim classificadas: leishmaniose cutânea (LC) ou tegumentar, mucocutânea (LMC) e visceral (LV), esta última também conhecida como calazar (AKHOUNDI *et al.*, 2016; SUNDAR & CHAKRAVARTY, 2013).

Caracterizadas como doenças negligenciadas, apresentam formas clínicas distintas, sendo a LV a mais severa e a que apresenta maior número de óbitos. A *Leishmania infantum* (*syn. Leishmania chagasi*) é o agente causador da LV nas Américas, na China e na bacia do Mediterrâneo, apresentando o cão (*Canis familiaris*) como reservatório de importância epidemiológica (ANVERSA *et al.*, 2018). Os casos caninos, na maioria das vezes, precedem os casos humanos, principalmente devido à proximidade destes. Além da presença do vetor e do reservatório, há outros fatores importantes para a progressão da doença, como a imunidade do hospedeiro e a virulência do parasito (ALVAR *et al.*, 2004; KRAUSPENHAR *et al.*, 2007).

Segundo a OPAS (2020), na América latina, as leishmanioses são zoonoses com diferentes padrões de transmissão, sendo o ciclo silvestre o principal da leishmaniose cutânea e o doméstico rural e urbano da leishmaniose visceral. Embora ainda mantenha algumas características rurais, a LV se apresenta em processo de urbanização com significativa expansão geográfica. A grande população de cães que fica nas ruas dos grandes centros pode abrigar animais assintomáticos que tem grande importância na saúde pública, pois também são fontes de infecção para os flebotomíneos e assim apresentam papel ativo na cadeia de transmissão da doença (MULE *et al.*, 2020).

Até o presente momento, o tratamento básico da LV e LC baseia-se em poucas opções terapêuticas. Estibogluconato de sódio e antimoniato de meglumina são a base da quimioterapia de primeira escolha em países endêmicos,

especialmente no subcontinente indiano, sendo os fármacos de segunda escolha a anfotericina B e sua formulação lipossomal, paromomicina e miltefosina. De acordo Srivastava *et al.* (2016), além de poucas opções terapêuticas, o uso destes fármacos é limitado devido à alta toxicidade, a via de administração parental, exceto a miltefosina, a ineficácia devido ao surgimento de cepas resistentes aos fármacos e elevado custo de tratamento no caso de formulações lipídicas da anfotericina B.

Em se tratando do diagnóstico de rotina, este baseia-se em métodos diretos, os quais detectam o estágio intracelular do parasito por microscopia em tecido de biópsia ou punção aspirativa do baço, fígado, medula óssea ou linfonodos. No entanto, estes procedimentos invasivos requerem microscopista experiente e não fornecem diagnóstico positivo em todos os casos, pois a distribuição dos parasitos nos tecidos afetados não é homogênea. Além disso, para uma investigação diagnóstica completa é importante avaliar o estado imunológico do hospedeiro e a evolução clínica da doença (NOLI; SARIDOMICHELAKIS, 2014; SAKKAS; GARTZONIKA; LEVIDIOTOU, 2016).

Portanto, é de notória importância o estudo de novos métodos de diagnóstico para doenças negligenciadas a exemplo das leishmanioses. Também torna-se relevante o estudo sob novas metodologias de manipulação de células a fim de baratear os custos de experimentos laboratoriais.

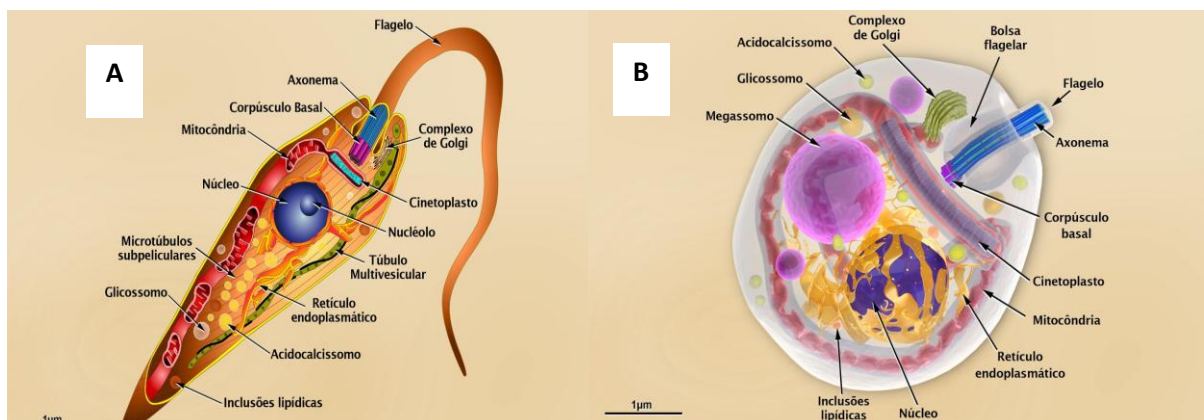
## 2. REVISÃO DA LITERATURA

Para fins de exposição de nossa revisão de literatura, a seguir apontaremos um apanhado dos nossos pressupostos, começando pelo agente etiológico e seu ciclo de vida, bem como a imunopatogenia e as manifestações clínicas, passando pelos vetores e reservatórios, concluindo com a epidemiologia, tratamento, diagnóstico e os avanços em Biotecnologia.

### 2.1 Agente etiológico e ciclo de vida

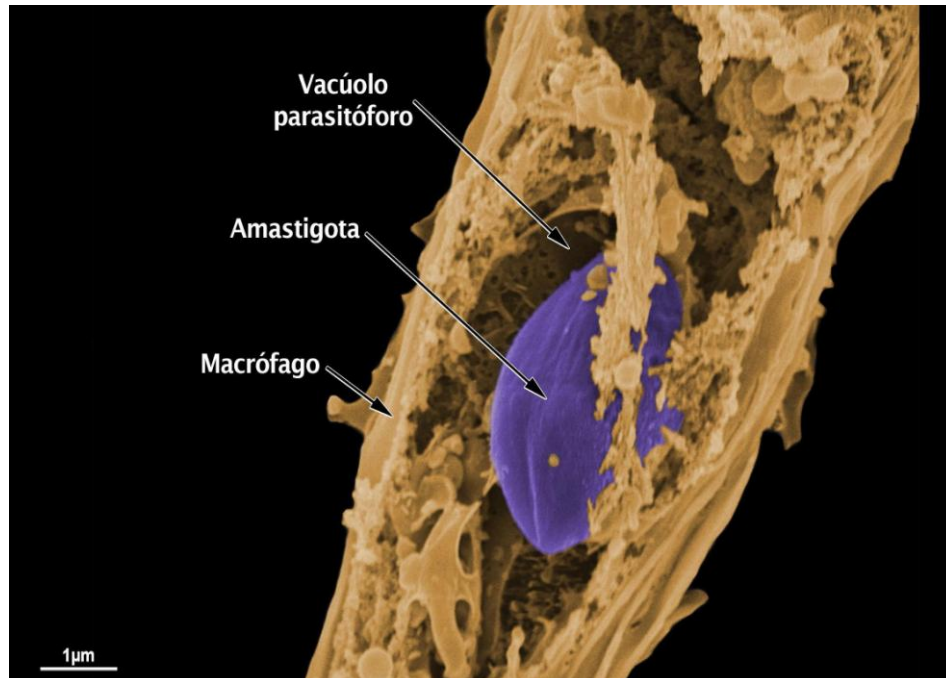
A *Leishmania* é um parasito intracelular que possui ciclo de vida digenético, o qual existe sob duas formas evolutivas: amastigota e promastigota. As promastigotas metacíclicas são alongadas (Figura 1a), possuem um flagelo bastante desenvolvido, são encontradas dentro do intestino das fêmeas dos flebotomíneos (inseto vetor) e são as formas infectantes, seu corpo celular mede entre 6 e 8  $\mu\text{m}$  de comprimento. As amastigotas são esféricas (Figura 1b), medem cerca de 3  $\mu\text{m}$  de largura e 6  $\mu\text{m}$  de comprimento, possuem flagelo externalizado e estão presentes dentro dos fagócitos mononucleares dos hospedeiros vertebrados, como exposto na Figura 2. (DE ALMEIDA *et al.*, 2003).

**Figura 1** – Esquema tridimensional das formas promastigota metacíclica e amastigota de *L. amazonensis* mostrando as principais estruturas, sendo A - Forma promastigota e B - Forma amastigota



Fonte: Teixeira *et al.*, 2013.

**Figura 2** – Micrografia da forma amastigota dentro de um vacúolo parasitóforo no interior de um macrófago através de um microscópio eletrônico de varredura



Fonte: Rodrigues *et al.*, 2008.

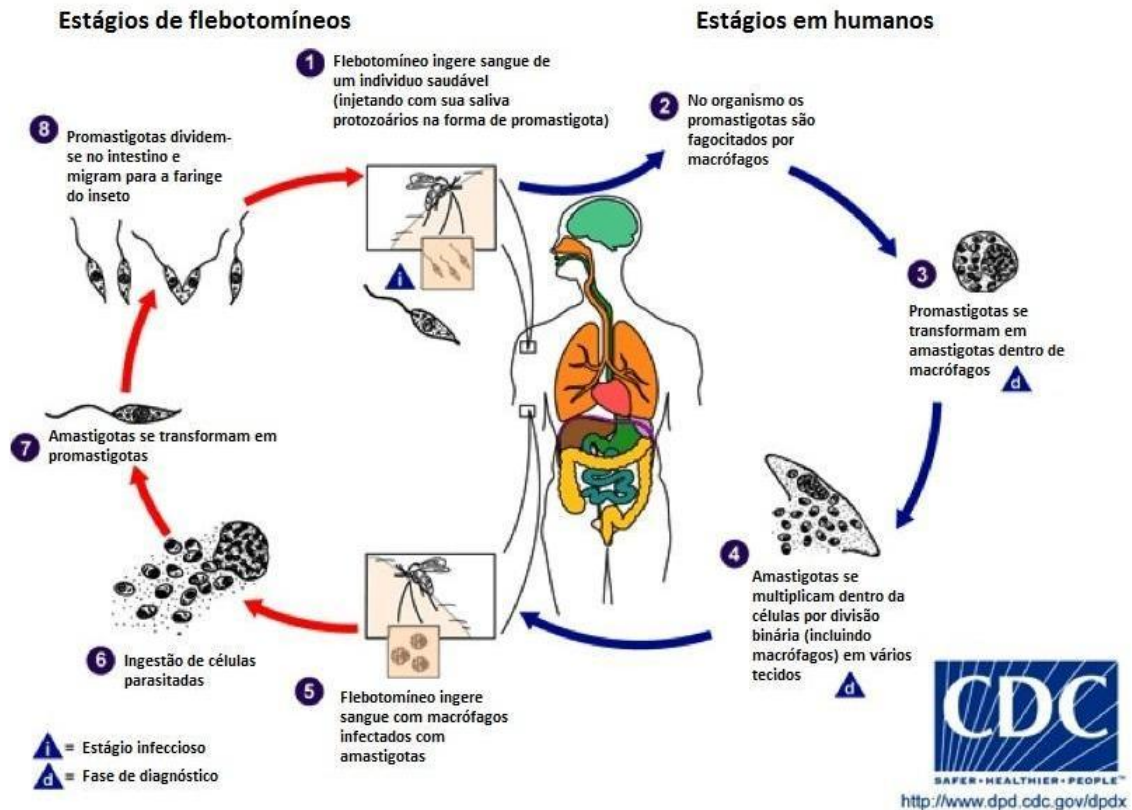
Como reforçam autores como Burza, Croft e Boelaert (2018) e Paho (2019), no Brasil, existem sete espécies distintas do parasito, sendo que destas, seis (*Leishmania braziliensis*, *Leishmania amazonensis*, *Leishmania guyanensis*, *Leishmania lansoni*, *Leishmania shawii*, e *Leishmania naiffi*) são responsáveis pela LC e uma espécie (*Leishmania chagasi*) responsável pela LV.

Durante o repasto sanguíneo, o inseto vetor regurgita as formas promastigotas metacíclicas no hospedeiro vertebrado. Estas formas são fagocitadas, iniciando a fase de desenvolvimento intracelular do parasito e, quando internalizadas, se localizam dentro do vacúolo parasitóforo ou fagolisossomo, onde ocorre a diferenciação da forma promastigota para amastigota, as quais se multiplicam por divisão binária, levando ao rompimento dos macrófagos (Figura 2). Por sua vez, as amastigotas livres ou células infectadas podem ser ingeridas pelo flebotomíneo durante o repasto sanguíneo (SRIVASTAVA *et al.*, 2016) .

Na concepção de SRIVASTAVA *et al.* (2016) e BATES (2018), no interior do intestino dos insetos, as células infectadas se rompem, liberando as formas

amastigotas, que se transformam em promastigotas, recomeçando o ciclo biológico do parasito, como ilustrado na Figura 3 apresentada a seguir.

**Figura 3 – Ciclo de vida de *Leishmania* spp**



Fonte: Site sanarsaúde.com, 2019.<sup>1</sup>

## 2.2 Imunopatogenia e manifestações clínicas

Na perspectiva de Lukes *et al.* (2014), embora os macrófagos sejam células fagocitárias especializadas no combate a agentes infecciosos, as leishmanias desenvolveram mecanismos de defesa capazes de subverter sua capacidade microbicida, conseguindo sobreviver neste ambiente potencialmente tóxico e multiplicar-se até a ruptura da célula, quando são liberadas para infectar outros macrófagos, propagando a infecção.

A internalização das promastigotas ocorre por fagocitose mediada pelo reconhecimento receptor/ligante. Nesse processo geralmente participam os

<sup>1</sup> Disponível em: <https://www.sanarsaude.com/portal/residencias/artigos-noticias/leishmaniose-resumo-completo-tudo-que-o-veterinario-precisa-saber>. Acessado em: 08 nov. 2020.

receptores para complemento CR1 e CR3 dos macrófagos. As moléculas do complemento C3b e C3bi fixadas nas formas promastigotas de *Leishmania* ligam-se aos receptores de macrófagos CR1 e CR3, respectivamente, mostrando o importante papel do receptor de complemento na internalização do parasita na célula hospedeira (ROBLEDO, 1994).

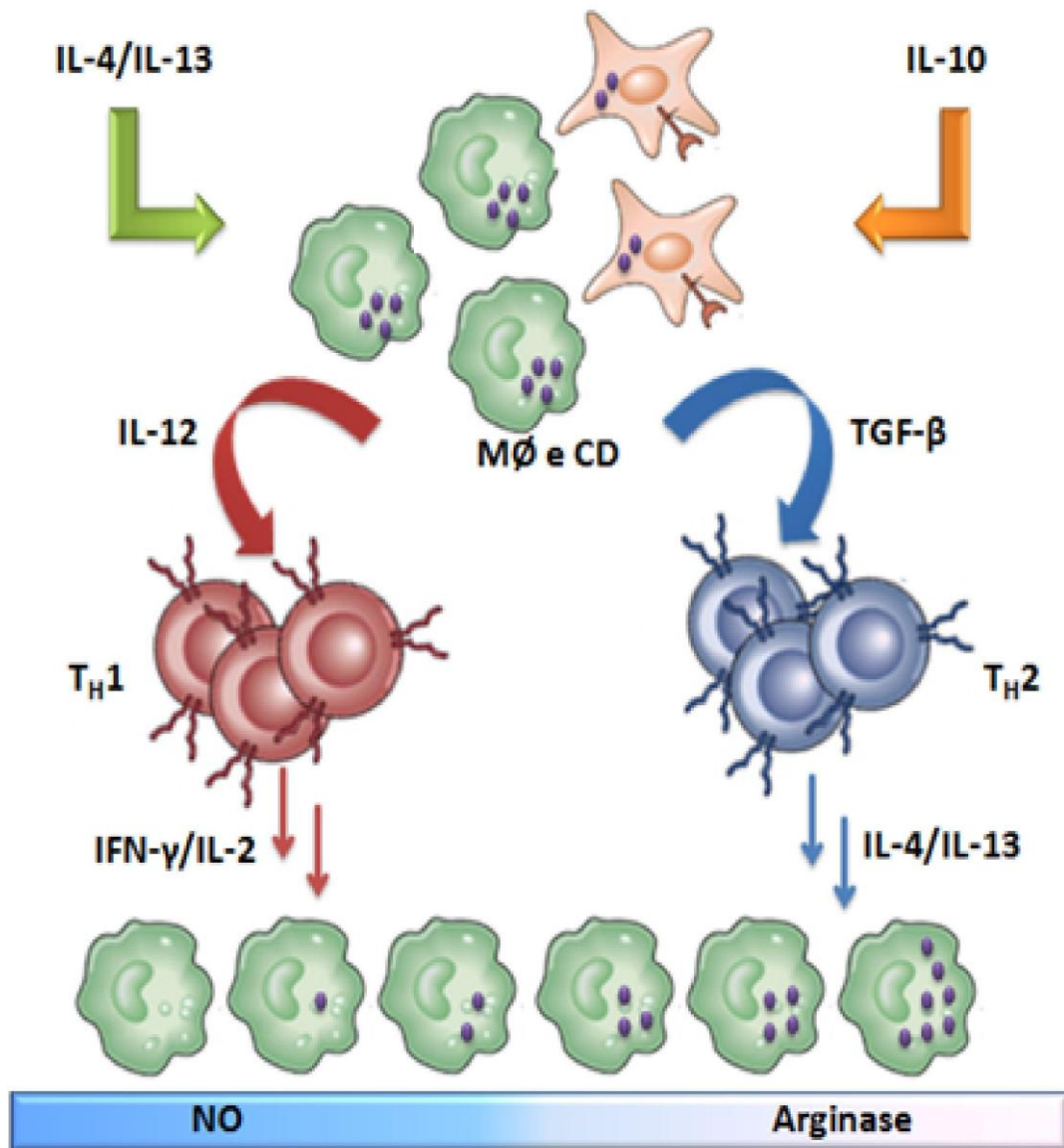
A resposta adaptativa contra os parasitos ocorre após a apresentação de antígenos por macrófagos e células dendríticas, via Complexo Principal de Histocompatibilidade (*Major Histocompatibility Complex* - MHC) classe II para as células T. Contudo, as leishmanias são também susceptíveis à ação dos neutrófilos que possuem grande capacidade de produzir peróxido de hidrogênio (H<sub>2</sub>O<sub>2</sub>) e óxido nítrico (NO). Porém, como afirmam Carvalho, Passos e Jesus (2005) e Alexander *et al.* (2012), ao penetrar no hospedeiro, o parasito infecta os macrófagos escapando do ataque dos neutrófilos.

Ainda na visão dos últimos autores supracitados, em consonância com os pressupostos de Scott e Novais (2016), as células T podem exercer sua função através da toxicidade mediada por células CD8<sup>+</sup> ou através da secreção de citocinas que vão ativar macrófagos para destruir os microorganismos intracelulares. Já as células T CD4<sup>+</sup> podem ser diferenciadas por várias subpopulações. Entre elas estão as células Th1 e Th2, que são respectivamente de fundamental importância para a defesa e susceptibilidade do hospedeiro contra as infecções.

Em resposta à estimulação, as células Th1 produzem IFN $\gamma$  e IL-2 e é necessária para controlar a infecção. A liberação de IFN $\gamma$  acarreta na ativação do macrófago e produção de NO, importantes na erradicação do parasito intracelular. A atividade leishminicida do macrófago induzida por IFN $\gamma$  pode ser aumentada por outras citocinas, como TNF $\alpha$  e Fator Inibitório de Migração (Migration Inhibitory Factor - MIF). Por outro lado, as células Th2 são responsáveis por produzir IL-4, IL-10, IL-13 e TGF- $\beta$  (SCOTT, NOVAIS, 2016).

No entendimento de McCall *et al.* (2013) e Tomiotto-Pelleissier *et al.* (2018), este tipo de resposta não é capaz de controlar a infecção, já que aumenta a expressão de arginase e multiplicação dos parasitos resultando no agravamento da doença, como ilustrado na Figura 4 a seguir.

**Figura 4** – Esquema do mecanismo imunológico que induz a diferenciação das células T CD4<sup>+</sup> nas subpopulações Th1 e Th2



Fonte: Adaptado de Alexander *et al.*, 2012.

### 2.2.1 Leishmaniose visceral

A LV é caracterizada por sinais clínicos incluindo hepatoesplenomegalia e caquexia, podendo levar à morte se não houver tratamento (Figura 5); no entanto, segundo Alvar *et al.* (2012), dependendo da fase da doença e da imunidade do hospedeiro, este por muitas vezes apresenta-se assintomático. O período de

incubação varia de duas semanas a 18 meses, podendo aparecer lesões cutâneas iniciais de dois a oito meses após a infecção, podendo os sintomas da LV demorarem anos para aparecer.

Efetivamente, a doença é bastante progressiva e se a infecção sintomática não for tratada é geralmente fatal, com uma taxa de mortalidade de 75 a 95%. Os parasitos proliferam onde há células do Sistema de Fagocítico Mononuclear, especialmente macrófagos. Estas são mais abundantes no baço e no fígado e, conseqüentemente, a infecção resulta em um aumento de ambos os órgãos. As células da medula óssea também são infectadas e os pacientes desenvolvem pancitopenia e imunossupressão, tornando-os susceptíveis a infecções secundárias (READY, 2014).

**Figura 5** – Hepatoesplenomegalia em paciente com leishmaniose visceral



Fonte: Teixeira *et al.*, 2013.

Os cães domésticos são os principais reservatórios para *L. infantum* em regiões endêmicas e a maioria deles é assintomática. De acordo com Shokri, Fakhari e Teshnizi (2017), os sinais clínicos da LV em cães infectados incluem caquexia, queda de pelo, feridas na derme, perda de peso, linfadenopatia e letargia, como evidenciado na Figura 6 abaixo.



**Figura 6** – Cães com sinais clínicos da leishmaniose visceral canina, como queda de pelo, feridas na derme e perda de peso



Fonte: Teixeira *et al.*, 2013; Noli e Saridomichelakis, 2014.

### 2.2.2 Leishmaniose cutânea

Segundo PAHO (2019), a forma cutânea ou tegumentar é tida como uma forma benigna da leishmaniose, apresenta acometimento da pele com lesões indolores, únicas ou múltiplas, bordas elevadas, concentrando-se em partes do corpo como a face, braços e pernas, que tendem a ter cura espontânea ou apresentam uma significativa resposta à terapêutica. Em consonância, Verma *et al* (2012) apontam que esta dispõe de formato arredondado que varia de alguns milímetros até centímetros de diâmetro, com base eritematosa e infiltrada, associada a bordas bem delimitadas e elevadas. O fundo da ferida é avermelhado e com granulações. A partir das úlceras ou isoladamente podem surgir lesões vegetantes e verrucosas, como retratado na Figura 7A.

Na LC, o período de incubação é relativamente variável, podendo a infecção evoluir após um período de incubação de uma a doze semanas, em uma pápula que aumenta de tamanho podendo formar úlcera. Na visão de Silveira (2019), a lesão típica, em aspecto de cratera de lua, é indolor e apresenta bordas salientes com fundo necrótico úmido e granuloso, ilustrado também na Figura 7.

A Leishmaniose Cutânea Difusa (LCD) é uma forma rara da leishmaniose, causada pela *L. amazonensis* ou pela *L. aethiopica*. Verma *et al.* (2012) e PAHO (2019) evidenciam que nesta forma é verificada a ocorrência de diversas lesões não ulceradas, nodulares ou em placas, que afetam principalmente a face, e podem chegar a cobrir o corpo inteiro, como mostra a Figura 7B). Assim sendo, conforme Burza, Croft e Boelaert (2018), a LMC compromete a mucosa, com destruição tissular progressiva da mucosa nasal e orofaríngea, podendo levar à perfuração do septo e ocasionar uma possível desfiguração da face e perda do septo, palato e pavilhão auditivo, devido à intensa resposta inflamatória, como exposto na Figura 7C.

**Figura 7** – Formas clínicas da Leishmaniose Cutânea (LC): A: Leishmaniose cutânea; B: Leishmaniose Cutânea difusa; C: Leishmaniose Muco-cutânea



Fonte: BRASIL, 2017.

Se não tratadas, as lesões podem evoluir para cura espontânea, deixando cicatrizes atróficas, no período de meses a poucos anos. Além disso, podem também permanecer ativas e coexistir com lesões mucosas que surgem posteriormente. Conforme apontam Mcgwire e Satoskar (2013), na maioria dos casos, a doença mucosa ocorre após as lesões cutâneas e o diagnóstico de comprometimento da mucosa é estabelecido apenas meses a anos depois da cura clínica da lesão cutânea primária, embora haja casos em que a mucosa é o local primário.

### 2.3 Vetores e reservatórios

Na natureza, todas as espécies de *Leishmania* são transmitidas ao homem ou a outros hospedeiros vertebrados durante o repasto sanguíneo de fêmeas hematófagas infectadas. Estes insetos denominados flebotomíneos (Figura 8), pertencem à ordem Díptera, família *Psychodidae*, subfamília *Phlebotominae* e gênero *Lutzomyia*, e são popularmente conhecidos como mosquito-palha, asa dura, birigui ou cangalhinha. Estes dípteros possuem o corpo revestido por pelos e são de coloração clara, medindo de 1 a 3 mm de comprimento. Possuem uma grande distribuição nos climas quentes e temperados, apresentando atividade crepuscular e pós-crepuscular e abrigando-se durante o dia em lugares úmidos, escuros e protegidos dos ventos. Rath *et al.* (2003) e Marques e Forattini (2005) reforçam que ambos os sexos necessitam de carboidratos como fonte energética, mas apenas as fêmeas se alimentam de sangue para o desenvolvimento de seus ovos.

**Figura 8** – Fêmea de flebotomíneo (Diptera: Psychodidae) ingurgitada durante repasto sanguíneo realizado em pele de isca humana



Fonte: Site do CDC – Centers for disease control and prevention, 2006. <sup>2</sup>

O gênero *Lutzomyia* é o responsável pela transmissão das leishmanioses nas Américas, existindo 350 espécies catalogadas, distribuídas desde o sul do Canadá até o norte da Argentina. De acordo com Rocha *et al.* (2010), destas, pelo menos 200 ocorrem na bacia amazônica. As principais espécies envolvidas na transmissão da leishmaniose tegumentar americana são: *Lutzomyia flaviscutellata*, *Lutzomyia whitmani*, *Lutzomyia umbratilis*, *Lutzomyia intermédia*, *Lutzomyia wellcome* e

<sup>2</sup> Disponível em: <https://phil.cdc.gov/Details.aspx?pid=10277>. Acesso em: 08 jan. 2020.

*Lutzomyia migone*. O principal vetor da leishmaniose visceral no Brasil é o *Lutzomyia longipalpis*, o qual está distribuída no peridomicílio de áreas rurais, subúrbios de baixa altitude e favelas de diversas regiões tropicais da América Latina (STEVERDING, 2017).

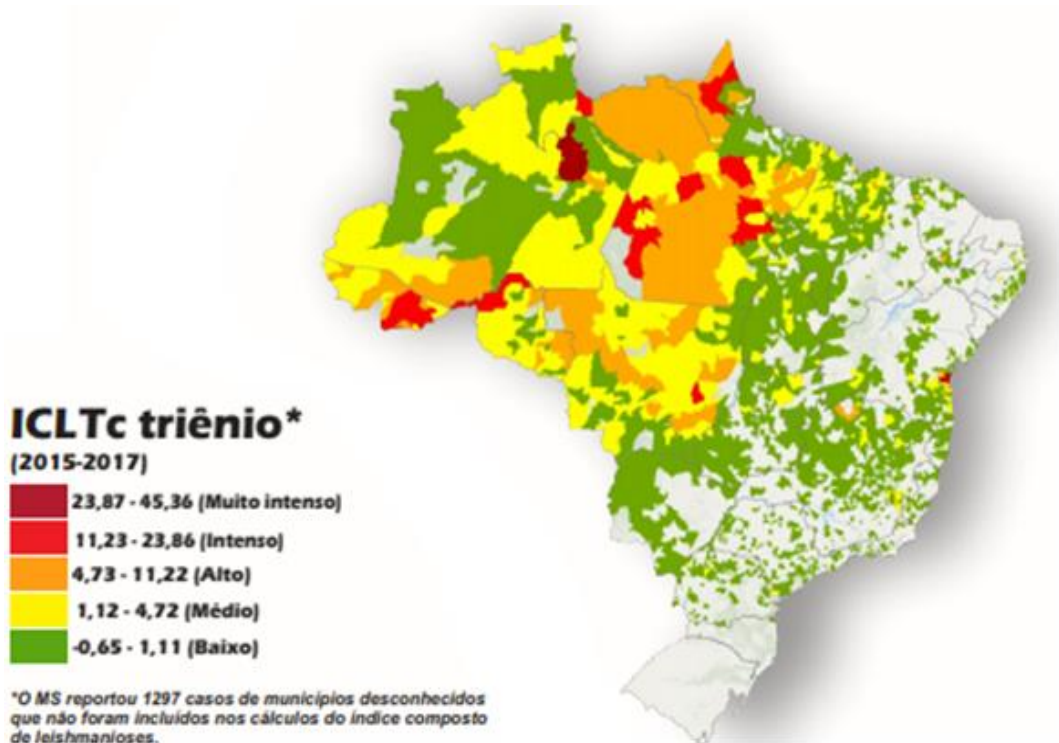
## 2.4 Epidemiologia

As leishmanioses estão presentes principalmente em países localizados em regiões tropicais e subtropicais, acometendo países mais pobres e em desenvolvimento, atingindo populações mais vulneráveis, sem e/ou com pouco acesso ao saneamento básico e com educação sanitária escassa. Sua expansão é multifatorial e geralmente está associada às condições subsistentes de habitação, desnutrição, baixa escolaridade e deficiência do sistema imunológico. Estas também representam uma problemática na saúde pública, pois são necessários grandes investimentos dos governos em prol da erradicação da doença, partindo da prevenção, como pulverização de ruas com inseticida, até o tratamento, o qual é custoso para os sistemas públicos (BRASIL, 2017; PAHO, 2019).

Este grupo de doenças é o segundo mais frequente em todo o mundo, e é endêmico em 102 países, com incidência anual de 1 milhão de novos casos, prevalência de 12 milhões de casos por ano e cerca de 30 mil óbitos por ano (WHO, 2021). Nas Américas, as leishmanioses acometem 18 países, sendo a LV a forma mais severa e quase sempre fatal, se não tratada, e a LC representa a forma clínica mais comum. Além disso, a LMC possui uma evolução crônica podendo causar deformidades e sequelas (OPAS, 2020).

Segundo dados da OPAS (2020), no Brasil, a LC e LMC apresentaram juntas uma incidência de 17,7 e ocorrência de 17.526 novos casos, sendo 95,3% de LC e 4,7% de LM, entre 2015 e 2017. Neste mesmo triênio foi observado que 91,8% das pessoas acometidas pela doença são maiores que 10 anos, onde 16,3% dos casos totais ocorreram nas fronteiras e que a doença prevalece no sexo masculino (72,7%). A Figura 9 mostra um panorama geral da situação no país, mostrando regiões que sofrem com a doença.

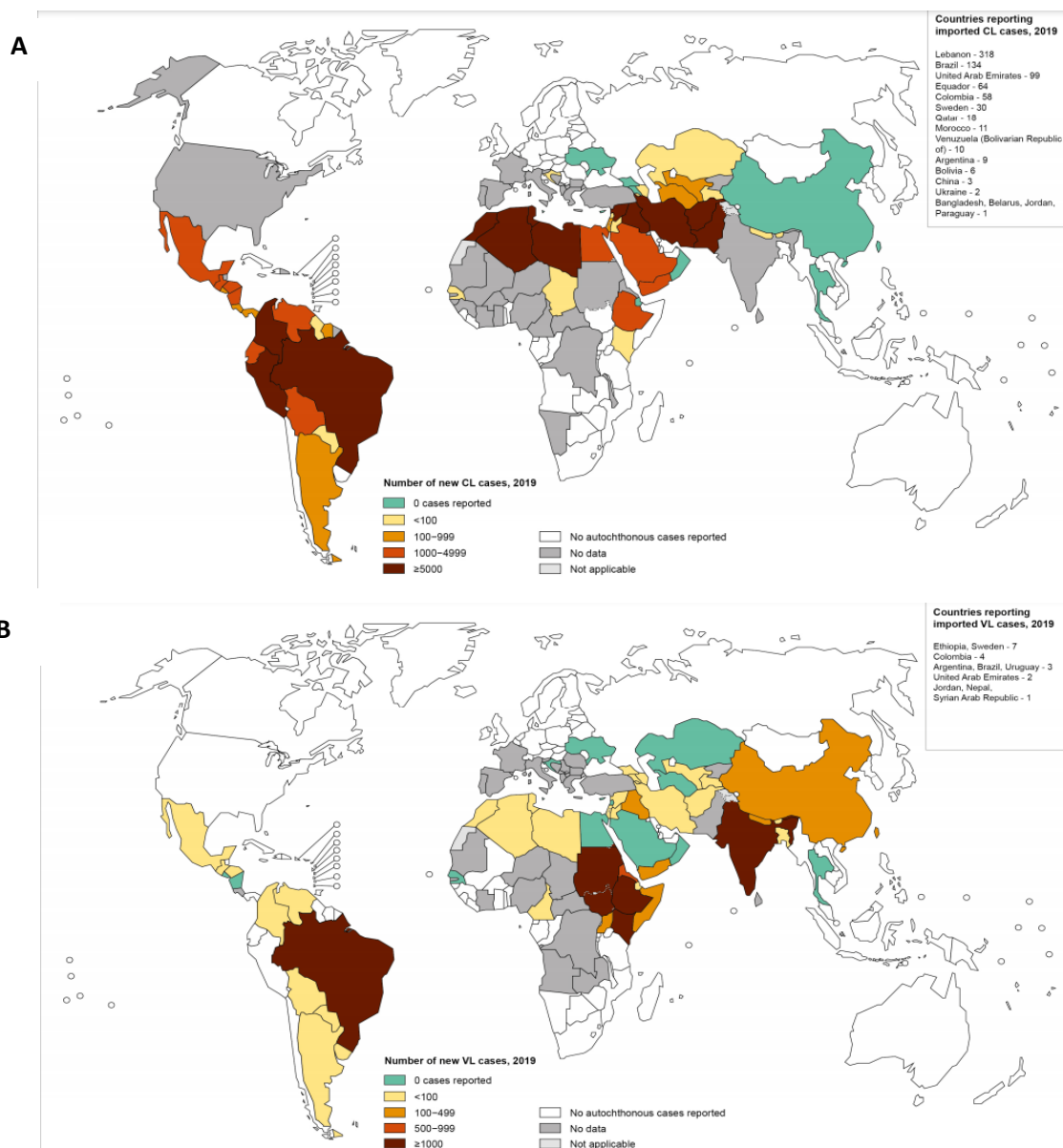
**Figura 9** – Incidência de leishmaniose cutânea e mucosa no Brasil



Fonte: OPAS, 2017.

A forma mais severa da doença, a LV, acomete todos os continentes do planeta (Figura 10), sendo que 90% destes relatados ocorrem em seis países: Índia, Bangladesh, Sudão, Sudão do Sul, Brasil e Etiópia. Mesmo com acesso ao tratamento, a LV pode resultar em taxas de letalidade de 10-20%. Essa parasitose apresenta 0,2 a 0,4 milhões de casos em todo o mundo, com incidência anual de 58 mil casos, exceto na Nova Zelândia e no Sul do Pacífico. (AKHOUNDI *et al.*, 2016; ALVAR *et al.*, 2012). A figura abaixo, demonstra geograficamente as regiões ao redor do mundo acometidas pela LT (Figura A) e LV (figura B) até o ano de 2019, segundo a Organização Mundial de Saúde.

**Figura 10 - Situação epidemiológica das leishmanioses no mundo no ano de 2019: A - Distribuição da leishmaniose tegumentar; B - Distribuição da leishmaniose visceral**



Fonte: WHO, 2019.<sup>3</sup>

<sup>3</sup> Disponível em: [https://www.who.int/health-topics/leishmaniasis#tab=tab\\_1](https://www.who.int/health-topics/leishmaniasis#tab=tab_1). Acesso em: 20 maio 2021.

Estima-se que no Brasil há uma incidência anual de 4.200 casos de LV (AKHOUNDI *et al.*, 2016; ALVAR *et al.*, 2012). Entre os anos de 2007 e 2013 foram registrados em nosso país mais de 26 mil casos de LV, sendo que a região Nordeste possui o maior percentual de casos registrados no país (51%). De acordo com os dados do SINAM (2014), o Brasil é o terceiro maior foco de LV do mundo e é responsável por 90% dos casos notificados nas Américas. No país, a LV é uma doença que requer a notificação compulsória, e que cujos medicamentos para o tratamento são fornecidos exclusivamente pelo governo (BELO *et al.*, 2013; DE ARAUJO *et al.*, 2013).

O Brasil é endêmico para as duas formas da doença, fato este que se justifica devido ao clima tropical do país, o que é favorável a proliferação do díptero transmissor da doença. Esse caráter endêmico é observado ao avaliar um período de 10 anos no Brasil, e a despeito da forma visceral, houve uma curva decrescente no mundo que não foi acompanhada pelo Brasil. (WHO, 2021).

## 2.5 Tratamento

A leishmaniose é uma doença antiga, tendo descrições de suas manifestações clínicas cutâneas que datam de 1500 a 2500 anos a.C. No entanto, os relatos sobre o seu tratamento são apenas do final do século XIX, quando se começou a usar ácido láctico puro para cauterizar as lesões. Além disso, foram utilizados sulfato de cobre, ácido de bateria velha e extratos de plantas. (OPS, 2020).

Conforme Rath *et al.* (2003) e Frezard, Demicheli e Ribeiro (2009), embora o uso medicinal de compostos de antimônio seja conhecido desde séculos antes da era cristã, para diversos fins terapêuticos, apenas em 1912 o tártaro emético foi utilizado pela primeira vez para tratar a Leishmaniose Cutânea pelo médico Gaspar de Oliveira Vianna, o qual era utilizado na época como substância emética, tratamento contra sífilis, gota, dentre outros. Entretanto, seu uso foi contestado por outros estudiosos os quais enalteceram os seus efeitos colaterais, o que levou ao desenvolvimento dos antimoniais pentavalentes, que apresentam maior taxa de cura e menos efeitos tóxicos que a forma trivalente. Tais informações serão exploradas ao longo das próximas subseções.

### 2.5.1 Antimoniais

Dentre os compostos de antimoniais utilizados no tratamento da leishmaniose destacam-se os complexos de antimônio trivalentes tais como o tartarato antimonial de potássio (Tártaro emético), antimoniato de bis-catecol-3,5-dissulfonato sódico (Stibophen<sup>®</sup>, Repodral<sup>®</sup>, Fuadina<sup>®</sup>) e tioglicolato de sódio e antimônio, bem como os antimoniais pentavalentes, antimoniato de *N*-metilglucamina (Glucantime<sup>®</sup>, antimoniato de meglumina), gluconato de antimônio sódico (Pentostan<sup>®</sup>, Solustibosan<sup>®</sup>, estibogluconato sódico) e ureia estibamina (Estibamine<sup>®</sup>) (BRASIL, 2014).

Estudiosos como Wyllie, Cunningham e Fairlamb (2004) sugerem que o antimônio compromete o potencial redox tiol da célula, induzindo o efluxo de tióis intracelulares e inibição de tripanotiona redutase. Outra hipótese, segundo Demicheli et al. (2002), diz respeito à capacidade do Sb<sup>V</sup> em formar complexos com nucleotídeos, inibindo a topoisomerase e interferindo no metabolismo do parasito. No entanto, devido a cardiotoxicidade e intolerância gastrointestinal dos antimoniais trivalentes (Sb<sup>III</sup>), são os antimoniais pentavalentes (Sb<sup>V</sup>) que apresentam maior uso terapêutico (SERENO *et al.*, 1998).

Ao longo dos anos diferentes regimes de dosagens foram propostos numa tentativa de alcançar a menor dose terapêutica eficaz e com menos efeitos colaterais. A Organização Mundial de Saúde (2014) preconiza que as doses de antimoniais não devem ultrapassar 20 mg/kg/dia, não se ultrapassando o limite de 850 mg de antimônio, devido à sua elevada toxicidade. Mialgias, dores abdominais, alterações hepáticas e distúrbios cardiológicos e renais são efeitos colaterais frequentemente associados ao uso destes fármacos.

Ainda que o antimoniato de metilglucamina seja bastante eficaz em regredir rapidamente as manifestações clínicas e hematológicas da doença e provocar esterilização do parasita, a crescente incidência de casos de resistência tem sido uma séria preocupação para a sua utilização em áreas endêmicas. Devido às baixas dosagens e tratamentos descontínuos, começaram a ocorrer falhas na terapia e consequente aumento da resistência de parasitos (RATH *et al.*, 2003; SUNDAR & CHAKRAVART, 2019).



O aumento da incidência de falha terapêutica nos últimos anos vem se tornando uma grande ameaça, principalmente aos pacientes coinfectados com *Leishmania* e HIV. A principal causa dessa emergência é o mau uso dos fármacos, que leva à seleção de pequenas populações resistentes. Esse fenômeno de falha terapêutica é complexo, uma vez que há vários fatores envolvidos: características do hospedeiro, como genética e resposta imunológica; fatores técnicos, como a qualidade do fármaco e a via de administração parenteral; a duração do tratamento; e a biologia do parasito, como uma variabilidade intrínseca em relação à susceptibilidade ao antimônio (CROFT; SUNDAR & FAIRLAMB, 2006).

Sendo assim, Plano *et al.* (2011) reforçam que os principais pontos contrários à terapia com antimoniais são o desenvolvimento de resistência de várias cepas frente a estes tratamentos, os regimes de tratamento com altas doses por longos períodos, administração parenteral, além de elevada toxicidade renal e cardíaca, muitas vezes levando os pacientes a abandonarem o tratamento.

### 2.5.2 Anfotericina B

É um antibiótico macrolídeo da classe dos polienos, derivado de uma cepa de *Streptomyces nodosus*, largamente utilizado para o tratamento de infecções fúngicas sistêmicas que pertence ao grupo de fármacos leishmanicidas de segunda geração, usada extensivamente no caso de falhas no tratamento com compostos antimoniais. O mecanismo de ação, assim como da toxicidade, envolve a formação de poros artificiais ao longo da membrana celular do parasito e hospedeiro, alterando a permeabilidade seletiva a cátions e levando à morte celular. A anfotericina B também interfere na síntese do ergosterol, um importante componente de membrana da *Leishmania* (LEMKE; KIDERLEN & KAYSER, 2005; SANGSHETTI *et al.*, 2015).

Apesar de sua eficácia a anfotericina B também é tóxica e está associada a efeitos secundários graves. No entanto, em áreas em que existem níveis elevados de resistência ao  $Sb^V$ , a anfotericina B é o fármaco de escolha (HAMILL, 2013; BRASIL, 2014). Alguns desses efeitos foram contornados por alterações em sua formulação, tais como lipossomal, dispersão coloidal e complexo lipídico. Estas formulações lipídicas da anfotericina B mantêm sua atividade e reduz a toxicidade.

Assim sendo, foi visto que a anfotericina B é efetiva no tratamento de leishmaniose visceral, com toxicidade mais baixa quando encapsulada em

lipossomas, porém o alto custo limita sua utilização, sendo utilizada apenas em LV (KLEMPNER *et al*, 2014; FUNABASHI *et al*, 2020).

### 2.5.3 Pentamidina

A pentamidina pertence ao grupo das diaminas aromáticas e sua atividade terapêutica foi descoberta casualmente. Basselin *et al.* (1997) descreveram que a pentamidina, utilizada na clínica contra casos de leishmaniose resistente aos antimoniais pentavalentes, apresenta resultados significantes em pacientes imunodeprimidos. No entanto requer administração parenteral e têm sido observados efeitos adversos significantes após sua administração. Dentre os principais efeitos estão hipoglicemia, hipotensão, mialgias, alterações cardiológicas e nefrotoxicidade. Além disso, há relatos de morte repentina, o que limita seu emprego terapêutico (HAFIZ; KYRIAKOPOULOS, 2021).

Embora o mecanismo preciso pelo qual a pentamidina atue não esteja claro, sabe-se que as diamidinas interferem na síntese de poliaminas, bloqueando a utilização de S-adenosil-L-metionina ao inibir enzimas como a ornitina descarboxilase e a espermidina sintetase, impedindo, assim, a síntese de biomoléculas de importância em vários processos bioquímicos da fisiologia celular do parasita. Além disso, outra teoria bastante aceita tem proposto que ocorre inibição da topoisomerase mitocondrial. Já o mecanismo de resistência pode estar associado à redução do potencial da membrana mitocondrial e redução do acúmulo do fármaco em terapias prolongadas (MUKHERJEE; DAS & SEN, 2006; PORCHEDDU *et al.*, 2012).

### 2.5.4 Miltefosina

A miltefosina é um antineoplásico alquilfosfolipídico que se mostrou eficaz contra *Leishmania* spp. *in vitro* e *in vivo*. No entanto, a grande vantagem do uso desse fármaco é o fato de ser o primeiro e único usado por via oral, quer seja para tratar a LV ou LC. A dose de miltefosina atualmente recomendada, como monoterapia, é de 2,5 mg/kg/dia durante 28 dias, embora na prática clínica outras doses sejam administradas. De maneira geral ela tem sido bem tolerada, com

exceção de leves efeitos colaterais gastrointestinais, embora o seu potencial teratogênico dificulte seriamente a sua utilização generalizada na clínica e em programas nacionais de eliminação (BRASIL, 2018; BRASIL, 2020).

As dificuldades encontradas no tratamento da leishmaniose, como o alto custo, o longo período de tratamento, a via de administração, os efeitos colaterais, as contraindicações e a resistência são fatores que relatam o quanto a quimioterapia da leishmaniose está distante de ser satisfatória. Assim, é imprescindível o desenvolvimento de novos fármacos capazes de apresentarem alta seletividade, um alto índice terapêutico e ser de fácil administração.

## 2.6 Diagnóstico

O diagnóstico de rotina baseia-se em métodos diretos, os quais detectam o estágio intracelular do parasito por microscopia em tecido de biópsia ou punção aspirativa do baço, fígado, medula óssea ou linfonodos. No entanto, estes procedimentos invasivos requerem microscopista experiente e não fornecem diagnóstico positivo em todos os casos, pois a distribuição dos parasitos nos tecidos afetados não é homogênea. Além disso, para uma investigação diagnóstica completa é importante avaliar o estado imunológico do hospedeiro e a evolução clínica da doença (NOLI; SARIDOMICHELAKIS, 2014; SAKKAS; GARTZONIKA; LEVIDIOTOU, 2016; TRONCARELLI *et al.*, 2009).

O diagnóstico parasitológico, utilizando aspirado de medula óssea como amostras, constitui o padrão ouro para o diagnóstico da LV. De acordo com Goto e Lindoso (2010) e Srivastava *et al.* (2011), para o diagnóstico etiológico, as alternativas incluem técnicas moleculares para a detecção de DNA de *Leishmania* spp. por meio de métodos baseados na Reação em Cadeia da Polimerase (PCR), que pode detectar o gênero *Leishmania* para confirmar a leishmaniose ou até mesmo identificar as espécies de *Leishmania*. O método de diagnóstico por PCR é realizado utilizando DNA do parasito, que pode ser extraído de fragmento de pele, mucosa, sangue periférico, medula óssea ou baço (BRASIL, 2014; BRASIL, 2017).

No diagnóstico laboratorial, os parasitos são geralmente identificados quanto ao gênero *Leishmania* por microscopia, onde, por sua vez, a forma amastigota é geralmente detectada microscopicamente após a coloração com Giemsa. Os exames de sangue são os mais fáceis de realizar, porém há pouquíssimas células

parasitadas circulantes. Os aspirados de baço são uma fonte rica de células parasitadas, no entanto a biópsia deve ser realizada somente por profissionais treinados, por existir o risco de ruptura ou sangramento do órgão. A aspiração da medula óssea é frequentemente utilizada, mas é uma técnica especializada com menor sensibilidade. A inoculação de materiais de biópsia em meios de cultura ou em roedores de laboratório pode ser um método sensível, porém requer um tempo elevado para chegar ao resultado do diagnóstico, como destacam Noli e Saridomichelakis (2014) e Sakkas, Gartzonika e Levidiotou (2016).

Os métodos mais utilizados para o diagnóstico sorológico das leishmanioses são imunofluorescência indireta (IFI) e o ensaio imunoenzimático (ELISA), também são utilizados o teste rápido imunocromatográfico, aglutinação direta e imunobloting. Esses testes são sensíveis, porém a especificidade pode variar, principalmente em áreas endêmicas de *Trypanosoma* spp. Os anticorpos antileishmania permanecem detectáveis durante meses ou anos após o tratamento, porém, quando há baixos níveis de infecção é difícil diagnosticar.

Ademais, é comum que o resultado sorológico positivo seja encontrado em um paciente infectado que não tem LV, mas outra doença. Dessa forma, novamente autores como Noli e Saridomichelakis (2014) e Sakkas, Gartzonika e Levidiotou (2016) enfatizam a importância de uma análise cuidadosa para o maior número possível de diferenciais de reação cruzada, especialmente quando o quadro clínico não é típico da doença.

Sabe-se que cães com leishmaniose são reservatórios dos parasitos e, por conseguinte, contribuem para a transmissão da doença, o diagnóstico precoce e tratamento são considerados um componente essencial no controle da doença (RIBEIRO et al., 2013). Destarte, Baneth e Aroch (2008) afirmam que alguns cães apresentam sintomas clínicos, como lesões oculares e na pele, alterações no esqueleto ósseo e emagrecimento. Porém, há casos não sintomáticos, que por sua vez representam as maiores dificuldades para identificação da doença.

A maioria das infecções é diagnosticada clinicamente com sintomas de febre irregular, leucopenia e anemia, hepatoesplenomegalia e supressão da medula óssea. Para o diagnóstico laboratorial de cães assintomáticos ou que apresentam poucos sintomas (oligossintomáticos) são requeridos testes de alta sensibilidade e especificidade. De modo a proporcionar mais sensibilidade aos testes, novas

ferramentas baseadas em métodos moleculares estão sendo desenvolvidas (LEITE et al., 2010; MOHAMMADIHA et al., 2013; MOTAZEDIAN et al., 2008).

Recentemente, o Ministério da Agricultura, Pecuária e Abastecimento (MAPA) aprovou a venda e uso do teste rápido para leishmanioses, o qual foi desenvolvido pela empresa *Victory Square Health*<sup>®</sup> em parceria com a Universidade Federal de Minas Gerais (UFMG). A *VS Health* desenvolveu e validou o desempenho clínico de seu teste de diagnóstico para leishmaniose com resultados que excede os testes atualmente disponíveis, com maior sensibilidade (93,2%) e especificidade (91,3%) em diagnosticar corretamente a leishmaniose tanto em animais quanto em humanos (*VS TECHNOLOGIES*, 2020).

## **2.7 Avanços na biotecnologia em saúde**

A biotecnologia pode ser definida como um conjunto de disciplinas, como engenharia química, biologia e física, inter-relacionadas no desenvolvimento de novos conhecimentos. A bioinformática, por exemplo, reúne aspectos da biologia e ciências da computação; a nanociência, apresenta características da física e da química. A modalidade da biotecnologia tem tornado pesquisadores mais interdisciplinares, que desenvolvem projetos de maior complexidade, contribuindo com o desenvolvimento da Ciência, Tecnologia e Inovação (CT&I) (FOLEY, 2016).

As técnicas e aplicações da biotecnologia para a saúde humana são inúmeras e abrange uma diversidade de profissões. Classificando-as em quatro grupos, o primeiro é composto por substâncias biotecnológicas, como as proteínas recombinantes, anticorpos monoclonais, genes e células-tronco para uso terapêutico. O segundo, reúne os biofármacos. O terceiro, os reagentes e kits utilizados em diagnósticos de análises clínicas. E o quarto grupo compreende as vacinas preventivas e terapêuticas (REIS *et al.*, 2009).

Na visão de Madureira (2011), a importância do avanço na biotecnologia frente às doenças negligenciadas é relevante para a erradicação destas doenças, que em sua maioria estão presentes nos países menos desenvolvidos e que apresentam recursos humanos e financeiro devastados. Pode-se citar a aplicação da biotecnologia no diagnóstico molecular para detectar possíveis doenças como dengue, leishmaniose, malária, doença de chagas, tuberculose, sífilis e leptospirose, apenas para destacar algumas dentre o amplo espectro de doenças.

Dentre as ciências citadas, a física se destaca por estar presente em diversos avanços biotecnológicos, como raios X, tomografias, PET-SCAN (do inglês *Positron Emission Tomography*), ressonância magnética e radioterapia. Alguns dispositivos físicos se encontram presentes em áreas como farmácia e biotecnologia, como o controle e medição de fluidos biológicos nas atividades científicas e industriais. Deste modo, há a possibilidade de uma atuação mais rápida e precisa sobre o escalamento das dimensões celulares, como exemplo na utilização de dispositivos microfluídicos, que serão abordados nas subseções seguintes.

### 2.7.1 Microfluídica

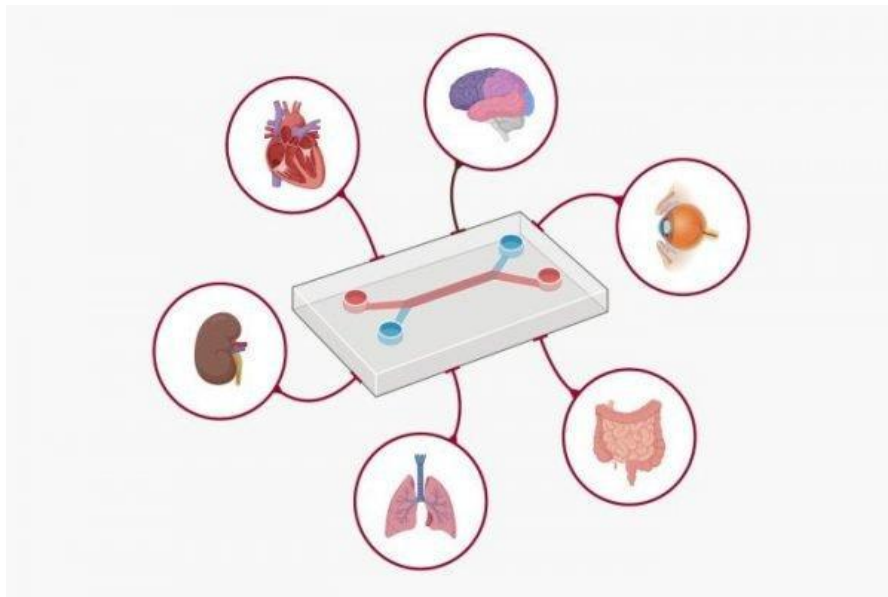
A microfluídica é uma ciência tecnológica que se encontra em crescente expansão, podendo ser aplicada em diversas ferramentas, as quais são promissoras para estudos em áreas como engenharia e medicina. Exemplos de dispositivos microfluídicos utilizados no cotidiano do ser humano são os testes de medição de glicemia e de gravidez, que no século passado eram realizados apenas com testes robustos em laboratório. As técnicas de microfabricação foram desenvolvidas pela *Bell Labs* na década de 1970 e após 10 anos houve o registro da primeira aplicação da microfluídica na biologia celular (SACKMANN; FULTON & BEEBE, 2014).

O avanço nas tecnologias de microfabricação abriu caminho para novas abordagens para manipular e monitorar células em um ambiente que mimetiza as condições *in vivo*. Conforme Vickerman *et al.* (2008), os recursos encontrados nos experimentos *in vivo*, como presença de vários tipos de células em uma única região e em imagem tridimensional (3D) são facilmente alcançáveis por técnicas atuais de microfabricação e podem ser combinados com protocolos de cultura de células. As principais vantagens dos sistemas de cultura de células nos dispositivos microfluídicos são a capacidade de usar pequenas quantidades de células e de reagentes, possuir controle preciso do ambiente espacial e temporal e visualização de alta resolução de eventos celulares em tempo real.

A microfluídica também está inserida no âmbito da indústria farmacêutica, a qual fornece soluções inovadoras. A P&D (pesquisa e desenvolvimento) está concentrada na capacidade de replicação das funções vitais de órgãos humanos em um *microchip*, conhecida como tecnologia de órgão em um chip (do inglês “*organ-on-a-chip*”) (Figura 11). Esta técnica nasceu da junção da tecnologia de

microfabricação e da engenharia de tecidos, o que possibilitou o desenvolvimento de dispositivos para testes de novos medicamentos (XIONG *et al.*, 2014).

**Figura 11:** Esquema representativo de um órgão em um chip (do inglês “organ-on-a-chip”)



Fonte: Ufluidix, 2022.

O desenvolvimento e aplicação de *microchips* simples e acessíveis está ascendendo mundialmente e é constantemente aplicado na área da saúde. Pode-se citar o resultado do trabalho realizado com colaborações de cientistas americanos, europeus e africanos que desenvolveram um dispositivo para diagnosticar o vírus da imunodeficiência humana (HIV).

Na verdade, o diferencial do dispositivo em relação às técnicas já existentes foi a utilização de cerca de um milésimo de mililitro do sangue periférico dos pacientes, e o HIV foi diagnosticado com sucesso na maior parte dos pacientes. Segundo Chin *et al.* (2011), este estudo demonstrou o potencial dos dispositivos microfluídicos para substituir testes de laboratório convencionais, a fim de contribuir para a saúde em países em desenvolvimento.

### 2.7.2 A técnica de acustofluídica e suas aplicações biotecnológicas

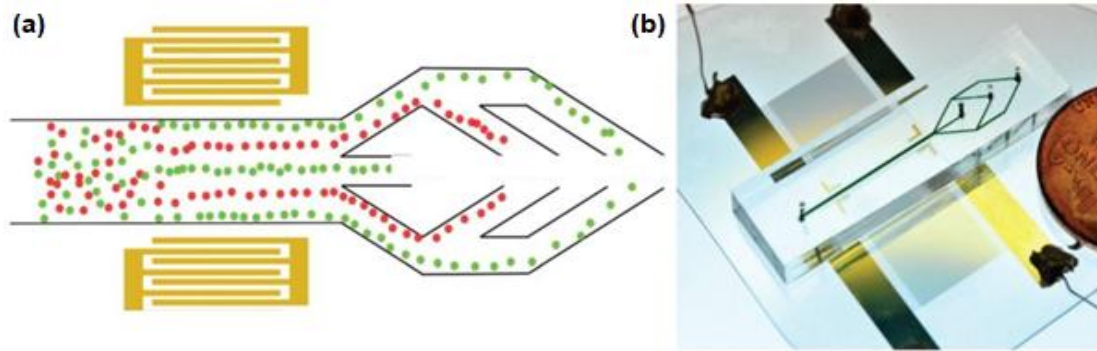
A técnica de acustofluídica conjuntura a metodologia microfluídica com ondas de ultrassom em cavidades com submilímetro. A técnica de ultrassom agregou tecnologias para manipulação sem contato de micropartículas, tais como células e outros microorganismos para separação, enriquecimento e bioensaios. A acustofluídica apresenta aspectos promissores nos ensaios de células que podem ser levitadas e padronizadas em 1D e 2D em uma cavidade acústica com dimensões da ordem de alguns milímetros. O aprisionamento acústico é realizado no regime ultrassônico através de ondas estacionárias que exercem a força de radiação acústica sobre uma micropartícula (PATEL *et al.*, 2014; WESER *et al.*, 2020).

Dispositivos microfluídicos acústicos são ferramentas que utilizam ondas sonoras para manusear objetos ou fluidos em micro ou nanoescala em biomedicina e química analítica. Eles apresentam *designs* simples e compacto e sua operação é biocompatível, o que os caracterizam como plataformas ideais para pesquisa básica, de diagnóstico e terapêutica. Além disso, na microfluídica acústica, as células ou materiais não necessitam estar fisicamente em contato com outros alvos para serem manipulados. De acordo com Zhang *et al.* (2020), isso implica em impactos mecânicos mínimos, bem como redução do calor conduzido pelos transdutores utilizados, diminuindo os danos físicos e biológicos nos materiais em estudo.

Sabe-se que os dispositivos de acustofluídica apresentam a capacidade de manipular células em fluidos, podendo apresentar uma vasta variabilidade, por exemplo, utilização do sangue total e periférico, saliva e urina, independente das propriedades físicas da partícula ou célula alvo. Outrossim, torna-se viável manipular vários grupos de células dentro de um domínio fluido simultaneamente, sendo possível separá-los. A técnica de acustofluídica também é empregada na separação de célula, baseando-se em um dispositivo capaz de distinguir diferenças na densidade celular e nas propriedades mecânicas, como demonstra a Figura 12. (XIE *et al.*, 2020; ZHANG *et al.*, 2020).

**Figura 12:** (a) Esquema e (b) foto do dispositivo de separação de células acústicas





Fonte: Xie *et al.*, 2020.

Em vista disso, o Grupo de Acústica Física (GAF-UFAL) planejou a fabricação de dispositivos de acustofluídica com tecnologia de impressão 3D para realização de ensaios celulares com *Leishmania* spp. e macrófagos realizados no Laboratório de Farmacologia e Imunidade (LaFI) para investigar a influência do aprisionamento por acustofluídica e da nano-termometria, assim como desenvolver um protótipo de teste de diagnóstico por aglutinação direta aprimorados por ultrassom.

### 3. JUSTIFICATIVA

Sabe-se que as doenças negligenciadas carecem de investimentos financeiros e humanos, sendo necessário otimizar aspectos como diagnóstico e tratamento das leishmanioses. A pesquisa científica, por sua vez, apresenta uma oportunidade de novos conhecimentos, otimizando técnicas já descritas na literatura e inovando tecnologicamente, eventualmente resultando em novos métodos de diagnóstico e tratamento, visando menor toxicidade para as células hospedeiras. Além da toxicidade seletiva contra as diferentes espécies de *Leishmania* spp., com alvos farmacológicos específicos para o parasito, é capaz de reduzir a probabilidade de efeitos colaterais, tornando-se assim uma alternativa mais eficaz para o tratamento das leishmanioses.

Como destacam Edmondson *et al.* (2014), os ensaios celulares baseados em microarranjos têm grande importância no processo de *drug-discovery*, fornecendo um processo que utiliza ferramentas simples, rápidas e econômicas, evitando dessa maneira testes em animais em grande escala e com alto custo. Assim sendo, as plataformas de separação baseadas em microfluidos são promissoras, pois podem realizar a separação com uma amostra de volume reduzida, diminuindo o consumo de reagentes e assim ocupam menos espaço. Além do mais, as escalas de comprimento da microfluídica são da mesma ordem de magnitude que as células manipuladas, o que torna a técnica de microfluídica uma plataforma de separação ideal para aplicações em células (REBOUD *et al.*, 2012).

Sabe-se que a busca de novos métodos para o diagnóstico de doenças infecciosas é de benfeitoria para a saúde pública, o que permite o rastreamento de enfermidades, como exemplo, a leishmaniose, que por sua vez facilita a erradicação

da doença. Partindo disso, este trabalho visou contribuir no desenvolvimento de um método diagnóstico inovador através de uma plataforma de opto-acustofluídica inédita projetada para a identificação de amostras microfluídicas contendo *Leishmania*.

## 4. OBJETIVOS

Para a realização desta pesquisa, destacam-se os objetivos listados a seguir.

### 4.1 Objetivo geral

Investigar a influência do aprisionamento por acustofluídica e nanotermometria de *Leishmania* spp. e macrófagos como inovação metodológica para o monitoramento de eventos em ensaios biológicos.

### 4.2 Objetivos específicos

- Desenvolver protocolos para manipulação e posicionamento de formas promastigotas e amastigotas de *Leishmania* spp. e de células hospedeiras (linhagem J774.A1) em armadilhas acústicas geradas por ondas estacionárias de ultrassom em dispositivos de acustofluídica;
- Contribuir para o desenvolvimento de técnicas em dispositivos de acustofluídica a fim de avaliar células e parasitos individualmente, extraindo informações sobre reações enzimáticas, propriedades mecânicas das células e taxa de divisão celular, através de espectroscopia Raman.

## **5. METODOLOGIA**

Os procedimentos de armazenamento das células e parasitos e a experimentação foram realizados no Laboratório de Farmacologia e Imunidade (LaFI) da UFAL sob coordenação da Profa. Dra. Magna Suzana Alexandre Moreira. O dispositivo utilizado nos experimentos foi desenhado e fabricado pelo doutorando, Giclênio Cavalcante, orientado pelo professor Dr. Glauber Thomaz do Grupo de Acústica Física (GAF). O manuseio do equipamento foi realizado pelo Dr. Harisson Santos, em colaboração com o professor Dr. Carlos Jacinto no LabRAM.

### **5.1 Experimentos realizados no LAFI**

A seguir, serão detalhados os procedimentos envolvidos nos experimentos realizados no LAFI.

#### **5.1.1 Macrófagos murinos J774.A1**

A linhagem de macrófagos murinos fenótipo aderente, J774.A1, foi cultivada em meio RPMI (Sigma<sup>®</sup>), em garrafas para cultura de 75 cm<sup>2</sup>, suplementado com 10% de SFB (soro fetal bovino) em estufa a 37°C com atmosfera úmida de 95% contendo 5% de CO<sub>2</sub>.

Assim sendo, os macrófagos foram cultivados até atingirem 90% de confluência, e em seguida foram centrifugados a 1500 rpm, por 5 minutos na

temperatura de 4°C para a separação de células vivas e mortas. Após a centrifugação, as células foram contadas com microscópio óptico em câmara de Neubauer. Para a realização do experimento, utilizou-se  $2 \times 10^7$  células/mL diluídas em 1mL de PBS (tampão fosfato salina, do inglês "*phosphate buffer saline*").

#### 5.1.2 Promastigotas de *Leishmania* spp

As formas promastigotas do parasito foram mantidas *in vitro* em meio *Schneider's*, suplementado com 10% de SFB e 2% urina humana a 27 °C em estufa de Demanda Bioquímica de Oxigênio (BOD). No momento do uso, os parasitos foram colocados em tubos tipo *falcon* e centrifugados à 3.500 rpm durante 10 minutos à 25 °C. Em seguida, o sobrenadante foi descartado e o *pellet* formado foi ressuspenso em PBS. Fez-se, então, a contagem dos parasitos em câmara de Neubauer, para posterior realização dos experimentos.

#### 5.1.3 Amastigotas de *Leishmania amazonensis*

Macrófagos foram plaqueados sobre garrafas de cultivo e infectados com formas promastigotas de *L. amazonensis*, na proporção de 10 parasitos: 1 macrófago. A garrafa com as células infectadas foi incubada por 4 horas em estufa de CO<sub>2</sub> a 37°C com atmosfera úmida contendo 5% de CO<sub>2</sub>. Após este tempo de infecção, os macrófagos foram "lavados" com PBS para remoção dos parasitos não fagocitados. Os macrófagos infectados foram desaderidos da placa por força mecânica, e as células foram contadas com o auxílio da câmara de Neubauer.

#### 5.1.4 Armadilhamento das células e parasitos

Os experimentos de armadilhamento foram realizados no GAF e LabRAM com as células e os parasitos diluídos em PBS. Para isso, foi injetado 10 µL de células e/ou parasitos no dispositivo acustofluídico com o auxílio de seringa e *scalp*. Em continuidade, o fluido foi submetido à frequência de ondas de ultrassom de 3.319 MHz e tensão pk-pk menor que 5 volts, dentro do dispositivo, a fim de aprisionar promastigotas das espécies de *L. amazonensis* e *L. chagasi*, macrófagos

infectados e não infectados. Os experimentos foram realizados em triplicata experimental e biológica.

## 5.2 Experimentos realizados no GAF

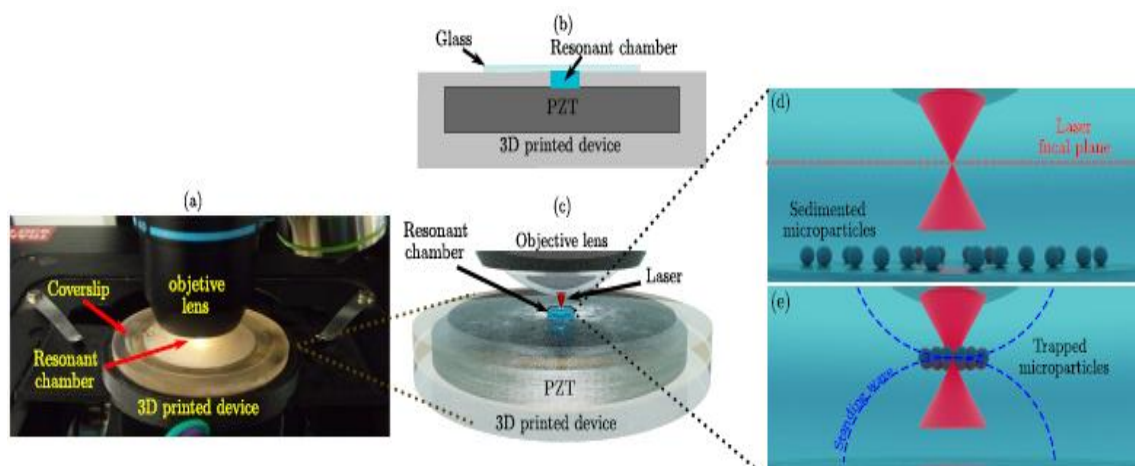
A seguir, serão detalhados os procedimentos envolvidos nos experimentos realizados no GAF.

### 5.2.1 Fabricação do dispositivo de acustofluídica

O armadilhamento acústico de micropartículas ou células é realizado em uma câmara acústica cilíndrica com uma altura de  $H = 750 \mu\text{m}$  e diâmetro de  $2R = 4 \text{ mm}$ . A câmara é produzida dentro de um disco cilíndrico, que é fabricado com uma impressora 3D (*Moonray D75, Sprintray, Inc., EUA*) através da técnica de processamento digital de luz. Um atuador piezocerâmico (titanato zirconato de chumbo, PZT-8) com um diâmetro de 25 mm é colado por baixo da câmara ressonante com epóxi (*Huntsman, Corp., EUA*). Uma lâmina de vidro de  $150 \mu\text{m}$  de espessura é colocada no topo da câmara, funcionando como um refletor acústico (Figura 13).

Este dispositivo foi desenhado e fabricado pelo doutorando, Giclênio Cavalcante, orientado pelo professor Dr. Glauber Thomaz.

**Figura 13.** Demonstração do dispositivo de acustofluídica



Fonte: Santos, 2021.

### 5.2.2 Espectroscopia Raman

As medições Raman foram realizadas por um microscópio Raman confocal (LabRam HR Evolution, HORIBA, França). O microscópio compreende uma lente objetiva de 40x (com uma abertura numérica  $NA = 0,65$ ) e um diodo laser CW que gera um laser de 785 nm com uma potência abaixo de 100 mW. O sinal Raman espalhado posteriormente é coletado pela mesma lente e é disperso por 300 ranhuras/mm. O sistema é calibrado usando uma banda de fônon de silício a  $520 \text{ cm}^{-1}$  como referência. O laser Raman é posicionado por um estágio translacional controlável xyz. O manuseio do equipamento foi realizado pelo Dr. Harisson Santos, em colaboração com o professor Dr. Carlos Jacinto no LabRAM.

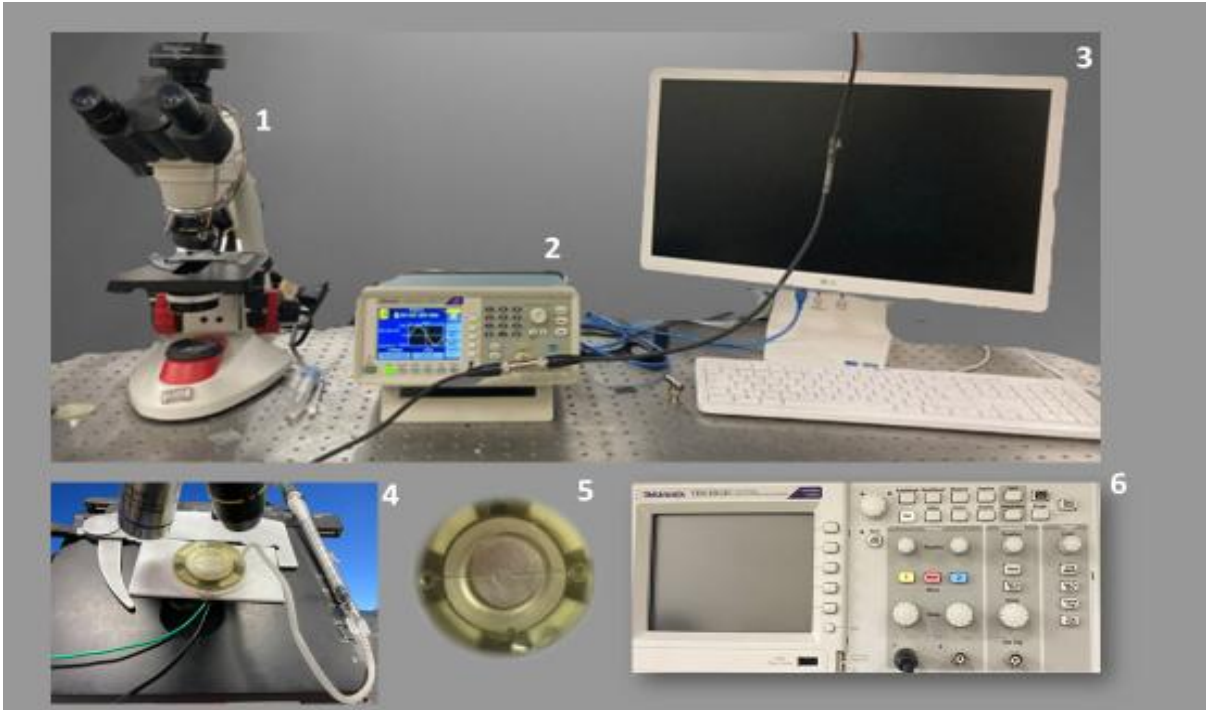
### 5.2.3 Instrumentação Eletrônica

O atuador piezocerâmico do dispositivo acusticofluídico, como demonstrado na figura 14 abaixo, é excitado com um sinal senoide produzido por um gerador de função (AFG1022, *Tektronix, Inc.*, EUA) e amplificado por um amplificador de potência RF (240L, *Electronics & Innovation, Ltd.*, EUA). Os sinais de condução são monitorados com um osciloscópio de dois canais (TDS 2012C, *Tektronix, Inc.*, EUA)

Também na Figura 14 a seguir é possível ver a seguinte ordem de materiais:

1. Microscópio óptico com câmera utilizado para a visualização das células no dispositivo;
2. Gerador de funções;
3. Computador para visualização e registro das imagens.
4. Seringa acoplada a um scalp para inserção do fluido no dispositivo;
5. Dispositivo acustofluídico;
6. Osciloscópio.

**Figura 14:** Instrumentos eletrônicos utilizados no experimento



Fonte: Silva, 2022.

## 6. RESULTADO E DISCUSSÃO

Em continuidade ao apresentado, serão detalhados os resultados e discussões da presente pesquisa, tomando como base o artigo derivado da tese.

### 6.1 Artigo derivado da tese



# 3D-Printed Acoustofluidic Devices for Raman Spectroscopy of Cells

Harrisson D. A. Santos,\* Amanda E. Silva, Giclélio C. Silva, Everton B. Lima, Alisson S. Marques, Magna S. Alexandre-Moreira, Aline C. Queiroz, Carlos Jacinto, J. Henrique Lopes, Uéslen Rocha,\* and Glauber T. Silva\*

Acoustofluidics technology can be used to trap live cells (and also micro/nanoparticles) in microenvironments suitable for cell assays. Herein, a cheap and easy-to-fabricate device is proposed that works with Raman spectroscopy for biosensing applications. The device comprises a 3D-printed microchamber working as a half-wavelength acoustic resonator. By tuning the resonance frequency with a low voltage ( $\approx 4$  V), cells or particles are aggregated and levitated in seconds by the action of the acoustic radiation force. Based on finite element simulations, the radiation force field produced inside the device is described. In the cellular enrichment (aggregation) process, a metastable honeycomb lattice is formed mostly due to the cell-to-cell attraction caused by the secondary acoustic radiation force. Orderly and metastable levitating aggregates provide an excellent arrangement for Raman spectroscopy to investigate cells individually. Polystyrene particles are used for the device characterization and Raman acquisition process. Biosensing applications are showcased with live murine macrophages J774.A1, which are used in infection assay of leishmaniasis disease. The unique features of the device, e.g., simple fabrication process with cheap materials, simple operation, fast time response, and formation of metastable cellular aggregates; hold a noteworthy potential for applications in life sciences and biotechnology involving cell assays.

torque)<sup>[6–10]</sup> generated by ultrasonic waves in microfluidic lab-on-a-chip devices. In a typical arrangement, microparticles or cells are injected into a small-volume resonant microchamber or microchannel of an acoustofluidic device (with a few microliters or less), and the acoustic radiation force aggregates them in a levitating state.<sup>[11,12]</sup> Most acoustofluidic devices are easily integrated into microscopy settings.<sup>[13]</sup> Moreover, it has been demonstrated that acoustically trapped cells have been kept alive for as long as seven days.<sup>[14]</sup> Compared with optical tweezer methods, which are also used for cell handling, acoustofluidics generally uses less power upon cells.<sup>[15]</sup>


Raman spectroscopy<sup>[16]</sup> is a label-free optical method that can determine the cell chemical structure, including proteins, lipids, and DNA assessed according to their molecular vibrational modes. There has been an increasing interest in Raman spectroscopy of live cells,<sup>[17]</sup> in part because it may allow observations of how cellular dynamics and metabolism change under the influence of an external agent (drug or substance).<sup>[18]</sup> Commonly, Raman signals obtained from seeded cells onto a substrate can be masked by information pertaining to the substrate's surface. The acoustic levitation of a sample under analysis can significantly reduce the background signal to the acquired spectrum. The unique features of the aforementioned acoustofluidics, e.g., a microenvironment for a

## 1. Introduction

Acoustofluidics harbors a collection of methods that are promoting a revolution in the manipulation, patterning, and analysis of cells and particles at the micro/nanoscale.<sup>[1–5]</sup> These methods use the mean acoustic fields (i.e., the acoustic radiation force and

H. D. A. Santos, A. E. Silva, G. C. Silva, E. B. Lima, A. S. Marques, U. Rocha, G. T. Silva  
 Physical Acoustics Group, Institute of Physics  
 Federal University of Alagoas  
 Maceió, Brazil  
 E-mail: harrisson2011@gmail.com; ueslen.silva@fis.ufal.br; gtomaz@fis.ufal.br

J. Henrique Lopes  
 Acoustics and Applications Group, Exact Sciences Nucleus  
 Federal University of Alagoas (Campus Arapiraca)  
 Arapiraca, Brazil

 The ORCID identification number(s) for the author(s) of this article can be found under <https://doi.org/10.1002/adem.202100552>.

DOI: 10.1002/adem.202100552

A. E. Silva, M. S. Alexandre-Moreira  
 Laboratory of Pharmacology and Immunology  
 Institute of Biological Sciences and Health  
 Federal University of Alagoas  
 Maceió, Brazil

A. C. Queiroz  
 Center of Medical Sciences and Nursing  
 Federal University of Alagoas  
 Campus Arapiraca, Maceió, Brazil

C. Jacinto, U. Rocha  
 Group of Nanophotonics and Images, Institute of Physics  
 Federal University of Alagoas  
 Maceió, Brazil

metastable aggregation and levitation of cells with low-power consumption, and easy integration with microscope setups, offer a pathway indeed to improve the Raman biosensing of live cells.

Acoustofluidics and Raman spectroscopy have worked hand in hand for revealing molecular information of microparticles suspended in liquid flows<sup>[19]</sup> and in suspensions.<sup>[20,21]</sup> Ultrasonic aggregation-induced enrichment with surface-enhanced Raman scattering (SERS) was introduced in an acoustofluidic device built with polydimethylsiloxane (PDMS) circular walls, a piezoelectric actuator, and a glass slide reflector.<sup>[22]</sup> The enhanced Raman was achieved via gold nanorods, which were used to enhance the detection of nucleic acids. Another acoustofluidic device, comprising a microchannel made with a double-sided adhesive tape glued on a quartz substrate, sealed with a glass slide reflector, and driven by a lithium-niobate actuator, was proposed for SERS real-time biosensing of live mycobacteria (*Mycobacterium smegmatis*) in the presence of isoniazid (antibiotic) for over eight hours.<sup>[23]</sup> A biosensor based on surface acoustic waves (SAWs) actuating on a functionalized glass capillary was developed to perform immunofluorescence and SERS of nanosized exosomes.<sup>[24]</sup> The detection of biomarkers such as miRNA molecules with fluorescence microscopy has also benefited from acoustofluidics. A microchip formed by four orthogonal ultrasonic actuators was developed to produce a 2D array where biomarkers were enriched and detected.<sup>[25]</sup> Acoustofluidics can also regulate the collective behavior of particles such as catalytic nanomotors, which holds promise for practical applications of biosensing.<sup>[26]</sup>

The acoustofluidics-assisted biosensing systems mentioned previously share the same attractive features for bioanalytical applications: simple operation and integration with sensing techniques and sample enrichment with minute acoustic forces in a sealed microenvironment for long-term monitoring. However, the cost and complexity to fabricate the referenced devices might be an obstacle for their widespread use, especially on the research of neglected tropical diseases in developing countries. Hence, an invaluable ingredient to be added to acoustofluidics-assisted Raman spectroscopy (in short, Raman acoustofluidics) is to have an easy fabrication process using cheap materials without compromising the aforementioned key functionalities.

The digital light processing (DLP) 3D printing method is emerging as a low-cost and easy-to-fabricate technique in microfluidics lab-on-a-chip technology.<sup>[27]</sup> In this work, we introduce a 3D-printed acoustofluidic device with the DLP technique using a liquid photopolymerizing resin to assist in Raman spectroscopy of cells. The device's fabrication cost is under 50 USD. The device has a cylindrical chamber of a 10  $\mu\text{l}$  volume sealed by a glass cover slide and a piezoelectric emitter that operates in a low-voltage regime ( $\approx 4$  V) at 1 MHz resonance frequency. Although 3D printing fabrication techniques have been discussed in the acoustofluidics context,<sup>[28]</sup> we provide for the first time a detailed description of the acoustic radiation force within 3D-printed chambers using finite element simulations. Using 10 and 30  $\mu\text{m}$  diameter polystyrene microparticles, we find the levitation plane at 285  $\mu\text{m}$  height, which is in good agreement with numerical predictions. We also explain the observed honeycomb aggregate formation using a scale analysis of the secondary radiation force.<sup>[29]</sup> A confocal microscope takes the Raman spectrum of single polystyrene particles with virtually no interference of the device parts. We also observed the ejection of 10  $\mu\text{m}$  particles

from the aggregate's periphery<sup>[30]</sup> as a result of the laser interaction.

As a proof of concept, we obtain the Raman spectrum of live murine macrophages J774.A1 without special preparations. These cells serve as a model for infection and drug discovery assays of *Leishmania amazonensis* that causes leishmaniasis disease.<sup>[31]</sup> The influence of acoustic microstreaming and temperature on metastable cell aggregates is discussed. Some aspects of cell viability such as morphology as well as safe operating of the Raman laser power are also addressed. The acquired Raman spectra are remarkably consistent with previously reported results obtained by standard Raman spectroscopy.<sup>[31]</sup> Hence, the proposed 3D-printed acoustofluidic chip is a reliable tool to assist the Raman monitoring of biological assays. Finally, the acoustofluidic device can be readily integrated to other microfluidic units (microchannels, valves, and pumps) into customized 3D-printed lab-on-a-chip platforms for applications in life sciences, clinical diagnosis, and biotechnology.

## 2. Experimental Section

### 2.1. Acoustofluidic Device Fabrication

The acoustic trapping of microparticles or cells was performed in a cylindrical acoustic chamber with a height of  $H = 750$   $\mu\text{m}$  and diameter of  $2R = 4$  mm. The chamber was cast inside a cylindrical disk, which was fabricated with a 3D printer (Moonray D75, Sprintray, Inc., USA) through the digital light-processing technique. A piezoceramic actuator (lead zirconate titanate, PZT-8) with a diameter of 25 mm was glued with epoxy (Huntsman Corp., USA) as the bottom of the resonant chamber. A glass cover slide of 150  $\mu\text{m}$  thickness was placed at the chamber's top, working as an acoustic reflector. In **Figure 1**, the acoustofluidic device is shown.

### 2.2. Raman Spectroscopy

The Raman measurements are conducted by a confocal Raman microscope (LabRam HR Evolution, Horiba, France). The microscope comprises a 0.65/40 $\times$  objective lens (series PLCN, Olympus Corp., Japan) and a 785 nm laser with power under 100 mW. The Raman backscattered signal is collected by the same lens and is dispersed by 300  $\text{gr mm}^{-1}$ . The system is calibrated using the silicon phonon band at 520  $\text{cm}^{-1}$  as reference. A notch filter smooths out the backscattered light from the undesirable elastic signal, e.g., the so-called Rayleigh scattering, which has the same wavelength as the excitation laser. The inelastically scattered light passes toward the detection system to form the Raman spectrum.

### 2.3. Electronic Instrumentation

The piezoceramic actuator of the acoustofluidic device was excited with a sinusoidal signal produced by a function generator (AFG1022, Tektronix Inc., USA) and amplified by an RF power amplifier (240L, Electronics & Innovation, Ltd., USA). The driving signals were monitored with a two-channel oscilloscope (TDS 2012C, Tektronix Inc., USA).

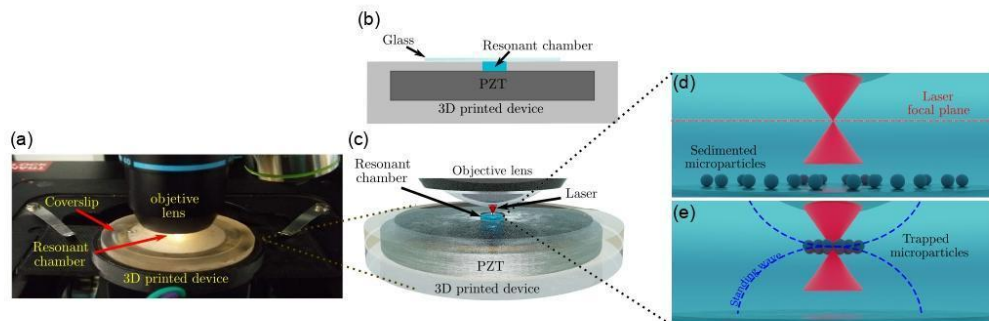


**Figure 1.** a) Photograph of the Raman-acoustofluidic integrated system comprising a cylindrical acoustic chamber and a confocal Raman apparatus. b) Transverse cut of the device with the resonant chamber (40 mm diameter and 750  $\mu\text{m}$  height) in light blue. A piezoceramic actuator (PZT) and glass slide form the bottom and top of the chamber, respectively. c) Zoom-in illustration of the acoustofluidic device. d) Microparticles sedimented at the chamber bottom. The focused Raman laser is displayed as red cones. e) After switching on the device, the microparticles are trapped in the central area of the nodal pressure plane. The blue-dashed curve show the acoustic standing wave in the axial direction.

#### 2.4. Preparation of J774.A1 Murine Macrophages

The adherent-phenotype macrophage line J774.A1 was cultured in Dulbecco's Modified Eagle's Medium (DMEM, Merck KGaA, Germany) supplemented with 10% fetal bovine serum (FBS) at 37  $^{\circ}\text{C}$ , 95% humidity, and 5%  $\text{CO}_2$ . Cells were cultured to 90% confluence and later centrifuged at 1500 rpm for 5 min at 4  $^{\circ}\text{C}$  to separate dead cells from living cells. Subsequently, the living cells were counted using an optical microscope and a Neubauer's chamber.

### 3. Results and Discussion

#### 3.1. Raman-Acoustofluidics-Integrated Method

In Figure 1, we display the Raman-acoustofluidic system proposed for cell enrichment and enhancement of the Raman signal-to-background ratio. A photograph of the device mounted on the confocal Raman microscope is shown in panel (a). In panel (b), we show the acoustofluidic device's schematics. Ultrasonic waves at 1.056 MHz frequency are pumped into the resonant chamber by the piezoceramic actuator. Microparticles are expected to levitate in a pressure nodal plane of height  $h \approx \lambda_{ac}/2 = 325 \mu\text{m}$ . The acoustic levitation plane should match the confocal plane of the objective lens. Hence, the Raman-acoustofluidic system should have a lens working distance satisfying

$$\text{WD} \geq \delta_{\text{ref}} + h \quad (1)$$

where  $\delta_{\text{ref}}$  is the thickness of the acoustic reflector. The working distance for our system reads  $\text{WD} \geq 475 \mu\text{m}$ . This gives us reasons to use a  $40\times$  objective lens, with numerical aperture  $\text{NA} = 0.65$  and working distance of  $600 \mu\text{m}$ , to focus the Raman laser on the levitation plane (see Figure 1).

#### 3.2. Acoustofluidic Fields

We assume the fluid inside the chamber is characterized by mass density  $\rho_0$  and adiabatic compressibility  $\beta_0$ . The piezoelectric vibrations at angular frequency  $\omega$  induce a harmonic acoustic pressure and fluid velocity whose spatial amplitude is denoted by  $p_{\text{ch}}$  and  $v_{\text{ch}}$ , respectively, where the subindex "ch" refers to the device's chamber. For applications in the Raman spectroscopy system, we seek for radially symmetric resonant modes. In so doing, we use Comsol Multiphysics Software (Comsol Inc., USA) to compute the acoustic fields numerically through the finite element method. The numerical model considers the device geometry and its material composition (fluid, viscoelastic and elastic solid, and piezoelectric parts) for the numerical simulations—see details in the Supporting Information. The pressure and fluid velocity are used in the next section to calculate the acoustic radiation force.

##### 3.2.1. Primary Acoustic Radiation Force

The acoustic radiation force exerted on microparticles and cells results from a change in the linear-momentum flux of an incident wave during the scattering process. In our approach, we assume that the radius of a microparticle, denoted by  $a$ , much smaller than the acoustic wavelength, e.g.,  $a \ll \lambda_{ac}$ . In this case, the primary radiation force is given as minus the gradient of a potential function<sup>[6,32]</sup>

$$\mathbf{F}^{\text{rad}} = -\nabla U^{\text{rad}} \quad (2)$$

$$U^{\text{rad}} = \frac{4\pi a^3}{3} \left( \frac{f_0}{2} \beta_0 |p_{\text{ch}}|^2 - \frac{3f_1}{4} \rho_0 |v_{\text{ch}}|^2 \right) \quad (3)$$

The coefficients  $f_0$  and  $f_1$  represent the compressibility and density contrast factors between the particle and surrounding liquid. The minimum of the radiation force potential  $U^{\text{rad}}$  at the chamber's center corresponds to the metastable acoustic trap.<sup>[33]</sup>

The computed pressure field inside the resonant chamber is used to calculate the acoustic radiation force exerted on a

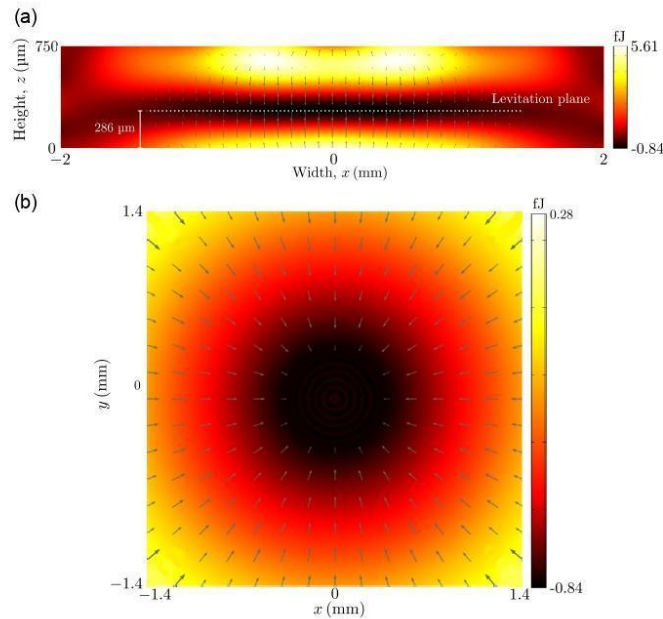


**Figure 2.** The finite element simulation of the acoustic radiation force field represented by gray arrows exerted on a 10  $\mu\text{m}$  polystyrene bead. The background images correspond to the radiation force potential. The device is simulated with a 1.19 MHz frequency and a peak-to-peak voltage of 3.8 V. a,b) The potential in the axial ( $xz$  plane) and levitation plane ( $xy$  plane) at  $h = 286 \mu\text{m}$ , respectively. In panel (a), the white dotted line shows the potential minimum position, which corresponds to the levitation plane.

10  $\mu\text{m}$  polystyrene bead (see details of the computational simulations in the Supporting Information). The acoustofluidic device is simulated with a frequency of 1.19 MHz and a 3.8 V peak-to-peak voltage. In **Figure 2**, the radiation force potential is shown with the origin of the coordinate system set in the principal chamber axis at the bottom. Panel (a) shows the axial plane's radiation force potential ( $xz$  plane), whereas panel (b) shows the same as (a) but in the levitation plane ( $xy$  plane). The gray arrows represent the radiation force vector field. In panel (a), the potential minimum is shown in the white dotted line, which corresponds to the levitation plane at  $h = 286 \mu\text{m}$ . This is in good agreement with the experimentally measured height  $h = 285 \pm (15) \mu\text{m}$  at a frequency of 1.056 MHz. Note that the frequencies in the experiment and simulation are apart by 0.037 MHz. The radiation force action will make particles aggregate in the central portion of the chamber.

The estimation of the ultrasonic wave's pressure amplitude inside the chamber is important in the cell viability analysis.<sup>[13]</sup> To perform this task, we use the gravity–radiation force balance method presented for a particle in a standing plane wave.<sup>[11]</sup> Considering a 10  $\mu\text{m}$  polystyrene bead in water at room temperature with a 1.056 MHz frequency and 3.8 V<sub>pp</sub> voltage, we have the following model parameters  $a = 5 \mu\text{m}$ ,  $f_0 = 0.31$ ,  $f_1 = 0.03$ ,  $\rho_0 = 998 \text{ kg m}^{-3}$ , and  $c_0 = 1493 \text{ ms}^{-1}$ . Hence, the experimental pressure amplitude is about  $p_0 = 50 \text{ kPa}$ , with a stored acoustic energy density of  $E_0 = 0.55 \text{ J m}^{-3}$ .

### 3.2.2. Secondary Acoustic Radiation Force

When two or more microparticles in the nodal plane are in close proximity, the *secondary* radiation force (also known as the acoustic interaction force) arises on the microparticles due to rescattering events.<sup>[29,34]</sup> Consider a pair of identical trapped particles, namely, particle 1 and 2, with interparticle distance  $d$ . Say particle 1 scatters the incoming wave, with the scattered wave's fluid velocity  $\mathbf{v}_{sc}$  being given regarding the reference frame in particle 1. The acoustic interaction force on particle 2 is<sup>[29]</sup>

$$\mathbf{F}^{\text{int}} = -\nabla_{\perp} U^{\text{int}} \quad (4)$$

$$U^{\text{int}} = -\pi a^3 f_1 \rho_0 \text{Re}[\mathbf{v}_{ch}^* \cdot \mathbf{v}_{sc}] \quad (5)$$

where  $\nabla_{\perp}$  is the transverse gradient, “Re” means the real part of a complex function, and the dot denotes the scalar product.

As indicated by Equation (2b) and (3b), both radiation force potentials  $U^{\text{rad}}$  and  $U^{\text{int}}$  rely upon the particle sizes; so do the related force amplitudes. Nonetheless, the aggregate position, which corresponds to the minimum of  $U^{\text{rad}}$ , depends on the pressure and velocity fields inside the microcavity. These fields are not influenced by particles as long as the aggregate's volume is small, contrasted to the microchamber's volume.

In the levitation plane, we expect the acoustic interaction force to be a central force; i.e., the interaction potential  $U^{\text{int}}$  depends on the interparticle distance. To estimate the acoustic interaction force, we first notice that the nearfield scattered-wave velocity is proportional to<sup>[35]</sup>  $v_{\text{sc}} \sim a^3 f_1 v_{\text{ch}}/r^3$ , with  $r$  being the distance from the center of particle 2 to the observation point. Hence, the nearfield interaction potential reads  $U^{\text{int}} \sim -\pi a^6 f_1^2 \rho_0 |v_{\text{ch}}|^2/r^3$ . Moreover, the only transverse variations of the acoustic fields are of the order of the chamber radius  $R$ ; then  $\nabla_{\perp} |v_{\text{ch}}|^2 \sim |v_{\text{ch}}|^2/R$ . Therefore, we estimate the acoustic interaction force as  $F^{\text{int}} = |\nabla_{\perp} U^{\text{int}}|_{r=d} \sim \pi a^6 f_1^2 \rho_0 |v_{\text{ch}}|^2/d^4$ .

To compare the interaction force with the primary radiation force (in the nodal plane), we use Equation (2) to obtain the ratio

$$\frac{F^{\text{int}}}{F_{\text{rad}}} \sim \frac{a^3 R f_1}{d^4} \quad (6)$$

For two 10  $\mu\text{m}$  diameter polystyrene particles in water, this ratio is 0.75, with  $d = 2a$ . We see that in close proximity, the primary and secondary radiation forces are about the same order of magnitude. It is important to fully determine the secondary radiation force in the levitation plane as it provides us with a basic understanding of microparticle close-packing arrangements. However, the aforesaid analysis is beyond the scope of this study.

### 3.2.3. Acoustic Microstreaming

In addition to transverse radiation forces in the levitation plane, acoustic microstreaming exerts a drag on aggregated particles, causing their in-plane movement.<sup>[36]</sup> Nonetheless, Raman spectroscopy should be performed on a standstill particle for as long as the acquisition process requires. Microstreaming can then be a show-stopper of the Raman acoustofluidics as a tool for selectively monitoring single cells. Particles with a diameter smaller than 15  $\mu\text{m}$  are more prone to microstreaming effects.<sup>[37]</sup> A possible route to suppress acoustic microstreaming is to develop shape-optimized chambers.<sup>[38]</sup> Furthermore, the method selectivity may benefit from patterned particles in the one-cell-per-trap configuration.<sup>[5,39]</sup>

## 3.3. Raman-Acoustofluidics Case Studies

### 3.3.1. Polystyrene Particles

Our first experiment using the Raman-acoustofluidic settings was performed with monodispersed polystyrene beads immersed in distilled water. Here, the acoustofluidic device operates with 1.056 MHz and a low peak-to-peak voltage of  $V_{\text{pp}} = 3.8\text{V}$ .

In Figure 3, we show the micrographs of aggregated polystyrene beads in the device chamber. Panels (a)–(d) show 10  $\mu\text{m}$  diameter beads, whereas panels (e)–(h) show 30  $\mu\text{m}$  diameter particles. The particle concentration ranges from  $C = 50$  to 900 particles  $\mu\text{L}^{-1}$ , with a  $20\times$  and  $40\times$  objective lens (see Figure S1 and S2, Supporting Information). The microparticles are trapped in a single layer in less than 1 min after switching on the device. The aggregation efficiency is defined as the ratio between the number of particles  $N$  counted in the central area of the levitation plane and the particle concentration  $C$  times the chamber's volume  $V_{\text{ch}}$ .

$$\varepsilon = \frac{N}{CV_{\text{ch}}} \quad (7)$$

Clearly,  $\varepsilon = 1$  means all diluted particles are trapped in the levitation plane. Based on the number of particles seen in panels (b) and (f), the efficiencies are  $\varepsilon_{10} = 0.28$  and  $\varepsilon_{30} = 0.40$ , for the 10 and 30  $\mu\text{m}$  particles, respectively. The efficiency  $\varepsilon_{30}$  is larger because the primary radiation force is proportional to the particle cross-section area.

Regarding the close-packed arrangement seen in Figure 3, we note that the aggregations form a hexagonal lattice. This geometrical arrangement has been noticed in other acoustic resonant chambers.<sup>[2,40,41]</sup> Computer simulations considering rigid particles demonstrate that a central force leads to hexagonal lattice packing.<sup>[42]</sup> A possible central force in the levitation plane is the interparticle secondary radiation force. As the observed aggregates remain stable for at least a few hours, we could selectively complete Raman acquisitions of any particle in the bead ensemble. With small particle concentrations ( $C < 50$  particles  $\mu\text{L}^{-1}$ ), we observed displacements of a few tens of micrometers of the 10  $\mu\text{m}$  bead aggregate due to acoustic microstreaming. Aggregates with larger beads remained at standstill. Furthermore, we note that the Raman laser could eject peripheral particles out of an aggregate. Indeed the acoustic trap breakup by light has been experimentally observed.<sup>[30]</sup> We found that the particle-ejection effect by light is more likely on 10  $\mu\text{m}$  beads with laser intensities greater than 5 mW.

In Figure 4, we show the average Raman spectrum out of ten measurements of a levitating (a) 10  $\mu\text{m}$  and (c) 30  $\mu\text{m}$  diameter bead. The Raman laser acted on a single bead with 2 mW power. In all measurements, the exposure time is 30 s, without accumulations. The blue line in panels (a) and (c) show the spectrum taken at a particle in the levitation plane (referenced as  $z = 0$  in depth). The obtained spectra are very alike and compatible with previously reported results,<sup>[43]</sup> although there is a small band around 1320  $\text{cm}^{-1}$  found to be assigned to the glass slide used to seal the microfluidic device. In contrast, the red line corresponds to the spectrum at  $z = -80\ \mu\text{m}$  (underneath the levitation plane). As no particle is trapped at this height, the Raman signal polystyrene is almost negligible. To further investigate the single-particle spectrum in depth, we laser scanned along the axial line from  $-60$  to  $60\ \mu\text{m}$ . Then we took the average Raman intensity around 1000  $\text{cm}^{-1}$  (e.g., the Raman signal is numerically integrated into a narrow interval around the peak intensity at 1000  $\text{cm}^{-1}$ ). After fitting the obtained data with a Gaussian curve, we estimate the full width at half maximum (FWHM) for the particles as FWHM = 15  $\mu\text{m}$  (10  $\mu\text{m}$  diameter) and FWHM = 33  $\mu\text{m}$  (30  $\mu\text{m}$  diameter). This result is consistent with focusing the Raman laser within a single particle, albeit a deviation in diameter of the smaller particle is noted. We may attribute this discrepancy to a laser depth close to 2.0  $\mu\text{m}$  and variations in the particle's size distribution. This result reasonably supports that a single layer of beads is formed at the levitation plane, even considering higher concentrations in the range of  $C = 50$ –900 particles  $\mu\text{L}^{-1}$  (see Figure S3, Supporting Information). For concentrations such as  $C \geq 50$ –900 particles  $\mu\text{L}^{-1}$ , the FWHM broadens due to the formation of other microparticle layers underneath the levitation plane (see Figure S4, Supporting Information).

Another aspect of the Raman-acoustofluidic platform concerns the signal-to-background ratio (SBR) defined as

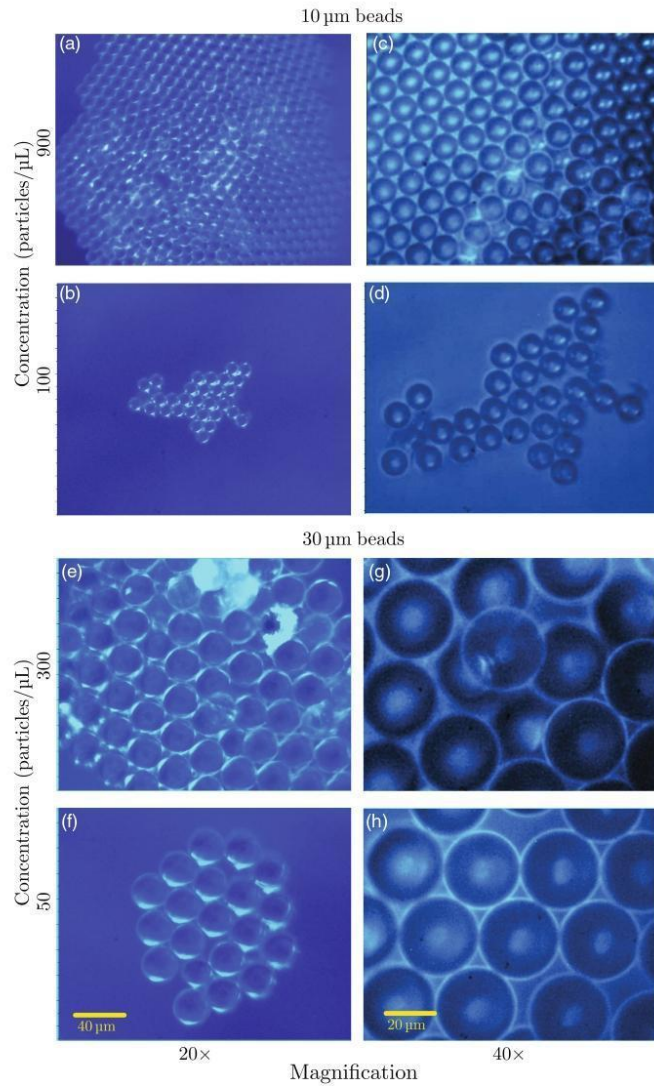


**Figure 3.** Micrographs of monodispersed polystyrene beads immersed in distilled water in the acoustofluidic device: a–d) 10 μm diameter beads; e–h) 30 μm diameter beads. The microparticles are trapped at 280 μm height in the center of the resonant chamber. The device operates at 1.056 MHz with a voltage amplitude of 3.8 V. Different concentrations are shown versus optical magnification.

$$SBR = 10 \log \left| 1 - \frac{\langle I_R \rangle}{\langle I_B \rangle} \right| \quad (8)$$

where  $\langle I_R \rangle$  and  $\langle I_B \rangle$  are the integrated Raman intensity over the acquisition bandwidth of a sample and background (sample is

absent), respectively. We want to determine the SBR considering 30 μm diameter particles in two distinct configurations as shown in **Figure 5**. In panel (a), we show the Raman spectrum of an acoustically trapped particle in the device (blue solid line), and the spectrum a particle sandwiched between a silicon (Si) wafer

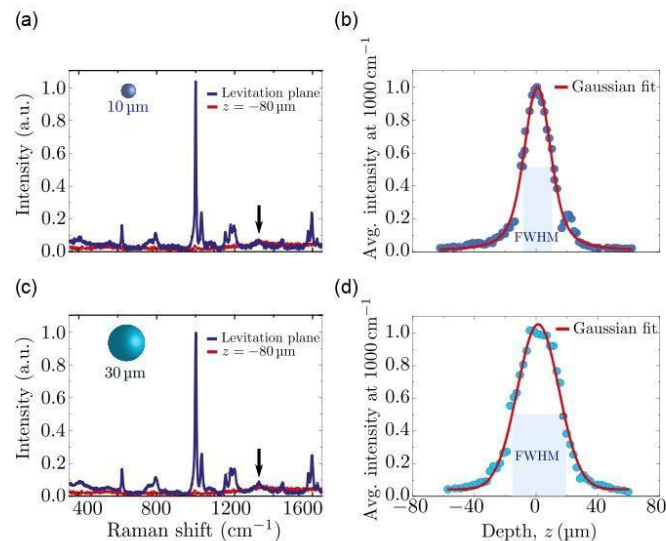


**Figure 4.** The average Raman spectrum of a) a 10  $\mu\text{m}$  and c) 30  $\mu\text{m}$  diameter polystyrene particle at different depths  $z = 0$  (levitation plane) and  $z = -80 \mu\text{m}$  inside the resonant chamber. No baseline correction was applied to the spectra. The polystyrene particles were dispersed in distilled water with concentrations of  $C = 50$  and  $100 \text{ particles } \mu\text{L}^{-1}$  for sizes of 10 and 30  $\mu\text{m}$ , respectively. In both cases, the Raman spectrum is taken by a 785 nm excitation laser of 2 mW power with 30 s acquisition time. The average value around the  $100 \text{ cm}^{-1}$  peak is used to assess the Raman signal axial broadening, as shown in panels (b) and (d). During the acquisition, the axial scan step size was 2  $\mu\text{m}$ . The FWHM is (b) 15  $\mu\text{m}$  and (d) 33  $\mu\text{m}$ , with the red line showing a Gaussian fit of the measured data.

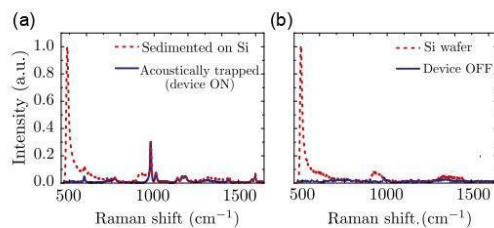


**Figure 5.** The average Raman spectrum is shown for a 30  $\mu\text{m}$  diameter polystyrene bead in two experimental settings, namely, particles sandwiched between a silicon (Si) wafer at the bottom and a glass slide at the top (red dotted lines), and particles in the acoustofluidic device (blue solid lines). a) In the sandwiched configuration, the particles are sedimented on the silicon wafer, whereas in the device the particles are trapped at  $h = 286 \mu\text{m}$ . b) The background Raman signal (without focusing on a particle) of the Si wafer and in the switched-off device. The signal-to-background ratios of the sandwiched and acoustofluidic device are, respectively,  $SBR = 32 \pm 1.5 \text{ dB}$  and  $SBR = 3.0 \pm 0.1 \text{ dB}$ .

and a glass slide (red dotted line). The glass slide is the same used to seal the device. We then take the spectra of the background on the Si wafer and in the device switched off. A remarkable difference in the results of the two acquisition methods is noted. In the sandwiched setup, a very large peak at  $520 \text{ cm}^{-1}$  is noted, which corresponds to the Si wafer. Outstanding discrepancies are seen

in the  $500\text{--}775$ ,  $915\text{--}990$ , and  $1275\text{--}1430 \text{ cm}^{-1}$  bands. The glass slide peak at  $1320 \text{ cm}^{-1}$  is barely noticed in both settings. The SBR of the device and that of the sandwiched apparatus are  $32 \pm 1.5$  and  $3.2 \pm 0.1 \text{ dB}$ , respectively. About 30 dB improvement is brought in by the acoustofluidic method.

### 3.3.2. Murine Macrophages J774.A1

Let us now present our results considering biological cells. We have conducted experiments on macrophages of mice (cell line J774.A1), with an averaged diameter of 20  $\mu\text{m}$ . These cells have been chosen as they are commonly used in infection assays of *L. Amazonensis* with the purpose of new drug discovery for leishmaniasis treatment.<sup>[31]</sup> The cells were immersed in phosphate buffer saline (PBS) solution and injected in the resonant chamber. The acoustic trapping protocol was the same as that used for polystyrene beads. As the Raman scattering efficiency of biological cells is much smaller than that of inorganic compounds,<sup>[44,45]</sup> we had to increase the laser power from 2 to 75 mW. Also, a longer acquisition time of 1 min with an average of 40 accumulations was required to obtain the cellular spectrum. The obtained Raman spectrum is the population average over five measurements taken on different cells. Here no cell ejection by light interaction was observed.

Raman acoustofluidics may induce collateral damage due to laser (photodamage) and acoustic interaction with cells, as

well as temperature rise and acoustic cavitation. We have not observed photodamage in the probed cell after the Raman acquisition. In fact, photodamage may not occur for a laser power as high as 115 mW for nearly 1 h of cell exposure to light.<sup>[46]</sup> Temperature rise may be caused by ultrasonic absorption in the liquid and biosample, heat losses in the piezoelectric actuator, and in thin glue layers used to bond different device parts.<sup>[36]</sup> We have measured the overall chamber temperature with an infrared thermographic camera (E40bx, FLIR Systems, USA) with thermal sensitivity of 0.045 °C in the -20 to 120 °C range. At voltages as low as 8 V, the temperature variations remained under 1 °C over a few hours' measurement, as shown in Figure S5, Supporting Information. Nonetheless, the local temperature of the Raman-investigated cell was not measured. An approach based on luminescent nanothermometers, which provide intracellular temperature readings,<sup>[47–49]</sup> can be used for this task. Also, the ultrasonic effects on cellular viability and metabolic activity were not investigated. For reference, human dermal fibroblasts have good viability (above 80%) for a voltage range of 6–8 V and a time interval under 15 min, when conducted at room temperature.<sup>[50]</sup> Finally, a few words should be said about inertial cavitation that may provoke cell lysis and death. Inertial cavitation is caused by a large bubble oscillation over a few cycles ending in a violent bubble collapse. Because the cavitation threshold depends on the wave pressure amplitude, cavitation is less likely to take place in a pressure node. In addition, for a frequency of 1–10 MHz, the estimated pressure amplitude for cavitation is 0.1–1 MPa.<sup>[13]</sup> This is well above the estimated pressure amplitude inside the device chamber, e.g.,  $p_0 = 0.05$  MPa. Therefore, it is unlikely that inertial cavitation occurs in the levitation plane wherein cells are investigated.

In Figure 6a–c, we present trapped macrophages with a concentration of 50 cells  $\mu\text{L}^{-1}$  and the average macrophage spectrum at room temperature. The bright-field images show a collection of macrophages in the levitation plane after a Raman acquisition ( $\approx 40$  min). The observed macrophages are well packed in a stable configuration during the acquisition, without notable acoustic microstreaming effects. By visual inspection, we see the membrane integrity and cell morphology are good indicators of the cell preserved viability. In panel (c), we exhibit the experimentally measured Raman spectra (gray lines) for the acoustofluidic device “ON” and “OFF.” The red and blue lines correspond to the average over five measurements. We should mention that the polystyrene particle and cell aggregations were formed at the same height with a very similar geometrical arrangement (honeycomb array). This hints that their compressibility ( $f_0$ ) and density ( $f_1$ ) contrast factors should have the same sign to produce similar qualitative behavior.

The differences between the spectra are straightforward. Indeed, before turning on the device, no Raman signal from a cell could be detected. The more visible contributions are observed around 1320 and 1640  $\text{cm}^{-1}$ , probably assigned to the culture medium (PBS) and glass slide used to seal the device. The green line represents the average spectrum after subtracting the background signal. This Raman signature is in accordance with previously reported results (pink curve) for the fixed cell of the same line.<sup>[31]</sup> We observe that several peaks in both spectra are alike. The spectrum delivered by Raman acoustofluidics

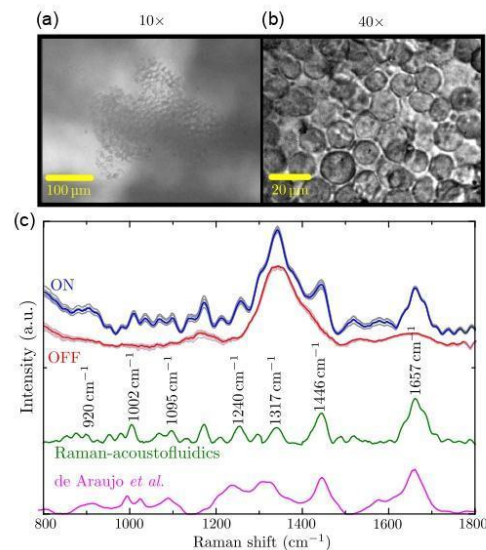


**Figure 6.** Bright-field images of macrophages in the levitation plane taken by a) a 10 $\times$  and b) a 40 $\times$  objective lens. The cell concentration is 50 cells  $\mu\text{L}^{-1}$ . c) The room-temperature Raman spectra (gray lines) of a single macrophage obtained with the 40 $\times$  objective lens. The red and blue curves correspond to the average spectrum with the device “OFF” and “ON,” respectively. The green curve is the averaged Raman spectrum after background subtraction. For comparison, the spectrum obtained from fixed macrophages is also shown (pink curve), which was adapted from Ref.<sup>[31]</sup>

shows prominent peaks in the 900–1400  $\text{cm}^{-1}$  band, which are smoothed out in the mentioned reference. According to Tfaily et al.,<sup>[51]</sup> some Raman bands are described as follows. The band around 1240  $\text{cm}^{-1}$  corresponds to random coil amide III, while at 1371  $\text{cm}^{-1}$ , the peak relates to  $\delta(\text{CH}_2)$  lipids, adenine, and cytosine in DNA/RNA. The peak around 1446  $\text{cm}^{-1}$  is associated with  $\delta(\text{CH})$  in lipids and proteins and is also attributed to cholesterol. The band at 1657  $\text{cm}^{-1}$  could be associated with the carbonyl stretching ( $\nu\text{C}=\text{O}$ ) in peptide bonds and  $\text{C}=\text{C}$  stretching in lipids.

#### 4. Conclusion

We have presented a detailed description of Raman spectroscopy of cells in a 3D-printed acoustofluidic device. The key aspects of the acoustofluidic system include particle aggregation and levitation in a metastable configuration, fast response, and low-power consumption with a slight temperature variation ( $\approx 1$  °C).

By controlling the concentration of polystyrene beads in the chamber, we observed the formation of a 2D hexagonal lattice, which appears to be caused by the secondary radiation force between neighbor particles. These results are achieved with an aggregation efficiency of 30–40%. At low voltages  $\approx 4$  V, the



acoustic microstreaming does not affect the trapping stability of any of the particle concentrations investigated. The obtained Raman spectrum of a single polystyrene bead in the device is in excellent agreement with previous observations.<sup>[4,3]</sup> As a proof of concept, we took the Raman spectrum at room temperature of live levitating macrophages. We obtained a good agreement with previously reported results based on Raman acquisition from fixed cells of the same line.<sup>[31]</sup>

Our study has expounded that the acoustofluidic-assisted Raman spectroscopy based on a cheap, easy-to-fabricate, and robust 3D-printed device can be a valuable technique for cell monitoring in biological assays. At last, the acoustofluidic device presented here can be incorporated as a unit into a 3D-printed microfluidic lab-on-a-chip system. Also, enhanced Raman spectroscopy methods such as SERS can be assisted by the acoustofluidic chip. These envisioned possibilities, along with the attractive features previously discussed to assist Raman spectroscopy, point out the proposed device can become a platform of widespread use in a variety of applications in life sciences, medical diagnostics, and biotechnology.

### Supporting Information

Supporting Information is available from the Wiley Online Library or from the author.

### Acknowledgements

The authors acknowledge the financial support from Brazilian agencies: Funding Authority for Studies and Projects-FINEP (grants INFRAPESQ-11 and INFRAPESQ-12), Council for Scientific and Technological Development-CNPq (grant numbers 439106/2018-4, 310412/2018-8, 431736/2018-9, 304967/2018-1, 308357/2019-1). H.D.A.S. thanks the Federal University of Alagoas for the postdoctoral scholarship.

### Conflict of Interest

The authors declare no conflict of interest.

### Data Availability Statement

Data available in article supplementary material The data that supports the findings of this study are available in the supplementary material of this article.

### Keywords

acoustofluidics, cell analysis, lab-on-a-chip, Raman spectroscopy

Received: May 7, 2021

Revised: July 28, 2021

Published online: August 19, 2021

- [1] M. Antfolk, T. Laurell, *Anal. Chim. Acta* **2017**, 965, 9.  
 [2] K. Olofsson, B. Hammarström, M. Wiklund, *Micromachines* **2018**, 9, 594.  
 [3] A. Ozcelik, J. Rufo, F. Guo, Y. Gu, P. Li, J. Lata, T. J. Huang, *Nat. Methods* **2018**, 15, 1021.

- [4] W. Connacher, N. Zhang, A. Huang, J. Mei, S. Zhang, T. Gopesh, J. Friend, *Lab Chip* **2018**, 18, 1952.  
 [5] G. T. Silva, J. H. Lopes, J. P. Leão-Neto, M. K. Nichols, B. W. Drinkwater, *Phys. Rev. Appl.* **2019**, 11, 054044.  
 [6] G. T. Silva, *J. Acoust. Soc. Am.* **2014**, 136, 2405.  
 [7] J. P. Leão-Neto, G. T. Silva, *Ultrasonics* **2016**, 71, 2177.  
 [8] J. P. Leão-Neto, J. H. Lopes, G. T. Silva, *J. Acoust. Soc. Am.* **2020**, 147, 1.  
 [9] M. Baudoin, J.-L. Thomas, *Annu. Rev. Fluid Mech.* **2020**, 52, 205.  
 [10] A. Vargas-Jiménez, M. Camacho, J. Muñoz, I. González, *Wave Motion* **2021**, 101, 102701.  
 [11] J. F. Spengler, M. Jekel, K. T. Christensen, R. J. Adrian, J. J. Hawkes, W. T. Coakley, *Bioseparation* **2001**, 9, 329.  
 [12] A. Lenshof, M. Evander, T. Laurell, J. Nilsson, *Lab Chip* **2012**, 12, 684.  
 [13] M. Wiklund, H. Brismar, B. Önfelt, *Lab on a Chip* **2012**, 12, 3221.  
 [14] A. E. Christakou, B. O. Mathias Ohlin, M. Wiklund, *Lab Chip* **2015**, 15, 3222.  
 [15] K. Dholakia, B. W. Drinkwater, M. Ritsch-Martel, *Nat. Rev. Phys.* **2020**, 2, 480.  
 [16] R. R. Jones, D. C. Hooper, L. Zhang, D. Wolverson, V. K. Valev, *Nanoscale Res. Lett.* **2019**, 14, 231.  
 [17] R. Smith, K. L. Wright, L. Ashton, *Analyst* **2016**, 141, 3590.  
 [18] D. Wang, P. He, Z. Wang, G. Li, N. Majed, A. Z. Gu, *Curr. Opin. Biotechnol.* **2020**, 64.  
 [19] M. J. Ruedas-Rama, A. Domínguez-Vidal, S. Radel, B. Lendl, *Anal. Chem.* **2007**, 79, 7853.  
 [20] S. Radel, J. Schnöller, A. Domínguez, B. Lendl, M. Gröschl, E. Benes, *Elektrotech. Inform.* **2008**, 125, 82.  
 [21] K. Wieland, S. Tauber, C. Gasser, L. A. Rettenbacher, L. Lux, S. Radel, B. Lendl, *Anal. Chem.* **2019**, 91, 14231.  
 [22] T. Xu, Y. Luo, C. Liu, X. Zhang, S. Wang, *Anal. Chem.* **2020**, 92, 7816.  
 [23] V. O. Baron, M. Chen, B. Hammarstrom, R. J. H. Hammond, P. Glynne-Jones, S. H. Gillespie, K. Dholakia, *Commun. Biol.* **2020**, 3, 236.  
 [24] N. Hao, Z. Pei, P. Liu, H. Bachman, T. D. Naquin, P. Zhang, J. Zhang, L. Shen, S. Yang, K. Yang, S. Zhao, T. J. Huang, *Small* **2020**, 16, e2005179.  
 [25] Q. Zhu, T. Xu, Y. Song, Y. Luo, L. Xu, X. Zhang, *Biosens. Bioelectron.* **2020**, 158, 112185.  
 [26] Q. Zhu, T. Xu, Y. Song, Y. Luo, L. Xu, X. Zhang, *J. Am. Chem. Soc.* **2015**, 137, 2163.  
 [27] A. V. Nielsen, M. J. Beauchamp, G. P. Nordin, A. T. Woolley, *Annu. Rev. Anal. Chem.* **2020**, 13, 45.  
 [28] E. Cesevski, A. P. Haring, Y. Tong, M. Singh, R. Thakur, S. Laheri, K. A. Read, M. D. Powell, K. J. Oestreich, B. N. Johnson, *Lab Chip* **2018**, 18, 2087.  
 [29] G. T. Silva, H. Bruus, *Phys. Rev. E* **2014**, 90, 063007.  
 [30] G. Dumy, M. Hoyos, J.-L. Aider, *J. Acous. Soc. Am.* **2019**, 146, 4557.  
 [31] M. V. Araújo, A. C. Queiroz, J. F. M. Silva, A. E. Silva, J. K. S. Silva, G. R. Silva, E. C. O. Silva, S. T. Souza, E. J. S. Fonseca, C. A. Camara, T. M. S. Silva, M. S. Alexandre-Moreira, *Analyst* **2019**, 144, 5232.  
 [32] H. Bruus, *Lab Chip* **2012**, 12, 1014.  
 [33] J. P. Leão-Neto, M. Hoyos, J.-L. Aider, G. T. Silva, *J. Acous. Soc. Am.* **2021**, 149, 285.  
 [34] J. H. Lopes, M. Azarpeyvand, G. T. Silva, *IEEE Trans. Ultrasonics Ferroelectrics Frequency Control* **2016**, 63, 186.  
 [35] A. D. Pierce, *Acoustics: An Introduction to Its Physical Principles and Applications*, 3rd ed., Springer, Cham **2019**.  
 [36] M. Wiklund, R. Green, M. Ohlin, *Lab Chip* **2012**, 12, 2438.  
 [37] J. F. Spengler, W. T. Coakley, K. T. Christensen, *AIChE J.* **2003**, 49, 2773.  
 [38] J. S. Bach, H. Bruus, *Phys. Rev. Lett.* **2020**, 124, 21.  
 [39] D. J. Collins, B. Morahan, J. Garcia-Bustos, C. Doerig, M. Plebanski, A. Neild, *Nat. Commun.* **2015**, 6, 8686.

- [40] D. Bazou, W. T. Coakley, K. M. Meek, M. Yang, D. T. Pham, *Colloids Surf., A* **2004**, *243*, 97.
- [41] D. Bazou, G. A. Foster, J. R. Ralphs, W. T. Coakley, *Mol. Membr. Biol.* **2005**, *22*, 229.
- [42] E. M. B. Campello, K. R. Cassares, *Latin Am. J. Solids Struct.* **2016**, *13*, 23.
- [43] W. M. Sears, J. L. Hunt, J. R. Stevens, *J. Chem. Phys.* **1981**, *75*, 1589.
- [44] N. Kuhar, S. Sil, T. Verma, S. Umapathy, *RSC Adv.* **2018**, *8*, 25888.
- [45] G. Puppels, *Exp. Cell Res.* **1991**, *195*, 361.
- [46] I. Notingher, S. Verrier, H. Romanska, A. E. Bishop, J. M. Polak, L. L. Hench, *Spectroscopy* **2002**, *16*, 43.
- [47] D. Jaque, F. Vetrone, *Nanoscale* **2012**, *4*, 4301.
- [48] C. Brites, A. Millán, L. Carlos, *Including Actinides*, Elsevier **2016**, pp. 339–427.
- [49] H. D. A. Santos, E. C. Ximendes, M. del Carmen Iglesias-de la Cruz, I. Chaves-Coira, B. del Rosal, C. Jacinto, L. Monge, I. Rubia-Rodríguez, D. Ortega, S. Mateos, J. GarcaSolé, D. Jaque, N. Fernández, *Adv. Funct. Mater.* **2018**, *28*, 1803924.
- [50] P. B. Victoria Levario-Diaz, M. C. Galan, A. C. Barnes, *Sci. Rep.* **2020**, *10*, 8493.
- [51] S. Tfaili, A. Al Assaad, N. Fournier, F. Allaoui, J.-L. Paul, P. Chaminade, A. Tfayli, *Talanta* **2019**, *199*, 54.

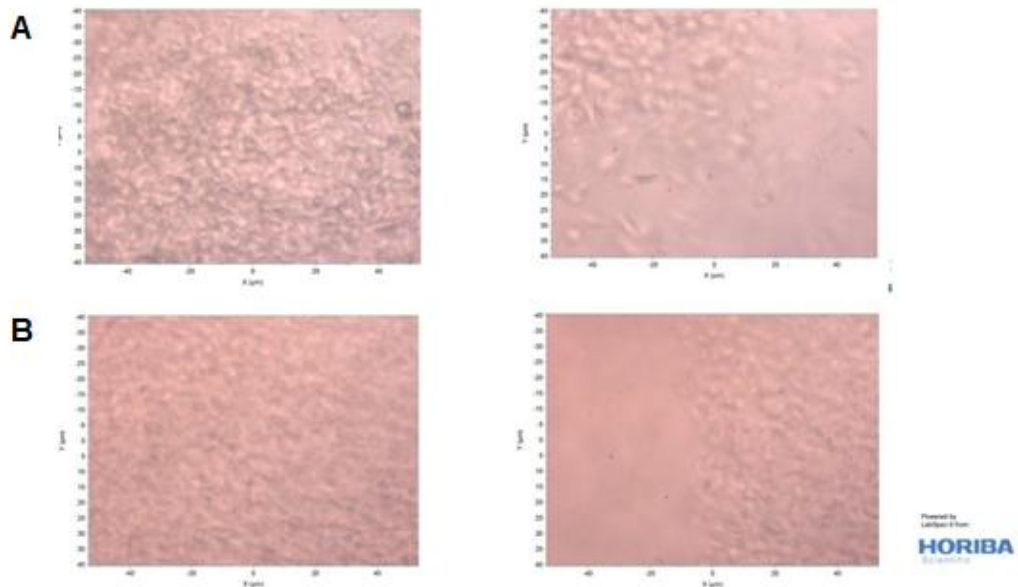
O artigo exposto apresenta resultados preliminares do desenvolvimento de um dispositivo de acustofluídica desenvolvido por membros do GAF do IF-UFAL, coordenado pelo professor Dr. Glauber T. Silva. Os resultados confirmam a capacidade do dispositivo em aprisionar células macrofágicas e de melhorar as informações oriundas das células através da espectrometria de massas obtida por RAMAN.

Neste trabalho, foi demonstrado o uso de métodos de nanoscopia e nanotermometria integrados em dispositivos de micro-acusticofluídica para monitoramento de eventos em ensaios celulares. Esta técnica permite a investigação de uma célula isolada ou um aglomerado de células que serão acusticamente armadilhadas e levitadas em uma cavidade (biorreator) com dimensões da ordem de alguns milímetros. Através das análises de nanotermometria, pode-se extrair informações sobre reações enzimáticas, taxa de divisão celular, propriedades mecânicas da membrana celular, e processos fundamentais, como distinção entre células cancerosas e saudáveis, dentre outras.

A investigação dessas propriedades foi realizada através de nanosensores fluorescentes multifuncionais capazes de realizar imagens e sensoriamento termo-óptico simultaneamente. Além disso, é de fundamental importância que as bandas de emissão e absorção destes nanosensores fluorescentes operem nas janelas biológicas (regiões espectrais onde as células são parcialmente transparentes, devido a uma baixa absorção e espalhamento da luz incidente e emitida).

Após a execução dos experimentos preliminares, procedeu-se com a investigação da aplicação da acustofluídica e nano-termometria como inovação tecnológica para o estudo das leishmanioses, utilizando o dispositivo para o aprisionamento dos macrófagos e dos parasitos. Para isto, promastigotas de *L. amazonensis* (agente etiológico da leishmaniose tegumentar) e *L. chagasi* (agente etiológico da leishmaniose visceral) foram submetidas à frequência de ondas de ultrassom de 3.319 MHz e tensão pk-pk menor que 5 volts, dentro do dispositivo. Observa-se na figura 15 o aprisionamento de promastigotas das espécies de *L. amazonensis* e *L. chagasi*, que se mantiveram estáticas durante o experimento.

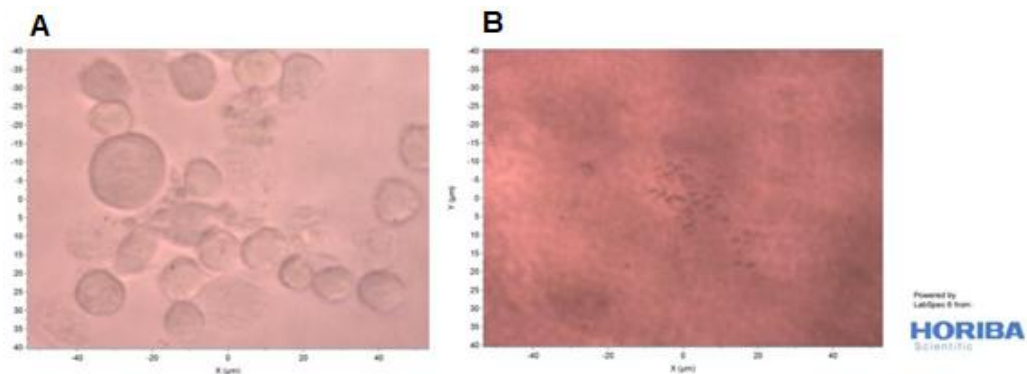
**Figura 15:** Promastigotas de *L. amazonensis* (A) e *L. chagasi* (B), estáticas durante o aprisionamento, no aumento de 40x



Fonte: Silva, 2022.

Para demonstrar a capacidade do dispositivo acustofluídico em aprisionar formas amastigotas de *Leishmania*, macrófagos J774.A1 foram infectados com promastigotas de com *L. amazonensis* (Figura 16). O resultado da análise foi promissor, demonstrando que através da acustofluídica o dispositivo apresenta a capacidade de aprisionar não somente células saudias como também células infectadas, as quais são os alvos de testes de diagnóstico.

**Figura 16:** Macrófagos infectados com *L. amazonensis*, estáticos durante o aprisionamento, nos aumentos de 40x (A) e 10x (B).



Fonte: Silva, 2022.

No trabalho descrito por Xie *et al.* (2020), os autores demonstram a separação de células por acustofluídica, baseando-se na densidade e compressibilidade, independentemente de seus tamanhos e manipulando as propriedades acústicas em meio fluídico. A separação foi realizada devido a variação das dimensões dos canais microfluídicos, os comprimentos de onda dos sinais acústicos e as propriedades do meio fluido. O método foi aplicado para separar células Hela selvagens e tratadas com paraformaldeído com base nas diferenças das propriedades mecânicas; foi alcançada uma taxa de recuperação de 85% para células fixadas. Também foi aplicado para separar glóbulos vermelhos (RBCs) e glóbulos brancos (WBCs) que têm densidades diferentes. Assim sendo, conforme os autores supracitados, uma taxa de recuperação de 80,5% para WBCs foi alcançada.

Cardoso *et al.* (2009) desenvolveram um dispositivo acustofluídico para medir ácido úrico em saliva humana, o qual foi baseado em medições espectrofotométricas ópticas e em fluxo acústico, que potencializa a reação dos fluidos devido ao aquecimento e agitação. A transmissão acústica foi fornecida por um piezoelétrico de  $\beta$ -PVDF depositado sob a matriz microfluídica do dispositivo. Além disso, um dispositivo eletrônico foi utilizado para a detecção, leitura, processamento de dados e atuação de sinal. Segundo os autores acima mencionados, os resultados experimentais comprovaram que a transmissão acústica baseada neste polímero piezoelétrico é vantajosa e reduz em 55% o tempo necessário para a obtenção dos resultados das análises.

Por sua vez, no trabalho de Papadakis *et al.* (2019) foi possível desenvolver um método e plataforma para detecção de ácidos nucleicos portátil utilizando ondas fluídicas como ferramenta. A amplificação do DNA da *Salmonella* foi realizada em três amostras biológicas, swab nasal, sangue total e saliva. Como apontam os autores abordados acima, a simplicidade do método combinada com a operação e detecção do smartphone, o rápido tempo de análise amostra-resposta (30 min) e alto desempenho em três das amostras humanas mais importantes em diagnóstico, sugerem que a metodologia poderia se tornar uma ferramenta móvel de escolha para detecção de ácidos nucleicos.

## 7. CONCLUSÃO

O presente estudo confirma a robustez dos métodos acustofluídicos como uma plataforma capaz de armadilhar células macrofágicas da linhagem J774.A1, promastigotas de *Leishmania amazonensis* e *Leishmania chagasi*, e também células J774.A1 infectadas com amastigotas de *L. amazonensis*, as quais são alvos de testes de diagnóstico. Também comprovou-se que o dispositivo acustofluídico desenvolvido pelo grupo de pesquisa foi capaz de armadilhar macrófagos da linhagem J774.A1 para bio-Raman espectroscopia, como demonstrado no artigo derivado desta tese, intitulado, “*3D-Printed Acoustofluidic Devices for Raman Spectroscopy of Cells*”. A tese desenvolvida pode facilitar e aperfeiçoar o diagnóstico das leishmanioses, utilizando amostras biológicas menos invasivas.

O trabalho apresentado ressalta um caráter inovador, bem como a interdisciplinaridade, envolvendo profissionais de áreas diversas, como engenheiros, físicos, farmacêuticos, biólogos, entre outros. Além disso, a tese descrita está correlacionada com o projeto do PPSUS (Programa de Pesquisa para o SUS), coordenado pela professora Dra. Aline Cavalcanti de Queiroz, intitulado, Desenvolvimento de um novo método de diagnóstico para as leishmanioses utilizando acustofluídica - Fase 1 - Processo nº E:60030.0000000194/2021, aprovado no Programa de pesquisa para o SUS/Chamada FAPEAL Nº 06/2020 – PPSUS.

Mais recentemente a autora da tese, junto com colaboradores liderados pelo Me. Giclênio Cavalcante concorreram ao edital do Catalisa ICT do SEBRAE e foram aprovados. A proposta é projetar e desenvolver dispositivos com a tecnologia acustofluídica de baixo custo para aplicações às ciências da vida e biotecnologia. Utilizaremos impressão 3D para prototipagem em resina e termoplásticos, e técnicas industriais de réplica como moldagem por injeção e *hot embossing*, uma vez que o uso de métodos de fabricação industrial visa a escalabilidade de nossos produtos.

Além disso, a tese consta com a exposição de quatro artigos demonstrados no “Material Suplementar”, onde a autora participou de outros projetos acadêmicos durante o seu doutoramento, contribuindo para a sua formação e outros alunos de

pós-graduação e graduação do LaFI, coordenado pela professora Dra. Magna Suzana Alexandre Moreira.

## **8. MATERIAL SUPLEMENTAR**

**Artigos desenvolvidos durante o doutorado em colaboração:**



Contents lists available at ScienceDirect

Journal of Inorganic Biochemistry

journal homepage: [www.elsevier.com/locate/jinorgbio](http://www.elsevier.com/locate/jinorgbio)

## Synthesis and evaluation of the antibiotic and adjuvant antibiotic potential of organotin(IV) derivatives



Ana Soraya Lima Barbosa<sup>a</sup>, Jéssica de Siqueira Guedes<sup>a</sup>, Douglas Rozendo da Silva<sup>a</sup>, Simoni Margareti Plentz Meneghetti<sup>a</sup>, Mario Roberto Meneghetti<sup>a,\*</sup>, Amanda Evelyn da Silva<sup>b</sup>, Morgana Vital de Araujo<sup>b</sup>, Magna Suzana Alexandre-Moreira<sup>b</sup>, Thiago Mendonça de Aquino<sup>a,c</sup>, José Pinto de Siqueira Junior<sup>d</sup>, Rodrigo Santos Aquino de Araújo<sup>e</sup>, Ryldene Marques Duarte da Cruz<sup>f</sup>, Francisco Jaime Bezerra Mendonça-Junior<sup>e,f,\*\*</sup>

<sup>a</sup> Group of Catalysis and Chemical Reactivity, Institute of Chemistry and Biotechnology, Federal University of Alagoas, 57072-970 Maceió, AL, Brazil

<sup>b</sup> Laboratory of Pharmacology and Immunity, Institute of Biological Sciences and Health, Federal University of Alagoas, 57020-720 Maceió, AL, Brazil

<sup>c</sup> Nucleus of Analysis and Research in Nuclear Magnetic Resonance - NAPRMN, Institute of Chemistry and Biotechnology, Federal University of Alagoas, 57020-720 Maceió, AL, Brazil

<sup>d</sup> Laboratory of Genetics of Microorganism, Federal University of Paraíba, 58051-900 João Pessoa, PB, Brazil

<sup>e</sup> Laboratory of Synthesis and Drug Delivery, Biological Science Department, State University of Paraíba, 58071-160 João Pessoa, PB, Brazil

<sup>f</sup> Graduate Program in Natural and Synthetic Bioactive Products, Federal University of Paraíba, 58071-160 João Pessoa, PB, Brazil

### ARTICLE INFO

#### Keywords:

Organotin compounds  
*Staphylococcus aureus*  
 Antibiotic activity  
 Adjuvant antibiotic activity  
 Efflux pump inhibitors  
 Cytotoxicity

### ABSTRACT

A series of organotin(IV) derivatives was investigated *in vitro* for their antibiotic and adjuvant antibiotic properties (efflux pump inhibitors) against *Staphylococcus aureus* strains that overexpress efflux pump proteins for norfloxacin (SA-1199B), erythromycin (RN-4220) and tetracycline (IS-58). Most organotin(IV) compounds showed significant antibacterial activity with small Minimum Inhibitory Concentration (MIC) values, some of which were close to 1.0 µg/mL (3.1 µM), but this feature was also associated with substantial cytotoxicity. Nevertheless, the cytotoxicity of these organotin(IV) compounds can be overcome when they are used as antibiotic adjuvants. Their remarkable adjuvant antibiotic properties allow potentiation of the action of tetracycline (against IS-58 strain) by up to 128-fold. This likely indicates that they can act as putative inhibitors of bacterial efflux pumps. These results reinforce organotin(IV) complexes as promising antibacterial agents, and many of these complexes, if associated with antibiotics, can act as potential adjuvant antibiotic candidates.

### 1. Introduction

The increasing incidence of bacterial resistance in clinical practice has become a significant public health problem since resistance is not restricted to a specific antibiotic, but affects many drugs. According to the report published in 2013 by the Center for Disease Control and Prevention of the USA, every year, in the United States, > 2 million people are infected by resistant bacteria, of which at least 23,000 are killed by these infections, due to the ineffectiveness of the antibiotics available in the clinic. “Superbugs” (organisms that are resistant to most antibiotics used clinically) are emerging at a fast pace. In particular, *Staphylococcus aureus* is responsible for many cases of infection each year [1,2].

Indeed, *S. aureus* is a major cause of hospital-acquired infections and lower respiratory tract infections. In addition, it is the second major cause of nosocomial pneumonia bacteremia and cardiovascular infections [3]. Infections caused by this microorganism are particularly difficult to treat due to the evolution of resistance to antimicrobial drugs [4].

The inefficiency of the antibacterial agents used, which have a high therapeutic limitation of systemic infections, high risk of toxicity, and bacterial inefficiency, as well as the emergence of resistant bacterial strains [5], combines with the increasing indiscriminate use of these drugs, leading to selective pressure, which is responsible for the development of or increase in resistant pathogenic bacteria [6].

Of the main mechanisms of bacterial resistance, efflux pumps,

\* Corresponding author.

\*\* Correspondence to: F.J.B. Mendonça-Junior, Laboratory of Synthesis and Drug Delivery, Biological Science Department, State University of Paraíba, 58071-160 João Pessoa, PB, Brazil.

E-mail addresses: [nrm@qui.ufal.br](mailto:nrm@qui.ufal.br) (M.R. Meneghetti), [franciscojaime@ccbsa.uepb.edu.br](mailto:franciscojaime@ccbsa.uepb.edu.br) (F.J.B. Mendonça-Junior).

<https://doi.org/10.1016/j.jinorgbio.2017.12.004>

Received 23 August 2017; Received in revised form 4 December 2017; Accepted 5 December 2017

Available online 08 December 2017

0162-0134/ © 2017 Elsevier Inc. All rights reserved.



which are constituted by transmembrane proteins, stand out as being responsible for pumping drugs to the extracellular medium. This lowers the antimicrobial intracellular concentration and therefore allows the survival of bacteria [7].

These data reinforce the need for immediate action [8], mainly with regard to the development of new active compounds [9,10] to combat one of the greatest clinical challenges of the 21st century [11]. Strategies against bacterial resistance include an increase in the clinical utility of existing antibiotics, the use of drug resistance modulators, and the development of efflux pump inhibitors, which can be co-administered with known antibiotics [12].

Organotin compounds are currently the most widely produced organometallic complexes in the world [13,14]. In industrial applications, they are largely employed as catalysts in reactions to produce esters [15], polyesters [16,17] and lactones [18] at high yields. Furthermore, organotin compounds also show a wide range of important biological applications [19,20], for example, they have been demonstrated to have significant antitumor [21,22], antifungal [23,24], antiviral [25], and antibacterial [26,27] activities.

In terms of their chemical and structural properties, organotin(IV) compounds are known to display significant Lewis acid characteristics and expand their coordination number *via* interactions with non-bonding electron pairs of atoms. Thus, these compounds have additional ligands and intramolecular coordination or association to produce dimers, oligomers, or polymers [14,28].

Organotin(IV) chloride and carboxylate complexes are the most studied organotin derivatives [14], but the carboxylate derivatives are the most studied for biological application because of the enormous number of compounds that can be envisaged and prepared but also because of the different biological properties that can be achieved [29]. Indeed, the most interesting feature for such compounds is the fact that the carboxylate moiety already displays important biological activity [30,31]; this, together with the organotin fragment, can modulate the biological application of the whole complex.

Fatty acids are one of the most abundant groups of organic compounds in nature, which are associated with various biological activities. Most of them are related to defense against pathogenic or opportunistic microorganisms and mainly act through inhibition of growth or direct killing. Thus, for this work, we chose three bioactive fatty acids to prepare organotin(IV) carboxylate derivatives, namely, undecylenic, caprylic, and ricinoleic acids.

Undecylenic acid (UndH), an unsaturated 11-carbon fatty acid, is a terminal unsaturated fatty acid that has antifungal [32], antibacterial [33] and antiviral activity [34]. Although rarely found in great abundance in nature, it can be found in tears and sweat. It is used as a topical antifungal agent to treat dermatomycoses, aphthae [35] and denture stomatitis [36]. This acid is primarily a fungistatic agent, and its fungicidal activity can be observed with prolonged exposure to high concentrations [37]. Caprylic acid, a saturated 8-carbon fatty acid, is found in its natural form in milk and palm, coconut and babassu oils. It is reported an antifungal, antibacterial, anti-protozoal, anthelmintic and larvicidal agent [38] and is considered to be a reliable substance by the FDA (Food and Drug Administration, USA) for use as a preservative [39]. Ricinoleic acid, an unsaturated 18-carbon fatty acid, is derived from castor oil and is primarily known for its laxative properties, but may present pro-anti-inflammatory or anti-inflammatory actions through acute or repeated topical application, respectively, resembling those described for capsaicin as well as its vanilloid analogues, but has the advantage of no poignant or painful effects, a drawback of capsaicin [40]. This fatty acid and its derivatives are used in dressings as a chemical debriding and facilitator of the healing process [41] as well as in the treatment of infected wounds as an adjunct to systemic antibiotic therapy [42,43]. In addition, ricinoleic acid easily penetrates deep into the skin and enhances trans-dermal penetration of other chemicals [44]. Thus, the association of organotin(IV) moieties with bioactive fatty acids can extend the range of action of drugs *via* the metal-ligand

synergistic effect and consequently lead to the development of new metallodrug prototypes [45].

In this context, the aim of this work was to synthesize and evaluate the antibiotic and antibiotic adjuvant activities (efflux pump inhibitor) of a series of organotin(IV) compounds against *Staphylococcus aureus* strains.

## 2. Experimental

### 2.1. Organometallic Sn(IV) derivatives

Two sets of organotin(IV) compounds were evaluated in this work: organotin(IV) chlorides and organotin(IV) carboxylates. The organotin(IV) chloride derivatives – dimethyltin dichloride ( $\text{Me}_2\text{SnCl}_2$ ), dibutyltin dichloride ( $n\text{-Bu}_2\text{SnCl}_2$ ), tributyltin dichloride ( $n\text{-Bu}_3\text{SnCl}$ ), and di-*t*-butyltin dichloride ( $t\text{-Bu}_2\text{SnCl}_2$ ) – were purchased from Gelest (Morrisville, PA, USA) and used without further purification (NMR analysis was used to confirm their state - available in Supplementary material). The organotin(IV) carboxylates were prepared from the former organotin(IV) chlorides in the presence of the respective fatty acid sodium salts. Chloroform-*d* (99.8 at% D), metallic sodium, and the fatty acids undecylenic (UndH), caprylic (CapH), and ricinoleic (RicH) acids were purchased from Sigma-Aldrich (Saint Louis, MO, USA) and used without further purification. Methanol was purchased from Dinâmica (Diadema, SP, Brazil) and used without further purification. Toluene was purchased from Tedia Brasil (Rio de Janeiro, RJ, Brazil), dried from Na/Benzophenone under reflux and argon atmosphere, and stored under argon before use. The IR spectra were recorded on a Varian 640-IR with an ATR device. The  $^1\text{H}$ ,  $^{13}\text{C}$ , and  $^{119}\text{Sn}$  NMR spectra were recorded at 400.130, 100.613, and 149.211 MHz, respectively, on a Bruker Avance 400 instrument and were externally referenced to tetramethylsilane for  $^1\text{H}$ , and  $^{13}\text{C}$  and tetramethyltin for  $^{119}\text{Sn}$ . Chemical shifts ( $\delta$ ) and coupling constants ( $J$ ) were expressed in ppm and Hz, respectively. High resolution mass spectrometry (HRMS) was performed at the LTQ Orbitrap XL Hybrid Ion Trap-Orbitrap Mass Spectrometer by electrospray ionization (ESI).

#### 2.1.1. Synthesis of organotin(IV) carboxylate derivatives

The reactions involving the synthesis of the organotin(IV) carboxylates—dimethyltin diricinoleate ( $\text{Me}_2\text{SnRic}_2$ ), dimethyltin diundecylenate ( $\text{Me}_2\text{SnUnd}_2$ ), dimethyltin dicaprylate ( $\text{Me}_2\text{SnCap}_2$ ), dibutyltin diricinoleate ( $n\text{-Bu}_2\text{SnRic}_2$ ), dibutyltin diundecylenate ( $n\text{-Bu}_2\text{SnUnd}_2$ ), dibutyltin dicaprylate ( $n\text{-Bu}_2\text{SnCap}_2$ ), tributyltin ricinoleate ( $n\text{-Bu}_3\text{SnRic}$ ), tributyltin undecylenate ( $n\text{-Bu}_3\text{SnUnd}$ ), tributyltin caprylate ( $n\text{-Bu}_3\text{SnCap}$ ), di-*t*-butyltin diricinoleate ( $t\text{-Bu}_2\text{SnRic}_2$ ), di-*t*-butyltin diundecylenate ( $t\text{-Bu}_2\text{SnUnd}_2$ ), and di-*t*-butyltin dicaprylate ( $t\text{-Bu}_2\text{SnCap}_2$ )—were prepared, according to previously described practices [46]. Briefly, all of the sodium salts of fatty acids were prepared (quantitatively) under a common atmosphere by dropwise addition of an equimolar amount of an aqueous solution (30 mL) of  $\text{NaHCO}_3$  (4.16 g; 50 mmol) into a methanolic solution (20 mL) of fatty acid. These solutions were stirred for approximately 2 h at room temperature, and the volatiles were removed under reduced pressure to give white solids, which were vacuum dried. The organotin(IV) carboxylates were prepared using the same strategy, respecting the equivalence between the number of chlorides and carboxylates. These reactions were performed under an argon atmosphere using a dual vacuum/argon line and standard Schlenk techniques. Example: to a 50-mL two-neck round-bottom flask, a solution of  $n\text{-Bu}_2\text{SnCl}_2$  (0.61 g; 2.0 mmol) in dry toluene (15 mL), and suitable equivalents of powdered sodium undecylenate (1.24 g; 6.0 mmol) were added. After 24 h under reflux, the mixture was cooled to room temperature, diethyl ether (15 mL) is added, and the mixture filtered. The solution was transferred to a rotary evaporator to remove the volatiles. The product was finally dried under vacuum, leading to a light yellow oil.

*n*-Bu<sub>2</sub>SnUnd<sub>2</sub> – Colorless oil. Yield: 68%. HRMS-ESI for C<sub>30</sub>H<sub>56</sub>O<sub>4</sub>Sn (*m/z*): calculated 623.3093 (M + Na<sup>+</sup>); found 623.3082 (M + Na<sup>+</sup>). IR (ν<sub>max</sub>/cm<sup>-1</sup>): 3078 (ν =CH), 2956 and 2886 (ν<sub>as</sub>/ν<sub>s</sub> CH<sub>3</sub>), 2923 and 2852 (ν<sub>as</sub>/ν<sub>s</sub> CH<sub>2</sub>), 1738 (ν C=O), 1639 (ν C=C), 1599 and 1381 (ν<sub>as</sub>/ν<sub>s</sub> COO), 1460 (δ<sub>as</sub> CH<sub>3</sub> and δ<sub>s</sub> CH<sub>2</sub>), 991 and 908 (γ =CH); 722 (ρ CH<sub>2</sub>), 633 and 560 (ν<sub>as</sub>/ν<sub>s</sub> Sn–C), 538 (ν Sn–O). <sup>1</sup>H NMR (CDCl<sub>3</sub>, ppm): δ 5.82 (m, 2H, =CH), 4.97 (m, 4H, =CH<sub>2</sub>), 2.36 (t, 2H, CH<sub>2</sub>COO, *J* = 7.44 Hz), 2.04 (q, 4H, CH<sub>2</sub>CH=, *J* = 7.17 Hz), 1.65 (m, 12H, Sn(CH<sub>2</sub>)<sub>2</sub> + CH<sub>2</sub>CH<sub>2</sub>COO), 1.34 (m, 24H, Sn(CH<sub>2</sub>)<sub>2</sub>CH<sub>2</sub> + (CH<sub>2</sub>)<sub>3</sub>), 0.91 (t, 6H, Sn(CH<sub>2</sub>)<sub>3</sub>CH<sub>3</sub>, *J* = 7.27 Hz). <sup>13</sup>C NMR (CDCl<sub>3</sub>, ppm): δ 184.07 (CH<sub>2</sub>CH(CH<sub>2</sub>)<sub>8</sub>COO), 139.15 (CH<sub>2</sub>CH(CH<sub>2</sub>)<sub>8</sub>COO), 114.12, (CH<sub>2</sub>CH(CH<sub>2</sub>)<sub>8</sub>COO), 34.12 (CH<sub>2</sub>CH(CH<sub>2</sub>)<sub>2</sub>CH<sub>2</sub>COO), 33.14 (CH<sub>2</sub>CHCH<sub>2</sub>(CH<sub>2</sub>)<sub>7</sub>COO), 29.30, 29.24, 29.19, 29.04, and 28.90 (CH<sub>2</sub>CHCH<sub>2</sub>(CH<sub>2</sub>)<sub>5</sub>(CH<sub>2</sub>)<sub>2</sub>COO), 26.67 and 26.30 (SnCH<sub>2</sub>(CH<sub>2</sub>)<sub>2</sub>CH<sub>3</sub>), 25.50 (CH<sub>2</sub>CH(CH<sub>2</sub>)<sub>6</sub>CH<sub>2</sub>CH<sub>2</sub>COO), 24.90 (SnCH<sub>2</sub>(CH<sub>2</sub>)<sub>2</sub>CH<sub>3</sub>), 13.53 (Sn(CH<sub>2</sub>)<sub>3</sub>CH<sub>3</sub>). <sup>119</sup>Sn NMR (CDCl<sub>3</sub>, ppm): –148.19.

*t*-Bu<sub>2</sub>SnUnd<sub>2</sub> – Light yellow oil. Yield: 64%. HRMS-ESI for C<sub>30</sub>H<sub>56</sub>O<sub>4</sub>Sn (*m/z*): calculated 623.3093 (M + Na<sup>+</sup>); found 623.3090 (M + Na<sup>+</sup>). IR (ν<sub>max</sub>/cm<sup>-1</sup>): 3075 (ν =CH), 2974 and 2883 (ν<sub>as</sub>/ν<sub>s</sub> CH<sub>3</sub>), 2925 and 2853 (ν<sub>as</sub>/ν<sub>s</sub> CH<sub>2</sub>), 1737 (ν C=O), 1638 (ν C=C), 1602 and 1367 (ν<sub>as</sub>/ν<sub>s</sub> COO), 1460 (δ<sub>as</sub> CH<sub>3</sub> and δ<sub>s</sub> CH<sub>2</sub>), 1387 (δ<sub>s</sub> CH<sub>3</sub>), 993 and 908 (γ =CH), 723 (ρ CH<sub>2</sub>), 640 and 555 (ν<sub>as</sub>/ν<sub>s</sub> Sn–C), 532 (ν Sn–O). <sup>1</sup>H NMR (CDCl<sub>3</sub>, ppm): δ 5.81 (m, 2H, =CH), 4.96 (m, 4H, =CH<sub>2</sub>), 2.37 (t, 4H, CH<sub>2</sub>COO, *J* = 7.57 Hz), 2.08 (q, 4H, CH<sub>2</sub>CH=, *J* = 7.13 Hz), 1.65 (qt, 4H, CH<sub>2</sub>CH<sub>2</sub>COO, *J* = 7.48 Hz), 1.31 (m, 38H, Sn–C(CH<sub>3</sub>)<sub>3</sub> + (CH<sub>2</sub>)<sub>5</sub>). <sup>13</sup>C NMR (CDCl<sub>3</sub>, ppm): δ 183.20 (CH<sub>2</sub>CH(CH<sub>2</sub>)<sub>8</sub>COO), 139.16 (CH<sub>2</sub>CH(CH<sub>2</sub>)<sub>8</sub>COO), 114.14 (CH<sub>2</sub>CH(CH<sub>2</sub>)<sub>8</sub>COO), 45.13 (SnC(CH<sub>3</sub>)<sub>3</sub>), 34.10 (CH<sub>2</sub>CH(CH<sub>2</sub>)<sub>7</sub>CH<sub>2</sub>COO), 33.79 (CH<sub>2</sub>CHCH<sub>2</sub>(CH<sub>2</sub>)<sub>7</sub>COO), 29.78 (SnC(CH<sub>3</sub>)<sub>3</sub>), 29.34, 29.30, 29.19, 29.03 and 28.88 (CH<sub>2</sub>CHCH<sub>2</sub>(CH<sub>2</sub>)<sub>5</sub>(CH<sub>2</sub>)<sub>2</sub>COO), 25.61 (CH<sub>2</sub>CH(CH<sub>2</sub>)<sub>6</sub>CH<sub>2</sub>CH<sub>2</sub>COO). <sup>119</sup>Sn NMR (CDCl<sub>3</sub>, ppm): δ –211.65.

*n*-Bu<sub>3</sub>SnUnd – Light yellow oil. Yield: 66%. HRMS-ESI for C<sub>23</sub>H<sub>46</sub>O<sub>2</sub>Sn (*m/z*): calculated 497.2412 (M + Na<sup>+</sup>); found 497.2403 (M + Na<sup>+</sup>). IR (ν<sub>max</sub>/cm<sup>-1</sup>): 3076 (ν =CH), 2954 and 2870 (ν<sub>as</sub>/ν<sub>s</sub> CH<sub>3</sub>), 2923 and 2853 (ν<sub>as</sub>/ν<sub>s</sub> CH<sub>2</sub>), 1738 (ν C=O), 1641 (ν C=C), 1559 and 1376 (ν<sub>as</sub>/ν<sub>s</sub> COO), 1460 (δ<sub>as</sub> CH<sub>3</sub> and δ<sub>s</sub> CH<sub>2</sub>), 994 and 906 (γ =CH), 724 (ρ CH<sub>2</sub>), 668 and 609 (ν<sub>as</sub>/ν<sub>s</sub> Sn–C), 536 (ν Sn–O). <sup>1</sup>H NMR (CDCl<sub>3</sub>, ppm): δ 5.78 (m, 1H, =CH), 4.95 (m, 2H, =CH<sub>2</sub>), 2.28 (t, 2H, CH<sub>2</sub>COO, *J* = 7.15 Hz), 2.01 (q, 2H, CH<sub>2</sub>CH=, *J* = 7.15 Hz), 1.58 (m, 8H, SnCH<sub>2</sub> + CH<sub>2</sub>CH<sub>2</sub>COO), 1.27 (m, 22H, SnCH<sub>2</sub>(CH<sub>2</sub>)<sub>2</sub> + (CH<sub>2</sub>)<sub>3</sub>), 0.88 (t, 9H, Sn(CH<sub>2</sub>)<sub>3</sub>CH<sub>3</sub>, *J* = 7.15 Hz). <sup>13</sup>C NMR (CDCl<sub>3</sub>, ppm): δ 179.49 (CH<sub>2</sub>CH(CH<sub>2</sub>)<sub>8</sub>COO), 139.18 (CH<sub>2</sub>CH(CH<sub>2</sub>)<sub>8</sub>COO), 114.07 (CH<sub>2</sub>CH(CH<sub>2</sub>)<sub>8</sub>COO), 34.91 (CH<sub>2</sub>CH(CH<sub>2</sub>)<sub>2</sub>CH<sub>2</sub>COO), 33.77 (CH<sub>2</sub>CHCH<sub>2</sub>(CH<sub>2</sub>)<sub>7</sub>COO), 29.34, 29.30, 29.28, 29.07 and 28.91 (CH<sub>2</sub>CHCH<sub>2</sub>(CH<sub>2</sub>)<sub>5</sub>(CH<sub>2</sub>)<sub>2</sub>COO), 27.84 and 27.00 (SnCH<sub>2</sub>(CH<sub>2</sub>)<sub>2</sub>CH<sub>3</sub>), 25.83 (CH<sub>2</sub>CH(CH<sub>2</sub>)<sub>6</sub>CH<sub>2</sub>CH<sub>2</sub>COO), 16.37 (SnCH<sub>2</sub>(CH<sub>2</sub>)<sub>2</sub>CH<sub>3</sub>), 13.61 (SnCH<sub>2</sub>(CH<sub>2</sub>)<sub>2</sub>CH<sub>3</sub>). <sup>119</sup>Sn NMR (CDCl<sub>3</sub>, ppm): δ 103.93.

Me<sub>2</sub>SnUnd<sub>2</sub> – Light yellow oil. Yield: 69%. HRMS-ESI for C<sub>24</sub>H<sub>44</sub>O<sub>4</sub>Sn (*m/z*): calculated 539.2154 (M + Na<sup>+</sup>); found 539.2144 (M + Na<sup>+</sup>). IR (ν<sub>max</sub>/cm<sup>-1</sup>): 3076 (ν =CH), 2979 and 2863 (ν<sub>as</sub>/ν<sub>s</sub> CH<sub>3</sub>), 2923 and 2852 (ν<sub>as</sub>/ν<sub>s</sub> CH<sub>2</sub>), 1734 (ν C=O), 1639 (ν C=C), 1556 and 1393 (ν<sub>as</sub>/ν<sub>s</sub> COO), 1457 (δ<sub>as</sub> CH<sub>3</sub> and δ<sub>s</sub> CH<sub>2</sub>), 993 and 908 (γ =CH), 722 (ρ CH<sub>2</sub>), 634 and 574 (ν<sub>as</sub>/ν<sub>s</sub> Sn–C), 540 (ν Sn–O). <sup>1</sup>H NMR (CDCl<sub>3</sub>, ppm): δ 5.81 (m, 2H, =CH), 4.97 (m, 4H, =CH<sub>2</sub>), 2.35 (br, 4H, CH<sub>2</sub>COO), 2.04 (q, 4H, CH<sub>2</sub>CH=, *J* = 7.01 Hz), 1.63 (br, 4H, CH<sub>2</sub>CH<sub>2</sub>COO), 1.32 (m, 20H, (CH<sub>2</sub>)<sub>5</sub>), 0.98 (br, 6H, SnCH<sub>3</sub>). <sup>13</sup>C NMR (CDCl<sub>3</sub>, ppm): δ 184.32 (CH<sub>2</sub>CH(CH<sub>2</sub>)<sub>8</sub>COO), 139.14 (CH<sub>2</sub>CH(CH<sub>2</sub>)<sub>8</sub>COO), 114.12 (CH<sub>2</sub>CH(CH<sub>2</sub>)<sub>8</sub>COO), 34.05 (CH<sub>2</sub>CH(CH<sub>2</sub>)<sub>2</sub>CH<sub>2</sub>COO), 33.76 (CH<sub>2</sub>CHCH<sub>2</sub>(CH<sub>2</sub>)<sub>7</sub>COO), 29.68, 29.27, 29.17, 29.02 and 28.88 (CH<sub>2</sub>CHCH<sub>2</sub>(CH<sub>2</sub>)<sub>5</sub>(CH<sub>2</sub>)<sub>2</sub>COO), 25.36 (CH<sub>2</sub>CH(CH<sub>2</sub>)<sub>6</sub>CH<sub>2</sub>CH<sub>2</sub>COO),

4.12 (SnCH<sub>3</sub>). <sup>119</sup>Sn NMR (CDCl<sub>3</sub>, ppm): δ –119.74.

*n*-Bu<sub>2</sub>SnCap<sub>2</sub> – Light yellow oil. Yield: 70%. HRMS-ESI for C<sub>24</sub>H<sub>48</sub>O<sub>4</sub>Sn (*m/z*): calculated 543.2467 (M + Na<sup>+</sup>); found 543.2460 (M + Na<sup>+</sup>). IR (ν<sub>max</sub>/cm<sup>-1</sup>): 2954 and 2869 (ν<sub>as</sub>/ν<sub>s</sub> CH<sub>3</sub>), 2923 and 2855 (ν<sub>as</sub>/ν<sub>s</sub> CH<sub>2</sub>), 1734 (ν C=O), 1596 and 1378 (ν<sub>as</sub>/ν<sub>s</sub> COO), 1458 (δ<sub>as</sub> CH<sub>3</sub> and δ<sub>s</sub> CH<sub>2</sub>), 722 (ρ CH<sub>2</sub>), 670 and 631 (ν<sub>as</sub>/ν<sub>s</sub> Sn–C), 530 (ν Sn–O). <sup>1</sup>H NMR (CDCl<sub>3</sub>, ppm): δ 2.35 (t, 4H, CH<sub>2</sub>COO, *J* = 7.66 Hz), 1.65 (m, 12H, CH<sub>2</sub>CH<sub>2</sub>COO + Sn(CH<sub>2</sub>)<sub>2</sub>), 1.31 (m, 20H, (CH<sub>2</sub>)<sub>4</sub>CH<sub>3</sub> + Sn(CH<sub>2</sub>)<sub>2</sub>CH<sub>2</sub>), 0.88 (m, 12H, (CH<sub>2</sub>)<sub>4</sub>CH<sub>3</sub> + Sn(CH<sub>2</sub>)<sub>3</sub>CH<sub>3</sub>). <sup>13</sup>C NMR (CDCl<sub>3</sub>, ppm): δ 183.70 (CH<sub>3</sub>(CH<sub>2</sub>)<sub>6</sub>COO), 34.09 (CH<sub>3</sub>(CH<sub>2</sub>)<sub>5</sub>CH<sub>2</sub>COO), 31.67 (CH<sub>3</sub>CH<sub>2</sub>CH<sub>2</sub>(CH<sub>2</sub>)<sub>4</sub>COO), 29.20 and 28.91 (CH<sub>3</sub>(CH<sub>2</sub>)<sub>2</sub>(CH<sub>2</sub>)<sub>2</sub>(CH<sub>2</sub>)<sub>2</sub>COO), 26.67 and 26.32 (SnCH<sub>2</sub>(CH<sub>2</sub>)<sub>2</sub>CH<sub>3</sub>), 25.43 (CH<sub>3</sub>(CH<sub>2</sub>)<sub>4</sub>CH<sub>2</sub>CH<sub>2</sub>COO), 24.94 (SnCH<sub>2</sub>(CH<sub>2</sub>)<sub>2</sub>CH<sub>3</sub>), 22.59 (CH<sub>3</sub>CH<sub>2</sub>(CH<sub>2</sub>)<sub>5</sub>COO), 14.03 (CH<sub>3</sub>(CH<sub>2</sub>)<sub>6</sub>COO), 13.52 (Sn(CH<sub>2</sub>)<sub>3</sub>CH<sub>3</sub>). <sup>119</sup>Sn NMR (CDCl<sub>3</sub>, ppm): δ –149.55.

*t*-Bu<sub>2</sub>SnCap<sub>2</sub> – Light yellow oil. Yield: 70%. HRMS-ESI for C<sub>24</sub>H<sub>48</sub>O<sub>4</sub>Sn (*m/z*): calculated 543.2467 (M + Na<sup>+</sup>); found 543.2455 (M + Na<sup>+</sup>). IR (ν<sub>max</sub>/cm<sup>-1</sup>): 2956 and 2870 (ν<sub>as</sub>/ν<sub>s</sub> CH<sub>3</sub>), 2926 and 2853 (ν<sub>as</sub>/ν<sub>s</sub> CH<sub>2</sub>), 1737 (ν C=O), 1602 and 1367 (ν<sub>as</sub>/ν<sub>s</sub> COO), 1458 (δ<sub>as</sub> CH<sub>3</sub> and δ<sub>s</sub> CH<sub>2</sub>), 1383 (δ<sub>s</sub> CH<sub>3</sub>), 724 (ρ CH<sub>2</sub>), 668 and 563 (ν<sub>as</sub>/ν<sub>s</sub> Sn–C), 532 (ν Sn–O). <sup>1</sup>H NMR (CDCl<sub>3</sub>, ppm): δ 2.37 (br, 4H, CH<sub>2</sub>COO), 1.65 (br, 4H, CH<sub>2</sub>CH<sub>2</sub>COO), 1.31 (m, 34H, (CH<sub>2</sub>)<sub>4</sub>CH<sub>3</sub> + Sn–C(CH<sub>3</sub>)<sub>3</sub>), 0.87 (br, 6H, (CH<sub>2</sub>)<sub>4</sub>CH<sub>3</sub>). <sup>13</sup>C NMR (CDCl<sub>3</sub>, ppm): δ 183.09 (CH<sub>3</sub>(CH<sub>2</sub>)<sub>6</sub>COO), 45.15 (SnC(CH<sub>3</sub>)<sub>3</sub>), 34.09 (CH<sub>3</sub>(CH<sub>2</sub>)<sub>5</sub>CH<sub>2</sub>COO), 31.68 (CH<sub>3</sub>CH<sub>2</sub>CH<sub>2</sub>(CH<sub>2</sub>)<sub>4</sub>COO), 29.78 (SnC(CH<sub>3</sub>)<sub>3</sub>), 29.30 and 28.92 (CH<sub>3</sub>(CH<sub>2</sub>)<sub>2</sub>(CH<sub>2</sub>)<sub>2</sub>(CH<sub>2</sub>)<sub>2</sub>COO), 25.58 (CH<sub>3</sub>(CH<sub>2</sub>)<sub>4</sub>CH<sub>2</sub>CH<sub>2</sub>COO), 22.58 (CH<sub>3</sub>CH<sub>2</sub>(CH<sub>2</sub>)<sub>5</sub>COO), 14.06 (CH<sub>3</sub>(CH<sub>2</sub>)<sub>6</sub>COO). <sup>119</sup>Sn NMR (CDCl<sub>3</sub>, ppm): δ –211.55.

*n*-Bu<sub>3</sub>SnCap – White oily solid. Yield: 73%. HRMS-ESI for C<sub>20</sub>H<sub>42</sub>O<sub>2</sub>Sn (*m/z*): calculated 457.2099 (M + Na<sup>+</sup>); found 457.2089 (M + Na<sup>+</sup>). IR (ν<sub>max</sub>/cm<sup>-1</sup>): 2954 and 2870 (ν<sub>as</sub>/ν<sub>s</sub> CH<sub>3</sub>), 2920 and 2853 (ν<sub>as</sub>/ν<sub>s</sub> CH<sub>2</sub>), 1545 and 1404 (ν<sub>as</sub>/ν<sub>s</sub> COO), 1457 (δ<sub>as</sub> CH<sub>3</sub> and δ<sub>s</sub> CH<sub>2</sub>), 1376 (δ<sub>s</sub> CH<sub>3</sub>), 725 (ρ CH<sub>2</sub>), 667 and 609 (ν<sub>as</sub>/ν<sub>s</sub> Sn–C), 532 (ν Sn–O). <sup>1</sup>H NMR (CDCl<sub>3</sub>, ppm): δ 2.30 (t, 2H, CH<sub>2</sub>COO, *J* = 7.35 Hz), 1.63 (m, 8H, CH<sub>2</sub>CH<sub>2</sub>COO + SnCH<sub>2</sub>), 1.30 (m, 20H, (CH<sub>2</sub>)<sub>4</sub>CH<sub>3</sub> + SnCH<sub>2</sub>(CH<sub>2</sub>)<sub>2</sub>), 0.91 (m, 12H, (CH<sub>2</sub>)<sub>4</sub>CH<sub>3</sub> + Sn(CH<sub>2</sub>)<sub>3</sub>CH<sub>3</sub>). <sup>13</sup>C NMR (CDCl<sub>3</sub>, ppm): δ 179.53 (CH<sub>3</sub>(CH<sub>2</sub>)<sub>6</sub>COO), 34.94 (CH<sub>3</sub>(CH<sub>2</sub>)<sub>5</sub>CH<sub>2</sub>COO), 31.74 (CH<sub>3</sub>CH<sub>2</sub>CH<sub>2</sub>(CH<sub>2</sub>)<sub>4</sub>COO), 29.29 and 29.01 (CH<sub>3</sub>(CH<sub>2</sub>)<sub>2</sub>(CH<sub>2</sub>)<sub>2</sub>(CH<sub>2</sub>)<sub>2</sub>COO), 27.85 and 27.03 (SnCH<sub>2</sub>(CH<sub>2</sub>)<sub>2</sub>CH<sub>3</sub>), 25.87 (CH<sub>3</sub>(CH<sub>2</sub>)<sub>4</sub>CH<sub>2</sub>CH<sub>2</sub>COO), 22.60 (CH<sub>3</sub>CH<sub>2</sub>CH<sub>2</sub>(CH<sub>2</sub>)<sub>4</sub>COO), 16.37 (SnCH<sub>2</sub>(CH<sub>2</sub>)<sub>2</sub>CH<sub>3</sub>), 14.05 (CH<sub>3</sub>(CH<sub>2</sub>)<sub>6</sub>COO), 13.63 (Sn(CH<sub>2</sub>)<sub>3</sub>CH<sub>3</sub>). <sup>119</sup>Sn NMR (CDCl<sub>3</sub>, ppm): δ 103.89.

Me<sub>2</sub>SnCap<sub>2</sub> – Light yellow oil. Yield: 69%. HRMS-ESI for C<sub>18</sub>H<sub>36</sub>O<sub>4</sub>Sn (*m/z*): calculated 459.1528 (M + Na<sup>+</sup>); found 459.1518 (M + Na<sup>+</sup>). IR (ν<sub>max</sub>/cm<sup>-1</sup>): 2954 and 2869 (ν<sub>as</sub>/ν<sub>s</sub> CH<sub>3</sub>), 2925 and 2855 (ν<sub>as</sub>/ν<sub>s</sub> CH<sub>2</sub>), 1714 (ν C=O), 1556 and 1404 (ν<sub>as</sub>/ν<sub>s</sub> COO), 1458 (δ<sub>as</sub> CH<sub>3</sub> and δ<sub>s</sub> CH<sub>2</sub>), 1378 (δ<sub>s</sub> CH<sub>3</sub>), 724 (ρ CH<sub>2</sub>), 640 and 571 (ν<sub>as</sub>/ν<sub>s</sub> Sn–C), 532 (ν Sn–O). <sup>1</sup>H NMR (CDCl<sub>3</sub>, ppm): δ 2.34 (br, 4H, CH<sub>2</sub>COO), 1.63 (br, 4H, CH<sub>2</sub>CH<sub>2</sub>COO), 1.29 (m, 16H, (CH<sub>2</sub>)<sub>4</sub>CH<sub>3</sub>), 0.96 (m, 12H, (CH<sub>2</sub>)<sub>4</sub>CH<sub>3</sub> + SnCH<sub>3</sub>). <sup>13</sup>C NMR (CDCl<sub>3</sub>, ppm): δ 183.57 (CH<sub>3</sub>(CH<sub>2</sub>)<sub>6</sub>COO), 34.19 (CH<sub>3</sub>(CH<sub>2</sub>)<sub>5</sub>CH<sub>2</sub>COO), 31.65 (CH<sub>3</sub>CH<sub>2</sub>CH<sub>2</sub>(CH<sub>2</sub>)<sub>4</sub>COO), 29.16 and 28.90 (CH<sub>3</sub>(CH<sub>2</sub>)<sub>2</sub>(CH<sub>2</sub>)<sub>2</sub>(CH<sub>2</sub>)<sub>2</sub>COO), 25.36 (CH<sub>3</sub>(CH<sub>2</sub>)<sub>4</sub>CH<sub>2</sub>CH<sub>2</sub>COO), 22.57 (CH<sub>3</sub>CH<sub>2</sub>CH<sub>2</sub>(CH<sub>2</sub>)<sub>4</sub>COO), 14.03 (CH<sub>3</sub>(CH<sub>2</sub>)<sub>6</sub>COO), 6.40 (SnCH<sub>3</sub>). <sup>119</sup>Sn NMR (CDCl<sub>3</sub>, ppm): δ –121.82.

*n*-Bu<sub>2</sub>SnRic<sub>2</sub> – Light yellow oil. Yield: 78%. HRMS-ESI for C<sub>44</sub>H<sub>84</sub>O<sub>6</sub>Sn (*m/z*): calculated 827.5206 (M – H); found 827.5195 (M – H). IR (ν<sub>max</sub>/cm<sup>-1</sup>): 3011 (ν =CH), 2957 and 2870 (ν<sub>as</sub>/ν<sub>s</sub> CH<sub>3</sub>), 2925 and 2853 (ν<sub>as</sub>/ν<sub>s</sub> CH<sub>2</sub>), 1723 (ν C=O), 1598 and 1378 (ν<sub>as</sub>/ν<sub>s</sub> COO), 1461 (δ<sub>as</sub> CH<sub>3</sub> and δ<sub>s</sub> CH<sub>2</sub>), 667 and 611 (ν<sub>as</sub>/ν<sub>s</sub> Sn–C), 529 (ν Sn–O). <sup>1</sup>H NMR (CDCl<sub>3</sub>, ppm): δ 5.45 (m, 4H, CH=CH), 4.88 (qt, 1H, CH–OH), 3.61 (qt, 1H, CH–OH), 2.29 (m, 8H, CH<sub>2</sub>CH = CHCH<sub>2</sub>), 2.03 (br, 4H, CH<sub>2</sub>COO), 1.52 (m, 52H, Sn(CH<sub>2</sub>)<sub>3</sub> + (CH<sub>2</sub>)<sub>5</sub>CH<sub>2</sub>COO + (CH<sub>2</sub>)<sub>3</sub>CH<sub>3</sub>), 0.90 (m, 12H,

$(\text{CH}_2)_5\text{CH}_3 + \text{Sn}(\text{CH}_2)_3\text{CH}_3$ .  $^{13}\text{C}$  NMR ( $\text{CDCl}_3$ , ppm):  $\delta$  173.50 ( $(\text{CH}_2)_7\text{COO}$ ), 133.27 ( $\text{CH}(\text{CH}_2)_7\text{COO}$ ), 125.23 ( $\text{CHCH}(\text{CH}_2)_7\text{COO}$ ), 71.51 ( $\text{CHCH}_2(\text{CH}_2)_2(\text{CH}_2)_7\text{COO}$ ), 36.86 ( $\text{CH}_3(\text{CH}_2)_4\text{CH}_2$ ), 35.36 ( $\text{CH}_2(\text{CH}_2)_2(\text{CH}_2)_7\text{COO}$ ), 34.02 ( $(\text{CH}_2\text{COO})$ ), 31.81 ( $\text{CH}_3\text{CH}_2\text{CH}_2(\text{CH}_2)_3$ ), 29.57, 29.53, 29.22 and 29.12 ( $(\text{CH}_2)_4(\text{CH}_2)_2\text{COO}$ ), 29.33 ( $\text{CH}_3(\text{CH}_2)_2\text{CH}_2$ ), 27.33 ( $\text{CH}_2(\text{CH}_2)_6\text{COO}$ ) 26.65 and 26.28 ( $\text{SnCH}_2(\text{CH}_2)_2\text{CH}_3$ ), 25.69 ( $\text{CH}_3(\text{CH}_2)_3\text{CH}_2$ ), 25.50 ( $\text{SnCH}_2(\text{CH}_2)_2\text{CH}_3$ ), 25.09 ( $\text{CH}_2\text{CH}_2\text{COO}$ ), 22.59 ( $\text{CH}_3\text{CH}_2(\text{CH}_2)_4$ ), 14.02 ( $\text{CH}_3(\text{CH}_2)_5$ ), 13.51 ( $\text{Sn}(\text{CH}_2)_3\text{CH}_3$ ).  $^{119}\text{Sn}$  NMR ( $\text{CDCl}_3$ , ppm):  $\delta$  -147.76.

$t\text{-Bu}_2\text{SnRic}_2$  - Light yellow oil. Yield: 79%. HRMS-ESI for  $\text{C}_{44}\text{H}_{84}\text{O}_6\text{Sn}$  ( $m/z$ ): calculated 827.5206 (M - H); found 827.5199 (M - H). IR ( $\nu_{\text{max}}/\text{cm}^{-1}$ ): 3008 ( $\nu = \text{CH}$ ), 2952 and 2867 ( $\nu_{\text{as}}/\nu_{\text{s}}$   $\text{CH}_3$ ), 2925 and 2853 ( $\nu_{\text{as}}/\nu_{\text{s}}$   $\text{CH}_2$ ), 1731 ( $\nu \text{C}=\text{O}$ ), 1602 and 1367 ( $\nu_{\text{as}}/\nu_{\text{s}}$   $\text{COO}$ ), 1458 ( $\delta_{\text{as}}$   $\text{CH}_3$  and  $\delta_{\text{s}}$   $\text{CH}_2$ ), 727 ( $\rho$   $\text{CH}_2$ ), 665 and 566 ( $\nu_{\text{as}}/\nu_{\text{s}}$   $\text{Sn}-\text{C}$ ), 534 ( $\nu \text{Sn}-\text{O}$ ).  $^1\text{H}$  NMR ( $\text{CDCl}_3$ , ppm):  $\delta$  5.44 (m, 4H,  $\text{CH}=\text{CH}$ ), 4.88 (qt, 1H,  $\text{CH}-\text{OH}$ ), 3.62 (qt, 1H,  $\text{CH}-\text{OH}$ ), 2.33 (m, 8H,  $\text{CH}_2\text{CH}=\text{CHCH}_2$ ), 2.03 (br, 4H,  $\text{CH}_2\text{COO}$ ), 1.44 (m, 58H,  $\text{Sn}-\text{C}(\text{CH}_2)_3 + (\text{CH}_2)_5\text{CH}_2\text{COO} + (\text{CH}_2)_5\text{CH}_3$ ), 0.88 (br, 6H,  $(\text{CH}_2)_5\text{CH}_3$ ).  $^{13}\text{C}$  NMR ( $\text{CDCl}_3$ , ppm):  $\delta$  173.50 ( $(\text{CH}_2)_7\text{COO}$ ), 133.30 ( $\text{CH}(\text{CH}_2)_7\text{COO}$ ), 125.22 ( $\text{CHCH}(\text{CH}_2)_7\text{COO}$ ), 71.51 ( $\text{CHCH}_2(\text{CH}_2)_2(\text{CH}_2)_7\text{COO}$ ), 45.12 ( $\text{Sn}(\text{CH}_2)_3$ ), 36.86 ( $\text{CH}_3(\text{CH}_2)_4\text{CH}_2$ ), 35.36 ( $\text{CH}_2(\text{CH}_2)_2(\text{CH}_2)_7\text{COO}$ ), 34.65 ( $(\text{CH}_2\text{COO})$ ), 31.82 ( $\text{CH}_3\text{CH}_2\text{CH}_2(\text{CH}_2)_3$ ), 29.76 ( $\text{Sn}(\text{CH}_2)_3$ ), 29.55, 29.51, 29.22 and 29.13 ( $(\text{CH}_2)_4(\text{CH}_2)_2\text{COO}$ ), 29.26 ( $\text{CH}_3(\text{CH}_2)_2\text{CH}_2$ ), 27.36 ( $\text{CH}_2(\text{CH}_2)_6\text{COO}$ ), 25.70 ( $\text{CH}_3(\text{CH}_2)_3\text{CH}_2$ ), 25.08 ( $\text{CH}_2\text{CH}_2\text{COO}$ ), 22.59 ( $\text{CH}_3\text{CH}_2(\text{CH}_2)_4$ ), 14.04 ( $\text{CH}_3(\text{CH}_2)_5$ ).  $^{119}\text{Sn}$  NMR ( $\text{CDCl}_3$ , ppm):  $\delta$  -106.69 and -211.63.

$n\text{-Bu}_3\text{SnRic}$  - Light yellow oil. Yield: 75%. HRMS-ESI for  $\text{C}_{30}\text{H}_{60}\text{O}_3\text{Sn}$  ( $m/z$ ): calculated 587.3481 (M - H); found 587.3466 (M - H). IR ( $\nu_{\text{max}}/\text{cm}^{-1}$ ): 3007 ( $\nu = \text{CH}$ ), 2952 and 2867 ( $\nu_{\text{as}}/\nu_{\text{s}}$   $\text{CH}_3$ ), 2023 and 2852 ( $\nu_{\text{as}}/\nu_{\text{s}}$   $\text{CH}_2$ ), 1732 ( $\nu \text{C}=\text{O}$ ), 1618 and 1376 ( $\nu_{\text{as}}/\nu_{\text{s}}$   $\text{COO}$ ), 1458 ( $\delta_{\text{as}}$   $\text{CH}_3$  and  $\delta_{\text{s}}$   $\text{CH}_2$ ), 724 ( $\rho$   $\text{CH}_2$ ), 670 and 609 ( $\nu_{\text{as}}/\nu_{\text{s}}$   $\text{Sn}-\text{C}$ ), 530 ( $\nu \text{Sn}-\text{O}$ ).  $^1\text{H}$  NMR ( $\text{CDCl}_3$ , ppm):  $\delta$  5.42 (m, 2H,  $\text{CH}=\text{CH}$ ), 4.87 (qt, 1H,  $\text{CH}-\text{OH}$ ), 3.60 (qt, 1H,  $\text{CH}-\text{OH}$ ), 2.26 (m, 4H,  $\text{CH}_2\text{CH}=\text{CHCH}_2$ ), 2.01 (br, 2H,  $\text{CH}_2\text{COO}$ ), 1.33 (m, 38H,  $\text{Sn}(\text{CH}_2)_3 + (\text{CH}_2)_5\text{CH}_2\text{COO} + (\text{CH}_2)_5\text{CH}_3$ ), 0.85 (br, 12H,  $(\text{CH}_2)_5\text{CH}_3 + \text{Sn}(\text{CH}_2)_3\text{CH}_3$ ).  $^{13}\text{C}$  NMR ( $\text{CDCl}_3$ , ppm):  $\delta$  173.48 ( $(\text{CH}_2)_7\text{COO}$ ), 133.25 ( $\text{CH}(\text{CH}_2)_7\text{COO}$ ), 125.24 ( $\text{CHCH}(\text{CH}_2)_7\text{COO}$ ), 71.48 ( $\text{CHCH}_2(\text{CH}_2)_2(\text{CH}_2)_7\text{COO}$ ), 36.85 ( $\text{CH}_3(\text{CH}_2)_4\text{CH}_2$ ), 35.35 ( $\text{CH}_2(\text{CH}_2)_2(\text{CH}_2)_7\text{COO}$ ), 34.63 ( $(\text{CH}_2\text{COO})$ ), 31.81 ( $\text{CH}_3\text{CH}_2\text{CH}_2(\text{CH}_2)_3$ ), 29.58, 29.53, 29.23 and 29.11 ( $(\text{CH}_2)_4(\text{CH}_2)_2\text{COO}$ ), 29.33 ( $\text{CH}_3(\text{CH}_2)_2\text{CH}_2$ ), 27.82 and 26.98 ( $\text{SnCH}_2(\text{CH}_2)_2\text{CH}_3$ ), 27.36 ( $\text{CH}_2(\text{CH}_2)_6\text{COO}$ ) 25.68 ( $\text{CH}_3(\text{CH}_2)_3\text{CH}_2$ ), 25.06 ( $\text{CH}_2\text{CH}_2\text{COO}$ ), 22.58 ( $\text{CH}_3\text{CH}_2(\text{CH}_2)_4$ ), 16.37 ( $\text{SnCH}_2(\text{CH}_2)_2\text{CH}_3$ ), 14.02 ( $\text{CH}_3(\text{CH}_2)_5$ ), 13.59 ( $\text{Sn}(\text{CH}_2)_3\text{CH}_3$ ).  $^{119}\text{Sn}$  NMR ( $\text{CDCl}_3$ , ppm):  $\delta$  104.31.

$\text{Me}_2\text{SnRic}_2$  - Light yellow oil. Yield: 71%. HRMS-ESI for  $\text{C}_{38}\text{H}_{72}\text{O}_6\text{Sn}$  ( $m/z$ ): calculated 743.4267 (M - H); found 743.4248 (M - H). IR ( $\nu_{\text{max}}/\text{cm}^{-1}$ ): 3008 ( $\nu = \text{CH}$ ), 2923 and 2852 ( $\nu_{\text{as}}/\nu_{\text{s}}$   $\text{CH}_2$ ), 1731 ( $\nu \text{C}=\text{O}$ ), 1557 and 1378 ( $\nu_{\text{as}}/\nu_{\text{s}}$   $\text{COO}$ ), 1457 ( $\delta_{\text{as}}$   $\text{CH}_3$  and  $\delta_{\text{s}}$   $\text{CH}_2$ ), 724 ( $\rho$   $\text{CH}_2$ ), 623 and 581 ( $\nu_{\text{as}}/\nu_{\text{s}}$   $\text{Sn}-\text{C}$ ), 543 ( $\nu \text{Sn}-\text{O}$ ).  $^1\text{H}$  NMR ( $\text{CDCl}_3$ , ppm):  $\delta$  5.43 (m, 4H,  $\text{CH}=\text{CH}$ ), 4.88 (qt, 1H,  $\text{CH}-\text{OH}$ ), 3.62 (qt, 1H,  $\text{CH}-\text{OH}$ ), 2.29 (m, 8H,  $\text{CH}_2\text{CH}=\text{CHCH}_2$ ), 2.03 (br, 4H,  $\text{CH}_2\text{COO}$ ), 1.43 (m, 40H,  $(\text{CH}_2)_5\text{CH}_2\text{COO} + (\text{CH}_2)_5\text{CH}_3$ ), 1.01 (br, 6H,  $\text{SnCH}_2$ ), 0.88 (br, 6H,  $(\text{CH}_2)_5\text{CH}_3$ ).  $^{13}\text{C}$  NMR ( $\text{CDCl}_3$ , ppm):  $\delta$  173.53 ( $(\text{CH}_2)_7\text{COO}$ ), 133.28 ( $\text{CH}(\text{CH}_2)_7\text{COO}$ ), 125.23 ( $\text{CHCH}(\text{CH}_2)_7\text{COO}$ ), 71.53 ( $\text{CHCH}_2(\text{CH}_2)_2(\text{CH}_2)_7\text{COO}$ ), 36.85 ( $\text{CH}_3(\text{CH}_2)_4\text{CH}_2$ ), 35.34 ( $\text{CH}_2(\text{CH}_2)_2(\text{CH}_2)_7\text{COO}$ ), 34.65 ( $(\text{CH}_2\text{COO})$ ), 31.82 ( $\text{CH}_3\text{CH}_2\text{CH}_2(\text{CH}_2)_3$ ), 29.58, 29.54, 29.22 and 29.12 ( $(\text{CH}_2)_4(\text{CH}_2)_2\text{COO}$ ), 29.33 ( $\text{CH}_3(\text{CH}_2)_2\text{CH}_2$ ), 27.35 ( $\text{CH}_2(\text{CH}_2)_6\text{COO}$ ), 25.69 ( $\text{CH}_3(\text{CH}_2)_3\text{CH}_2$ ), 25.08 ( $\text{CH}_2\text{CH}_2\text{COO}$ ), 22.59 ( $\text{CH}_3\text{CH}_2(\text{CH}_2)_4$ ), 14.04 ( $\text{CH}_3(\text{CH}_2)_5$ ), 6.14 ( $\text{SnCH}_2$ ).  $^{119}\text{Sn}$  NMR ( $\text{CDCl}_3$ , ppm):  $\delta$  -119.30.

## 2.2. Biological assays

### 2.2.1. *Staphylococcus aureus* strains

*S. aureus* strains that overexpress efflux pump proteins for norfloxacin (SA-1199B), erythromycin (RN-4220) and tetracycline (IS-58) were provided by Dr. Simon Gibbons (University of London). All strains were kept in inclined blood agar culture medium (Blood Agar Base – BAB, Difco), and before use, cells were grown in infusion nutritious broth (Brain Heart Infusion – BHI, Difco) for 18–24 h at 37 °C.

### 2.2.2. Evaluation of antibacterial activity

The Minimum Inhibitory Concentrations (MICs) were determined by nutritious broth (BHI) with a microdilution technique using a suspension of approximately  $10^5$  CFU/mL, with varying concentrations from 256 to 0.25  $\mu\text{g}/\text{mL}$  or from 128 to 0.125  $\mu\text{g}/\text{mL}$  (serial dilutions 1/2) [47]. The MIC was defined as the lowest concentration that completely inhibited bacterial growth. For better visualization of bacterial growth after 24 h, a resazurin dye solution (0.01%) was used (Sigma-Aldrich).

### 2.2.3. Antibiotics

Solutions of norfloxacin (NOR), tetracycline (TET) and erythromycin (ERI), were prepared according to a previous procedure [48].

### 2.2.4. Evaluation of modulatory activity

The *S. aureus* strains resistant to antibiotics were SA-1199B, RN-4220 and IS-58. For evaluation of organotin(IV) compounds as modifying antibiotic activity agents (putative efflux pump inhibitors), the MIC of antibiotics were determined in the presence and absence of the organotin(IV) compounds [49]. The concentration for the studied compounds corresponded to 1/4 of their MIC (subinhibitory concentration) [50]. For better visualization of bacterial growth before 24 h, a resazurin indicator solution (0.01%) (Sigma-Aldrich) was used.

Stock solutions of all antibiotics were prepared according to NCCLS procedures [48] and ethidium bromide was prepared in sterile distilled water. The stock solutions of the organotin derivatives analyzed were prepared in DMSO/sterile distilled water solutions. The highest final concentration of DMSO after dilution in broth was 4%. At this concentration no bacterial growth inhibition occurred by the solvent.

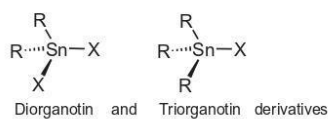
## 2.3. Cell lines and growth inhibitory assay (MTT assay)

The toxicity profiles of the fatty acids (UndH, RicH, and CapH) and all organotin derivatives against mammalian cells was prepared using the cell viability test MTT assay [51], MTT = 3-(4,5-dimethylthiazol-2-yl)-2,5-diphenyltetrazolium bromide.

The murine macrophage line J774 was treated with the compounds at different concentrations (0.1–100  $\mu\text{M}$ ), and the  $\text{LC}_{50}$  (necessary concentration to induce the death of 50% of the cells) was determined [52].

## 2.4. Statistics

Data were expressed as the mean  $\pm$  standard error of the mean (S.E.M.) and significant differences between the treated and control groups were evaluated using ANOVA and Dunnett post-hoc tests by Graph Pad Prism 5.0 software, and the 95% confidence intervals were included. Lethal concentration of 50% ( $\text{LC}_{50}$ ) calculated through toxic concentration-response curves. The maximum effect was considered significant compared to the DMSO group. Values were considered significant when  $^*p < 0.05$ ,  $^{**}p < 0.01$  and  $^{***}p < 0.001$ . NT = Non-toxic to concentrations above 100  $\mu\text{M}$  [52].



R= *n*-Bu, *t*-Bu, and Me

X= Cl and carboxylates of fatty acids, such as:

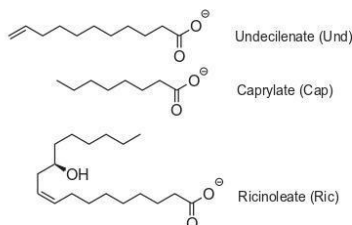


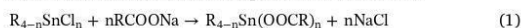
Fig. 1. Chemical structures of organotin(IV) compounds evaluated.

### 3. Results and discussion

#### 3.1. Organotin(IV) derivatives

All of the organotin(IV) compounds evaluated in this work have the general formula:  $R_4-nSnX_n$ , where  $n = 1$  or  $2$ ; R = alkyl substituents: *n*-Bu, *t*-Bu, or Me; and X = Cl, or fatty carboxylates: Undecylate (Und), Caprylate (Cap), and Ricinoleate (Ric) (see Fig. 1).

As mentioned before, the organotin(IV) chloride compounds were purchased from commercial sources, but the organotin(IV) carboxylate derivatives were synthesized from organotin(IV) chloride by reacting them with the corresponding fatty acid sodium salts (see Eq. (1)) [46]. In terms of their chemical structure, these compounds have intramolecular coordination and intermolecular association due to the intrinsic Lewis acid character of the metal [14,53]. All of the organotin(IV) carboxylate derivatives isolated were light yellow oils or white oily solids, and their chloride counterparts were white solids.



where  $n = 1$  or  $2$ , and  $RCOO = \text{Und, Cap, Ric}$ .

All of the synthesized compounds were verified according to their  $^1\text{H}$  NMR spectra; most signals related to carboxylate moieties are easily identified, as are the expected signals (chemical shift and intensities) for hydrogens of alkyl substituents (R = *n*-Bu, *t*-Bu, or Me). This was also observed for the  $^{13}\text{C}$  and  $^{119}\text{Sn}$  spectra. In particular, from  $^{119}\text{Sn}$  NMR analysis, it was verified that the chemical shift of the di- and triorganotin(IV) carboxylate derivatives were as expected due to the type and nature of the substituent around the metal center (see Table 1), i.e., between  $-140$  and  $-160$  ppm for  $n\text{-Bu}_2\text{Sn(OOCR)}_2$ ;  $-200$  and  $-220$  ppm for  $t\text{-Bu}_2\text{Sn(OOCR)}_2$ ;  $100$  and  $110$  ppm for  $n\text{-Bu}_3\text{Sn(OOCR)}$ ; and  $-110$  and  $-130$  ppm for  $\text{Me}_2\text{Sn(OOCR)}_2$  [14,54,55,56,57]. Furthermore, the  $^{119}\text{Sn}$  spectra of the respective di- and triorganotin(IV) chloride precursors had signals in completely different regions (see Supplementary material), indicating that substitution of the chlorides by the carboxylates occurred. The synthesized complexes were also characterized by infrared spectroscopy via ATR. The Sn–C and Sn–O stretching vibrations were found in all carboxylic complexes at  $670\text{--}555$  and  $543\text{--}529\text{ cm}^{-1}$ , respectively [53]. According to previous studies, the difference between  $\nu_{\text{as}}(\text{COO}^-)$  and  $\nu_{\text{s}}(\text{COO}^-)$  ( $\Delta\nu$ ) can be used to classify the coordination modes for metal carboxylates. In general, comparison of the  $\Delta\nu$  value of the complex to the  $\Delta\nu$  value of the respective sodium salt can be used for assignment following the guiding principle: (i) bidentate coordination occurs when  $\Delta(\text{COO}^-)_{\text{studied complex}} \ll \Delta\nu(\text{COO}^-)_{\text{sodium salt}}$ ; (ii) bridging carboxylate exists when  $\Delta\nu(\text{COO}^-)_{\text{studied complex}} \leq \Delta\nu(\text{COO}^-)_{\text{sodium salt}}$ ; (iii) monodentate coordination is characterized by  $\Delta\nu(\text{COO}^-)_{\text{studied}}$

Table 1

Selected data from infrared (IR) and nuclear magnetic resonance (NMR) spectroscopies of the organotin(IV) carboxylate derivatives synthesized.

Compounds	IR. COO $\nu_{\text{as}}, \nu_{\text{s}}$ ( $\Delta\nu$ ) <sup>a</sup>	NMR. $^{119}\text{Sn}$ (ppm)
<i>n</i> -Bu <sub>2</sub> SnUnd <sub>2</sub>	1599, 1381 (218)	– 148.19
<i>t</i> -Bu <sub>2</sub> SnUnd <sub>2</sub>	1602, 1367 (235)	– 211.65
<i>n</i> -Bu <sub>3</sub> SnUnd	1559, 1376 (183)	103.93
Me <sub>2</sub> SnUnd <sub>2</sub>	1556, 1393 (163)	– 119.74
<i>n</i> -Bu <sub>2</sub> SnCap <sub>2</sub>	1596, 1378 (218)	– 149.55
<i>t</i> -Bu <sub>2</sub> SnCap <sub>2</sub>	1602, 1367 (235)	– 211.55
<i>n</i> -Bu <sub>3</sub> SnCap	1545, 1404 (141)	103.89
Me <sub>2</sub> SnCap <sub>2</sub>	1556, 1404 (152)	– 121.82
<i>n</i> -Bu <sub>2</sub> SnRic <sub>2</sub>	1598, 1378 (220)	– 147.76
<i>t</i> -Bu <sub>2</sub> SnRic <sub>2</sub>	1603, 1368 (235)	– 211.63
<i>n</i> -Bu <sub>3</sub> SnRic	1618, 1376 (242)	104.31
Me <sub>2</sub> SnRic <sub>2</sub>	1557, 1378 (179)	– 119.30

<sup>a</sup> Respective values for fatty acid sodium salts - UndNa: 1559, 1415 (144); CapNa: 1557, 1423 (134); and RicNa: 1557, 1423 (134).

complex  $\gg \Delta\nu(\text{COO}^-)_{\text{sodium salt}}$  [58,59]. In line with this classification, all of the carboxylate derivatives had a monodentate coordination, or at least an asymmetric bidentate coordination [60], in their isolated forms. Table 1 shows the main characterization data that confirmed the general chemical structure of the organotin(IV) carboxylate derivatives prepared in this work.

#### 3.2. Evaluation of antibacterial activity

In this study, we used three resistant *Staphylococcus aureus* strains: i) SA-1199B, which overexpresses the *NorA* gene encoding the NorA efflux protein that is responsible for the efflux of fluoroquinolones [61,62] and other substances that bind to nucleic acids [63], such as quaternary ammonium compounds (e.g., benzalkonium chloride and centrimide), and intercalating dyes (e.g., acriflavine and ethidium bromide); ii) RN-4220, which contains the UL5054 plasmid that carries the gene encoding the protein for macrolide efflux (*MsrA*) [64]; and iii) IS-58, which contains the efflux protein of tetracycline (*TetK*) [65]. In Table 2, the Minimum Inhibitory Concentration (MIC) of tin organometallics complexes against these *Staphylococcus aureus* strains is shown.

As expected, most of the organotin derivatives showed antibacterial activity, some with MIC values up to  $1.0\text{ }\mu\text{g/mL}$  ( $3.1\text{ }\mu\text{M}$ , for *n*-Bu<sub>3</sub>SnCl) [66,67].

In general, the organotin(IV) chloride derivatives were more active against the *S. aureus* strains tested compared to their respective carboxylate equivalents. Among them, the trialkyl derivative *n*-Bu<sub>3</sub>SnCl

**Table 2**  
Minimum Inhibitory Concentration (MIC) of organotin(IV) compounds against *Staphylococcus aureus* strains.

Organotin(IV) derivative	MIC, µg/mL (µM)		
	RN-4220	IS-58	SA-1199B
<i>n</i> -Bu <sub>2</sub> SnUnd <sub>2</sub>	256 (427)	> 256 (> 427)	> 256 (> 427)
<i>t</i> -Bu <sub>2</sub> SnUnd <sub>2</sub>	64 (106)	128 (213)	256 (427)
<i>n</i> -Bu <sub>3</sub> SnUnd	32 (67)	64 (135)	32 (67)
Me <sub>2</sub> SnUnd <sub>2</sub>	> 256 (> 497)	> 256 (> 497)	> 256 (> 497)
<i>n</i> -Bu <sub>2</sub> SnRic <sub>2</sub>	> 256 (> 309)	> 256 (> 309)	> 256 (> 309)
<i>t</i> -Bu <sub>2</sub> SnRic <sub>2</sub>	128 (154)	128 (154)	256 (309)
<i>n</i> -Bu <sub>3</sub> SnRic	8 (13)	8 (13)	8 (13)
Me <sub>2</sub> SnRic <sub>2</sub>	> 256 (> 344)	> 256 (> 344)	> 256 (> 344)
<i>n</i> -Bu <sub>2</sub> SnCap <sub>2</sub>	> 256 (> 493)	> 256 (> 493)	> 256 (> 493)
<i>t</i> -Bu <sub>2</sub> SnCap <sub>2</sub>	64 (123)	128 (246)	128 (246)
<i>n</i> -Bu <sub>3</sub> SnCap	16 (37)	16 (37)	16 (37)
Me <sub>2</sub> SnCap <sub>2</sub>	> 256 (> 588)	> 256 (> 588)	> 256 (> 588)
<i>n</i> -Bu <sub>2</sub> SnCl <sub>2</sub>	16 (53)	16 (53)	32 (106)
<i>t</i> -Bu <sub>2</sub> SnCl <sub>2</sub>	8 (26)	16 (53)	16 (53)
<i>n</i> -Bu <sub>3</sub> SnCl	1.0 (3.1)	1.0 (3.1)	1.0 (3.1)
Me <sub>2</sub> SnCl <sub>2</sub>	64 (292)	128 (584)	128 (584)

had the highest activity, with MIC values of 1.0 µg/mL (3.1 µM) for all tested strains. This trend was also observed for the *n*-Bu<sub>3</sub>Sn<sup>+</sup> carboxylate counterparts, highlighting the results obtained for *n*-Bu<sub>3</sub>SnRic and *n*-Bu<sub>3</sub>SnCap, with MIC values of 8 and 16 µg/mL (13 and 37 µM), respectively, against all evaluated strains. These results indicate that the presence of three *n*-butyl substituents on tin(IV) has an important contribution to the antibacterial activity of organotin(IV) derivatives. This tendency was expected since the bactericidal activity of this class of compounds is normally associated with the number and type of organic groups bonded to the Sn(IV)-center (R<sub>3</sub>Sn<sup>+</sup> > R<sub>2</sub>Sn<sup>2+</sup> > RSn<sup>3+</sup> > Sn<sup>4+</sup>, bactericidal activity and toxicity scale) and has been well documented in many scientific reports [68]. Furthermore, it is important to note that when we only consider bactericidal activity, the substitution of chlorides by carboxylate substituents leads to a decrease in activity. Indeed, all of the organotin(IV) carboxylate complexes were less active than their chloride analogues [27]. For the most active species, *n*-Bu<sub>3</sub>SnCl, the chloride substitution for ricinoleate, *n*-Bu<sub>3</sub>SnRic, led to a decrease in potentiality of eight-fold in terms of µg/mL (but only 2.6 times in terms of µM) for the three strains. For *n*-Bu<sub>2</sub>SnCl<sub>2</sub>, the decrease in activity due to chloride substitution was seen for all strains, regardless of the carboxylate derivative used. The Me<sub>2</sub>Sn<sup>2+</sup> species, in general, demonstrated low activity, confirming that the wide-ranging biological activity of the organotin (IV) compounds is associated with the size of the alkyl chain. For example, it was observed for diorganotin(IV) compounds that the biological activity decreased when the alkyl moiety is too large or too small (octyl or methyl groups) [69]. Most characteristics must be related to the ratio between the solubility and lipophilicity of these compounds [60]. Indeed, the mechanism of the biological action of organotin derivatives is still not clear. However, due to their lipophilic feature, organotins are membrane-active and the cytoplasmic membrane is an obvious target of action [55,70].

Despite the decrease in activity due to the replacement of chlorides with carboxylates, it is possible that there is an improvement in antibacterial activity associated with reduced side effects, e.g., toxicity. The lipophilic characteristics of the carboxylate derivatives can yield an important improvement in antibacterial activity, allowing easier crossing of biological barriers [71], which is important for biocidal efficacy against many microorganisms [72,73,74,75]. This action can be associated with the formation of new bonds between the tin(IV) center, with electron donor species in active biological centers [76,77,78,79].

**Table 3**  
Effect of the organotin derivatives, fatty acids, and pentamidine (concentrations of 1.0, 10 and 100 µM) on the viability of J774 macrophages according to the MTT assay.

Compounds	LC <sub>50</sub> (µM ± S.E.M.) <sup>a</sup>	Maximum cytotoxicity (% ± S.E.M.) <sup>b</sup>
<i>n</i> -Bu <sub>2</sub> SnUnd <sub>2</sub>	30 ± 0	100 ± 0***
<i>t</i> -Bu <sub>2</sub> SnUnd <sub>2</sub>	2.5 ± 1.5	100 ± 0***
<i>n</i> -Bu <sub>3</sub> SnUnd	2.3 ± 0.3	100 ± 0***
Me <sub>2</sub> SnUnd <sub>2</sub>	> 100	NT
UndH	41 ± 7	100 ± 0***
<i>n</i> -Bu <sub>2</sub> SnRic <sub>2</sub>	3.9 ± 1.5	100 ± 0***
<i>t</i> -Bu <sub>2</sub> SnRic <sub>2</sub>	4.1 ± 0.6	100 ± 0***
<i>n</i> -Bu <sub>3</sub> SnRic	44 ± 12	100 ± 0***
Me <sub>2</sub> SnRic <sub>2</sub>	1.2 ± 0.5	68.4 ± 12
RicH	79 ± 1	46.7 ± 6.3***
<i>n</i> -Bu <sub>2</sub> SnCap <sub>2</sub>	< 1.0	95.4 ± 7.9***
<i>t</i> -Bu <sub>2</sub> SnCap <sub>2</sub>	< 1.0	100 ± 0***
<i>n</i> -Bu <sub>3</sub> SnCap	< 1.0	100 ± 0***
Me <sub>2</sub> SnCap <sub>2</sub>	13 ± 4	66.6 ± 13.4*
CapH	> 100	NT
<i>n</i> -Bu <sub>2</sub> SnCl <sub>2</sub>	< 1.0	100 ± 0***
<i>t</i> -Bu <sub>2</sub> SnCl <sub>2</sub>	< 1.0	100 ± 0***
<i>n</i> -Bu <sub>3</sub> SnCl	< 1.0	100 ± 0***
Me <sub>2</sub> SnCl <sub>2</sub>	> 100	NT
Pentamidine <sup>c</sup>	88 ± 1	42.8 ± 7.3***

<sup>a</sup> Lethal concentration of 50% (LC<sub>50</sub>) calculated through toxic concentration-response curves.

<sup>b</sup> Mean ± standard error of the mean maximum cytotoxicity in triplicate for representative experiments. The maximum effect was considered significant compared to the DMSO group. Values were considered significant when \**p* < 0.05, \*\**p* < 0.01 and \*\*\**p* < 0.001. NT = Non-toxic to concentrations above 100 µM.

<sup>c</sup> Positive control [81].

### 3.3. Cytotoxicity assay

Toxicity, together with the desired biological activity, is a very important parameter that must also be evaluated. In general, the toxicity of organotin(IV) derivatives is mainly due to their action on the cell membrane and their high plasmatic membrane permeability [80]. In our study, the toxicity of the organotin(IV) compounds, as well the fatty acids used to prepare the organotin(IV) carboxylate derivatives, was estimated via a cytotoxicity assay (MTT) performed with the murine macrophage line J774. The results are summarized in Table 3 in terms of the lethal concentration (LC).

To better understand these results, consider that a higher LC<sub>50</sub> value indicates a less toxic substance. In general, in the MTT assay, non-toxic compounds have an LC<sub>50</sub> > 100 µM. Thus, according to Table 3, only the dimethyltin(IV) derivatives Me<sub>2</sub>SnUnd<sub>2</sub>, Me<sub>2</sub>SnCl<sub>2</sub> and CapH were considered to be nontoxic against the J774 line macrophages (Table 3). Moreover, for compounds bearing butyl substituents, one can verify that, in general, the exchange of chloride by fatty carboxylates leads to decreased toxicity of the respective compound.

We also evaluated the toxicity related to the fatty acids themselves to verify the toxic features from these moieties. In general, the toxicity of fatty acids is related to the induction of apoptosis and necrosis of cells via a mechanism that involve changes in the transmembrane potential of mitochondria and accumulation of neutral lipids; it is not simply related to the length of the carbon chain and the number of double bonds in their structure [82].

Most organotin(IV) compounds are relatively toxic if one compares the MIC values of the compounds against *Staphylococcus aureus*-resistant strains (Table 2) and the cellular viability of J774 macrophages (Table 3).

Despite the general low selectivity demonstrated by the organotin (IV) derivatives against *S. aureus* resistant strains against macrophages, their use at lower concentrations but in association with other well-established antibiotic drugs can overcome the resistance strategy of the strains evaluated here, i.e., we were able to evaluate their antibiotic

**Table 4**  
Organotin(IV) modulating activity against *Staphylococcus aureus* strains. The standard antibiotics for treating the RN-4220, IS-58, and SA-1199B strains were erythromycin, tetracycline, and norfloxacin, respectively.

Compound	MIC, $\mu\text{g}/\text{mL}^a$ /modulation ratio <sup>b</sup>		
	RN-4220	IS-58	SA-1199B
Standard antibiotic	> 256	64	128
<i>n</i> -Bu <sub>2</sub> SnUnd <sub>2</sub>	> 256/1	64/1	128/1
<i>n</i> -Bu <sub>2</sub> SnRic <sub>2</sub>	> 256/1	32/2	128/1
<i>n</i> -Bu <sub>2</sub> SnCap <sub>2</sub>	> 256/1	64/1	128/1
<i>t</i> -Bu <sub>2</sub> SnUnd <sub>2</sub>	> 256/1	2/32	128/1
<i>t</i> -Bu <sub>2</sub> SnRic <sub>2</sub>	> 256/1	0.5/128	32/4
<i>t</i> -Bu <sub>2</sub> SnCap <sub>2</sub>	> 256/1	64/1	128/1
<i>n</i> -Bu <sub>3</sub> SnUnd	> 256/1	32/2	128/1
<i>n</i> -Bu <sub>3</sub> SnRic	> 256/1	32/2	128/1
<i>n</i> -Bu <sub>3</sub> SnCap	> 256/1	64/1	128/1
Me <sub>2</sub> SnUnd <sub>2</sub>	> 256/1	64/1	128/1
Me <sub>2</sub> SnRic <sub>2</sub>	> 256/1	64/1	128/1
Me <sub>2</sub> SnCap <sub>2</sub>	> 256/1	64/1	128/1
<i>n</i> -Bu <sub>2</sub> SnCl <sub>2</sub>	> 256/1	4/16	64/2
<i>t</i> -Bu <sub>2</sub> SnCl <sub>2</sub>	> 256/1	0.5/128	32/4
<i>n</i> -Bu <sub>3</sub> SnCl	> 256/1	0.5/128	128/1
Me <sub>2</sub> SnCl <sub>2</sub>	> 256/1	16/4	128/1

<sup>a</sup> Concentration corresponded to 1/4 of their MIC (subinhibitory concentration).

<sup>b</sup> MIC of standard antibiotic/MIC of standard antibiotics with organotin derivatives.

adjuvant activity properties.

### 3.4. Evaluation of antibiotic modulatory activity

The modulatory activities of the antibiotic action of the organotin (IV) derivatives are shown in Table 4. The first entry in the table, the standard antibiotics for each strain alone (erythromycin to RN-4220 strain, tetracycline to IS-58 strain, and norfloxacin to SA-1199B strain), was utilized (*i.e.*, in the absence of the organotin derivatives). In further entries, these standard antibiotics were tested in association with the organotin derivatives at subinhibitory concentrations (1/4 of their MIC values - presented on Table 2).

As expected, the standard antibiotics in the absence of the organotin derivatives, were not able to inhibit the growth of strains at the highest concentrations evaluated (256, 64 and 128  $\mu\text{g}/\text{mL}$ , respectively to RN-4220, IS-58 and SA-1199B) since the strains evaluated possess genes that overexpress the respective efflux proteins (bacterial resistance mechanism). These strains expel antibiotics from the cellular interior, making them completely ineffective [83].

In further tests performed with standard antibiotics in association with organotin derivatives at subinhibitory concentrations, many organotin derivatives potentiated the action of tetracycline (IS-58 strain) antibiotics, allowing inhibition of the growth of strains with lower MIC values and rescuing the effectiveness of the antibiotics against the microorganisms. For the RN-4220 strain overexpressing the *MsrA* protein, potentiation of erythromycin activity was not observed [84].

When antibiotic action was potentialized due modulation, we believe that the organotin(IV) derivatives not only allowed “reactivation” of standard antibiotics, hindering the bacterial resistance mechanism, but also reduced the amount of these antibiotics that were needed. This reduction was as high as 128-fold (tetracycline in association with the carboxylate derivative *t*-Bu<sub>2</sub>SnRic<sub>2</sub> and chlorine *t*-Bu<sub>2</sub>SnCl<sub>2</sub>). The same trend was observed for *n*-Bu<sub>3</sub>SnCl, which had high modulation against the IS-58 strain (128-fold). Indeed, these results are significant since a decrease in the risk of antibiotic side effects and organotin(IV) toxicity due to the reduction of the dose of both compounds can be significantly reduced.

From all of the compounds, we highlighted *t*-Bu<sub>2</sub>SnRic<sub>2</sub> as the most promising in this study. Its toxicity was lowest among the compounds, with a modulation effect of up to 128 against the IS-58 strain.

These results show, for the first time, the potential for organotin(IV)

compounds as putative inhibitors of bacterial efflux systems, especially against tetracycline resistant strains, which contains the efflux protein of tetracycline (TetK) with a modulation ratio up to 128. It is important to perform further studies to reduce the toxicity of these compounds to adopt them as possible antibiotic adjuvants against antibiotic-resistant bacterial lines.

## 4. Conclusion

In this work, we observed that the substitution of chlorine by fatty carboxylates on organotin(IV) compounds led, in most cases, to a decrease in the antibacterial potentiality as well as cytotoxicity. This particular substitution can tune the relationship of biological activity and cytotoxicity in several ways and can be used as a strategy to prepare effective new antibacterial drugs, mainly against resistant strains.

Despite the relative high toxicity observed for most organotin compounds, some complexes demonstrated promising antibacterial activity and, particularly, modulatory activity at lower concentrations, indicating that the strategy adopted, *i.e.*, the use of bioactive compounds as substituents on organotin(IV) derivatives, is a good strategy to overcome challenges in the development of new alternative antimicrobial agents.

Briefly, we believe that the association of conventional antibiotics with organotin(IV) compounds can allow the renewed use of these antibiotics against resistant strains, with lower amount of antibiotic, decreasing the possibility of toxicity and development of resistant strains as well as lowering drug production cost. Therefore, these compounds may represent a new alternative method to modify antibiotic activity by acting as antibiotic adjuvants.

## Table of abbreviations

$\delta$	Chemical shifts
ANOVA	Analysis of variance
ATR	Attenuated total reflection
BAB	Blood Agar Base
BHI	Brain Heart Infusion
Cap	Caprylate
CapH	Caprylic acid
CapNa	Sodium caprylate
CFU	Colony-forming unit
DMSO	Dimethyl sulfoxide
ERI	Erythromycin
ESI	Electrospray ionization
FDA	Food and Drug Administration
HRMS	High resolution mass spectrometry.
IR	Infrared spectroscopy
IS-58	<i>S. aureus</i> strains resistant to tetracycline
<i>J</i>	Coupling constants
LC <sub>50</sub>	Lethal concentration to induce death of 50% of cells
Me <sub>2</sub> SnCap <sub>2</sub>	Dimethyltin dicaprylate
Me <sub>2</sub> SnCl <sub>2</sub>	Dimethyltin dichloride
Me <sub>2</sub> SnRic <sub>2</sub>	Dimethyltin diricinoleate
Me <sub>2</sub> SnUnd <sub>2</sub>	Dimethyltin diundecylenate
MIC	Minimum Inhibitory Concentration
<i>MsrA</i>	Macrolide efflux pump
MTT	3-(4,5-dimethylthiazol-2-yl)-2,5-diphenyltetrazolium bromide
NaHCO <sub>3</sub>	Sodium bicarbonate
<i>n</i> -Bu <sub>2</sub> SnCap <sub>2</sub>	Dibutyltin dicaprylate
<i>n</i> -Bu <sub>2</sub> SnCl <sub>2</sub>	Dibutyltin dichloride
<i>n</i> -Bu <sub>2</sub> SnRic <sub>2</sub>	Dibutyltin diricinoleate
<i>n</i> -Bu <sub>2</sub> SnUnd <sub>2</sub>	Dibutyltin diundecylenate
<i>n</i> -Bu <sub>3</sub> SnCap	Tributyltin caprylate
<i>n</i> -Bu <sub>3</sub> SnCl	Tributyltin chloride
<i>n</i> -Bu <sub>3</sub> SnRic	Tributyltin ricinoleate

<i>n</i> -Bu <sub>3</sub> SnUnd	Tributyltin undecylenate
NCCLS	National Committee for Clinical Laboratory Standards
NMR	Nuclear magnetic resonance
NOR	Norflaxacin
NorA	Norflaxacin efflux pump
<i>p</i>	Range of statistical significance
Ric	Ricinoleate
RicH	Ricinoleic acid
RicNa	Sodium ricinoleate
RN-4220	<i>S. aureus</i> strains resistant to erythromycin
SA-1199B	<i>S. aureus</i> strains resistant to norflaxacin
SEM	Standard Error of the Mean
<i>t</i> -Bu <sub>2</sub> SnCap <sub>2</sub>	di- <i>t</i> -butyltin dicaprylate
<i>t</i> -Bu <sub>2</sub> SnCl <sub>2</sub>	di- <i>t</i> -butyltin dichloride
<i>t</i> -Bu <sub>2</sub> SnRic <sub>2</sub>	di- <i>t</i> -butyltin diricinoleate
<i>t</i> -Bu <sub>2</sub> SnUnd <sub>2</sub>	di- <i>t</i> -butyltin diundecylenate
TET	Tetracycline
TetK	Tetracycline efflux pump
Ligand	Undecylenate
UndH	Undecylenic acid
UndNa	Sodium undecylenate

### Acknowledgements

Authors gratefully acknowledge the Brazilian research founding agencies, Research and Projects Financing (FINEP), National Counsel of Technological and Scientific Development (CNPq), and the Alagoas Research Support Foundation (FAPEAL) for financial support. FJBMJr and JPSJ thank Dr. Simon Gibbons (University of London) for the *S. aureus* strains. MRM and SMPM thank CNPq for research fellowships. MRM and JSG thank Dr. Simone Carvalho Chiapetta and National Institute of Technology (INT) for high resolution mass spectrometry analysis.

### Appendix A. Supplementary data

Supplementary data to this article can be found online at <https://doi.org/10.1016/j.jinorgbio.2017.12.004>.

### References

- [1] Antibiotic resistance threats in the United States, <https://www.cdc.gov/drugresistance/threat-report-2013/index.html>, (2013), Accessed date: 22 September 2017.
- [2] A.L. Demain, S. Sanchez, Microbial drug discovery: 80 years of progress, *J. Antibiot.* 62 (2009) 5–16.
- [3] M.J. Richards, J.R. Edwards, D.H. Culver, R.P. Gaynes, Nosocomial infections in medical intensive care units in the United States, *Crit. Care Med.* 17 (1999) 887–892.
- [4] H. Wisplinghoff, T. Bischoff, S.M. Tallent, H. Seifert, R.P. Wenzel, M.B. Edmond, Nosocomial bloodstream infections in US hospitals: analysis of 24,179 cases from a prospective nationwide surveillance study, *Clin. Infect. Dis.* 39 (2004) 309–317.
- [5] N.C. Desai, K.M. Rajpara, V.V. Joshi, Synthesis of pyrazole encompassing 2-pyridone derivatives as antibacterial agents, *Bioorg. Med. Chem. Lett.* 23 (2013) 2714–2717.
- [6] S.L. Barriere, Clinical, economic and societal impact of antibiotic resistance, *Expert Opin. Pharmacother.* 16 (2015) 151–153.
- [7] L.J.V. Piddock, Clinically relevant chromosomally encoded multidrug resistance efflux pumps in bacterial, *Clin. Microbiol. Rev.* 19 (2006) 382–402.
- [8] WHO – World Health Organization, Antimicrobial Resistance: Global Report on Surveillance, World Health Organization, Geneva, Switzerland, 2014.
- [9] M. Grare, M. Mourer, S. Fontanay, J.-B. Regnouf-de-Vains, C. Finance, R.E. Duval, *In vitro* activity of *para*-guanidinomethylcalix[4]arene against susceptible and antibiotic-resistant gram-negative and gram-positive bacteria, *J. Antimicrob. Chemother.* 60 (2007) 575–581.
- [10] R.M. Klevens, M.A. Morrison, J. Nadle, S. Petit, K. Gershman, S. Ray, L.H. Harrison, R. Lynfield, G. Dumyati, J.M. Townes, A.S. Craig, E.R. Zell, G.E. Fosheim, L.K. McDougal, R.B. Carey, S.K. Fridkin, Invasive methicillin-resistant *Staphylococcus aureus* infections in the United States, *J. Am. Med. Assoc.* 298 (2007) 1763–1771.
- [11] C. Patel, J.P. Bassin, M. Scott, J. Flye, A.P. Hunter, L. Matin, M. Goyal, Synthesis and antimicrobial activity of 1,2-benzothiazine derivatives, *Molecules* 21 (2016) 1–16.
- [12] A.S. Lynch, Efflux system in bacterial pathogens: an opportunity for therapeutic intervention? An industry view, *Biochem. Pharmacol.* 71 (2006) 949–956.
- [13] M.R. Meneghetti, S.M.P. Meneghetti, Sn(IV)-based organometallics as catalysts for the production of fatty acid alkyl esters, *Cat. Sci. Technol.* 5 (2015) 765–771.
- [14] A.G. Davies, *Organotin Chemistry*, 2nd ed., Wiley-VCH Verlag GmbH & Co. KGaA, 3-527-31023-1, 2004.
- [15] Y.C. Brito, D.A.C. Ferreira, D.M.A. Fragoso, P.R. Mendes, C.M.J. de Oliveira, M.R. Meneghetti, S.M.P. Meneghetti, Simultaneous conversion of triacylglycerides and fatty acids into fatty acid methyl esters using organometallic tin(IV) compound as catalysts, *Appl. Catal. A.* 443–444 (2012) 202–206.
- [16] G. Deshayes, F.A.G. Mercier, P. Degee, I. Verbruggen, M. Biesemans, R. Willem, P. Dubois, Mechanistic study of Bu<sub>2</sub>SnCl<sub>2</sub>-mediated ring-opening polymerization of  $\epsilon$ -Caprolactone by multinuclear NMR spectroscopy, *Chem. Eur. J.* 9 (2003) 4346–4352.
- [17] S. Shyamroy, B. Gamaik, S. Sivaram, Structure of poly(*L*-lactic acid)s prepared by the dehydropolycondensation of *L*-lactic acid with organotin catalysts, *J. Polym. Sci. A Polym. Chem.* 43 (2005) 2164–2177.
- [18] I. Shiina, Total synthesis of natural 8- and 9-membered lactones: recent advancements in medium-sized ring formation, *Chem. Rev.* 107 (2007) 239–273.
- [19] A.B. Alama, F. Tasso, F. Sparatore, Organometallic compounds in oncology: implications of novel organotin as antitumor agents, *Drug Discov. Today* 14 (2009) 500–508.
- [20] M.A. Affan, S.W. Foo, I. Jusho, S. Hanapi, E.R.T. Tiekiak, Synthesis, characterization and biological studies of organotin(IV) complexes with hydrazone ligand, *Inorg. Chim. Acta* 362 (2009) 5031–5037.
- [21] M. Mohan, A. Agarwal, N.K. Jha, Synthesis, characterization, and antitumor properties of some metal complexes of 2,6-diacetylpyridine bis([N.sup.4]-azacyclicthiosemicarbazones), *J. Inorg. Biochem.* 34 (1988) 41–54.
- [22] B. Ruan, Y. Tian, H. Zhou, J. Wu, R. Hu, C. Zhu, J. Yang, H. Zhu, Synthesis, characterization and *in vitro* antitumor activity of three organotin(IV) complexes with carbazole ligand, *Inorg. Chim. Acta* 365 (2011) 302–308.
- [23] N. Manav, N. Gandhi, N.K. Kaushik, Some tribenzyltin(IV) complexes with thiohydrazides and thiodiamines. Synthesis, characterization and thermal studies, *J. Therm. Anal. Calorim.* 61 (2000) 127–134.
- [24] R. Singh, N.K. Kaushik, Spectral and thermal studies with anti-fungal aspects of some organotin(IV) complexes with nitrogen and sulphur donor ligands derived from 2-phenylethylamine, *Spectrochim. Acta A* 71 (2008) 669–675.
- [25] N.K. Singh, A. Srivastava, A. Sodhi, P. Ranjan, *In vitro* and *in vivo* antitumor studies of a new thiosemicarbazide derivative and its complexes with 3D-metal ions, *Transit. Met. Chem.* 25 (2000) 133–140.
- [26] A. Maiti, A.K. Guha, S. Ghosh, Ligational behavior of two biologically active N-S donors toward oxovanadium(IV) ion and potentiation of their antibacterial activities by chelation to, *J. Inorg. Biochem.* 33 (1988) 57–65.
- [27] B. Gleeson, J. Claffey, D. Ertler, M. Hogan, H. Muller-Bunz, F. Paradisi, D. Wallis, M. Tacke, Novel organotin antibacterial and anticancer drugs, *Polyhedron* 27 (2008) 3619–3624.
- [28] D.M. Reinoso, M.L. Ferreira, G.M. Tonetto, Study of the reaction mechanism of the transesterification of triglycerides catalyzed by zinc carboxylates, *J. Mol. Catal. A Chem.* 377 (2013) 29–41.
- [29] S.K. Hadjilakou, N. Hadjiladis, Antiproliferative and anti-tumor activity of organotin compounds, *Coord. Chem. Rev.* 253 (2009) 235–249.
- [30] R. Di Stefano, M. Scopelliti, C. Pellerito, G. Casella, T. Fiore, G.C. Stocco, R. Vitturi, M. Colomba, L. Ronconi, I.D. Sciacca, L. Pellerito, *J. Inorg. Biochem.* 98 (2004) 534.
- [31] M. Gielen, Organotin compounds and their therapeutic potential: a report from the Organometallic Chemistry Department of the Free University of Brussels, *Appl. Organomet. Chem.* 16 (2002) 481–494.
- [32] D. Shi, Y. Zhao, H. Yan, H. Fu, Y. Shen, G. Lu, H. Mei, Y. Qiu, D. Li, W. Liu, Antifungal effects of undecylenic acid on the biofilm formation of *Candida albicans*, *Int. J. Clin. Pharmacol. Ther.* 54 (2016) 343–353.
- [33] S.D. Shafran, S.L. Sacks, F.Y. Aoki, D.L. Tyrrell, W.F. Schleich III, J. Mendelson, D. Rosenthal, M.J. Gill, R.L. Bader, I. Chang, Topical undecylenic acid for herpes simplex labialis: a multicenter, placebo-controlled trial, *J. Infect. Dis.* 176 (1997) 78–83.
- [34] N. Bourne, J. Ireland, L.R. Stanberry, D.I. Bernstein, Effect of undecylenic acid as a topical microbicide against genital herpes infection in mice and guinea pigs, *Antivir. Res.* 40 (1999) 139–144.
- [35] X.C. Li, M.R. Jacob, S.I. Khan, M.K. Ashfaq, K.S. Babu, A.K. Agarwal, H.N. Elshohly, S.P. Manly, A.M. Clark, *Antimicrob. Agents Chemother.* 52 (2008) 2442–2448.
- [36] N. McLain, R. Asciano, C. Baker, R.A. Strohaber, J.W. Dolan, *Antimicrob. Agents Chemother.* 44 (2000) 2873–2875.
- [37] J.E. Bennett, Chapter 57: antifungal agents, in: L.L. Brunton, B.A. Chabner, B.C. Knollmann (Eds.), Goodman & Gilman's: The Pharmacological Basis of Therapeutics, 12nd ed., McGraw-Hill, 2011, pp. 1571–1592.
- [38] A.P. Desbois, V.J. Smith, Antibacterial free fatty acids: activities, mechanisms of action and biotechnological potential, *Appl. Microbiol. Biotechnol.* 85 (2010) 1629–1642.
- [39] W. Johnson, Final report on the safety assessment of Ricinus communis (castor) seed oil, hydrogenated castor oil, glyceryl ricinoleate, glyceryl ricinoleate se, ricinoleic acid, potassium ricinoleate, sodium ricinoleate, zinc ricinoleate, cetyl ricinoleate, ethyl ricinoleate, glycol ricinoleate, isopropyl ricinoleate, methyl ricinoleate, and octyldodecyl ricinoleate, *Int. J. Toxicol.* 26 (2007) 31–77.
- [40] C. Vieira, S. Evangelista, R. Cirillo, A. Lippi, C.A. Maggi, S. Manzini, *Mediat. Inflamm.* 9 (2000) 223–228.
- [41] A.C. Dweck, The internal and external use of medicinal plants, *Clin. Dermatol.* 27 (2009) 148–158.
- [42] C.D.R.M. D'Oca, T. Coelho, T.G. Marinho, C.R.L. Hack, R. da Costa Duarte, P.A. da

- Silva, M.G.M. D'Oca, Synthesis and antituberculosis activity of new fatty acid amides, *Bioorg. Med. Chem. Lett.* 20 (2010) 5255–5257.
- [43] Y. Mohini, R.B.N. Prasad, M.S.L. Karuna, Y. Poornachandra, C.G. Kumar, Synthesis, antimicrobial and anti-biofilm activities of novel Schiff base analogues derived from methyl-12-aminooctadec-9-enoate, *Bioorg. Med. Chem. Lett.* 24 (2014) 5224–5227.
- [44] E.A. Mein, D.G. Richards, D.L. McMillin, C.D. Nelson, Transdermal adsorption of Castor oil, *Evid. Based Integr. Med.* 2 (2005) 239–244.
- [45] K.D. Mjos, C. Orvig, *Chem. Rev.* 114 (2014) 4540–4563.
- [46] N. Muhammad, A. Shah, Z. Rehman, S. Shuja, S. Ali, R. Qureshi, A. Meetsma, M.N. Tahir, Organotin(IV) 4-nitrophenylethanoates: synthesis, structural characteristics and intercalative mode of interaction with DNA, *J. Organomet. Chem.* 694 (2009) 3431–3437.
- [47] E. Smith, M. Williamson, M. Zloh, S. Gibbons, Isopimaric acid from *Pinus nigra* shows activity against multidrug-resistant and EMRSA strains of *Staphylococcus aureus*, *Phytother. Res.* 19 (2005) 538–542.
- [48] NCCLS – National Committee for Clinical Laboratory Standards, Performance Standards for Antimicrobial Susceptibility Testing; Fifteenth Information Supplement. CLSI/NCCLS Document M100-S15, 200 Clinical and Laboratory Standards Institute, Wayne, PA, USA, 2005.
- [49] S. Gibbons, M. Oluwatuyi, N.C. Veitch, A.I. Gray, Bacterial resistance modifying agents from *Lycopodium europaeus*, *Phytochemistry* 62 (2003) 83–87.
- [50] M. Stavri, L.J.V. Piddock, S. Gibbons, Bacterial efflux pump inhibitors from natural sources, *J. Antimicrob. Chemother.* 59 (2007) 1247–1260.
- [51] R.F. Hussain, A.M. Nouri, R.T. Oliver, A new approach for measurement of cytotoxicity using colorimetric assay, *J. Immunol. Methods* 160 (1993) 89–96.
- [52] M.A. Alves, A.C. Queiroz, M.S. Alexandre-Moreira, J. Varela, H. Cerecetto, M. Gonzalez, A.C. Doriguetto, I.M. Landre, E.J. Barreira, L.M. Lima, *Eur. J. Med. Chem.* 100 (2015) 24–33.
- [53] M. Nath, H. Singh, P. Kumar, A. Kumar, X. Song, G. Eng, *Appl. Organomet. Chem.* 23 (2009) 347–358.
- [54] V.S. Petrosyan, NMR spectra and structures of organotin compounds, *Prog. Nucl. Magn. Reson. Spectrosc.* 11 (1977) 115–148.
- [55] M. Gielen, A. Davies, K. Pannell, E. Tiekink, *Tin Chemistry: Fundamentals, Frontiers, and Applications*, John Wiley & Sons. Ltd., 978-0-470-51771-0, 2008.
- [56] J.P.V. da Silva, Y.C. Brito, D.M.A. Fragozo, P.R. Mendes, A.S.L. Barbosa, J.H. Bortoluzzi, M.R. Meneghetti, S.M.P. Meneghetti, Influence of different alkyl and carboxylate substituents on Sn(IV) organometallic catalysts during fatty acid methyl ester production, *Catal. Commun.* 58 (2015) 204–208.
- [57] V.B. Mokal, V.K. Jain, Steric effects on the formation of isolable products in the reactions of dibutyltin oxides with carboxylic acids, *J. Organomet. Chem.* 441 (1992) 215–226.
- [58] V. Zelenak, Z. Vargova, K. Gyoryova, Correlation of infrared spectra of zinc(II) carboxylates with their structures, *Spectrochim. Acta A* 66 (2007) 262–272.
- [59] K. Nakamoto, *Infrared and Raman Spectra of Inorganic and Coordination Compounds*, John Wiley & Sons, New York, 1997.
- [60] L.C. Dias, G.M. de Lima, J.A. Takahashi, J.D. Ardisson, New di- and triorganotin(IV) carboxylates derived from a Schiff base: synthesis, characterization and in vitro antimicrobial activities, *Appl. Organomet. Chem.* 29 (2015) 305–313.
- [61] G.W. Kaatz, S.M. Seo, C.A. Ruble, Efflux-mediated fluoroquinolone resistance in *Staphylococcus aureus*, *Antimicrob. Agents Chemother.* 37 (1993) 1086–1094.
- [62] G.W. Kaatz, S.M. Seo, Inducible NorA-mediated multidrug resistance in *Staphylococcus aureus*, *Antimicrob. Agents Chemother.* 39 (1995) 2650–2655.
- [63] K.R. Ensle, D.E. Townsend, W.B. Grubb, A resistance determinant to nucleic acid-binding compounds in methicillin resistance *Staphylococcus aureus*, *J. Med. Microbiol.* 20 (1995) 139–145.
- [64] J.I. Ross, A.M. Farelli, E.A. Eady, J.H. Cove, W.J. Cunliffe, Characterization and molecular cloning of the novel macrolide-streptogramin B resistance determinant from *Staphylococcus epidermidis*, *J. Antimicrob. Chemother.* 24 (1989) 851–862.
- [65] S. Gibbons, E.E. Udo, The effect of reserpine, a modulator of multidrug efflux, on the *in vivo* activity of tetracycline against clinical isolates of methicillin resistance *Staphylococcus aureus* (Mrsa) possessing the Tet(K) determinant, *Phytother. Res.* 14 (2000) 139–140.
- [66] A.S.L. Barbosa, M.R. Meneghetti, J.S. Guedes, M.L.A. Bastos, S.M.P. Meneghetti, Compostos Organoestânicos derivados de ácidos carboxílicos naturais bioativos e seus usos, (BR 10 2014 019055-4), (2014) (Brazil).
- [67] A. Saeed, P.A. Channar, F.A. Larik, F. Jabeen, U. Muqadar, S. Saeed, U. Flörke, H. Ismail, E. Dilshad, B. Mirza, *Inorg. Chim. Acta* 464 (2017) 204–213.
- [68] A. Gianguzza, O. Giuffrè, D. Piazzese, S. Sammartano, Aqueous solution chemistry of alkyltin(IV) compounds for speciation studies in biological fluids and natural waters, *Coord. Chem. Rev.* 256 (2012) 222–239.
- [69] C.E. Carraher Jr., M.R. Roner, Organotin polymers as anticancer and antiviral agents, *J. Organomet. Chem.* 751 (2014) 67–82.
- [70] J.S. White, J.M. Tobin, J.J. Cooney, Organotin compounds and their interactions with microorganisms, *Can. J. Microbiol.* 45 (1999) 541–554.
- [71] T.S.B. Baul, Antimicrobial activity of organotin(IV) compounds: a review, *Appl. Organomet. Chem.* 22 (2008) 195–204.
- [72] M.S. Refat, I.M. El-Deen, Z.M. Anwer, Z.E. Ghol, Bivalent transition metal complexes of coumarin-3-yl thiosemicarbazone derivatives: spectroscopic, antibacterial activity and thermogravimetric studies, *J. Mol. Struct.* 920 (2009) 149–162.
- [73] R.V. Singh, P. Chaudhary, S. Chauhan, M. Swami, Microwave-assisted synthesis, characterization and biological activities of organotin(IV) complexes with some thio schiff bases, *Spectrochim. Acta A* 72 (2009) 260–268.
- [74] M.T. Kaczmarek, R. Jastrzab, E.H. Kedzia, W.R. Paryzek, Self-assembled synthesis, characterization and antimicrobial activity of zinc(II) salicylaldehyde complexes, *Inorg. Chim. Acta* 362 (2009) 3127–3133.
- [75] M.V. Angelusiu, S.F. Barbuceanu, C. Draghich, G.L. Almajan, New Cu(II), Co(II), Ni(II) complexes with aryl-hydrazono based ligand. Synthesis, spectroscopic characterization and *in vitro* antibacterial evaluation, *Eur. J. Med. Chem.* 45 (2010) 2055–2062.
- [76] R.V. Singh, N. Fahmi, M.K. Biyala, Coordination behavior and biopotency of N and S/O donor ligands with their palladium(II) and platinum(II) complexes, *J. Iran. Chem. Soc.* 2 (2005) 40–46.
- [77] S.K. Dubey, U. Roy, Biodegradation of tributyltins (organotins) by marine bacteria, *Appl. Organomet. Chem.* 17 (2003) 3–8.
- [78] N.N. Goh, C.K. Chu, L.E. Khoo, D. Whalen, G. Eng, F.E. Smith, R.C. Hynes, The synthesis, structural characterization and biocidal properties of some triorganotin(IV) esters of *N*-arylidene- $\omega$ -amino acids, *Appl. Organomet. Chem.* 12 (1998) 457–466.
- [79] L.S.Z. Rivera, R.G. Tellez, G.L. Mendonza, A.M. Pacheco, E. Flores, H. Hopfl, V. Barba, F.J. Fernandez, N. Caribol, H.I. Beltran, Synthesis, characterization, biocidal and toxicological activities of di-*n*-butyl- and diphenyl-tin(IV)-Salicyliden- $\beta$ -amino alcohol derivatives, *Inorg. Chem.* 44 (2005) 5370–5378.
- [80] H. Pruchnik, T.T. Kral, D. Poradowski, A. Pawlak, A. Drynda, B. Obminka-Mrukowicz, M. Hof, New cytotoxic butyltin complexes with 2-sulfobenzoic acid: molecular interaction with lipid bilayers and DNA as well as *in vitro* anticancer activity, *Chem. Biol. Interact.* 243 (2016) 107–118.
- [81] M. Sands, M.A. Kron, R.B. Brown, Pentamidine: a review, *Rev. Infect. Dis.* 7 (1985) 625–634.
- [82] T.M. Lima, M.F. Cury-Boaventura, G. Giannocco, M.T. Nunes, R. Curi, Comparative toxicity of fatty acids on a macrophage cell line (J774), *Clin. Sci.* 111 (2006) 307–317.
- [83] D.B. Longley, P.G. Johnston, Molecular mechanisms of drug resistance, *J. Pathol.* 205 (2005) 275–292.
- [84] E. Reynolds, J.I. Ross, J.H. Cove, Msr(A) and related macrolide/streptogramin resistance determinants: incomplete transporters? *Int. J. Antimicrob. Agents* 22 (2003) 228–236.



Cite this: *Analyst*, 2019, **144**, 5232

## Flavonoids induce cell death in *Leishmania amazonensis*: *in vitro* characterization by flow cytometry and Raman spectroscopy

Morgana V. Araújo,<sup>a</sup> Aline C. Queiroz,<sup>a</sup> João F. M. Silva,<sup>a</sup> Amanda E. Silva,<sup>a</sup> João K. S. Silva,<sup>a</sup> Girliane R. Silva,<sup>b</sup> Elaine C. O. Silva,<sup>c</sup> Samuel T. Souza,<sup>c</sup> Eduardo J. S. Fonseca,<sup>c</sup> Celso A. Camara,<sup>b</sup> Tania M. S. Silva<sup>b</sup> and Magna S. Alexandre-Moreira<sup>b</sup>\*

Leishmaniasis comprises a group of infectious diseases with worldwide distribution, of which both the visceral and cutaneous forms are caused by *Leishmania* parasites. In the absence of vaccines, efficacious chemotherapy remains the basis for leishmaniasis control. The available drugs are expensive and associated with several secondary adverse effects. Due to these limitations, the development of new antileishmanial compounds is imperative, and plants offer various perspectives in this regard. The present study evaluated the *in vitro* leishmanicidal activity of flavonoids isolated from *Solanum paludosum* Moric. and investigated the mechanisms of cell death induced by them. These compounds were evaluated *in vitro* for their antileishmanial activity against *Leishmania amazonensis* promastigotes and they showed prominent leishmanicidal activity. The EtOAc fraction, gossypetin 3,7,8,4'-tetra-*O*-methyl ether (**1**), and kaempferol 3,7-di-*O*-methyl ether (**3**) were selected to be used in an *in vitro* assay against *L. amazonensis* amastigotes and cell death assays. The flavonoids (**1**) and (**3**) presented significant activity against *L. amazonensis* amastigotes, exhibiting the IC<sub>50</sub> values of 23.3 ± 4.5 μM, 34.0 ± 9.6 μM, and 10.5 ± 2.5 μM for the EtOAc fraction, (**1**), and (**3**), respectively, without toxic effects to the host cells. Moreover, (**1**) and (**3**) induced blocked cell cycle progression at the G1/S transition, ultimately leading to G1/G0 arrest. Flavonoid (**3**) also induced autophagy. Using Raman spectroscopy in conjunction with principal component analysis, the biochemical changes in the cellular components induced by flavonoids (**1**) and (**3**) were presented. The obtained results indicated that the mechanisms of action of (**1**) and (**3**) occurred through different routes. The results support that the flavonoids derived from *S. paludosum* can become lead molecules for the design of antileishmanial prototypes.

Received 23rd May 2019.

Accepted 6th July 2019

DOI: 10.1039/c9an00948e

rsc.li/analyst

## Introduction

Leishmaniasis comprises a group of diseases caused by the protozoa of the genus *Leishmania*, which can affect human beings. Leishmaniasis is considered to be a neglected disease with a major impact on the economically weaker individuals, especially in underdeveloped countries.<sup>1,2</sup> It is the second main cause of death, after malaria, among parasitic diseases caused by protozoa.<sup>3</sup> Despite being a disease affecting millions

of people worldwide, the currently available treatment for leishmaniasis is restricted to a few drugs of the first choice such as pentavalent antimonials, pentamidine, miltefosine, amphotericin B with its derivatives, and paromomycin. The main problem of conventional treatments is the intrinsic or acquired resistance developed by the protozoan. Other restrictions related to the available drugs are a high incidence of adverse effects and toxicity.<sup>4</sup> The clinical symptoms are diverse and are associated with antigenic differences among the *Leishmania* species in addition to hosting genetic and immunological factors.<sup>5</sup>

Due to the lack of better therapies, the identification of novel drugs, compounds, and targets is of interest to researchers worldwide. Natural products are potential sources of new agents for the treatment of neglected tropical diseases, especially those caused by protozoan parasites.<sup>6</sup> Various secondary plant metabolites such as quinones, phenolics and

<sup>a</sup>Laboratory of Pharmacology and Immunity, Institute of Biological Sciences and Health, Federal University of Alagoas, 57020-720 Maceió, Alagoas, Brazil. E-mail: suzana.magna@gmail.com

<sup>b</sup>Phytochemical Bioprospecting Laboratory, Chemistry Department, Federal Rural University of Pernambuco, 52171-900 Recife, Pernambuco, Brazil

<sup>c</sup>Optics and Nanoscopy Group, Institute of Physics, Federal University of Alagoas, 57072-970 Maceió, Alagoas, Brazil

their derivatives, alkaloids, terpenes, and saponins are beneficial for human beings due to their antiparasitic properties and highly selective mode of action. Furthermore, the skeletons of many metabolites have been successfully used to design more pharmacologically active compounds.<sup>7</sup>

An alternative strategy used against *Leishmania* is the use of natural products. Included in the Brazilian biodiversity, the *Solanum* genus is the best representative of the Solanaceae family with 1400 species<sup>8</sup> and is characterized by the production of a variety of glycoalkaloids<sup>9–11</sup> and high occurrence of flavonoids.<sup>12,13</sup>

Some *Solanum* species have been reported to have anti-inflammatory, sedative, anti-spasmodic, anti-epileptic,<sup>14</sup> hypoglycemic, anti-obesity, cholesterol-lowering,<sup>15,16</sup> leishmanicidal, and trypanosomal activities.<sup>17,18</sup> In addition, studies have demonstrated their anticancer activity against hepatoma cells (Hep3B) and tumor cells of lung lines (H441, H520, H661, and H69).<sup>19,20</sup>

In order to identify the biochemical changes induced by flavonoids in the cell behavior, a combined analysis of Raman spectroscopy and principal component analysis was performed. Raman spectroscopy is a highly sensitive vibrational spectroscopic technique that can provide information about the molecular compositions of biological samples.<sup>21,22</sup> For example, by the use of Raman spectroscopic analysis, the secondary structure of the promastigote surface protease was determined<sup>23</sup> in addition to the determination of the uptake of nanoparticles by macrophages,<sup>24</sup> antibiotic resistance,<sup>25</sup> and anticancer drug evaluation.<sup>26</sup> Due to the advantages of being noninvasive and nondestructive, this technique has become a useful tool in the identification of the biochemical changes caused by treatments in biological cells.<sup>27,28</sup> This approach can contribute useful molecular information to assess the effects of flavonoids on cells, which can be applicable to the development of new therapies for the treatment of leishmaniasis.

Therefore, the present study aimed to investigate the leishmanicidal activity, the mechanisms of cell death, and the biochemical changes induced by the flavonoids isolated from *Solanum paludosum* Moric.

## Materials and methods

### Extraction and isolation of flavonoids

The flavonoids were obtained according to the method reported by Silva *et al.*<sup>12</sup> A fraction of the flavonoid mixture (532.5 mg) obtained from the aerial parts of *S. paludosum* was purified by semipreparative high-pressure liquid chromatography with Diode Array Detection (HPLC-DAD). HPLC was conducted using a Shimadzu Prominence chromatograph model CMB-20A (Shimadzu Corporation, Kyoto, Japan) equipped with a UV-Vis detector (SPD-20A), column oven (CTO-20A), solvent pump (LC-20AD), and Luna Phenomenex C-18 column (21 mm × 250 mm × 5 μm, Phenomenex, Aschaffenburg, Germany). The solvents H<sub>2</sub>O (A) and

methanol:acetonitrile (1 : 1, B) were used as the mobile phase. Methanol and acetonitrile were obtained from J.T. Baker (Deventer, The Netherlands), and MilliQ water was used in the following gradient elution: from 0–5 min, 65% B; 5–15 min, 70% B; 15–30%, 75%; 30–32, 100% and detection at 320 nm at a flow rate of 16 mL min<sup>-1</sup>. Five principal flavonoids were isolated: 1 (30.0 mg), 2 (25.0 mg), 3 (29.0 mg), 4 (18.8 mg), and 5 (30.0 mg).

The purity of the compounds was examined by ultra-high pressure liquid chromatography along with quadrupole time of flight mass spectrometry (UHPLC-QTOF-MS/MS) HPLC-DAD-qTOF-MS. The XEVO-G2XSQTOF mass spectrometer (Waters, Manchester, UK) was connected to the ACQUITY UPLC system (Waters, Milford, MA, USA) via an electrospray ionization (ESI) interface. Chromatographic separation of the compounds was performed on ACQUITY UPLC with a conditioned autosampler at 4 °C using an Acquity BEH C18 column (50 mm × 2.1 mm i.d., 1.7 μm particle size) (Waters, Milford, MA, USA). The column temperature was maintained at 40 °C. The mobile phase consisting of water with 0.1% formic acid in water (solvent A) and acetonitrile (solvent B) was pumped at a flow rate of 0.4 mL min<sup>-1</sup>. The gradient elution program was as follows: 0–8 min, 10–80% B; 9–1 min, 80–100% B. The injection volume was 5 μL. MS analysis was performed on Xevo G2 QTOF (Waters MS Technologies, Manchester, UK), a quadrupole time-of-flight tandem mass spectrometer coupled with an electrospray ionisation source in the positive ion mode. The scan range was from 50 to 1200 *m/z* for data acquisition. In addition, the MS<sup>E</sup> experiments were carried out, which allowed both the precursor and production data to be acquired in one injection. The source conditions were as follows: capillary voltage, 3.0 kV; sample cone, source temperature, 120 °C; desolvation temperature 450 °C; cone gas flow rate 50 L h<sup>-1</sup>; desolvation gas (N<sub>2</sub>) flow rate 800 L h<sup>-1</sup>. All analyses were performed using the lock spray, which ensured accuracy and reproducibility. Leucine-enkephalin (5 ng mL<sup>-1</sup>) was used as a standard or reference compound to calibrate the mass spectrometers during analysis and was introduced by a lock spray at 10 μL min<sup>-1</sup> for accurate mass acquisition. All the acquisition and data analyses were controlled using the Waters MassLynx v 4.1 software.

### Parasites

*L. anazonensis* [MHOM/BR/77/LTB0016] strain was maintained *in vitro* as proliferating promastigotes at 26 °C in Schneider's medium (Sigma-Aldrich) supplemented with 10% heat-inactivated fetal bovine serum (Sigma-Aldrich), gentamycin (1 mg L<sup>-1</sup>) (Sigma-Aldrich), L-glutamine (2 mM) (Sigma-Aldrich), and 2% sterile human urine. In the culture, the promastigote forms were cultured extracellularly and took an estimated 7 days to complete their life cycle. After the third day, the promastigote forms were in the exponential phase of growth and then, they were used in the third passage, a phase in which the parasites could infect the macrophages in the assay of *in vitro* infection.

### Animals

Swiss mice (six-to-eight weeks old) were obtained from the Central Animal House of the Federal University of Alagoas in order to obtain the peritoneal macrophages. These studies were approved by the Ethics Committee for Animal Experimentation of the Federal University of Alagoas (Brazil) (protocol no. 2015.01).

### Macrophages

Peritoneal macrophages were obtained from Swiss mice (weighing 20–25 g) through peritoneal lavage with 10 mL of cold PBS (Phosphate-Buffered Saline; 137 mM NaCl, 8 mM Na<sub>2</sub>HPO<sub>4</sub> (Vetec Química fina), 2.7 mM KCl (Vetec Química fina), 1.5 mM KH<sub>2</sub>PO<sub>4</sub> (Vetec Química fina), pH 7.0). The peritoneal exudate cells were centrifuged at 1500 rpm for 5 min and the pellet was resuspended in an RPMI-1640 medium (Sigma-Aldrich) supplemented with 10% heat-inactivated fetal bovine serum, gentamycin (1 mg L<sup>-1</sup>), L-glutamine (2 mM), and sodium pyruvate solution (2 mM) (Sigma-Aldrich). The cells were then counted and seeded into 96-well plates for the cytotoxicity assay and into 24-well plates for the intracellular amastigote assay.

### Cytotoxicity assay using the macrophages

Peritoneal macrophages were seeded ( $3 \times 10^4$  cells per well) in 96-well plates containing 100  $\mu$ L of media. The cells were allowed to attach to the bottom of the well for 24 h at 37 °C and then treated with different concentrations (1, 10, and 100  $\mu$ M) of flavonoids or pentamidine (Sigma-Aldrich) previously diluted in RPMI-1640 medium with dimethyl sulfoxide (0.1% DMSO) (Sigma-Aldrich). The plates were maintained in a 5% CO<sub>2</sub> incubator at 37 °C for 48 h. The cells were also cultured in media free from compounds, a vehicle (basal growth control), or media with 0.1% DMSO (vehicle control). Thereafter, the supernatant was removed and the cells were incubated with 3-(4,5-dimethylthiazol-2-yl)-2,5-diphenyltetrazolium bromide (MTT) (Sigma-Aldrich) (100  $\mu$ L per well) for 1 h in the dark at 37 °C. The MTT solution was then removed, the cells were resuspended in 100  $\mu$ L of DMSO, and the absorbance was measured using an ELISA reader at 550 nm.

### Leishmanicidal activity assay

*L. amazonensis* promastigotes ( $2 \times 10^6$  cells per mL) were maintained *in vitro* in Schneider's medium supplemented with 10% FBS and 2% human urine in the presence of various concentrations of flavonoids and pentamidine (0.1, 1.0, 10, and 100  $\mu$ M) for 48 h at 26 °C. The cells were also cultured in media free from compounds (basal growth control) or with 0.1% DMSO (vehicle control). The promastigotes were adjusted to a concentration of  $10^2$  cells per mL in PBS and the viable cells were counted in a Neubauer's chamber.

### Intracellular amastigote assay

Peritoneal cavity macrophages of Swiss mice were seeded on glass coverslips (13 mm diameter) in 24-well plates and incu-

bated at 37 °C with 5% CO<sub>2</sub> for 12 hours for adhesion. The macrophages were infected with *L. amazonensis* promastigotes using a ratio of 1:10 at 37 °C overnight in isolated experiments. Non-internalized promastigotes were removed by washing (three times) with PBS. The infected macrophages were treated with concentrations of 0.1, 1.0, and 100  $\mu$ M of the EtOAc fraction, (1), and (3) flavonoids and maintained at 37 °C in 5% CO<sub>2</sub> for 48 h. The glass coverslips were fixed with methanol and stained with May-Grünwald-Giemsa (Sigma-Aldrich) and then, the intracellular amastigotes were counted (one hundred macrophages were evaluated per glass coverslip). The data were expressed as the infection index (percentage of infected macrophages multiplied by the average number of amastigotes per macrophage).

### Cell cycle analysis

The cell cycle assay was performed according to the instructions of the Muse® Cell Cycle Kit. *L. amazonensis* promastigotes ( $10^5$  cells per mL) were treated with pentamidine, (1), and (3) at a concentration of 100  $\mu$ M for 48 h. After the incubation period, the cells were centrifuged and the pellets were resuspended in 1 mL of PBS supplemented with 1% FBS to wash the cells; then, they were fixed with 70% ethanol for 3 hours at -20 °C. After fixation, 200  $\mu$ L of each cell suspension was centrifuged and washed with PBS, and the pellets were resuspended in 200  $\mu$ L of Muse® Cell Cycle reagent. After incubation for 30 min at room temperature and protection from light, data acquisition was carried out by flow cytometry on a Muse® Cell Analyzer and analyzed using the Muse™ 1400 Analysis software.

### Analysis of phospholipid externalization in *L. amazonensis* promastigotes by flow cytometry

The quantification of the percentage of parasites undergoing apoptosis or necrosis was performed according to the instructions of the Annexin Muse® & Dead Cell Kit. Exponential-phase *L. amazonensis* promastigotes ( $10^5$  cells per mL) were incubated with pentamidine, (1), and (3) (10  $\mu$ M and 100  $\mu$ M for 48 h). After the incubation period, the cells were centrifuged and resuspended in PBS supplemented with 1% FBS to wash the cells. Subsequently, 100  $\mu$ L of each cell suspension was incubated with 100  $\mu$ L of the reagent containing Annexin V-PE and 7-AAD for 30 min at room temperature with protection from light. Data acquisition was carried out by flow cytometry on a Muse® Cell Analyzer and the analysis was performed using the Muse® 1400 Analysis software.

### Determination of caspase-like proteases

To determine the percentage of caspase-positive cells, the Muse® Multicaspase kit was used to perform the analysis according to the instructions of the manufacturer. *L. amazonensis* promastigotes were grown to the concentration of  $10^5$  cells per mL and then treated with pentamidine, (1), and (3) at a concentration of 100  $\mu$ M and incubated at 26 °C. After 48 h, 1 mL of the cell culture was pelleted and resuspended in 1 mL of PBS buffer supplemented with 1% FBS.

Muse® Multicaspase Reagent followed by 7-AAD was added. Data acquisition was carried out using a Muse® Cell Analyzer and analyzed using the Muse® 1400 Analysis software.

#### Assay of autophagy

The determination of autophagy induction was performed according to the instructions of the Muse® Autophagy LC3-based antibody kit. *L. amazonensis* promastigotes ( $5 \times 10^4$  cells per mL) were incubated with pentamidine, (1) and (3) at a concentration of 100  $\mu$ M for 48 h. After the incubation period, the contents of each well were transferred to microcentrifuge tubes and centrifuged, and the pellets were resuspended in PBS supplemented with 1% FBS to wash the cells. Subsequently, the content was treated with reagent autophagy A for 3 hours at 37 °C. Each cell suspension was then centrifuged and the pellet was resuspended in 200  $\mu$ L of a solution containing reagent autophagy B and anti-LC3 Alexa Fluor®555. After 30 min of incubation on ice and protection from light, the tubes were centrifuged and the pellets were resuspended in the assay buffer. Data analysis was performed using the Muse® 1400 Analysis software.

#### Raman spectroscopic measurements

Raman spectroscopy was performed on infected macrophages according to the methodology described in "Intracellular Amastigote Assay"; however, the fixation process was with 4% glutaraldehyde (Sigma-Aldrich) for 5 min. Raman spectra were obtained using a Horiba XploRA spectrometer coupled to an Olympus microscope and equipped with a 532 nm laser that was focused on the nucleus of the cells through a 100 $\times$  objective lens (NA = 0.9). The same objective lens was used for collecting the Raman scattered light after interaction with the sample in a backscattering geometry. The frequency calibration was set by the reference to the 520  $\text{cm}^{-1}$  vibrational band of a silicon wafer. Under the same conditions, 50 cell spectra for each group were obtained in the spectral range from 800 to 1800  $\text{cm}^{-1}$ . In order to minimize the laser-induced heating of the specimens, a lower power irradiation at the sample surface was used of about 5 mW for a short exposure time (1 s laser exposure for 15 accumulations). The diffraction grating used had 1200 lines per millimeter, and the spectral resolution of the system was 1.5  $\text{cm}^{-1}$ .

#### Data preprocessing and spectral analysis

Before conducting the spectral analysis, all the spectra were smoothed, background-adjusted, and normalized using an algorithm implemented in the MatLab software. After removing the fluorescence background from the spectra, principal component analysis (PCA) was performed. PCA is a multivariate technique that transforms the given data into a set of new orthogonal variables called the principal components (PCs), which are responsible for the significant spectral variation. This technique extracts the important information from the data and identifies the patterns that reveal the main characteristics of the analyzed set. The PCs are ordered so that the first few retain most of the variations present in all of the

original variables. Each successive component accounts for the residual variance that is not captured by the previous component and so on.<sup>29</sup> Usually, most of the variance is contained in the first three principal components (PC1, PC2, and PC3). PCA is a suitable statistical method for biological samples due to its successful applications in cell sorting.<sup>30,31</sup>

#### Statistical analysis

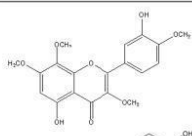
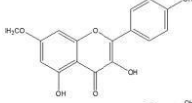
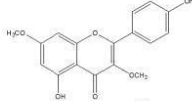
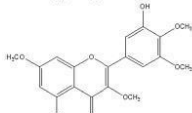
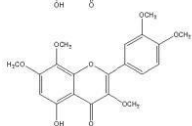
Data were expressed as the mean  $\pm$  S.E.M. and significant differences between the treated and control groups were evaluated using ANOVA and Dunnett's *post-hoc* tests using the Graph Pad Prism 5.0 software; 95% confidence intervals were also included.

## Results

### Chemistry

The chemical study of the fraction of flavonoids obtained from the aerial parts of *S. paludosum* resulted in the characterization of five flavonoids by UPLC-DAD-TOF-MS/MS. Five principal compounds (1–5, Table 1) were isolated and the structures of 1, 2, 3, and 5 were compared with the patterns of flavonoids previously isolated from *S. paludosum*.<sup>12,13</sup> The flavonoid 4 was

**Table 1** Chemical data of flavonoids 1–5. 3,7,3',4'-Tetra-*O*-methyl myricetin (4) ion at  $m/z$  389.1230 [ $M + H$ ]<sup>+</sup> (calcd for  $C_{20}H_{21}O_8$ , 389.1230) and gossypetin 3,7,8,3',4'-penta-*O*-methyl ether (5) 389.1230 [ $M + H$ ]<sup>+</sup> (calcd for  $C_{20}H_{21}O_8$ , 389.1230)

Compounds	Molecular weight (g)	Chemical name
1 	300	Gossypetin 3,7,8,4'-tetra- <i>O</i> -methyl ether
2 	374	Kaempferol 7- <i>O</i> -methyl ether
3 	314	Kaempferol 3,7-di- <i>O</i> -methyl ether
4 	360	Myricetin 3,7,3',4'-tetra- <i>O</i> -methyl ether
5 	388	Gossypetin 3,7,8,3',4'-penta- <i>O</i> -methyl ether

identified by various spectroscopies (UV, IR,  $^1\text{H}$  NMR,  $^{13}\text{C}$  NMR, 2D NMR, and MS), and it was readily identified by the direct comparison of its spectroscopic data with the literature data.<sup>32</sup> This flavonoid is being reported for the first time in the *Solanum* genus.

The structures of the known isolated compounds were confirmed by their HR-ESI-MS spectra as gossypetin 3,7,8,4'-tetra-*O*-methyl ether (1) ion at  $m/z$  375.1072  $[\text{M} + \text{H}]^+$  (calcd for  $\text{C}_{19}\text{H}_{19}\text{O}_8$ , 375.1074), kaempferol 7-*O*-methyl ether (2) ion at  $m/z$  301.0707  $[\text{M} + \text{H}]^+$  (calcd for  $\text{C}_{16}\text{H}_{13}\text{O}_6$ , 301.0706), kaempferol 3,7-di-*O*-methyl ether (3) ion at  $m/z$  315.0565  $[\text{M} + \text{H}]^+$  (calcd for  $\text{C}_{17}\text{H}_{15}\text{O}_6$ , 315.0863), myricetin 3,7,3',4'-tetra-*O*-methyl ether (4) ion at  $m/z$  389.1230  $[\text{M} + \text{H}]^+$  (calcd for  $\text{C}_{20}\text{H}_{21}\text{O}_8$ , 389.1230), and gossypetin 3,7,8,3',4'-penta-*O*-methyl ether (5) 389.1230  $[\text{M} + \text{H}]^+$  (calcd for  $\text{C}_{20}\text{H}_{21}\text{O}_8$ , 389.1230).

#### Viability of peritoneal macrophages

The effect of the EtOAc fraction and flavonoids of *S. paludosum* on murine peritoneal macrophages was assessed by quantitative colorimetric MTT assays after 48 h of incubation. The macrophages were treated with flavonoid compounds (1, 10, and 100  $\mu\text{M}$ ) to investigate the potential toxic effects on mammalian cells. Table 2 shows the results for the flavonoid compounds and pentamidine (reference standard drug). Pentamidine and only flavonoid (3) showed the same deleterious activity to the host cells, as evidenced by the MTT assay, with the maximum cytotoxicities of  $72.1 \pm 4.8\%$  and  $47.9 \pm 8.2\%$ , respectively. However, flavonoid (3) exhibited a  $\text{CC}_{50}$  value (the concentration that causes 50% of the cytotoxicity in macrophages) greater than the maximum concentration tested; the standard drug pentamidine, on the other hand, showed  $\text{CC}_{50}$  of  $68.2 \pm 3.8$   $\mu\text{M}$ .

#### In vitro evaluation of the antipromastigote activity of flavonoids

An initial screening was carried out to evaluate and compare the *in vitro* leishmanicidal profiles of the flavonoid compounds

and pentamidine against the proliferation of the exponentially growing promastigote form of *L. amazonensis*. The maximum effects and the  $\text{IC}_{50}$  values (concentrations causing 50% inhibition of promastigote growth) were used as parameters for leishmanicidal activity (Table 2). After 48 h of incubation, the EtOAc fraction and the isolated compounds (1), (2), and (3) exhibited antileishmanial activities against *L. amazonensis* promastigotes with maximum effects of  $84.3 \pm 5.5\%$ ,  $82.6 \pm 7.6\%$ ,  $48.8 \pm 1.7\%$ , and  $83.7 \pm 2.6\%$ , respectively. The EtOAc fraction, (1), and (3) exhibited the  $\text{IC}_{50}$  values of  $63.0 \pm 2.3$   $\mu\text{M}$ ,  $44.0 \pm 6.0$   $\mu\text{M}$ , and  $54.2 \pm 2.2$   $\mu\text{M}$ , respectively; they were as potent and effective as pentamidine (with the efficacy of  $90.4 \pm 5.5\%$  and  $\text{IC}_{50}$  of  $24.3 \pm 5.3$   $\mu\text{M}$ ) against *L. amazonensis* promastigotes. In contrast, (4) and (5) did not present activity against the promastigote form of *L. amazonensis* up to 100  $\mu\text{M}$  (Table 2). Based on the viability of the macrophage cells and *L. amazonensis* promastigotes, it was possible to calculate the selectivity index (SI) of the compounds (Table 2). Thus, when comparing the SI values of the macrophage and *L. amazonensis* promastigote, the flavonoids (2), (4), and (5) did not show selectivity for *L. amazonensis*. In addition, the EtOAc fraction and flavonoids (1) and (3) were probably selective for *L. amazonensis*; however, as their  $\text{CC}_{50}$  values were not determined, it was not possible to calculate SI for *L. amazonensis*. Pentamidine showed 2.81 times more selectivity for the parasites (Table 2).

#### In vitro evaluation of the antiamastigote activity of flavonoids

The EtOAc fraction, (1), and (3) were selected for testing against the amastigote forms for displaying the best data with the activity against the promastigotes of the two tested *Leishmania* species. In this study, the EtOAc fraction, (1), and (3) inhibited the amastigote growth with the maximum efficacy values of  $85.6 \pm 0.0\%$ ,  $72.2 \pm 13.7\%$ , and  $88.8 \pm 0.9\%$ , respectively. The EtOAc fraction, (1), and (3) exhibited the  $\text{IC}_{50}$  values of  $23.3 \pm 4.5$   $\mu\text{M}$ ,  $34.0 \pm 9.6$   $\mu\text{M}$ , and  $10.5 \pm 2.5$   $\mu\text{M}$ , respectively (Table 3).

**Table 2** Effect of pentamidine, EtOAc fraction, and flavonoid compounds (1–5) of *S. paludosum* against the macrophages or the promastigote form of *L. amazonensis*

Substances	Peritoneal macrophages		<i>L. amazonensis</i> promastigotes		SI <sup>c</sup>
	$\text{CC}_{50}$ <sup>a</sup> ( $\mu\text{M}$ )	Maximum cytotoxicity <sup>b</sup> (%)	$\text{IC}_{50}$ <sup>a</sup> ( $\mu\text{M}$ )	Maximum effect <sup>b</sup> (%)	
Pentamidine	$68.2 \pm 3.8$	$72.1 \pm 4.8^{**}$	$24.3 \pm 5.3$	$90.4 \pm 5.5^{***}$	2.81
EtOAc fraction	>100	ND	$63.0 \pm 2.3$	$84.3 \pm 5.5^{***}$	>1.19
(1)	>100	ND	$44.0 \pm 6.0$	$82.6 \pm 7.6^{***}$	>2.27
(2)	>100	ND	>100	$48.8 \pm 1.7^{**}$	—
(3)	>100	$47.9 \pm 8.2^*$	$54.2 \pm 2.2$	$83.7 \pm 2.6^{***}$	>1.84
(4)	>100	ND	>100	NA	—
(5)	>100	ND	>100	NA	—

<sup>a</sup>Cytotoxic Concentration 50 ( $\text{CC}_{50}$ ) calculated by the concentration-response curves. <sup>b</sup>Maximum Cytotoxicity or Maximum Effect (ME) is expressed as a mean  $\pm$  standard error of maximum toxicity, average of the triplicates of a representative experiment. <sup>c</sup>Selectivity Index (SI) calculated from the ratio of  $\text{CC}_{50}$  values of the macrophage and  $\text{IC}_{50}$  of the promastigotes. (—): Substance does not have a deleterious effect on the macrophage or *Leishmania*. The values of cytotoxicity or maximum effect were considered significant when  $^*p < 0.05$ ,  $^{**}p < 0.01$ , and  $^{***}p < 0.001$  compared to the DMSO group. ND: Not determined. Maximum Cytotoxicity to cell until the concentration of 100  $\mu\text{M}$  compared to the DMSO group. NA: compound is not active.

**Table 3** Leishmanicidal activity of the flavonoid compounds against the growth of amastigotes of *L. amazonensis*

Treatment	IC <sub>50</sub> <sup>a</sup> (μM)	Efficacy <sup>b</sup> (%)
Pentamidine	6.4 ± 0.1	99.91 ± 0.04***
EtOAc fraction	23.3 ± 4.5	85.6 ± 0.0***
(1)	34.0 ± 9.6	72.2 ± 13.7***
(3)	10.5 ± 2.5	88.8 ± 0.9***

Data are reported as the mean ± standard error of the mean, S.E.M. <sup>a</sup>IC<sub>50</sub> is the concentration required to cause 50% inhibition. <sup>b</sup>The efficacy values were considered significant when \**p* < 0.05, \*\**p* < 0.01, and \*\*\**p* < 0.001 compared to the 0.1% DMSO group.

### Cell cycle analysis

After the *in vitro* leishmanicidal activity of (1) and (3) was characterized, other studies were conducted to investigate the mechanism of cell death by these compounds. The *Leishmania* cell cycle was analyzed by flow cytometry after treatment with pentamidine, (1), and (3) at a concentration of 100 μM for 48 hours (Fig. 1). The analysis of the cell population in different cell cycle phases was possible after staining with 7-AAD and subsequent analysis by flow cytometry. In Fig. 1, it is observed that pentamidine, (1), and (3) can induce changes in the cell cycle (in the G0/G1, S, and G2/M phases) of *L. amazonensis* promastigotes after 48 h of treatment.

### Analysis of externalized phosphatidylserine (PS)

In order to determine the mechanism by which the flavonoid compounds exert their antiproliferative activity against the parasites, flow cytometric analyses using Annexin V-PE and 7-AAD were performed to investigate the externalization of phospholipids or the rupture of the cytoplasmic membrane. As demonstrated in Fig. 2, flavonoids (1) and (3) do not induce cell death through the induction of necrosis or apoptosis in *L. amazonensis* promastigotes after 48 h of incubation at the concentrations of 10 and 100 μM. Additionally, the caspase-like activation did not occur in the promastigotes treated with flavonoids (1) or (3) at 100 μM for 48 hours (Fig. 3).

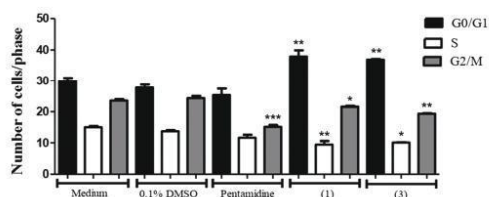


**Fig. 1** Cell cycle distribution of *L. amazonensis* promastigotes. Analysis using flow cytometry after treatment with 10 μM pentamidine and 100 μM (1) and (3) flavonoids for 48 h. Values represent means ± SEMs for three samples.

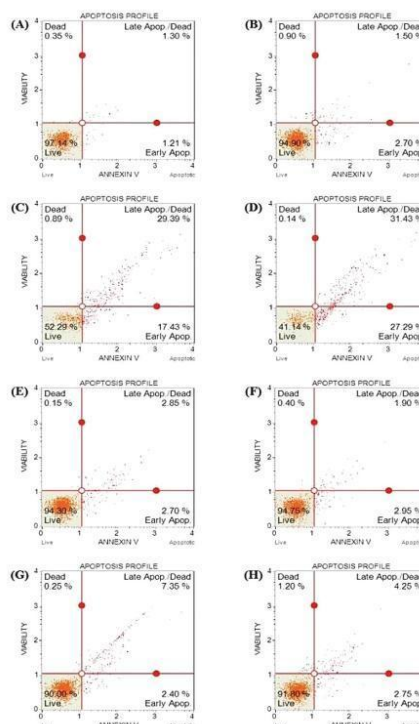


**Fig. 2** Phospholipid externalization of *L. amazonensis* promastigotes. Analysis using flow cytometry after treatment with 10 and 100 μM pentamidine and flavonoids (1) and (3) for 48 h. (A) Medium; (B) 0.1% DMSO; (C) 100 μM pentamidine; (D) 10 μM pentamidine; (E) 100 μM (1); (F) 10 μM (1); (G) 100 μM (3); (H) 10 μM (3).

### Detection of autophagy by flow cytometry

Next, we evaluated the induction of autophagic cell death in *L. amazonensis* promastigotes treated with (1) and (3) at a concentration of 100 μM for 48 hours. The treatment with (3) altered the mean of autophagy intensity in the promastigotes, showing that the antiproliferative activity of these compounds is probably also the result of an exacerbated autophagic process (Fig. 4).

### Raman spectra of the macrophages infected with *L. amazonensis*

Through a Raman spectrum, it is possible to evaluate the responses induced by the treatments in cells and identify the most important spectral differences among the cell groups. The main bands observed in the spectra of the cells were in the regions corresponding to the C–C stretching of the proline ring at 920 cm<sup>-1</sup>, the phenylalanine peaks at 1002 and 1030 cm<sup>-1</sup>, the DNA phosphodi-oxo group PO<sub>2</sub><sup>-</sup> symmetric stretching at 1095 cm<sup>-1</sup>, a band centered at 1240 cm<sup>-1</sup> related

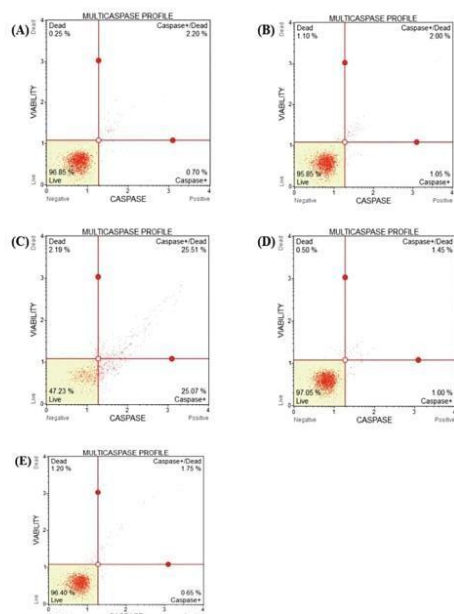


Fig. 3 Determination of the presence of active caspase-like proteases in *L. amazonensis* promastigotes. Analysis using flow cytometry after treatment with 100  $\mu\text{M}$  pentamidine and flavonoids (1) and (3) for 48 h. (A) Medium; (B) 0.1% DMSO; (C) 100  $\mu\text{M}$  pentamidine; (D) 100  $\mu\text{M}$  (1); (E) 100  $\mu\text{M}$  (3).

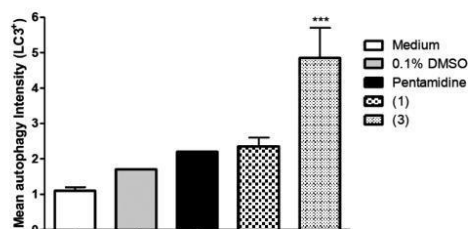


Fig. 4 Determination of the presence of autophagic LC3<sup>+</sup> in *L. amazonensis* promastigotes incubated with pentamidine and flavonoids (1) and (3) (100  $\mu\text{M}$ ) for 48 h and analyzed by flow cytometry. Values represent means  $\pm$  SEMs for three samples.

to RNA, the corresponding vibrations of the DNA bases adenine and guanine at 1317 and 1578  $\text{cm}^{-1}$ , the 1446  $\text{cm}^{-1}$  band corresponding to the C–H deformation vibrations, and the vibrations in the amide I band centered at 1657  $\text{cm}^{-1}$ . The Raman band assignments used in the interpretation of the spectral features were carried out based on the published literature.<sup>33</sup>

The spectral regions with the most significant variations were pointed out based on the calculated spectral difference between the cell groups. As illustrated in Fig. 5(A), the Raman spectra of the cells cultured in the medium free from compounds and those with 0.1% DMSO displayed similar patterns, indicating that these cell groups have very similar spectral characteristics. The differences between the Raman spectra of the DMSO group cells and pentamidine group cells can be seen in Fig. 5(B). The spectral changes can be observed in practically the entire analyzed region. The peaks at 920, 1002, 1030, 1446, and 1657  $\text{cm}^{-1}$  correspond to proteins, whereas the peaks at 1095, 1240, 1317, and 1578  $\text{cm}^{-1}$  correspond to nucleic acids. The differences in these regions indicate that there are variations in the amounts of proteins and nucleic acids among the cells.

In Fig. 5(C), it is observed that among the DMSO group cells and the cells treated with flavonoid (1), the main variations also occur in a large part of the analyzed spectral region. The cells treated with flavonoid (1) showed a smaller amount of proteins, as indicated by the less intense peaks at 1002, 1030, 1446, and 1657  $\text{cm}^{-1}$ . Although the peak at 1578  $\text{cm}^{-1}$  increased slightly, the amount of nucleic acids in the cells treated with flavonoid (1) seemed to be smaller, as indicated by the less intense peaks at 1240 and 1317  $\text{cm}^{-1}$ . Important spectral variations were also observed in the differ-

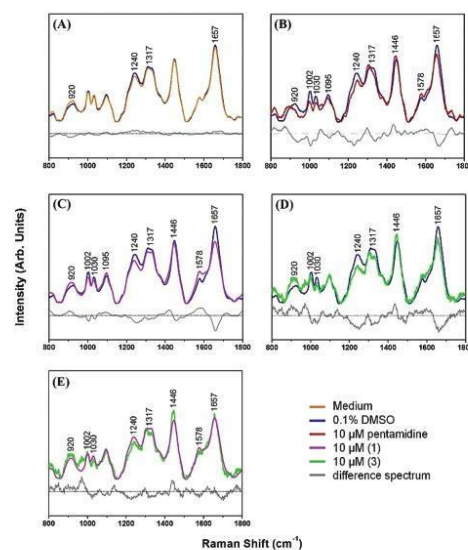


Fig. 5 Raman spectra of macrophages infected with *L. amazonensis* exposed to different treatments. The Raman spectra are the averages of 50 cells for each group in the fingerprint region (800–1800  $\text{cm}^{-1}$ ). (A) 0.1% DMSO and Medium; (B) 0.1% DMSO and 10  $\mu\text{M}$  pentamidine; (C) 0.1% DMSO and 10  $\mu\text{M}$  (1); (D) 0.1% DMSO and 10  $\mu\text{M}$  (3), and (E) 10  $\mu\text{M}$  (1) and 10  $\mu\text{M}$  (3). The gray lines represent the computed difference spectrum between the cell groups.

ence spectrum of the cells of the DMSO group and the cells treated with flavonoid (3), as can be observed in Fig. 5(D). Among the regions with the highest spectral variations are the bands at 920, 1002, 1030, 1446, and 1657  $\text{cm}^{-1}$ , corresponding to proteins, and the bands at 1240 and 1317  $\text{cm}^{-1}$  related to nucleic acids. The spectrum of the cells treated with flavonoid (3) showed considerable decrease in the intensity of the peaks corresponding to the nucleic acids. This indicates that the DNA of these cells was lowered greatly.

Finally, as shown in Fig. 5(E), an analysis was performed between the cells treated with flavonoids (1) and (3). The most significant spectral variations occurred in the following regions: 920, 1030, 1446, and 1657  $\text{cm}^{-1}$  (corresponding to proteins) and 1240, 1317, and 1578  $\text{cm}^{-1}$  (corresponding to nucleic acids). The decrease in the intensity of the peaks corresponding to the nucleic acids in the cells treated with flavonoid (3) reiterates the results reported in Fig. 5(D) and may indicate cell death.

### Spectral classification based on PCA

The small differences observed in the Raman spectra may be sufficient to differentiate and classify the different groups of cells. Through multivariate statistical methods, it was possible to make this differentiation and prove that the treatments had in fact affected the cellular biochemical composition. Herein, PCA was used for the classification of the cellular groups and interpretation of the spectral data. As seen in Fig. 6(A), the cells of the DMSO group (blue dots) can be separated from the cells of the Medium group (orange dots) by the first two PCs. This demonstrates that even in the groups of cells where the spectral characteristics are quite similar, PCA can successfully classify the samples. The first two PCs explained 51% of the

variance of the original data set, with PC1 describing 37% and PC2 describing 14% of the total variance.

The distribution of the cells of the DMSO, pentamidine (red dots), and flavonoid (1) (pink dots) groups is observed in Fig. 6(B). The cells were classified based on the first two PCs, which explained 59% of the total variance. Based on the distribution presented, the pentamidine treatment caused a large dispersion of the samples, indicating that in this group, there are cells quite different from each other. A region of overlap can also be observed for the samples under treatment, indicating that although there are significant differences between the groups, many spectra were similar. An analogous comparison between the cells of the DMSO, pentamidine, and flavonoid (3) (green dots) groups is presented in Fig. 6(C). The first two PCs explained 52% of the variance of the original data set, with PC1 describing 30% and PC2 describing 22%. In this analysis, it was observed that both treatments caused great dispersion of the samples, evidencing quite different spectra within each of the groups.

The PCA score plots presented in Fig. 6(D) show the distribution of the cells of the DMSO and (1) and (3) flavonoid groups. The first two PCs used in this comparison accounted for 64% of the variance of the original data set. The distribution presented evidenced the spectral differences among the groups exposed to the treatments, corroborating with the results of the analyses of flow cytometry, which demonstrated that the flavonoids (1) and (3) have different mechanisms of action. The grouping of the samples into three clusters indicated that the systematic differences between the Raman spectra can be revealed easily by PCA.

## Discussion

Considering the low efficacy of the available drugs for the treatment of leishmaniasis as well as their side effects and the resistance developed by parasites, research using natural products, mainly due to the properties of the bioactive compounds found in the crude extracts of medicinal plants, may lead to the discovery of new therapies with high efficiency, which are cheap and safe for patients.<sup>34</sup> Hence, the purpose of this research was to study the antileishmanial effects of the flavonoid compounds isolated from the EtOAc fraction of *S. paludosum* and to investigate the mechanisms involved in cell death.

Previous studies with *Solanum* species have demonstrated various pharmacological activities, including activity against trypanosomatids, such as *L. amazonensis* and *Trypanosoma cruzi*.<sup>17,18</sup> In this study, the flavonoids showed pronounced leishmanicidal activity against the promastigotes of *L. amazonensis* with emphasis on the EtOAc fraction and flavonoids (1) and (3), which have also exhibited leishmanicidal activity against promastigotes of *L. chagasi* (data not show).

The activities of the compounds against promastigotes and amastigotes can differ depending on the targets of the antileishmanial action, which may be selective for one of the two

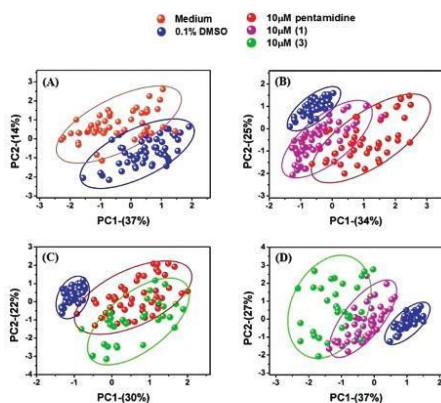


Fig. 6 Principal component analysis (PCA) of the macrophages infected with *L. amazonensis*. PCA score plots for (A) 0.1% DMSO and Medium; (B) 0.1% DMSO, 10  $\mu\text{M}$  pentamidine, and 10  $\mu\text{M}$  (1); (C) 0.1% DMSO, 10  $\mu\text{M}$  pentamidine, and 10  $\mu\text{M}$  (3); and (D) 0.1% DMSO, 10  $\mu\text{M}$  (1), and 10  $\mu\text{M}$  (3).



developmental forms. Overall, promastigotes may be more sensitive than intracellular amastigotes because amastigotes are adapted to survive in a hostile intracellular environment as well as due to the fact that the compounds have direct contact with promastigotes. In contrast, in order to have anti-amastigote activity, the substances must be capable of crossing the membrane of the host cell. The EtOAc fraction and flavonoids (1) and (3) were then subjected to the amastigote assay and besides the observed efficacy, they were found to be highly potent against the growth of *L. amazonensis* amastigotes, exhibiting the IC<sub>50</sub> values of 23.3 ± 4.5 μM (EtOAc fraction), 34.0 ± 9.6 μM (1 flavonoid), and 10.5 ± 2.5 μM (3 flavonoid). The data corroborated the results reported by Wong *et al.*;<sup>35,36</sup> they tested the flavonoid dimers and found potent leishmanicidal activity similar to the results observed by Abreu-Miranda *et al.*,<sup>18</sup> who tested the glycoalkaloids isolated from *S. lycocarpum* against the promastigotes of *L. amazonensis*.

In addition, there are few studies about flavonoids (1) and (3). It was found that the flavonoid (1) was isolated from *Fagoniaboveana*<sup>37</sup> and *Ricinocarpus stylosus*.<sup>38</sup> It was also demonstrated that this flavone did not induce the activation of apoptosis as it did not present antitubulin activity in HL60 cells.<sup>39</sup> In the case of flavonoid (3), this flavonolaglycone was isolated from *Siparunagigantotepala*<sup>40</sup> and *Cistus ladanifer*.<sup>41</sup> Thus, this paper demonstrated the leishmanicidal activity of these flavonoids for the first time.

Although a screening for leishmanicidal activity is important to select promising substances, understanding the mechanism of action by which they inhibit the parasitic growth or cause parasite death is necessary to find specific targets. In the cell cycle assay, flavonoids (1) and (3) induced significant increase in the proportion of cells in the G0/G1 phase, a stage of cell cycle which cells have split and the cells have only one copy of their DNA. These treatments significantly decreased the proportion of promastigotes at the S and G2/M phases. These data suggest that there is accumulation of cells in the G0/G1 phase due to prolonging of the G1 phase or arrest of cell cycle progression through the G1/S restriction point. Other studies also reported the induction of arrest in the G0/G1 phase by leishmanicidal compounds. For example, the dibenzalacetone treatment changed the profile of the cell cycle with an increase in the G0/G1 population associated with the decrease in the S (synthesis) and G2/M phases of the *L. donovani* promastigotes.<sup>42</sup>

Morphological, biochemical, or molecular changes lead to parasite death or prevent parasite proliferation.<sup>43</sup> The cell death pathways can be generally classified into apoptosis, necrosis, and exacerbation of the autophagic processes.<sup>44</sup> To determine the way by which the tested flavonoids exert their antiproliferative activity, flow cytometry analysis was performed using annexin V-PE to investigate the externalization of phospholipids, a typical characteristic of apoptosis in *Leishmania*.<sup>45</sup>

Lipids are essential for the structural and functional integrity of cells. As the predominant constituents of cellular membranes, lipids compartmentalize the cellular functions and are involved in various aspects of signal transduction.<sup>46</sup> Some

changes in the lipid distribution generally trigger a physiological event such as the clearance of apoptotic cells or the internalization of viruses by the host cells. Therefore, the externalization of phospholipids may indicate apoptotic death.<sup>47,48</sup> The binding of annexin V to the cell surface of *Leishmania* parasites is therefore likely to be a consequence of the changes in the plasma membrane lipid arrangement. In this study, flavonoids (1) and (3) at the concentration of 100 μM did not cause cell death through the induction of apoptosis in *L. amazonensis* promastigotes after 48 h of incubation. Intriguingly, it was observed that the parasites treated with pentamidine at 10 μM presented a higher percentage of cells in early apoptosis than that for the treatment at 100 μM. In parallel, the treatment with this reference antileishmanial drug at both concentrations also presented analogous effects in the induction of late apoptosis (the results were not significantly different). Thus, pentamidine is a potent antileishmanial drug; at 100 μM, it induced apoptosis in promastigotes. However, there was reduction in the element counts recorded by a flow cytometer in this treatment due to the high fragmentation of the parasitic cells. Moreover, pentamidine has been employed as a positive control to induce the apoptotic killing of the *Leishmania* parasites, but the exact mechanism by which this drug exerts its cytotoxic effect has not yet been fully elucidated, disregarding the identification of several molecular targets of pentamidine in the scientific literature.<sup>49–54</sup> Logically, the elevation of concentration may also cause loss of selectivity of the compound for other systems; for example, to inhibit topoisomerase II, another target of this drug acts on the DNA synthesis. These hypotheses explain how the treatment at 10 μM induced earlier apoptosis than that at the concentration of 100 μM, but other studies are needed to understand these findings.

Unlike a necrotic cell, which presents membrane rupture and release of intracellular content, a cell undergoing apoptosis is rapidly phagocytosed by tissue cells or phagocytes such as macrophages. Death by apoptosis can be triggered by various stimuli ranging from stress on intracellular organelles to receptor-mediated signalling. An important characteristic of this process is the activation of several cysteine proteases known as caspases. The proteolytic cleavage of different cell substrates by caspases determines the main characteristics of the process of cell death by apoptosis.<sup>55</sup> The pharmacological manipulation of apoptosis and caspases may have clinical applications and is a new frontier in the development of novel approaches to treat human diseases. In our study, we observed that flavonoids (1) and (3) did not cause caspase activation, which corroborated with our previous results about apoptosis.

Autophagy is a physiological process characterized by lysosome-mediated degradation and recycling of proteins and other cytoplasmic components; however, when it is exacerbated, autophagy is associated with the development of cell death.<sup>56,57</sup> In this regard, we evaluated autophagy induction in the promastigote forms of *L. amazonensis* treated with flavonoids (1) and (3). From these observations, it was seen that flavonoid (3) was capable of inducing autophagy at the concen-

tration of 100  $\mu\text{M}$ , therefore indicating the contribution of this process for the leishmanicidal activity of this flavonoid. Other studies also reported the induction of autophagic cell death in response to leishmanicidal compounds.<sup>58,59</sup> However, it is not clear whether autophagy regulates the G1/G0 cell cycle arrest in *Leishmania* sp. In fucoxanthin-treated HeLa cells, it was reported to be dose-responsively cytotoxic and G0/G1 arrest occurred without apoptosis change; autophagy-based cytotoxicity was found to involve the inhibition of the Akt/mTOR signaling pathway.<sup>60</sup>

Raman spectroscopy is a technique widely used to noninvasively monitor the cellular biochemical responses induced by substances. Recent studies have demonstrated the potential in the evaluation of the effects of drugs on cells.<sup>61–63</sup> In this study, Raman spectroscopy was used to characterize the flavonoids isolated from *S. paludosum* used in the treatment of macrophages infected with *L. amazonensis*. Initially, the spectra of the cells cultured in a medium free from compounds and those with 0.1% DMSO were analyzed. The analysis showed that these cell groups have similar spectral patterns, indicating that DMSO (vehicle control) does not cause significant changes in the cells.

The pentamidine treatment produced significant changes in the cell spectrum when compared to the spectrum of the DMSO group cells. As pentamidine is an aromatic diamidine, the reduction in the proline vibrations induced by this treatment might be related to the alterations induced by the drug in polyamine pathways.<sup>64</sup> Also, pentamidine reduced phenylalanine and amide I peaks, indicating conformational changes in the proteins.<sup>65–67</sup> In addition, this decrease in the protein content in the dying cells followed by the induction of the apoptosis proteins for cleavage and slicing is suggested by the decrease in most of the Raman bands of the proteins.<sup>66</sup> Moreover, there was decrease in the intensity of the peaks at 1240 and 1095  $\text{cm}^{-1}$ , indicating the disintegration of DNA/RNA related to cell death.<sup>66,67</sup>

The spectra of the cells treated with flavonoids (1) and (3) present changes in the same spectral regions. However, the cells treated with flavonoid (3) showed more dramatic changes in their Raman spectrum when compared to the DMSO group cells. Thus, the treatment of macrophages infected with *L. amazonensis* induced decrease in the Raman bands corresponding to the proteins (peaks at 1002, 1030, and 1657  $\text{cm}^{-1}$ ), and this result might indicate denaturation and conformational changes in the proteins related to cell death<sup>65</sup> since autophagy is a catabolic system that promotes the degradation of proteins and organelles.<sup>68,69</sup> Also, it is possible to observe decrease in the intensity of the peak at 1240  $\text{cm}^{-1}$ , indicating increase in the catabolism of RNA and the consequent reduction in protein synthesis.

To further highlight any differences between the treatments, the PCA analysis of the Raman spectra was performed. This multivariate method has been widely used to identify the spectral changes related to human diseases.<sup>70</sup> In most cases, the changes are subtle and difficult to interpret. By using PCA, the statistical difference between different types of cells can be

revealed effectively, which is similar to the difference spectrum. The PCA results obtained in this study presented a classification of the cell groups.

Although the cells of the Medium group and those of the DMSO group showed very similar spectral characteristics, it was possible to separate and classify the samples successfully by PCA, thus demonstrating the potential of this multivariate method. Subsequently, the DMSO, pentamidine, and flavonoid (1) groups were analyzed. This analysis suggested that despite the changes caused by both the treatments, pentamidine significantly modified the cellular structure compared to flavonoid (1). However, when we compared the DMSO, pentamidine, and flavonoid (3) groups, we observed that both flavonoid (3) and pentamidine significantly modified the cellular structure, forming overlapping regions that demonstrated greater similarity between these groups.

Ultimately, the distribution of the cells of the DMSO and flavonoid (1) and (3) groups was observed. This analysis revealed separated clusters and showed that the cells treated with flavonoid (1) presented more similar characteristics to that of the cells of the DMSO group, whereas the cells treated with flavonoid (3) presented very different spectra with greater dispersion of the samples. Summing up, the flavonoid (1) treatment caused lesser changes in the cell structure compared with the flavonoid (3) treatment. The PCA analysis suggested that the mechanisms of action of the flavonoids occur through different routes, that is, each flavonoid modifies the cell differently.

## Conclusions

In conclusion, it was demonstrated in this study that flavonoids showed excellent *in vitro* activity against *Leishmania*. In addition, in the investigation of the possible mechanisms of cell death, flavonoids (1) and (3) could increase the number of cells in the G0/G1 phases and reduce the number of cells in the S and G2/M phases of the cell cycle; flavonoid (3) also showed antiproliferative activity due to the induction of autophagy. Through the combination of Raman spectroscopy and PCA, it was possible to interpret and classify the spectral data accurately. This approach was proven to be useful in detecting the molecular mechanisms induced by flavonoids in cell behavior. The results support that the flavonoids isolated from *S. paludosum* can become lead compounds for the design of new prototypes of antileishmanial drugs.

## Conflicts of interest

There are no conflicts to declare.

## Acknowledgements

The authors would like to thank CAPES, CNPq, MCT, FINEP, INCT-INOVAR (573.564/2008-6), CNPQ (479822/2013-1), CNPQ

(404344/2012-7), FACEPE and FAPEAL (Pronem 20110722-006-0018-0010), FACEPE-PRONEM (APQ0741.1.06/14), and CENAPESQ for providing financial assistance for this research. Moreover, the authors would like to thank several colleagues working at UFAL for constructive criticism and assistance during the development of this study.

## References

- L. H. Freitas-Junior, E. Chatelain, H. A. Kim and J. L. Siqueira-Neto, Visceral leishmaniasis treatment: what do we have, what do we need and how to deliver it?, *Int. J. Parasitol.*, 2012, **2**, 11–19.
- Control of the leishmaniases: report of a meeting of the WHO expert committee on the control of leishmaniases. Control of the leishmaniases: report of a meeting of the WHO expert committee on the control of leishmaniases, ed. Organization WH, World Health Organization, 2010.
- J. Alvar, I. D. Velez, C. Bern, M. Herrero, P. Desjeux, J. Cano, *et al.*, Leishmaniasis worldwide and global estimates of its incidence, *PLoS One*, 2012, **7**(5), e35671.
- C. Graebin, F. Uchoa, L. Bernardes, V. Campo, I. Carvalho and V. Eifler-Lima, Antiprotozoal agents: an overview, *Anti-Infect. Agents Med. Chem.*, 2009, **8**(4), 345–366.
- F. Silveira, R. Lainson, C. De Castro Gomes, M. Laurenti and C. Corbett, Immunopathogenic competences of Leishmania (V.) braziliensis and L.(L.) amazonensis in American cutaneous leishmaniasis, *Parasite Immunol.*, 2009, **31**(8), 423–431.
- B. B. Mishra and V. K. Tiwari, Natural products: an evolving role in future drug discovery, *Eur. J. Med. Chem.*, 2011, **46**(10), 4769–4807.
- M. J. Chan-Bacab and L. M. Peña-Rodríguez, Plant natural products with leishmanicidal activity, *Nat. Prod. Rep.*, 2001, **18**(6), 674–688.
- L. Bohs, Major clades in Solanum based on ndhF sequences, in *A Festschrift for William G D'Arcy: The Legacy of a Taxonomist Monogr Syst Bot Missouri Bot Gard*, 2005, vol. 104, pp. 27–49.
- S. E. Milner, N. P. Brunton, P. W. Jones, N. M. O'Brien, S. G. Collins and A. R. Maguire, Bioactivities of glycoalkaloids and their aglycones from Solanum species, *J. Agric. Food Chem.*, 2011, **59**(8), 3454–3484.
- T. M. S. Silva, M. Agra and J. Bhattacharyya, Studies on the alkaloids of Solanum of northeastern Brazil, *Rev. Bras. Farmacogn.*, 2005, **15**(4), 292–293.
- T. M. S. da Silva, M. G. de Carvalho, R. Braz-Filho and M. de Fatima Agra, Ocorrência de flavonas, flavonóis e seus glicosídeos em espécies do gênero Solanum (Solanaceae), *Quim. Nova*, 2003, **26**(4), 517–522.
- T. Silva, M. Carvalho and R. Braz-Filho, Estudo espectroscópico em elucidación estrutural de flavonoides de Solanum jabrense Agra & Nee e S. paludosum Moric, *Quim. Nova*, 2009, **32**(5), 1119–1128.
- T. M. S. Silva, R. J. B. Nascimento, C. A. Câmara, R. N. Castro, R. Braz-Filho, M. de Fátima Agra, *et al.*, Distribution of flavonoids and N-trans-caffeoyl-tyramine in Solanum subg. Leptostemonum, *Biochem. Syst. Ecol.*, 2004, **32**(5), 513–516.
- G. Vieira Jr., P. Ferreira, L. Matos, E. Ferreira, W. Rodovalho, P. Ferri, *et al.*, Anti-inflammatory effect of Solanum lycocarpum fruits, *Phytother. Res.*, 2003, **17**(8), 892–896.
- R. Dall'Agnol and G. L. von Poser, The use of complex polysaccharides in the management of metabolic diseases: the case of Solanum lycocarpum fruits, *J. Ethnopharmacol.*, 2000, **71**(1–2), 337–341.
- A. Oliveira, D. Endringer, R. Araújo, M. Brandão and M. Coelho, The starch from Solanum lycocarpum St. Hill. fruit is not a hypoglycemic agent, *Braz. J. Med. Biol. Res.*, 2003, **36**(4), 525–530.
- C. A. Hall, T. Hobby and M. Cipollini, Efficacy and mechanisms of  $\alpha$ -solasonine and  $\alpha$ -solamargine-induced cytolysis on two strains of Trypanosoma cruzi, *J. Chem. Ecol.*, 2006, **32**(11), 2405–2416.
- M. Abreu Miranda, R. F. J. Tiozzi, M. R. da Silva, K. C. Rodrigues, C. C. Kuehn, L. G. Rodrigues Oliveira, *et al.*, In vitro leishmanicidal and cytotoxic activities of the glycoalkaloids from Solanum lycocarpum (Solanaceae) fruits, *Chem. Biodiversity*, 2013, **10**(4), 642–648.
- K.-W. Kuo, S.-H. Hsu, Y.-P. Li, W.-L. Lin, L.-F. Liu, L.-C. Chang, *et al.*, Anticancer activity evaluation of the Solanum glycoalkaloid solamargine: triggering apoptosis in human hepatoma cells, *Biochem. Pharmacol.*, 2000, **60**(12), 1865–1873.
- L.-F. Liu, C.-H. Liang, L.-Y. Shiu, W.-L. Lin, C.-C. Lin and K.-W. Kuo, Action of solamargine on human lung cancer cells—enhancement of the susceptibility of cancer cells to TNFs, *FEBS Lett.*, 2004, **577**(1–2), 67–74.
- P. Crow, J. Uff, J. Farmer, M. Wright and N. Stone, The use of Raman spectroscopy to identify and characterize transitional cell carcinoma in vitro, *BJU Int.*, 2004, **93**(9), 1232–1236.
- Y. H. Ong, M. Lim and Q. Liu, Comparison of principal component analysis and biochemical component analysis in Raman spectroscopy for the discrimination of apoptosis and necrosis in K562 leukemia cells, *Opt. Express*, 2012, **20**(20), 22158–22171.
- F. Jähnig and R. Etges, Secondary structure of the promastigote surface protease of Leishmania, *FEBS Lett.*, 1988, **241**(1–2), 79–82.
- V. Dugandžić, D. Drikermann, O. Ryabchykov, A. Undisz, I. Vilotijević, S. Lorkowski, *et al.*, Surface enhanced Raman spectroscopy-detection of the uptake of mannose-modified nanoparticles by macrophages in vitro: A model for detection of vulnerable atherosclerotic plaques, *J. Biophotonics*, 2018, **11**(12), e201800013.
- L. Cui, Y.-J. Zhang, W. E. Huang, B.-F. Zhang, F. L. Martin, J.-Y. Li, *et al.*, Surface-enhanced Raman spectroscopy for identification of heavy metal arsenic(v)-mediated enhan-

- cing effect on antibiotic resistance, *Anal. Chem.*, 2016, **88**(6), 3164–3170.
- 26 J. Binoy, J. P. Abraham, I. H. Joe, V. Jayakumar, G. Pettit and O. F. Nielsen, NIR-FT Raman and FT-IR spectral studies and ab initio calculations of the anti-cancer drug combretastatin-A4, *J. Raman Spectrosc.*, 2004, **35**(11), 939–946.
- 27 H. Nawaz, F. Bonnier, P. Knief, O. Howe, F. M. Lyng, A. D. Meade, *et al.*, Evaluation of the potential of Raman microspectroscopy for prediction of chemotherapeutic response to cisplatin in lung adenocarcinoma, *Analyst*, 2010, **135**(12), 3070–3076.
- 28 P. Gao, B. Han, Y. Du, G. Zhao, Z. Yu, W. Xu, *et al.*, The clinical application of Raman spectroscopy for breast cancer detection, *J. Spectrosc.*, 2017, **2017**, 5383948.
- 29 H. Abdi and L. J. Williams, Principal component analysis, *Wiley Interdiscip. Rev.: Comput. Stat.*, 2010, **2**(4), 433–459.
- 30 G. Das, R. La Rocca, T. Lakshminanth, F. Gentile, R. Tallero, L. Zambetti, *et al.*, Monitoring human leukocyte antigen class I molecules by micro-Raman spectroscopy at single-cell level, *J. Biomed. Opt.*, 2010, **15**(2), 027007.
- 31 R. Malini, K. Venkatakrishna, J. Kurien, K. M. Pai, L. Rao, V. Kartha, *et al.* Discrimination of normal, inflammatory, premalignant, and malignant oral tissue: a Raman spectroscopy study, *Biopolymers*, 2006, **81**(3), 179–193.
- 32 K. Dimas, C. Demetzos, D. Angelopoulou, A. Kolokouris and T. Mavromoustakos, Biological activity of myricetin and its derivatives against human leukemic cell lines in vitro, *Pharmacol. Res.*, 2000, **42**(5), 475–478.
- 33 Z. Movasaghi, S. Rehman and I. U. Rehman, Raman spectroscopy of biological tissues, *Appl. Spectrosc. Rev.*, 2007, **42**(5), 493–541.
- 34 P. Raveendran, J. Fu and S. L. Wallen, A simple and “green” method for the synthesis of Au, Ag, and Au–Ag alloy nanoparticles, *Green Chem.*, 2006, **8**(1), 34–38.
- 35 I. L. K. Wong, K.-F. Chan, Y.-F. Chen, Z.-R. Lun, T. H. Chan and L. M. C. Chow, In Vitro and In Vivo Efficacy of Novel Flavonoid Dimers against Cutaneous Leishmaniasis, *Antimicrob. Agents Chemother.*, 2014, **58**(6), 3379–3388.
- 36 I. L. Wong, K.-F. Chan, B. A. Burkett, Y. Zhao, Y. Chai, H. Sun, *et al.*, Flavonoid dimers as bivalent modulators for pentamidine and sodium stibogluconate resistance in Leishmania, *Antimicrob. Agents Chemother.*, 2007, **51**(3), 930–940.
- 37 S. R. Gedara, O. B. Abdel-Halim, S. H. El-Sharkawy, O. M. Salama, T. W. Shier and A. F. Halim, New erythroane-type diterpenoids from fagonia boveana (hadidi) hadidi & graf, *Z. Naturforsch., C: J. Biosci.*, 2003, **58**(1–2), 23–32.
- 38 C. Henrick and P. Jefferies, The chemistry of the Euphorbiaceae. VIII. New flavones from *Ricinocarpus stylosus*, *Aust. J. Chem.*, 1964, **17**(8), 934–942.
- 39 G. Lewin, A. Maciuk, S. Thoret, G. Aubert, J. Dubois and T. Cresteil, Semisynthesis of natural flavones inhibiting tubulin polymerization, from hesperidin, *J. Nat. Prod.*, 2010, **73**(4), 702–706.
- 40 H. G. T. Castañeda, A. J. C. Dulcey and J. H. I. Martínez, Flavonoid glycosides from *Siparuna gigantotepala* leaves and their antioxidant activity, *Chem. Pharm. Bull.*, 2016, **64**(5), 502–506.
- 41 C. Valares Masa, J. Alias Gallego, N. Chaves Lobon and T. Sosa Diaz, Intra-population variation of secondary metabolites in *Cistus ladanifer* L, *Molecules*, 2016, **21**(7), 945.
- 42 I. S. Chauhan, G. S. Rao, J. Shankar, L. K. S. Chauhan, G. J. Kapadia and N. Singh, Chemoprevention of Leishmaniasis: *In vitro* antiparasitic activity of dibenzalacetone, a synthetic curcumin analog leads to apoptotic cell death in *Leishmania donovani*, *Parasitol. Int.*, 2018, **67**(5), 627–636.
- 43 C. M. Adade, G. S. Chagas and T. Souto-Padron, Apis mellifera venom induces different cell death pathways in *Trypanosoma cruzi*, *Parasitology*, 2012, **139**(11), 1444–1461.
- 44 C. A. Guimarães and R. Linden, Programmed cell deaths, *Eur. J. Biochem.*, 2004, **271**(9), 1638–1650.
- 45 A. Debrabant and H. Nakhasi, Programmed cell death in trypanosomatids: is it an altruistic mechanism for survival of the fittest?, *Kinetoplastid Biol. Dis.*, 2003, **2**(1), 7.
- 46 P. F. Devaux, Static and dynamic lipid asymmetry in cell membranes, *Biochemistry*, 1991, **30**(5), 1163–1173.
- 47 A. D. Tepper, P. Ruurs, T. Wiedmer, P. J. Sims, J. Borst and W. J. van Blitterswijk, Sphingomyelin hydrolysis to ceramide during the execution phase of apoptosis results from phospholipid scrambling and alters cell-surface morphology, *J. Cell Biol.*, 2000, **150**(1), 155–164.
- 48 P. Williamson, M. S. Halleck, J. Malowitz, S. Ng, X. Fan, S. Krahling, *et al.*, Transbilayer phospholipid movements in ABCA1-deficient cells, *PLoS One*, 2007, **2**(8), e729.
- 49 N. Azas, C. Di Giorgio, F. Delmas, M. Gasquet and P. Timon-David, *Leishmania infantum* Promastigotes: Flow Cytometry as a Possible Tool for Assessing the Effects of Drugs on Cellular Functions, *Exp. Parasitol.*, 1997, **87**(1), 1–7.
- 50 A. Mehta and C. Shaha, Apoptotic Death in *Leishmania donovani* Promastigotes in Response to Respiratory Chain Inhibition Complex II Inhibition Results in Increased Pentamidine Cytotoxicity, *J. Biol. Chem.*, 2004, **279**(12), 11798–11813.
- 51 P. A. Nguewa, M. A. Fuertes, V. Cepeda, S. Iborra, J. Carrión, B. Valladares, *et al.*, Pentamidine is an antiparasitic and apoptotic drug that selectively modifies ubiquitin, *Chem. Biodiversity*, 2005, **2**(10), 1387–1400.
- 52 G. Singh and C. S. Dey, Induction of apoptosis-like cell death by pentamidine and doxorubicin through differential inhibition of topoisomerase II in arsenite-resistant *L. donovani*, *Acta Trop.*, 2007, **103**(3), 172–185.
- 53 A. Pućkowska, D. Drozdowska, M. Rusak, T. Bielawski, I. Bruzgo and K. Midura-Nowaczek, Amino and chlorambucil analogues of pentamidine—synthesis and biological examinations, *Acta Pol. Pharm.*, 2012, **69**(1), 63–73.

## Artigo II

View Article Online

Paper

Analyst

- 54 M. Islamuddin, D. Sahal and F. Afrin, Apoptosis-like death in *Leishmania donovani* promastigotes induced by eugenol-rich oil of *Syzygium aromaticum*, *J. Med. Microbiol.*, 2014, **63**(1), 74–85.
- 55 X.-M. Sun, M. MacFarlane, J. Zhuang, B. B. Wolf, D. R. Green and G. M. Cohen, Distinct caspase cascades are initiated in receptor-mediated and chemical-induced apoptosis, *J. Biol. Chem.*, 1999, **274**(8), 5053–5060.
- 56 Y. Liu and B. Levine, Autosis and autophagic cell death: the dark side of autophagy, *Cell Death Differ.*, 2015, **22**(3), 367.
- 57 T. Yonekawa and A. Thorburn, Autophagy and cell death, *Essays Biochem.*, 2013, **55**, 105–117.
- 58 U. Schurigt, C. Schad, C. Glowa, U. Baum, K. Thomale, J. K. Schnitzer, *et al.*, Aziridine-2, 3-dicarboxylate-based cysteine cathepsin inhibitors induce cell death in *Leishmania* major associated with accumulation of debris in autophagy-related lysosome-like vacuoles, *Antimicrob. Agents Chemother.*, 2010, **54**(12), 5028–5041.
- 59 A. Bera, S. Singh, R. Nagaraj and T. Vaidya, Induction of autophagic cell death in *Leishmania donovani* by antimicrobial peptides, *Mol. Biochem. Parasitol.*, 2003, **127**(1), 23–35.
- 60 L.-I. Hou, C. Gao, L. Chen, G.-q. Hu and S.-q. Xie, Essential role of autophagy in fucoxanthin-induced cytotoxicity to human epithelial cervical cancer HeLa cells, *Acta Pharmacol. Sin.*, 2013, **34**(11), 1403.
- 61 T. Tao, Q. Shen, X. Lu, Y. He and L. Zhong, Raman spectroscopy-based multivariate statistical analysis reveals the molecular mechanism of K562 cell apoptosis induced by adriamycin, *Spectrosc. Lett.*, 2014, **47**(4), 301–305.
- 62 E. C. O. da Silva, F. M. dos Santos, A. R. B. Ribeiro, S. T. de Souza, E. Barreto and E. Fonseca, Drug-induced anti-inflammatory response in A549 cells, as detected by Raman spectroscopy: a comparative analysis of the actions of dexamethasone and p-coumaric acid, *Analyst*, 2019, **144**(5), 1622–1631.
- 63 L. E. Jamieson and H. J. Byrne, Vibrational spectroscopy as a tool for studying drug-cell interaction: could high throughput vibrational spectroscopic screening improve drug development?, *Vib. Spectrosc.*, 2017, **91**, 16–30.
- 64 R. Balaña-Fouce, E. Calvo-Álvarez, R. Álvarez-Velilla, C. F. Prada, Y. Pérez-Pertejo and R. M. Reguera, Role of trypanosomatid's arginase in polyamine biosynthesis and pathogenesis, *Mol. Biochem. Parasitol.*, 2012, **181**(2), 85–93.
- 65 I. Notingher, J. Selvakumaran and L. L. Hench, New detection system for toxic agents based on continuous spectroscopic monitoring of living cells, *Biosens. Bioelectron.*, 2004, **20**(4), 780–789.
- 66 I. Notingher, S. Verrier, S. Haque, J. Polak and L. Hench, Spectroscopic study of human lung epithelial cells (A549) in culture: living cells versus dead cells, *Biopolymers*, 2003, **72**(4), 230–240.
- 67 S. Choi and Z. Jiang, Cardiac sound murmurs classification with autoregressive spectral analysis and multi-support vector machine technique, *Comput. Biol. Med.*, 2010, **40**(1), 8–20.
- 68 B. Levine and D. J. Klionsky, Development by self-digestion: molecular mechanisms and biological functions of autophagy, *Dev. Cell*, 2004, **6**(4), 463–477.
- 69 F. Reggiori and D. J. Klionsky, Autophagosomes: biogenesis from scratch?, *Curr. Opin. Cell Biol.*, 2005, **17**(4), 415–422.
- 70 J. W. Chan, D. S. Taylor, T. Zwerdling, S. M. Lane, K. Ihara and T. Huser, Micro-Raman spectroscopy detects individual neoplastic and normal hematopoietic cells, *Biophys. J.*, 2006, **90**(2), 648–656.



# Leishmanicidal Activity of Propolis Collected in the Semiarid Region of Brazil

Giani Maria Cavalcante<sup>1</sup>, Celso Amorim Camara<sup>1</sup>, Eva Monica Sarmiento Da Silva<sup>2</sup>, Mariana Silva Santos<sup>3</sup>, Anderson Brandão Leite<sup>3</sup>, Aline Cavalcanti Queiroz<sup>3,4</sup>, Amanda Evelyn Da Silva<sup>3</sup>, Morgana Vital Araújo<sup>3</sup>, Magna Suzana Alexandre-Moreira<sup>3</sup> and Tania Maria Sarmiento Silva<sup>1\*</sup>

<sup>1</sup>Phytochemical Bioprospecting Laboratory, Chemistry Department, Rural Federal University of Pernambuco, Pernambuco, Brazil, <sup>2</sup>Zootechnical Collegiate, Federal University of the São Francisco Valley, Pernambuco, Brazil, <sup>3</sup>Pharmacology and Immunity Laboratory, Institute of Biological and Health Sciences, Federal University of Alagoas, Alagoas, Brazil, <sup>4</sup>Microbiology, Immunology and Parasitology Laboratory, Campus Arapiraca, Federal University of Alagoas, Alagoas, Brazil

**Objective:** The aim of the current study is to investigate the chemical composition, cytotoxic effect, and leishmanicidal activity of propolis collected in the semi-arid region of Bahia, Brazil.

**Methods:** EtOH extract, hexane, EtOAc and MeOH fractions from propolis were analyzed by ultra-performance liquid chromatography coupled with diode array detector and quadrupole time-of-flight mass spectrometry. The identification was based on the exact mass, general fragmentation behaviors and UV absorption of the flavonoids. The *in vitro* cytotoxic effect and leishmanicidal activity of ethanolic extract, hexane, ethyl acetate, and methanolic fractions of propolis were evaluated.

**Results:** Five triterpenes and twenty-four flavonoids were identified. The propolis did not present toxicity to the host cell up to the maximum concentration tested. In addition, all tested samples showed statistically significant activity against promastigotes of *Leishmania chagasi* and *Leishmania amazonensis*. Regarding the activity against amastigote forms of *L. amazonensis*, the hexane fraction, presented statistically significant activity with IC<sub>50</sub> of 1.3 ± 0.1 µg/ml.

**Conclusion:** The results support the idea that propolis can be used for future antileishmania studies.

**Keywords:** flavonoids, propolis, leishmanicidal activity, *Leishmania (Leishmania) amazonensis*, *Leishmania (Leishmania) chagasi*

## INTRODUCTION

Leishmaniasis is one of the six major parasitic diseases targeted by the World Health Organization. It is endemic in 98 countries and more than 350 million people are at risk of infection. The disease causes 20,000–40,000 deaths per year globally (Sasidharan and Saudagar, 2021).

In humans, the clinical forms of leishmaniasis are broadly categorized into cutaneous leishmaniasis (CL) and visceral leishmaniasis (VL), and clinical manifestations depend on the pathogenicity of the parasite, which differs among species, and the genetically determined cell-mediated immune response of the human host (Singh et al., 2012).

## OPEN ACCESS

### Edited by:

John Ogbaji Igoli,  
Federal University of Agriculture  
Makurdi (FUAM), Nigeria

### Reviewed by:

David Watson,  
University of Strathclyde,  
United Kingdom  
Paula C Castilho,  
Centro de Química da Madeira,  
Universidade da Madeira, Portugal

### \*Correspondence:

Tania Maria Sarmiento Silva  
sarmientosilva@gmail.com

### Specialty section:

This article was submitted to  
Ethnopharmacology,  
a section of the journal  
Frontiers in Pharmacology

Received: 28 April 2021

Accepted: 16 June 2021

Published: 01 July 2021

### Citation:

Cavalcante GM, Camara CA,  
Silva EMSD, Santos MS, Leite AB,  
Queiroz AC, Evelyn Da Silva A,  
Araújo MV, Alexandre-Moreira MS and  
Silva TMS (2021) Leishmanicidal Activity  
of Propolis Collected in the Semiarid  
Region of Brazil.  
Front. Pharmacol. 12:702032.  
doi: 10.3389/fphar.2021.702032

Current leishmaniasis treatment strategy is based on chemotherapy with some attempts at immunotherapy, but the combination of factors including the development of parasite resistance to drug therapies, the absence of vaccines, problems with vector control, among other factors, has rendered the treatment options for leishmaniasis limited (Taslimi et al., 2018).

Pentavalent antimonials are the standard first line treatment, but the emergence of resistance has limited their usefulness. Alternative chemotherapeutic treatments with amphotericin B and its lipid formulation, miltefosine, and paromomycin are available but their use is limited either due to toxicity or the high cost of treatment (Braga, 2019).

Consequently, it is of the utmost importance to discover effective drugs and new drug targets for the treatment of leishmaniasis. Propolis has long been the subject of pharmaceutical interest because of its potent biological functions, such as antimicrobial, anti-inflammatory, anti-protozoan, and antitumoral activities (Popova et al., 2005; Dantas et al., 2006; Jin et al., 2008; Szliszka et al., 2013). The propolis resin is complex, and its common constituents include polyphenols (flavonoids, phenolic acids, and their esters, terpenoids, and steroids (Tran et al., 2012). Its chemical composition depends on the plant or plants from which the resin is collected, the geographical location, and the associated flora (Popova et al., 2005; Ishida et al., 2011).

Therefore, there has been an interest in the composition and biological properties of this natural product. Extensive investigations have been conducted with propolis from different countries in temperate and tropical areas (Sforzin, 2016); however, a limited number of investigations have been conducted to study the palynological analysis (Matos et al., 2014), chemical composition (Valcic et al., 1998; Hernandez et al., 2007) and biological activities of propolis from semiarid regions (Russo et al., 2004).

In our continuing studies of the chemical and biological activity of *Apis* and *Melipona* bee products (Silva et al., 2006; Silva et al., 2009; Freire et al., 2012; Silva et al., 2013; Souza et al., 2013; Souza et al., 2014; Sousa-Junior et al., 2019; Sousa-Fontoura et al., 2020), we investigated the chemical composition of propolis by ultra-performance liquid chromatography coupled with diode array detector and quadrupole time-of-flight mass spectrometry (UPLC-DAD-QTOF-MS/MS), and we also analyzed the cytotoxic effect and leishmanicidal activity of the ethanolic extract, hexane, ethyl acetate, methanolic fractions of propolis from semi-arid region of Bahia, Brazil.

## METHODS

### Propolis Sample and Extraction

Propolis was collected in Brazil, State of Bahia, municipality of Casa Nova, which is an area of the Caatinga, a Brazilian biome. The propolis (79.4 g) was successively extracted with ethanol (EtOH) in an ultrasonic bath and evaporation was performed using a rotary evaporator in a vacuum at 40°C. 20 g dry extract was dissolved in methanol:water (1:1, MeOH) and successively fractionated with hexane (hexane, 7.4 g) and ethyl acetate

(EtOAc, 9.1 g). The amount of MeOH fraction was 1.1 g. The EtOH extract, hexane, EtOAc, and MeOH fractions, were subjected to UPLC-PDA-QTOF-MS analysis.

### Analysis of Propolis by Ultra-Performance Liquid Chromatography Coupled With Diode Array Detector and Quadrupole Time-of-Flight Mass Spectrometry

The analysis was performed using a XEVO-G2XSQTOF mass spectrometer (Waters, Manchester, United Kingdom) connected to an ACQUITY UPLC system (Waters, Milford, MA, United States) via an electrospray ionization (ESI) interface. Chromatographic separation of the compounds was performed on the ACQUITY UPLC with a conditioned autosampler at 4°C, using an Acquity BEH C18 column (150 mm × 2.1 mm i.d., 1.7 μm particle size). The column temperature was maintained at 40°C. The mobile phase consisted of water with 0.1% formic acid (solvent A) and acetonitrile (solvent B), and it was pumped at a flow rate of 0.4 ml min<sup>-1</sup>. The gradient elution program was as follows: 0–5 min, 5–10% B; 5–9 min, 10–95% B. The injection volume was 10 μl. MS analysis was performed on a Xevo G2 QTOF (Waters MS Technologies, Manchester, United Kingdom), a quadrupole time-of-flight tandem mass spectrometer coupled with an electrospray ionization source in the negative ion mode. The scan range was from 50 to 1,200 *m/z* for data acquisition. In addition, MS<sup>E</sup> experiments were carried out which allow precursor and product ion data to be acquired in one injection. The source conditions were as follows: capillary voltage, 2.0 kV; sample cone, source temperature, 100°C; desolvation temperature 250°C; cone gas flow rate 20 Lh<sup>-1</sup>; desolvation gas (N<sub>2</sub>) flow rate 600 Lh<sup>-1</sup>. All analysis were performed using the lockspray, which ensured accuracy and reproducibility. Leucine-enkephalin (5<sup>+</sup>ngml<sup>-1</sup>) was used as a standard or reference compound to calibrate the mass spectrometers during analysis. All the acquisition and analysis of data were controlled using Waters MassLynx v 4.1 software.

### Cells and Parasites

J774.A1 macrophages were cultured *in vitro* in RPMI-1640 medium supplemented with 10% FBS, 2 mM L-glutamine, nonessential amino acids and pyruvate at 37°C with 95% humidity and 5% CO<sub>2</sub> in an incubator. Two strains of *Leishmania* were used in the present study: *Leishmania (Leishmania) amazonensis* [MHOM/BR/77/LTB0016] and *Leishmania (Leishmania) infantum chagasi* [MCAN/BR/89/BA262]. They were maintained *in vitro* at 26°C in Schneider's medium supplemented with 10% FBS, gentamycin (1 mg/L), L-glutamine (2 mM), and 2% sterile human urine.

### Cytotoxicity Assay

J774.A1 macrophages were seeded (1 × 10<sup>5</sup> cell/well) in 96-well plates with 100 μl of RPMI-1640 medium and incubated at 37°C for 1 h. After this period, the cells were treated with 0.1, 1, 10, and 100 μg/ml of EtOH extract and organic fractions hexane, EtOAc, MeOH; 0.1, 1, 10, and 100 μM of pentamidine (all treatments performed in triplicate) previously diluted in RPMI-1640

medium with 0.1% dimethyl sulfoxide (DMSO). The plates were maintained in a 5% CO<sub>2</sub> incubator at 37°C for 48 h. Cells were also cultured in media free of compounds, or media with 0.1% DMSO (vehicle control). Thereafter, the supernatant was removed and cells were incubated with 3-(4,5-dimethylthiazol-2-yl)-2,5-diphenyltetrazolium bromide (MTT) (0.5 mg/ml) for 1 h in the dark at 37°C. The MTT solution was removed, cells were resuspended in 100 ml of 0.1% DMSO, and the absorbance was measured using an ELISA reader at 550 nm (Hussain et al., 1993).

### Leishmanicidal Assay

Cells ( $1 \times 10^5$ /well) of promastigotes forms of *L. amazonensis* and *L. chagasi* were cultured in Schneider's medium supplemented with 10% FBS and 2% human urine, in the presence of various concentrations of EtOH extract, hexane, EtOAc and MeOH fractions (0.1, 1, 10 and 100 µg/ml), and pentamidine (0.1, 1, 10, and 100 µM) in triplicate for 48 h at 26°C. Cells were also cultured in a medium free of substances, a vehicle (basal growth control) or with 0.1% DMSO (vehicle control). After 48 h, the viability of the promastigotes forms was analyzed using the MTT assay. MTT (20 µL) was added to each well and incubated at 37°C for 2 h with 95% humidity and 5% CO<sub>2</sub>. Formazan extraction was performed using 120 µL of isopropanol and left at room temperature for 2 h. The absorbance was measured using an ELISA reader at 550 nm (Moraes et al., 2014). The intracellular amastigote assay was performed in 24-well microplates with rounded coverslips on the bottom. J774.A1 macrophages were seeded at a density of  $3 \times 10^5$  cells/well and maintained for 1 h in 5% CO<sub>2</sub> at 37°C for adhesion in a humidified atmosphere of 95% air and 5% CO<sub>2</sub> at 37°C. Afterward, the cells were infected *in vitro* with promastigote forms of *L. amazonensis* and *L. chagasi* at a ratio of 1:10 for 6 h in a humidified atmosphere of 95% air and 5% CO<sub>2</sub> at 37°C.

The parasites in the supernatant were removed by washing, and various concentrations of EtOH extract, hexane, EtOAc, and MeOH fractions (0.1, 1, 10, and 100 µg/ml) and pentamidine (0.1, 1, 10, and 100 µM) were added and maintained at 37°C in 5% CO<sub>2</sub> for 48 h. The glass coverslips were fixed with methanol, stained with May-Grünwald-Giemsa, and intracellular amastigotes were counted (one hundred macrophages were evaluated per glass coverslip). Data were expressed as infection index (percentage of infected macrophages multiplied by the average number of amastigotes per macrophage) (Hussain et al., 1993).

### Statistical Analysis

Results were expressed as the mean ± SEM of an experiment in triplicate. The tests were performed with controls: media free from compounds, a vehicle (basal growth control), or media with 0.1% DMSO (vehicle control). Significant differences between the treated and control groups were evaluated using ANOVA and Dunnett *post-hoc* tests by Graph Pad Prism 5.0 software, and 95% confidence intervals were included.

## RESULTS

The compounds were tentatively identified by ultra-performance liquid chromatography coupled with diode array detector and quadrupole time-of-flight mass spectrometry (UPLC-DAD-QTOF-MS/MS), as flavonoids (flavonol/flavone, flavanone, and chalcones) based on their characteristic UV-Vis (flavonoids) spectra peaks and mass detection as well as the accurate mass measurement of the precursor and product ions. Terpenes were suggested by the absence of absorption in the UV spectra, in addition to the high-resolution mass spectra. **Figure 1** shows the

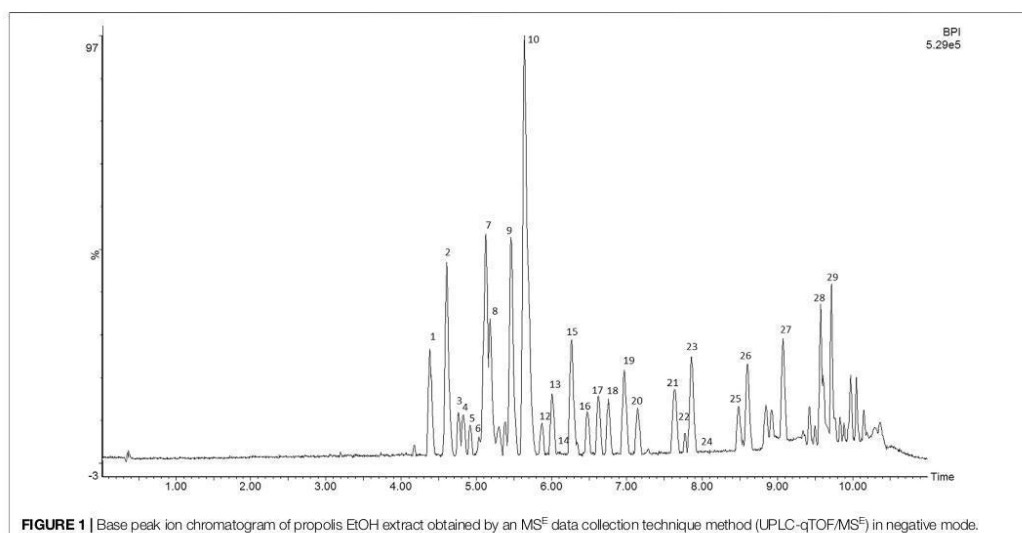




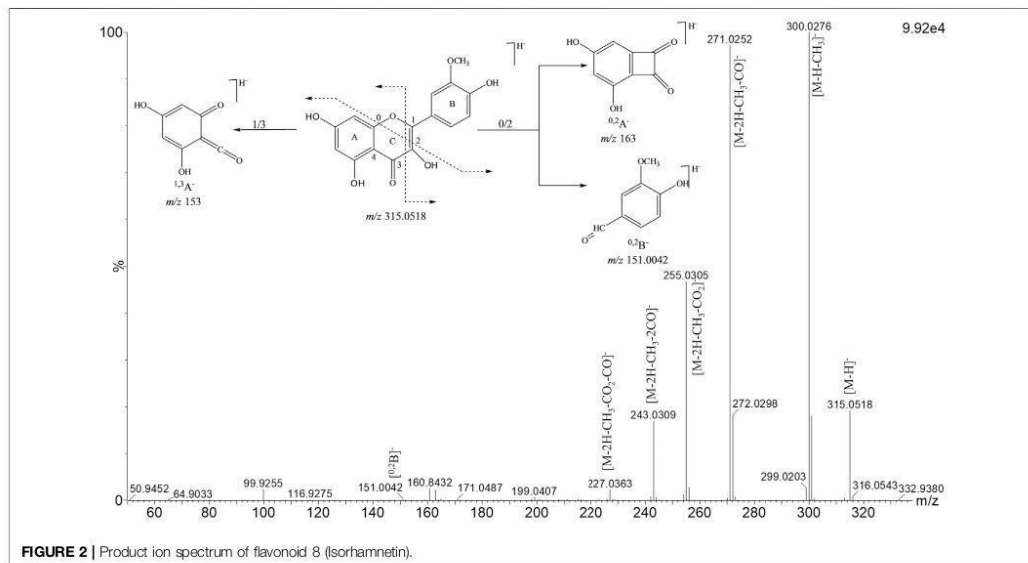
**TABLE 1** | Characterization of compounds from propolis EtOH extract, hexane, EtOAc and MeOH fractions analyzed by UPLC-DAD-ESI-qTOF-MS<sup>E</sup> in negative mode.

	RT (min)	$\lambda_{max}$ (nm)	[M-H] <sup>-</sup> (m/z)	[M-H] <sup>-</sup> (m/z) Calculated	MS <sup>2</sup> Fragments identification	Tentative identification <sup>a</sup>
1 <sup>e</sup>	4.38	359	301.0350	301.0353	271.0274 [M-2H-CO] <sup>-</sup> , 193.0133 [M-H-B] <sup>-</sup> ; 151.0045 [1 <sup>-3</sup> A] <sup>-</sup>	Quercetin <sup>a,c,d</sup>
2 <sup>e</sup>	4.60	356	315.0512	315.0510	300.0208 [M-H-CH <sub>3</sub> ] <sup>-</sup> , 271.0251 [M-2H-CH <sub>3</sub> -CO] <sup>-</sup> , 255.0307 [M-2H-CH <sub>3</sub> -CO-CH <sub>3</sub> ] <sup>-</sup> , 151.0044, 151.0045 [1 <sup>-3</sup> A] <sup>-</sup>	3-O-methyl-quercetin <sup>a,c,d</sup>
3	4.76	345	345.0615	345.0615	330.0388 [M-H-CH <sub>3</sub> ] <sup>-</sup> , 315.0159 [M-H-2CH <sub>3</sub> ] <sup>-</sup> , 287.0208 [M-H-2CH <sub>3</sub> -CO] <sup>-</sup>	Myricetin dimethyl-ether <sup>a,c</sup>
4 <sup>e</sup>	4.82	287	271.0610	271.0611	151.0029 [1 <sup>-3</sup> A] <sup>-</sup> , 119.0505 [1 <sup>-2</sup> B] <sup>-</sup>	Naringenin <sup>a,c</sup>
5	4.91	339	269.0455	269.0455	151.0037 [1 <sup>-3</sup> A] <sup>-</sup>	Trihydroxy-flavone <sup>a,c</sup>
6	5.02	364	285.0405	285.0404	257.0524 [M-H-CO] <sup>-</sup>	Tetrahydroxy-flavone <sup>a,c</sup>
7	5.48	346	299.0563	299.0563	284.0323 [M-H-CH <sub>3</sub> ] <sup>-</sup> , 227.0359 [M-2H-CH <sub>3</sub> -2CO] <sup>-</sup> , 151.0058 [1 <sup>-3</sup> A] <sup>-</sup>	Trihydroxy-methoxy-flavone <sup>a,c,d</sup>
8 <sup>e</sup>	5.16	346	315.0518	315.0510	300.0276 [M-H-CH <sub>3</sub> ] <sup>-</sup> , 271.0265 [M-2H-CH <sub>3</sub> -CO] <sup>-</sup> , 255.0305 [M-2H-CH <sub>3</sub> -CO] <sup>-</sup> , 243.0309 [M-2H-CH <sub>3</sub> -2CO] <sup>-</sup> , 227.0663 [M-2H-CH <sub>3</sub> -CO-CO <sub>2</sub> ] <sup>-</sup> , 151.0042 [1 <sup>-2</sup> B] <sup>-</sup>	Isorhamnetin <sup>a,c</sup>
9	5.44	346	299.0563	299.0561	284.0302 [M-H-CH <sub>3</sub> ] <sup>-</sup> , 255.0294 [M-2H-CH <sub>3</sub> -CO] <sup>-</sup> , 227.0347 [M-2H-CH <sub>3</sub> -2CO] <sup>-</sup>	Trihydroxy-methoxy-flavone <sup>a,c,d</sup>
10	5.64	345	329.0662	329.0667	314.0409 [M-H-CH <sub>3</sub> ] <sup>-</sup> , 299.0195 [M-H-2CH <sub>3</sub> ] <sup>-</sup> , 271.0248 [M-H-2CH <sub>3</sub> -CO] <sup>-</sup> , 243.0309 [M-H-2CH <sub>3</sub> -2CO] <sup>-</sup>	Quercetin dimethyl ether <sup>a,c,d</sup>
11	5.65	345	329.0660	329.0667	314.0409 [M-H-CH <sub>3</sub> ] <sup>-</sup> , 299.0195 [M-H-2CH <sub>3</sub> ] <sup>-</sup> , 271.0248 [M-H-2CH <sub>3</sub> -CO] <sup>-</sup> , 243.0309 [M-H-2CH <sub>3</sub> -2CO] <sup>-</sup>	Quercetin dimethyl ether <sup>a,c</sup>
12	5.83	369	285.0768	285.0768	270.0570 [M-H-CH <sub>3</sub> ] <sup>-</sup>	Hydroxy-methoxy-chalcone
13	5.98	286	301.0718	301.0717	285.0396 [M-2H-CH <sub>3</sub> ] <sup>-</sup> , 165.0206 [1 <sup>-2</sup> A] <sup>-</sup> , 135.0457 [1 <sup>-2</sup> A-CO] <sup>-</sup>	Trihydroxy-methoxy-flavanone <sup>a,c</sup>
14	6.07	275	269.0826	269.0819	241.7910 [M-H-CO] <sup>-</sup>	Hydroxy-methoxy-flavanone <sup>a,c</sup>
15	6.23	333	313.0716	313.0716	298.0477 [M-H-CH <sub>3</sub> ] <sup>-</sup> , 283.0245 [M-H-2CH <sub>3</sub> ] <sup>-</sup> , 255.0307 [M-H-2CH <sub>3</sub> -CO] <sup>-</sup>	Dihydroxy-dimethoxy-flavone <sup>a,c</sup>
16	6.44	356	315.0513	315.0510	300.0227 [M-H-CH <sub>3</sub> ] <sup>-</sup> , 135.9030 [1 <sup>-2</sup> A-CO] <sup>-</sup>	Tetrahydroxy-methoxy-flavone <sup>a,c</sup>
17	6.59	360	329.0666	329.0667	314.0409 [M-H-CH <sub>3</sub> ] <sup>-</sup> , 299.0195 [M-H-2CH <sub>3</sub> ] <sup>-</sup> , 271.0248 [M-H-2CH <sub>3</sub> -CO] <sup>-</sup> , 243.0309 [M-H-2CH <sub>3</sub> -2CO] <sup>-</sup>	Trihydroxy-dimethoxy-flavone <sup>a,c</sup>
18	6.72	339	343.0822	343.0823	328.0589 [M-H-CH <sub>3</sub> ] <sup>-</sup> , 313.0352 [M-H-2CH <sub>3</sub> ] <sup>-</sup> , 298.0122 [M-2H-3CH <sub>3</sub> ] <sup>-</sup> , 285.0414 [M-2H-3CH <sub>3</sub> -CO] <sup>-</sup>	Dihydroxy-trimethoxy-flavone <sup>a,c</sup>
19 <sup>e</sup>	6.93	287	285.0765	285.0768	269.0383 [M-2H-CH <sub>3</sub> ] <sup>-</sup> , 119.0505 [1 <sup>-2</sup> B] <sup>-</sup>	7-O-methyl naringenin <sup>a,b,c</sup> (sakuranetin) <sup>e</sup>
20	7.11	339	283.0618	283.0612	268.0373 [M-H-CH <sub>3</sub> ] <sup>-</sup> , 240.0427 [M-H-CH <sub>3</sub> -CO] <sup>-</sup>	Dihydroxy methoxy flavone <sup>a,b,c</sup>
21	7.32	346	313.0721	313.0718	298.0477 [M-H-CH <sub>3</sub> ] <sup>-</sup> , 283.0245 [M-H-2CH <sub>3</sub> ] <sup>-</sup> , 255.0307 [M-H-2CH <sub>3</sub> -CO] <sup>-</sup>	Dihydroxy-dimethoxy-flavone <sup>a,c</sup>
22	7.82	345	313.0718	313.0718	298.0477 [M-H-CH <sub>3</sub> ] <sup>-</sup> , 283.0245 [M-H-2CH <sub>3</sub> ] <sup>-</sup> , 255.0307 [M-H-2CH <sub>3</sub> -CO] <sup>-</sup>	Dihydroxy-dimethoxy-flavone <sup>a,b,c</sup>
23	7.84	339	343.0829	343.0823	328.0586 [M-H-CH <sub>3</sub> ] <sup>-</sup> , 313.0354 [M-H-2CH <sub>3</sub> ] <sup>-</sup> , 285.0407 [M-H-2CH <sub>3</sub> -CO] <sup>-</sup> , 270.0168 [M-H-3CH <sub>3</sub> -CO] <sup>-</sup>	Dihydroxy-trimethoxy-flavone <sup>a,b,c</sup>
24	7.93	363	269.0822	269.0819	235.9273 [M-2H-CH <sub>3</sub> -H <sub>2</sub> O] <sup>-</sup>	Dihydroxy-methoxy-chalcone <sup>a,c</sup>
25	8.48		515.3223	515.3226	469.3183 [M-H-CO-H <sub>2</sub> O] <sup>-</sup>	Triterpene <sup>a,b</sup>
26	8.60		515.3223	515.3226	485.3106 [M-H-2CH <sub>3</sub> ] <sup>-</sup> , 467.3019 [M-H-2CH <sub>3</sub> -H <sub>2</sub> O] <sup>-</sup> , 451.3044 [M-H-2CH <sub>3</sub> -H <sub>2</sub> O-CH <sub>3</sub> ] <sup>-</sup>	Triterpene <sup>a,b</sup>
27	8.92		499.3273	499.3276	453.3282 [M-H-CO-H <sub>2</sub> O] <sup>-</sup>	Triterpene <sup>a,b</sup>
27	9.57		515.3223	515.3226	497.3112 [M-H-H <sub>2</sub> O] <sup>-</sup> , 467.3008 [M-H-2CH <sub>3</sub> ] <sup>-</sup>	Triterpene <sup>a,b</sup>
29	9.72		499.3273	499.3276	469.3171 3.008 [M-H-2CH <sub>3</sub> ] <sup>-</sup>	Triterpene <sup>a,b</sup>

<sup>a</sup>Found in the EtOH extract.<sup>b</sup>Found in the hexane fraction.<sup>c</sup>Found in the EtOAc fraction.<sup>d</sup>Found in the MeOH fraction.<sup>e</sup>Compared to a previously isolated and identified standard.

base peak ion (BPI) chromatogram of the ethanol extract from propolis. The groups of flavonoids could be distinguished based on their UV-vis spectra which resembled that of flavone/flavonol (with two absorbance maxima near 250–260 and 350), flavanone (maximum near 280–290 nm), and chalcones (maxima near 242 and 364 nm). All the detected compounds were listed in **Table 1**. The analysis allowed the identification of 24 flavonoids including 13 flavonols/flavones (1, 2, 3, 5, 6, 7, 8, 9, 10, 11, 15, 16, 17, 18, 20,

21, 22 and 23), 2 chalcones (12 and 24) and 4 flavanones (4, 13, 14 and 19). The flavonoids 1, 2, 4, 8, and 19 were compared with standard samples. It is interesting to note that the identified flavonoids present only six main nuclei, and the difference was the presence of the methoxyl groups in the flavonoids. The fragments found for flavonoids are similar to the flavonoids reported by Santisteban et al., 2019. Methoxylated flavonoids lost preferentially nCH<sub>3</sub><sup>+</sup>, yielding the characteristic fragments of



$[M - H - n \times 15]^+$ . These methyl groups have been cleaved as methyl radicals in position-independent manners. Other fragments, such as the neutral loss of  $CH_4$  (14 Da),  $CO_2$  (44 Da), and  $CO$  (28 Da), were frequently detected. If there are protons adjacent to the methoxy on the flavonol rings, intramolecular proton transfer can occur, and one molecule of methane can be eliminated (Ma et al., 2013). Retro-Diels-Alder (RDA) reactions played key roles in the identification of flavonoids and their derivatives (Demarque et al., 2016). Consider isorhamnetin (8) as an example, the characteristic ion of methoxylated was observed by prominent ion at  $m/z$  300.0292  $[M - H - CH_3]^-$  by the loss of 15 Da ( $CH_3$ ) from the protonated molecular ion at  $m/z$  315.0518  $[M - H]^-$  (Figure 2). The abundant ion at  $m/z$  271.0265  $[M - 2H - CH_3 - CO]^-$ , might be obtained by the loss of  $CO$  (28 Da) from  $m/z$  300.0292. Subsequent neutral loss of  $CO_2$  or  $CO$  and gave a secondary abundant ion at  $m/z$  255.0305  $[M - 2H - CH_3 - CO_2]^-$  and  $m/z$  243.0309  $[M - 2H - CH_3 - 2CO]^-$ , respectively and another ion at  $m/z$  227.0663  $[M - 2H - CH_3 - CO - CO_2]^-$ . Additionally, the fragmentation pathways of RDA cleavage of the C-ring generated relative low abundance ion at  $m/z$  151.0042  $[0.2B]^-$  (Figure 2). The compounds shown at the end of the chromatogram of EtOH extract (Figure 1) can be identified as triterpenes because they do not absorb in the UV region and had a molecular constitution typical of triterpenes derivatives (25–29). The main product ions observed in the mass spectra were due to the loss of  $CH_3$  (15 Da) and  $H_2O$  (18 Da). These compounds are isomers and were not completely identified.

The *in vitro* leishmanicidal activity was evaluated with extract and fractions of propolis. The results presented in Table 2 show

**TABLE 2 |** Determination of the cytotoxicity of pentamidine, EtOH extract, and hexane, EtOAc, MeOH fractions, of propolis from the semi-arid region of Bahia, Brazil against J774.A1 cells using the MTT assay.

Treatment	IC <sub>50</sub> (μM) <sup>a</sup>	Maximum Cytotoxicity (%) <sup>b</sup>
Pentamidine	44.1 ± 0.8 μM	93.8 ± 0.7**+
EtOH	>100 μg/ml	ND
Hexane	>100 μg/ml	ND
EtOAc	>100 μg/ml	ND
MeOH	>100 μg/ml	ND

<sup>a</sup>Inhibitory concentration 50 (IC<sub>50</sub>) calculated by concentration-response curves toxic.

<sup>b</sup>Mean ± standard error of the mean maximum cytotoxicity in triplicates of a representative experiment. The values of maximum effect were considered significant when \*\*p < 0.01 compared to the 0.1% DMSO group. IC<sub>50</sub> is the concentration required to give 50% inhibition. ND: Not determined. Maximum cytotoxicity compared to the DMSO group.

the effects of the ethanol extract (EtOH), hexane fraction (hexane), ethyl acetate fraction (EtOAc), methanolic fraction (MeOH), and pentamidine against J774.A1 macrophages using the MTT assay. After 48 h of incubation, pentamidine showed deleterious activity to the host cell with maximum cytotoxicity of 93.8 ± 0.7% and IC<sub>50</sub> of 44.1 ± 0.8 μM. However, the extract, and fractions not showed deleterious activity to the host cell, presenting as promising substances for the other assays. Orsi et al. (2005), observed that Brazilian propolis was not toxic to macrophages, and using cytotoxicity assays, Blonska et al. (2004), observed that the ethanolic extract of propolis was not toxic to these macrophage cells.

**TABLE 3** | Effects of pentamidine, EtOH extract; hexane, EtOAc, MeOH fractions of propolis from the semi-arid region of Bahia, Brazil against promastigote forms of *L. amazonensis* and *L. chagasi*.

Treatment	<i>L. amazonensis</i>		<i>L. chagasi</i>	
	IC <sub>50</sub> <sup>a</sup>	Maximum effect (%) <sup>b</sup>	IC <sub>50</sub> <sup>a</sup>	Maximum effect (%) <sup>b</sup>
Pentamidine	4.7 ± 1.0 μM	97.8 ± 0.7***	6.1 ± 0.3 μM	96.5 ± 0.4***
EtOH	7.1 ± 1.1 μg/ml	94.3 ± 1.9***	4.2 ± 0.9 μg/ml	71.5 ± 2.3**
Hexane	8.2 ± 2.6 μg/ml	96.1 ± 0.2***	6.2 ± 1.9 μg/ml	68.6 ± 7.5**
EtOAc	5.8 ± 0.5 μg/ml	96.6 ± 1.2***	6.6 ± 0.3 μg/ml	71.5 ± 2.4**
MeOH	5.6 ± 1.0 μg/ml	95.8 ± 1.3***	7.3 ± 0.9 μg/ml	53.9 ± 7.5**

<sup>a</sup>Inhibitory concentration 50 (IC<sub>50</sub>) calculated by concentration-response curves toxic.

<sup>b</sup>Mean ± standard error of the mean maximum cytotoxicity in triplicates of a representative experiment. Differences with \*\*p < 0.01 and \*\*\*p < 0.001 were considered significant in relation to the 0.1% DMSO group. IC<sub>50</sub> is the concentration required to give 50% inhibition. The maximum effect was at concentrations 10 μg/ml.

The leishmanicidal activity of EtOH extract; hexane, EtOAc, MeOH fractions, and pentamidine against the promastigote forms of *L. amazonensis* and *L. chagasi* was assessed *in vitro*. The inhibitory effects and IC<sub>50</sub> values are shown in Table 3. Hexane, EtOAc, and MeOH fractions exhibited the most significant leishmanicidal activity to *L. amazonensis*. The EtOH extract, hexane and EtOAc fractions exhibited the most significant leishmanicidal activity to *L. chagasi*. Thus, it is observed that EtOH extract and EtOAc fraction showed the best inhibitory activity against the growth of promastigote forms of *L. amazonensis* and *L. chagasi*, respectively. Moreover, EtOAc and MeOH fractions showed the anti-amastigote activity against *L. amazonensis* and *L. chagasi*, respectively.

## DISCUSSION

The presence of flavonoids and terpenes were identified in the active EtOH extract, hexane and EtOAc fractions. In this study, the chemical profile of the flavonoids is similar to that found for the geopropolis samples of stingless bees collected in the semi-arid region (Sousa-Junior et al., 2019; Sousa-Fontoura et al., 2020). However, additional studies need to be carried out to know the origin of the plant species from which bees collect the resin in the semi-arid region of Brazil.

Propolis is an important source of substances applied in medicine due to its pharmacological activities (Potin et al., 2008) and wide range of biological properties, including

leishmanicidal activity (Duran et al., 2008; Potin et al., 2008; Nina et al., 2016). In another study, the ethanolic extract of propolis showed leishmanicidal activity against *L. tropica* at concentrations of 250, 500 and 750 μg/ml, and statistically significant differences in cell counts were observed compared to the control group (*p* < 0.05) (Duran et al., 2008), whereas the fractionated propolis-rich phenolic showed maximum efficacy against *L. amazonensis* (IC<sub>50</sub> = 12.1 μg/ml) and *L. brasiliensis* (IC<sub>50</sub> = 10.9 μg/ml) (Nina et al., 2016). Extracts of propolis were tested against protozoal pathogens, including *Crithidia fasciculata* a close relative of *Crithidia mellificae*, a parasite of bees. High levels of activity were obtained for all the samples of different extracts. In the case of *C. fasciculata* highest activity was associated with flavonoids methyl ethers of galangin and pinobanksin (Alotaibi et al., 2019). According to Ruiz-Gonzalez and Brown (2006), the spread of the protozoal infection occurs via feces, coating the surfaces in the hive with propolis that is active against trypanosomiasis could prevent transmission.

The results of the evaluation of leishmanicidal activity against intracellular forms of *L. amazonensis* revealed that hexane fraction induced the growth inhibition of amastigotes forms by 60.4 ± 1.4%, 63.4 ± 1.7%, 59.4 ± 1.9%, and they had IC<sub>50</sub> values of 1.3 ± 0.1 μg/ml, 1.9 ± 1.5 μM, and 1.4 ± 0.9 μM, respectively (Table 4).

According to Ayres et al. (2007), the ethanolic extract of propolis presented a direct effect on the amastigote forms of *L. amazonensis*, up to 96 h, at a concentration of 25 μg/ml.

Despite being widely studied, propolis remains an important source of metabolites for the treatment of diseases. Moreover,

**TABLE 4** | Effects of pentamidine, EtOH extract; hexane, EtOAc, MeOH fractions of propolis from the semi-arid region of Bahia, Brazil, against amastigote forms of *L. amazonensis* and *L. chagasi*.

Treatment	<i>L. amazonensis</i>		<i>L. chagasi</i>	
	IC <sub>50</sub> <sup>a</sup>	Maximum effect (%) <sup>b</sup>	IC <sub>50</sub> <sup>a</sup>	Maximum effect (%) <sup>b</sup>
Pentamidine	1.5 ± 1.2 μM	69.2 ± 0.4**	1.7 ± 0.5 μM	75.3 ± 2.0**
EtOH	>100 μg/ml	ND	>100 μg/ml	ND
Hexane	1.3 ± 0.1 μg/ml	60.4 ± 1.4**	>100 μg/ml	ND
EtOAc	>100 μg/ml	ND	>100	ND
MeOH	>100 μg/ml	ND	7.2 ± 0.4 μg/ml	55.2 ± 1.0*

Data are reported as the mean ± standard error of the mean, S.E.M. The values of efficacy were considered significant when \*p < 0.05, \*\*p < 0.01, and \*\*\*p < 0.001 compared to the 0.1% DMSO group. IC<sub>50</sub> is the concentration required to give 50% inhibition; ND: not determined; Maximum cytotoxicity compared to the DMSO group. The maximum effect was at concentrations 10 μg/ml to fractions.

leishmaniasis is a current public health issue with a high global social impact. The currently available treatments for this disease are limited in terms of toxicity, and they have variable efficacy and high costs, which potentiates the results obtained in this study.

## CONCLUSION

To the best of our knowledge, this is the first study which describes the chemical composition and biological activity of propolis collected from the semi-arid region in Northeast Brazil. The extract, and fractions from propolis anti-leishmanial effects. The observed effects could be associated with the presence of flavonoids. The chemical and biological characterization of the semi-arid region could be important for the development of alternative treatment strategies against *Leishmania* sp.

## DATA AVAILABILITY STATEMENT

The raw data supporting the conclusions of this article will be made available by the authors, without undue reservation.

## REFERENCES

- Alotaibi, A., Ebiloma, G. U., Williams, R., Alenezi, S., Alenezi, A.-M., Guillaume, S., et al. (2019). European Propolis Is Highly Active against Trypanosomatids Including *Crithidia Fasciculata*. *Sci. Rep.* 9 (9), 11364. doi:10.1038/s41598-019-47840-y
- Ayres, D. C., Marcucci, M. C., and Giorgio, S. (2007). Effects of Brazilian Propolis on *Leishmania Amazonensis*. *Mem. Inst. Oswaldo Cruz*, 102 (102), 215–220. doi:10.1590/S0074-02762007005000020
- Blonska, M., Bronikowska, J., Pietsz, G., Czuba, Z. P., Scheller, S., and Krol, W. (2004). Effects of Ethanol Extract of Propolis (EEP) and its Flavones on Inducible Gene Expression in J774A.1 Macrophages. *J. Ethnopharmacology* 91 (91), 25–30. doi:10.1016/j.jep.2003.11.011
- Braga, S. S. (2019). Multi-target Drugs Active against Leishmaniasis: A Paradigm of Drug Repurposing. *Eur. J. Med. Chem.* 183, 111660. doi:10.1016/j.ejmech.2019.111660
- Dantas, A. P., Olivieri, B. P., Gomes, F. H. M., and De Castro, S. L. (2006). Treatment of *Trypanosoma Cruzi*-infected Mice with Propolis Promotes Changes in the Immune Response. *J. Ethnopharmacology*. 103 (103), 187–193. doi:10.1016/j.jep.2005.07.018
- Demarque, D. P., Crotti, A. E. M., Vessecchi, R., Lopes, J. L. C., and Lopes, N. P. (2016). Fragmentation Reactions Using Electrospray Ionization Mass Spectrometry: an Important Tool for the Structural Elucidation and Characterization of Synthetic and Natural Products. *Nat. Prod. Rep.* 33 (33), 432–455. doi:10.1039/c5np00073d
- Duran, G., Duran, N., Culha, G., Ozcan, B., Oztas, H., and Ozer, B. (2008). *In Vitro* antileishmanial Activity of Adana Propolis Samples on *Leishmania Tropica*: a Preliminary Study. *Parasitol. Res.* 102, 1217–1225. doi:10.1007/s00436-008-0896-5
- Freire, K. R. L., Lins, A. C. S., Dórea, M. C., Santos, F. A. R., Camara, C. A., and Silva, T. M. S. (2012). Palynological Origin, Phenolic Content, and Antioxidant Properties of Honeybee-Collected Pollen from Bahia, Brazil. *Molecules* 17 (17), 1652–1664. doi:10.3390/molecules17021652
- Hernandez, J., Goycoolea, F., Quintero, J., Acosta, A., Castañeda, M., Dominguez, Z., et al. (2007). Sonoran Propolis: Chemical Composition and Antiproliferative Activity on Cancer Cell Lines. *Planta Med.* 73, 1469–1474. doi:10.1055/s-2007-990244
- Hussain, R. F., Nouri, A. M., and Oliver, R. T. (1993). A New Approach for Measurement of Cytotoxicity Using Colorimetric Assay. *J. Immunol. Methods* (160), 89–96. doi:10.1016/0022-1759(93)90012-v

## AUTHOR CONTRIBUTIONS

GC contributed to chemical and biological study and analysis of the biological data. CC and TS designed the chemical study, supervised the laboratory work, identification of chemical compounds, and contributed to critical reading of the manuscript. ES contributed to collecting propolis samples and identification. MA designed the biological study, supervised the laboratory work, and contributed to critical reading of the manuscript. MS, AL, AQ, AS, and MA contributed to the biological study. All authors reviewed and approved the final manuscript.

## FUNDING

This work was financially supported by grants from Conselho Nacional de Desenvolvimento Científico e Tecnológico (CNPq Grant no. MeliApis 462941/2014-0 and Universal 425493/2018-0) and Fundação de Amparo a Ciência e Tecnologia do Estado de Pernambuco (FACEPE PRONEM APQ-244 0741106/2014), and Coordenação de Aperfeiçoamento de Pessoal de Nível Superior (CAPES - Finance Code 001).

- Ishida, V. F. C., Negri, G., Salatino, A., and Bandeira, M. F. C. L. (2011). A New Type of Brazilian Propolis Prenylated Benzophenones in Propolis from Amazon and Effects against Cariogenic Bacteria. *Food Chem.* (125), 966–972. doi:10.1016/j.foodchem.2010.09.089
- Jin, U.-H., Song, K.-H., Motomura, M., Suzuki, I., Gu, Y.-H., Kang, Y.-J., et al. (2008). Caffeic Acid Phenethyl Ester Induces Mitochondria-Mediated Apoptosis in Human Myeloid Leukemia U937 Cells. *Mol. Cell Biochem* 310, 43–48. doi:10.1007/s11010-007-9663-7
- Júnior, U. P. S., Cabrera, S. P., Silva, T. M. G. d., Silva, E. M. S. d., Camara, C. A., and Silva, T. M. S. (2019). Geopropolis Gel for the Adjuvant Treatment of Candidiasis - Formulation and *In Vitro* Release Assay. *Revista Brasileira de Farmacognosia* 29 (3), 278–286. doi:10.1016/j.bjrp.2019.02.010
- Ma, C., Lv, H., Zhang, X., Chen, Z., Shi, J., Lu, M., et al. (2013). Identification of Regioisomers of Methylated Kaempferol and Quercetin by Ultra High Performance Liquid Chromatography Quadrupole Time-Of-Flight (UHPLC-QTOF) Tandem Mass Spectrometry Combined with Diagnostic Fragmentation Pattern Analysis. *Analytica Chim. Acta* 795 (795), 15–24. doi:10.1016/j.aca.2013.07.038
- Matos, V. R., Alencar, S. M., and Santos, F. A. R. (2014). Pollen Types and Levels of Total Phenolic Compounds in Propolis Produced by *Apis mellifera* L. (Apidae) in an Area of the Semi-arid Region of Bahia, Brazil. *Acad. Bras. Ciênc.* 86 (86), 407–418. doi:10.1590/0001-376520142013-0109
- Moraes, T. R., Costa-Silva, T. A., Tempone, A. G., Borborema, S. E. T., Scotti, M. T., Souza, R. M. F., et al. (2014). Antiparasitic Activity of Natural and Semi-synthetic Tirucallane Triterpenoids from *Schinus Terebinthifolius* (Anacardiaceae): Structure/activity Relationships. *Molecules* (19), 5761–5776. doi:10.3390/molecules19055761
- Nina, N., Lima, B., Feresin, G. E., Giménez, A., Salamanca Capusiri, E., and Schmeda-Hirschmann, G. (2016). Antibacterial and Leishmanicidal Activity of Bolivian Propolis. *Lett. Appl. Microbiol.* 62 (62), 290–296. doi:10.1111/lam.12543
- Orsi, R. O., Sforzin, J. M., Funari, S. R. C., and Bankova, V. (2005). Effects of Brazilian and Bulgarian Propolis on Bactericidal Activity of Macrophages against *Salmonella Typhimurium*. *Int. Immunopharmacology* 5 (5), 359–368. doi:10.1016/j.intimp.2004.10.003
- Popova, M., Silić, S., Kaftanoglu, O., and Bankova, V. (2005). Antibacterial Activity of Turkish Propolis and its Qualitative and Quantitative Chemical Composition. *Phytomedicine* 12 (12), 221–228. doi:10.1016/j.phymed.2003.09.007
- Potin, K., Silva-Filho, A. A., Santos, F. F., Silva, M. L. A., Cunha, W. R., Nanayukkara, N. P. D., et al. (2008). *In Vitro* and *In Vivo* Antileishmanial

## Artigo III

- Activities of a Brazilian green Propolis Extract. *Parasitol. Res.* 103, 487–492. doi:10.1007/s00436-008-0970-z
- Ruiz-Gonzalez, M. X., and Brown, M. J. (2006). Honey Bee and Bumblebee Trypanosomatids: Specificity and Potential for Transmission. *Ecol. Entomol.* 31, 616–622. doi:10.1111/j.1365-2311.2006.00823.x
- Russo, A., Cardile, V., Sanchez, F., Troncoso, N., Vanella, A., and Garbarino, J. A. (2004). Chilean Propolis: Antioxidant Activity and Antiproliferative Action in Human Tumor Cell Lines. *Life Sci.* 76, 554–558. doi:10.1016/j.lfs.2004.07.019
- Santisteban, R., Cabrera, S., Neto, J., Silva, E., Correia, R., Alves, R., et al. (2019). ANÁLISES MELISSOPALINOLÓGICAS, FÍSICO-Químicas, ATIVIDADE ANTIRRADICALAR E PERFIL QUÍMICO POR UPLC-DAD-QTOF-MS/MS DOS MÉIS DE Friescomelitta Doederleini (ABELHA BRANCA): COMPARAÇÃO COM OS FENÓLICOS PRESENTES NAS FLORES DE Mimosa Tenuiflora (JUREMA PRETA). *Quím. Nova* 42 (8), 874–884. doi:10.21577/0100-4042.20170407
- Sasidharan, S., and Saudagar, P. (2021). Leishmaniasis: where Are We and where Are We Heading? *Parasitol. Res.* 120, 1541–1554. doi:10.1007/s00436-021-07139-2
- Sforcin, J. M. (2016). Biological Properties and Therapeutic Applications of Propolis. *Phytother. Res.* 30, 894–905. doi:10.1002/ptr.5605
- Silva, T. M. S., Camara, C. A., da Silva Lins, A. C., Maria Barbosa-Filho, J., da Silva, E. M. S., Freitas, B. M., et al. (2006). Chemical Composition and Free Radical Scavenging Activity of Pollen Loads from Stingless Bee *Melipona Subnitida* Ducke. *J. Food Compos. Anal.* 19 (19), 507–511. doi:10.1016/j.jfca.2005.12.011
- Silva, T. M. S., Camara, C. A., Lins, A. C. S., Agra, M. d. F., Silva, E. M. S., Reis, I. T., et al. (2009). Chemical Composition, Botanical Evaluation and Screening of Radical Scavenging Activity of Collected Pollen by the Stingless Bees *Melipona Rufiventris* (Uruçu-Amarela). *Acad. Bras. Ciênc.* 81, 173–178. doi:10.1590/S0001-37652009000200003
- Silva, T. M. S., dos Santos, F. P., Evangelista-Rodrigues, A., da Silva, E. M. S., da Silva, G. S., de Novais, J. S., et al. (2013). Phenolic Compounds, Melissopalynological, Physicochemical Analysis and Antioxidant Activity of Jandaira (*Melipona Subnitida*) Honey. *J. Food Compos. Anal.* 29 (29), 10–18. doi:10.1016/j.jfca.2012.08.010
- Singh, N., Manish, K., and Singh, R. K. (2012). Leishmaniasis: Current Status of Available Drugs and New Potential Drug Targets. *Asian Pac. J. Trop. Dis.* (5), 485–497. doi:10.1016/S1995-7645(12)60084-4
- Sousa-Fontoura, D. M. N., Olinda, R. G., VianaCosta, G. A. K. M. F. M., Batista, J. S., Serrano, R. M. O. T., et al. (2020). Wound Healing Activity and Chemical Composition of Geopropolis from *Melipona Subnitida*. *Rev. Bras. Farmacogn.* 30, 367–373. doi:10.1007/s43450-020-00030-8
- Souza, S. A., Camara, C. A., Silva, E. M. S., and Silva, T. M. S. (2013). Composition and Antioxidant Activity of Geopropolis Collected by *Melipona Subnitida* (Jandaira) Bees. *Evid. Based Complement. Alternat. Med.*, 1–5. doi:10.1155/2013/801383
- Souza, S. A., Dias, T. L. M. F., Silva, T. M. G., Falcão, R. A., Alexandre-Moreira, M. S., Silva, E. M. S., et al. (2014). Chemical Composition, Antinociceptive and Free Radical-Scavenging Activities of Geopropolis from *Melipona Subnitida* Ducke (Hymenoptera: Apidae: Meliponini). *Sociobiology* (61), 560–565. doi:10.13102/sociobiology.v61i4.560-565
- Szliszka, E., Kucharska, A. Z., Sokół-Lętowska, A., Mertas, A., Czuba, Z. P., and Król, W. (2013). Chemical Composition and Anti-inflammatory Effect of Ethanol Extract of Brazilian green Propolis on Activated J774A.1 Macrophages. *Evidence-Based Complement. Altern. Med.* 2013, 1–13. doi:10.1155/2013/976415
- Taslami, Y., Zahedifard, F., and Rafati, S. (2018). Leishmaniasis and Various Immunotherapeutic Approaches. *Parasitology* 145 (4), 497–507. doi:10.1101/75003118201600216x
- Tran, V. H., Duke, R. K., Abu-Mellal, A., and Duke, C. C. (2012). Propolis with High Flavonoid Content Collected by Honey Bees from Acacia Paradoxa. *Phytochemistry* 81, 126–132. doi:10.1016/j.phytochem.2012.06.002
- Valčić, S., Montenegro, G., and Timmermann, B. N. (1998). Lignans From Chilean propolis. *J. Nat. Prod.* 61, 771–775.

**Conflict of Interest:** The authors declare that the research was conducted in the absence of any commercial or financial relationships that could be construed as a potential conflict of interest.

Copyright © 2021 Cavalcante, Camara, Silva, Santos, Leite, Queiroz, Evelyn Da Silva, Araújo, Alexandre-Moreira and Silva. This is an open-access article distributed under the terms of the Creative Commons Attribution License (CC BY). The use, distribution or reproduction in other forums is permitted, provided the original author(s) and the copyright owner(s) are credited and that the original publication in this journal is cited, in accordance with accepted academic practice. No use, distribution or reproduction is permitted which does not comply with these terms.



## Leishmanicidal activity of Morita-Baylis–Hillman adducts

Ana Carolina Santana Vieira<sup>1</sup> · Mariana da Silva Santos<sup>1</sup> · Anderson Brandão Leite<sup>1</sup> · Amanda Evelyn da Silva<sup>1</sup> · Luiz Henrique Agra Cavalcante-Silva<sup>2</sup> · Gabrielle de Souza Augusto Pereira<sup>3</sup> · Sany Delany Gomes Marques<sup>3</sup> · Barbara Viviana de Oliveira Santos<sup>3</sup> · Alysson Wagner Fernandes Duarte<sup>4</sup> · Aline Cavalcante de Queiroz<sup>1,4</sup> · Kristerson Reinaldo de Luna-Freire<sup>3</sup> · Magna Suzana Alexandre-Moreira<sup>1</sup>

Received: 22 July 2021 / Accepted: 27 December 2021

This is a U.S. government work and not under copyright protection in the U.S.; foreign copyright protection may apply 2022

### Abstract

Leishmaniasis is a neglected disease that affects millions of people, mostly in developing countries. Although this disease has a high impact on public health, there are few drug options to treat the different leishmaniasis forms. Additionally, these current therapies have various adverse effects, including gastrointestinal disturbances, headache, pancreatitis, and hepatotoxicity. Thus, it is essential to develop new drug prototypes to treat leishmaniasis. Accordingly, the present study aimed to evaluate the leishmanicidal activity of Morita-Baylis–Hillman adducts and their O-acetylates, carboxylic acid derivatives, and acid and ester derivatives of 2-methyl-phenylpropanoids against *Leishmania chagasi*. Initially, we evaluated the cytotoxicity of 16 derivatives (1–16G) against J774A.1 macrophages. Eight derivatives (2G, 4G, 5G, 7G, 9G, 10G, 13G, and 15G) showed no cytotoxicity at up to the maximum concentration tested (100 µM). When evaluated for antileishmanial effect against promastigote forms, 1G, 6G, 8G, 10G, 11G, 13G, 14G, 15G, and 16G displayed significant toxicity compared to the control (0.1% DMSO). Additionally, the compounds 1G, 5G, 7G, 9G, 11G, 13G, 14G, and 16G reduced macrophage infection by amastigotes. Thus, we conclude that these derivatives have antileishmanial effects, particularly 1G, which showed activity against promastigotes and amastigotes, and low toxicity against macrophages.

**Keywords** Leishmaniasis · Morita-Baylis–Hillman adducts · *L. chagasi*

Section Editor: Nawal Hijawi

✉ Magna Suzana Alexandre-Moreira  
suzana.magna@gmail.com

Ana Carolina Santana Vieira  
carola\_mcz@hotmail.com

Mariana da Silva Santos  
nananoquel@hotmail.com

Anderson Brandão Leite  
bioufal@hotmail.com

Amanda Evelyn da Silva  
amanda.evelyn13@hotmail.com

Luiz Henrique Agra Cavalcante-Silva  
luiz0710@gmail.com

Gabrielle de Souza Augusto Pereira  
gabriellesouza@hotmail.com

Sany Delany Gomes Marques  
sanydelany@gmail.com

Barbara Viviana de Oliveira Santos  
barbara@lft.ufpb.br

Alysson Wagner Fernandes Duarte  
alysson.duarte@arapiraca.ufal.br

Aline Cavalcante de Queiroz  
aline.queiroz@arapiraca.ufal.br

Kristerson Reinaldo de Luna-Freire  
kristerson@cbiotech.ufpb.br

<sup>1</sup> Laboratory of Pharmacology and Immunity, Institute of Biological Sciences and Health, Federal University of Alagoas, Maceió, AL 57020-720, Brazil

<sup>2</sup> Institute of Biological Sciences and Health, Federal University of Alagoas, Maceió, AL 57020-720, Brazil

<sup>3</sup> Laboratory of Organic Synthesis, Biotechnology Center, Federal University of Paraíba, João Pessoa, PB 58051-900, Brazil

<sup>4</sup> Laboratory of Microbiology, Immunology and Parasitology, Campus Arapiraca, Federal University of Alagoas, Arapiraca, AL 57072-970, Brazil

## Introduction

Neglected tropical diseases (NTDs) are a group of communicable diseases that affect 149 countries, mainly the poorest ones, prevailing in tropical and subtropical regions and causing social and economic damage. Despite reaching humans for centuries, they were considered neglected due to lack of funding, research, and concern of health authorities during the twentieth century (Engelman et al. 2016; WHO 2015).

Leishmaniasis, one of 17 neglected diseases, is endemic in 98 countries. Its various forms cause deep and permanent scars or destroy the mucous membranes of the nose, mouth, and throat. In the most severe form, if untreated, it can lead to death rapidly, as it mainly affects the liver and spleen (WHO 2013, 2015). This complex of diseases is classified as tegumentary or visceral and caused by different species of the genus *Leishmania*, obligate intracellular parasites. They are among the ten priority endemics of the World Health Organization (WHO) because of their significant impact on public health. It is estimated that around 20 to 40 thousand people die each year from leishmaniasis and that 400 million are at risk of contracting the disease (Alvar et al. 2012; WHO 2009, 2013).

Currently, pentavalent antimonials (Sb<sup>+5</sup>) are the drugs of choice for the treatment of all forms of leishmaniasis, followed by amphotericin B and pentamidine salts. As a second choice, if this treatment shows no response or if it cannot be applied, miltefosine and amphotericin B deoxycholate (antifungal antibiotic) are indicated. All these therapies have a high cost, adverse effects, and varied therapeutic response, which limits the patients' access to quality treatment. Currently, there is no approved vaccine available for humans (Sabbaga Amato et al. 2007; MacHado et al. 2015; WHO 2010).

The search for new drugs of natural or synthetic origin is a challenge for researchers nowadays (Neri et al. 2020; Ghodsian et al. 2020; Hounda Fokou et al. 2021; Maaroufi et al. 2021). In this context, Morita-Baylis–Hillman adducts (MBHA) and their derivatives have been studied as promising antiparasitic drugs, showing activity against promastigote forms of *Leishmania brasiliensis*, *L. chagasi*, and *L. donovani*. (Barbosa et al. 2011; Lima-Junior and Vasconcellos 2012; Silva et al. 2016a, b; Xavier et al. 2016; Souza et al. 2017). Likewise, the phenylpropanoids are described in the scientific literature for their antiparasitic potential against trypanosomatids (Abreu et al. 2020; Sulistyowaty et al. 2021), including the leishmanicidal activity (Abdel-Mageed et al. 2012; Costa-Silva et al. 2015; Chauhan et al. 2019). Therefore, the hypothesis of this study is that the production and biological evaluation of MBHA of phenylpropanoids as new leishmanicidal

derivatives is a promising strategy for the development of useful therapeutic alternatives for this neglected disease.

The Morita-Baylis–Hillman reaction provides polyfunctional, simple, and versatile molecules through carbon–carbon bond formation with high atom-economy. This sustainable transformation provides highly substituted small molecules, which can be used as valuable starting materials for the synthesis of natural products, heterocyclic compounds, and drugs (Das et al. 2006; Basavaiah et al. 2007; Basavaiah and Naganaboina 2018; Luna-Freire et al. 2011, 2014).

The low cost and ready availability of the reagents make the reaction advantageous and economical since all atoms are incorporated into the product. Moreover, it is considered green chemistry or a sustainable reaction, since it can be performed in aqueous media and in the absence of some solvents (Sheldon 2005).

According to WHO (2010, 2015), access to free and well-designed essential medicines is one of the ways to improve access to health for the most disadvantaged populations. Considering the exposed scenario, the search for new treatment alternatives is needed, mainly with greater effectiveness, less adverse effects, and better dosage forms. Thus, the present study aimed to evaluate the leishmanicidal activity of MBHA adducts and their O-acetylates, carboxylic acid derivatives, and acid and ester derivatives of 2-methyl-phenylpropanoids in the search for new drug prototypes, since these compounds contain chemical fragments privileged in relation to this biological activity.

## Material and methods

### Synthesis of compounds

The compounds 1G–16G tested in this work (Fig. 1) were synthesized according to procedures described in previous works (Fig. 2) (Stork et al. 1978; Basavaiah et al. 1999; Amarante et al. 2010; Luna-Freire et al. 2011, 2014).

80% yield. Methyl 2-[(2-chloroquinolin-3-yl)(hydroxy)methyl]prop-2-enoate (**1G**)—FTIR (KBr, cm<sup>-1</sup>): 3537, 3216, 3062, 2992, 2955, 1702, 1619, 1490, 1138, 1033, 759. <sup>1</sup>H NMR (250 MHz, CDCl<sub>3</sub>): δ (ppm) 3,8 (s, 3H); 5,65 (s, 1H); 6,1 (s, 1H); 6,40 (s, 1H); 7,5 (t, 1H); 7,75 (t, 1H); 7,8 (d, 1H); 8,0 (d, 1H); 8,4 (s, 1H). <sup>13</sup>C RMN (62,5 MHz, CDCl<sub>3</sub>): δ (ppm) 52,51; 69,45; 127,40; 127,46; 127,97; 128,05; 128,37; 130,81; 132,89; 137,29; 140,42; 147,33; 149,49; 167,06.

92% yield. 2-[(2-Chloroquinolin-3-yl)(hydroxy)methyl]prop-2-enoic acid (**2G**)—FTIR (KBr, cm<sup>-1</sup>): 3271, 1702, 1655, 1421, 1276, 1038, 957, 760. <sup>1</sup>H NMR (200 MHz, CD<sub>3</sub>OD): δ (ppm) 5,85 (d, 1H, *J* = 5,92 Hz); 6,35 (d, 1H, *J* = 5,90 Hz); 7,28 (dd, 1H, *J* = 7,85 e 15,52 Hz); 7,50 (m,

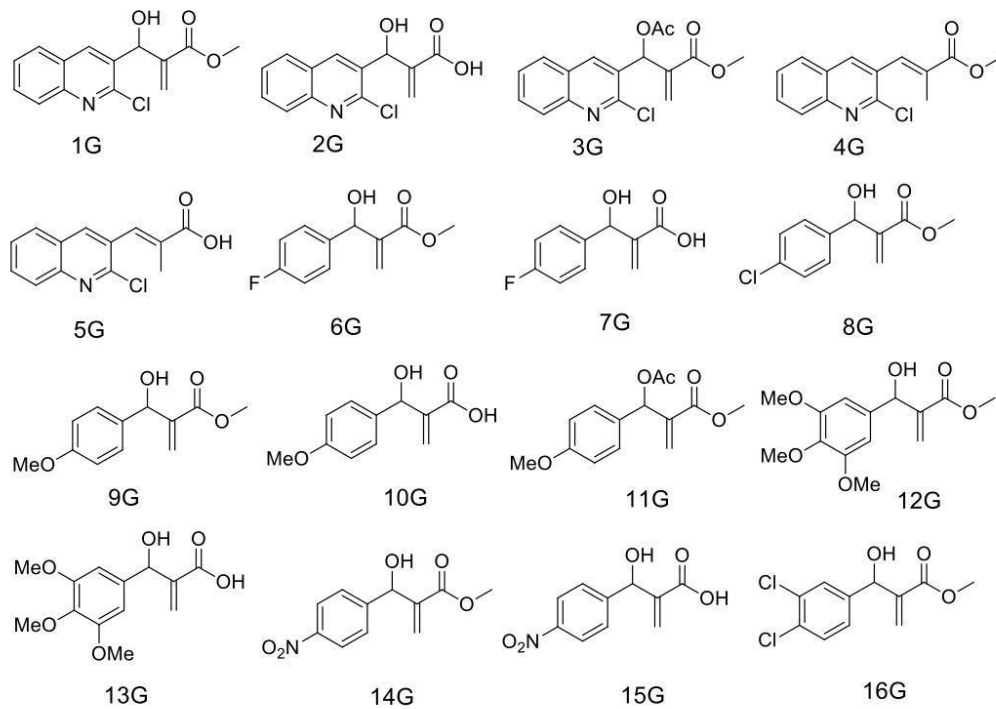


**Fig. 1** Chemical structures of the antileishmanial synthetic compounds tested

1H); 7,64 (d, 1H,  $J=7,70$  Hz); 7,92 (d, 1H,  $J=3,01$ ).  $^{13}\text{C}$  NMR (100 MHz,  $\text{CD}_3\text{OD}$ ):  $\delta$  (ppm) 67,29; 121,20; 123,90; 126,37; 129,20; 131,60; 138,18; 139,21; 143,39; 143,74; 169,17.

83% yield. Methyl 2-[(acetyloxy)(2-chloroquinolin-3-yl)methyl]prop-2-enoate (**3G**)—FTIR ( $\text{KBr}$ ,  $\text{cm}^{-1}$ ): 3079, 2949, 1726, 1623, 1435, 1246, 1053, 955, 750.  $^1\text{H}$  NMR (200 MHz,  $\text{CDCl}_3$ ):  $\delta$  (ppm) 2,31 (s, 3H); 3,89 (s, 3H); 5,96 (m, 1H); 6,72 (m, 1H); 7,72 (m, 1H); 7,89 (ddd, 1H,  $J=1,44$ ; 6,96 e 8,46 Hz); 7,97 (m, 1H); 8,17 (m, 1H); 8,28 (s, 1H).  $^{13}\text{C}$  NMR (50 MHz,  $\text{CDCl}_3$ ):  $\delta$  (ppm) 20,9; 52,37; 70,11; 126,93; 127,50; 127,84; 128,39; 128,60; 129,90; 131,08; 137,55; 137,66; 147,43; 149,86; 165,14; 169,16.

75% yield. Methyl (2*E*)-3-(2-chloroquinolin-3-yl)-2-methylprop-2-enoate (**4G**)—FTIR ( $\text{KBr}$ ,  $\text{cm}^{-1}$ ): 3443, 2925, 2851, 1718, 1437, 1266, 1226, 1051, 750.  $^1\text{H}$  NMR (200 MHz,  $\text{CDCl}_3$ ):  $\delta$  (ppm) 2,23 (s, 3H); 3,89 (s, 3H); 7,75 (d, 1H,  $J=7,20$  Hz); 7,93 (dd, 3H,  $J=8,19$  e 19,13 Hz); 8,19 (m, 1H); 8,28 (s, 1H).  $^{13}\text{C}$  NMR (50 MHz,  $\text{CDCl}_3$ ):  $\delta$  (ppm) 52,36; 79,1; 126,75; 126,92; 127,86; 128,41; 128,58; 129,86; 131,13; 131,89; 134,24; 137,56; 138,88; 147,42; 149,88; 169,22.

95% yield. (2*E*)-3-(2-Chloroquinolin-3-yl)-2-methylprop-2-enoic acid (**5G**)—FTIR ( $\text{KBr}$ ,  $\text{cm}^{-1}$ ): 3476, 2961, 2924, 2871, 1690, 1624, 1268, 1056, 759.  $^1\text{H}$  NMR (200 MHz,  $\text{CDCl}_3$ ):  $\delta$  (ppm) 2,04 (s, 3H); 8,20 (m, 1H); 8,38 (m, 1H); 8,63 (m, 1H); 8,86 (m, 1H).  $^{13}\text{C}$  NMR (100 MHz,  $\text{CD}_3\text{OD}$ ):  $\delta$  (ppm) 14,15; 128,28; 128,51; 128,81; 129,30; 129,84; 132,40; 133,79; 134,76; 140,59; 148,02; 151,14; 170,77.

81% yield. Methyl 2-[(4-fluorophenyl)(hydroxy)methyl]prop-2-enoate (**6G**)—FTIR ( $\text{KBr}$ ,  $\text{cm}^{-1}$ ): 3452, 3003, 2954, 2901, 2848, 1713, 1604, 960, 834.  $^1\text{H}$  NMR (200 MHz,  $\text{CDCl}_3$ ):  $\delta$  (ppm) 4,62 (s, 3H); 6,447 (s, 1H); 6,81 (s, 1H); 7,94 (t, 1H,  $J=8,65$  Hz); 8,26 (dd, 2H,  $J=5,59$  Hz, 8,36 Hz).  $^{13}\text{C}$  NMR (50 MHz,  $\text{CDCl}_3$ ):  $\delta$  (ppm) 51,81; 72,08; 114,94; 115,37; 125,76; 128,24; 128,44; 137,21; 142,01; 159,76; 164,68; 166,61.

89% yield. 2-[(4-Fluorophenyl)(hydroxy)methyl]prop-2-enoic acid (**7G**)—FTIR ( $\text{KBr}$ ,  $\text{cm}^{-1}$ ): 3358, 3878, 2547, 1689, 1605, 1511, 1235, 1028, 828.  $^1\text{H}$  NMR (200 MHz,  $\text{CDCl}_3$ ):  $\delta$  (ppm) 6,34 (s, 1H); 6,72 (s, 1H); 7,83 (t, 2H,  $J=8,38$ ); 8,12 (m, 2H).  $^{13}\text{C}$  NMR (50 MHz,  $\text{CDCl}_3$ ):  $\delta$  (ppm) 72,12; 115,21; 115,64; 128,45; 128,60; 136,58; 136,63; 141,37; 160,01; 164,9; 179,7.



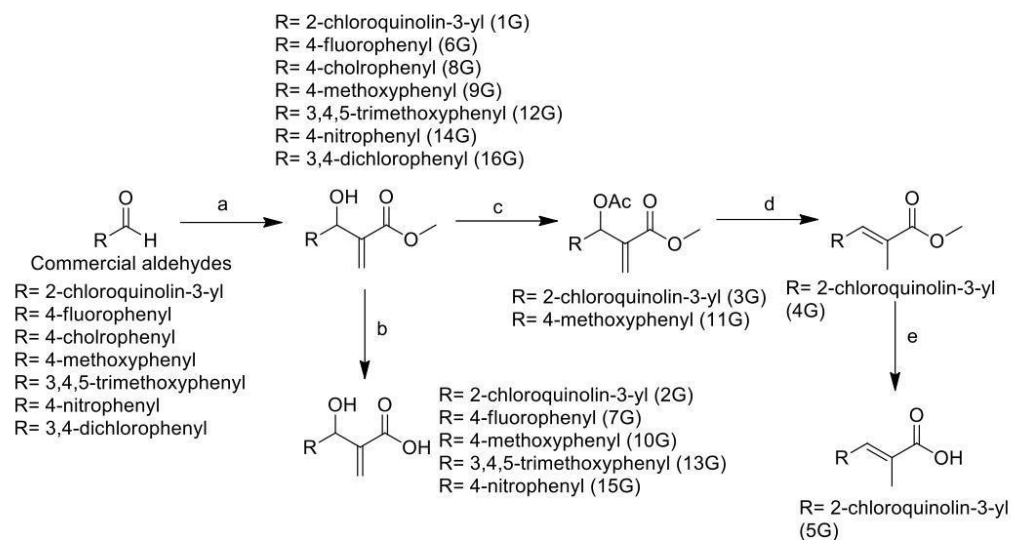


**Fig. 2** Scheme — Reagents and conditions: (a) methyl acrylate, DABCO, r.t.; (b, e) LiOH, acetonitrile:water (1:1), 50–60 °C; (c) acetic anhydride, pyridine, DMAP, DCM, r.t.; (d) NaBH<sub>4</sub>, t-BuOH, rt

78% yield. Methyl 2-[(4-chlorophenyl)(hydroxy)methyl]prop-2-enoate (**8G**)—FTIR (KBr, cm<sup>-1</sup>): 3359, 3102, 3018, 2959, 1718, 1635, 1437, 1275, 1037, 813, 744. <sup>1</sup>H NMR (200 MHz CDCl<sub>3</sub>): δ (ppm) 3,71 (s, 3H); 5,5 (s, 1H); 5,83 (s, 1H); 6,33 (s, 1H), 7,30 (s, 4H). <sup>13</sup>C NMR (50 MHz, CDCl<sub>3</sub>): δ (ppm) 52,17; 72,67; 126,43; 128,08; 128,65; 133,64; 139,89; 141,69; 166,70.

60% yield. Methyl 2-[hydroxy(4-methoxyphenyl)methyl]prop-2-enoate (**9G**)—FTIR (KBr, cm<sup>-1</sup>): 3358, 3001, 2952, 2833, 1717, 1512, 1259, 1023, 826, 579. <sup>1</sup>H NMR (250 MHz, CDCl<sub>3</sub>): δ (ppm) 2,94 (d, 1H); 3,6 (s, 3H); 3,79 (s, 3H); 5,53 (d, 1H); 5,85 (s, 1H); 6,32 (s, 1H); 6,85 (d, 2H); 7,29 (d, 2H). <sup>13</sup>C NMR (62,5 MHz, CDCl<sub>3</sub>): δ (ppm) 52,10; 55,45; 72,96; 114,03; 125,80; 128,09; 133,66; 142,38; 159,43; 166,99.

92% yield. 2-[Hydroxy(4-methoxyphenyl)methyl]prop-2-enoic acid (**10G**)—FTIR (KBr, cm<sup>-1</sup>): 3465, 2959, 2838, 1700, 1609, 1513, 1252, 1175, 1032, 829, 580. <sup>1</sup>H NMR (450 MHz, MeOD): δ (ppm) 3,73(s, 3H), 5,08 (s, 1H); 5,84 (s, 1H), 6,27 (s, 1H); 6,84 (d, 2H, *J*=9,5); 7,22 (d, 2H, *J*=9,5). <sup>13</sup>C NMR (112,5 MHz, MeOD): δ (ppm) 55,67, 81,76; 114,59; 130,00; 132,98; 136,63; 143,20; 145,91; 160,7; 173,42.

77% yield. Methyl 2-[(acetyloxy)(4-methoxyphenyl)methyl]prop-2-enoate (**11G**)—FTIR (KBr, cm<sup>-1</sup>): 3461, 3008, 2954, 2839, 1739, 1611, 1514, 1230, 1030, 828, 563. <sup>1</sup>H NMR (200 MHz, CDCl<sub>3</sub>): δ (ppm) 2,71 (s, 3H);

4,32 (s, 3H); 4,41 (s, 3H); 6,50 (s, 1H); 7,00 (s, 1H); 7,49 (d, 2H, *J*=8,73 Hz); 7,93 (d, 2H, *J*=8,68 Hz). <sup>13</sup>C NMR (50 MHz, CDCl<sub>3</sub>): δ (ppm) 21,25; 52,09; 55,34; 72,95; 113,03; 125,23; 129,27; 129,88; 139,79; 159,71; 165,56; 169,59.

77% yield. Methyl 2-[hydroxy(3,4,5-trimethoxyphenyl)methyl]prop-2-enoate (**12G**)—FTIR (KBr, cm<sup>-1</sup>): 3491, 2997, 2943, 2839, 1716, 1126, 1003, 838, 683. <sup>1</sup>H NMR (250 MHz, CDCl<sub>3</sub>): δ (ppm) 3,14 (s, 1H); 3,74 (s, 3H); 3,83 (s, 9H); 5,50 (s, 1H); 5,82 (s, 1H); 6,32 (s, 1H); 6,58 (s, 2H). <sup>13</sup>C NMR (62,5 MHz, CDCl<sub>3</sub>): δ (ppm) 52,14; 56,19; 60,89; 73,31; 103,69; 126,29; 136,98; 137,55; 141,97; 153,31; 166,97.

71% yield. 2-[Hydroxy(3,4,5-trimethoxyphenyl)methyl]prop-2-enoic acid (**13G**)—FTIR (KBr, cm<sup>-1</sup>): 3458; 3371; 2974; 2941; 2841; 2561; 1709; 822; 685; 667. <sup>1</sup>H NMR (250 MHz, CDCl<sub>3</sub>): δ (ppm) 3,83 (s, 9H); 5,50 (s, 1H); 5,90 (s, 1H); 6,45 (s, 1H); 6,57 (s, 2H). <sup>13</sup>C NMR (62,5 MHz, CDCl<sub>3</sub>): δ (ppm) 56,24; 60,95; 73,01; 103,81; 128,44; 136,73; 141,57; 153,37; 170,75.

90% yield. Methyl 2-[hydroxy(4-nitrophenyl)methyl]prop-2-enoate (**14G**)—FTIR (KBr, cm<sup>-1</sup>): 3511, 3104, 2958, 1708, 1529, 1348, 1146, 1044, 984, 751. <sup>1</sup>H NMR (250 MHz, CDCl<sub>3</sub>): δ (ppm) 3,29 (d, 1H); 3,75 (s, 3H); 5,65 (d, 1H); 5,87 (s, 1H); 6,40 (s, 1H); 7,58 (d, 2H); 8,25 (d, 2H); <sup>13</sup>C NMR (62,5 MHz, CDCl<sub>3</sub>): δ (ppm) 52,20; 72,8; 123,6; 127,3; 140,9; 147,4; 148,6; 166,4.

98% yield. 2-[Hydroxy(4-nitrophenyl)methyl]prop-2-enoic acid (**15G**)—FTIR (KBr,  $\text{cm}^{-1}$ ): 3568, 3456, 2917, 2848, 1690, 1513, 1350, 1038, 752.  $^1\text{H}$  NMR (200 MHz,  $\text{CDCl}_3$ ):  $\delta$  (ppm) 5,53 (s, 1H); 5,84 (s, 1H); 6,30 (s, 1H); 7,5 (d, 2H); 8,04 (d, 2H).  $^{13}\text{C}$  NMR (50 MHz,  $\text{CDCl}_3$ ):  $\delta$  (ppm) 71,72; 123,30; 126,52; 127,5; 141,91; 147,03; 149,73; 167,76.

85% yield. Methyl 2-[(3,4-dichlorophenyl)(hydroxy)methyl]prop-2-enoate (**16G**)—FTIR (KBr,  $\text{cm}^{-1}$ ): 1432, 2952, 2867, 1719, 1629, 1469, 1151, 1031, 961, 820.  $^1\text{H}$  NMR (200 MHz,  $\text{CDCl}_3$ ):  $\delta$  (ppm) 4,63 (s, 3H); 6,38 (s, 1H); 6,78 (s, 1H); 8,10 (d, 1H,  $J=8,19$  Hz); 8,32 (m, 2H).  $^{13}\text{C}$  NMR (50 MHz,  $\text{CDCl}_3$ ):  $\delta$  (ppm) 52,17; 71,82; 128,04; 128,66; 128,64; 130,30; 131,63; 132,40; 141,60; 141,73; 166,40.

### In vitro pharmacological tests

**Promastigote culture** The parasite of the Gonçalo Moniz—Fiocruz—BA Research Center, provided by Dr. Valéria de Matos Borges (MCAN/BR/89/BA262), was used to culture the *L. chagasi* promastigotes. These promastigotes were maintained in vitro in Schneider's medium supplemented with 10% fetal bovine serum (FBS) and 2% male human urine at 27 °C in a biochemical oxygen demand (BOD) incubator. For the experiments, the parasites were placed in Falcon tubes and centrifuged at 3500 rpm for 10 min. The supernatant was then discarded, and the pellet was resuspended in Schneider's medium. The parasites were then counted in a Neubauer chamber for plating and thus the subsequent assays.

**Macrophage culture** J774.A1 macrophages were maintained in culture flasks containing 10 mL of RPMI medium supplemented with 10% FBS, 2 mM L-glutamine, non-essential amino acids, and pyruvate. For the experiments, the cells were counted, adjusted in RPMI medium supplemented with 10% FBS, and then plated on a culture dish.

**Macrophage viability assay** For the study of cell viability of macrophages exposed to acyloxymethyl derivatives, we performed the MTT (3-(4,5-dimethylthiazol-2-yl)-2,5-diphenyltetrazolium bromide) reduction assay (Mosmann 1983; Hussain et al. 1993). J774.A.1 macrophages were seeded in 96-well plates for 1 h in ( $5 \times 10^4$ /well) and exposed to different concentrations of the diluted test compounds in supplemented RPMI medium (0.1, 1, 10, and 100  $\mu\text{M}$ ) for 24 h in a 37 °C incubator with a humid 5%  $\text{CO}_2$  atmosphere. Control wells contained cells with only culture medium or cells exposed to the diluent (0.1% DMSO). After incubation, the supernatant was discarded and 100  $\mu\text{L}$  of the MTT solution (5 mg/10 mL) was then added. The plates were incubated again for 1 h in a 37 °C incubator with a 5%  $\text{CO}_2$

atmosphere. After removing the supernatant, 100  $\mu\text{L}$  of DMSO was added and the plate read with a spectrophotometer at 550 nm. The cell viability of the wells treated with the synthesized compounds was compared to that of the death standard in the control cultures.

**Promastigote viability assay** Promastigote forms of *L. chagasi* at a density of  $1 \times 10^6$  parasites/well in a volume of 100  $\mu\text{L}$  were grown in triplicate in 96-well plates using Schneider's medium supplemented with 10% FBS, 2 mM L-glutamine, and 2% human urine. Different concentrations (0.1, 1, 10, and 100  $\mu\text{M}$ ) of the derivatives and controls (pentamidine, glucantime, RPMI medium, and 0.1% DMSO) were added to the wells containing the promastigote forms up to a final volume of 200  $\mu\text{L}$ . The plate was incubated in a BOD incubator at 27 °C for 48 h. Afterwards, 20  $\mu\text{L}$  of MTT solution was added to the wells, and the plates were placed in a  $\text{CO}_2$  incubator for 2 h. The MTT solution was then removed, and isopropyl alcohol was added to the wells to dissolve the formazan product. The plates were then read in a spectrophotometer at 550 nm. Cell viability of the wells treated with the synthesized compounds was compared to the death standard obtained in the control cultures.

**Macrophage infection with *L. chagasi* assay** J774.A1 macrophages were seeded at a density of  $5 \times 10^4$  cells/well in 24-well plates with coverslips for 1 h with supplemented RPMI medium. Macrophages were incubated overnight and subsequently infected with *L. chagasi* promastigotes, at a proportion of 10 parasites:1 macrophage. The plate was incubated for 6 h at 37 °C in a humid 5%  $\text{CO}_2$  atmosphere. Six hours after infection, the macrophages were washed with phosphate-buffered saline (PBS, pH 7.2), to remove the non-internalized parasites. Macrophages were cultured with RPMI supplemented with 10% FBS, 2 mM L-glutamine, 2 mM non-essential amino acids, and 2 mM sodium pyruvate, in the presence or absence of derivatives at a concentration of 10  $\mu\text{M}$ , and were kept in a 37 °C incubator with a humid 5%  $\text{CO}_2$  atmosphere for 24 h. Afterwards, the wells containing the coverslips were washed with PBS, and the cells were fixed with methanol, stained with May-Grünwald-Giemsa, and mounted on slides. The number of infected macrophages and the number of amastigotes in 100 macrophages were evaluated using a light microscope with 100 $\times$  oil-immersion objective (Nunes et al. 2005).

**Statistical analysis** All data are expressed as the mean  $\pm$  SEM and were analyzed by GraphPad Prism 8.0 software using one-way analysis of variance (ANOVA) followed by Dunnett's test. Differences were considered statistically significant when  $p < 0.05$ .

**Table 1** Effect of the test derivatives on the cell viability of J774.A1 macrophages in the MTT assay after 24 h

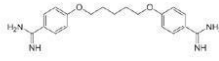
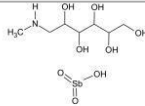
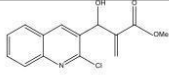
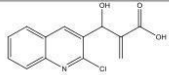
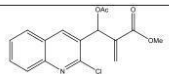
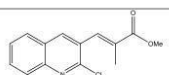
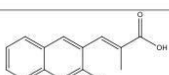
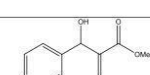
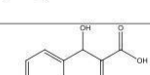
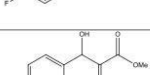
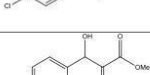
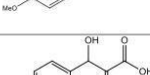
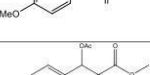
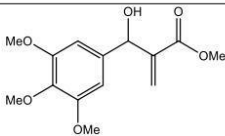
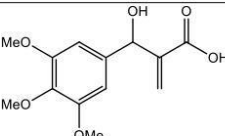
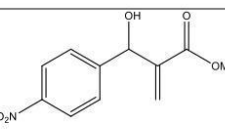
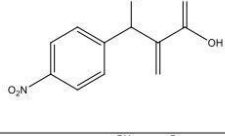
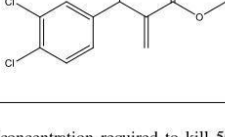
Derivative	Structure	IC <sub>50</sub> ( $\mu$ M) <sup>a</sup>	Maximum cytotoxicity (%) <sup>b</sup>	Cytotoxicity 10 $\mu$ M (%) <sup>c</sup>
Pentamidine		50.0 $\pm$ 2.8	89.7 $\pm$ 0.3***	16.4 $\pm$ 3.7***
Glucantime		> 100	25.4 $\pm$ 1.4 **	21.1 $\pm$ 0.2***
1G		> 100	48.6 $\pm$ 0.8***	NT
2G		> 100	NT	NT
3G		93.3 $\pm$ 1.2	53.3 $\pm$ 0.7***	NT
4G		> 100	NT	NT
5G		> 100	NT	NT
6G		> 100	79.1 $\pm$ 1.2***	NT
7G		> 100	NT	NT
8G		> 100	30.7 $\pm$ 1.8***	NT
9G		> 100	NT	10.2 $\pm$ 1.8*
10G		> 100	NT	NT
11G		> 100	75.2 $\pm$ 0.5***	62.5 $\pm$ 1.1***

Table 1 (continued)

12G		> 100	63.4 ± 3.2***	NT
13G		> 100	NT	NT
14G		93.3 ± 7.8	59.8 ± 4.7***	13.6 ± 1.6 *
15G		> 100	NT	NT
16G		> 100	75.1 ± 0.5***	71.4 ± 1.3***

The results refer to as follows: <sup>a</sup>concentration required to kill 50% of macrophages (IC<sub>50</sub>) determined by concentration–response curves; <sup>b</sup>mean ± standard error of the mean showing maximum cytotoxicity in triplicates of a representative experiment; and <sup>c</sup>cytotoxicity at 10 μM. *NT*, substance did not show significant lethal activity against macrophages at the concentrations of 100, 10, 1, or 0.1 μM compared to the DMSO group. Cytotoxicity was considered significant when \*\*\**p* < 0.001, \*\**p* < 0.01, or \**p* < 0.05 compared to the 0.1% DMSO group

## Results and discussion

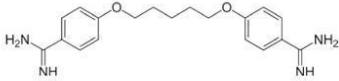
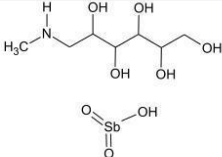
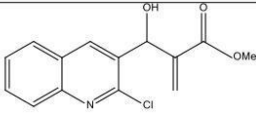
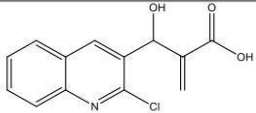
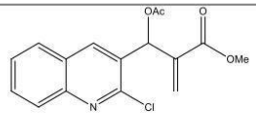
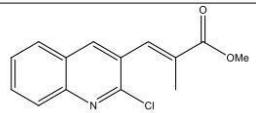
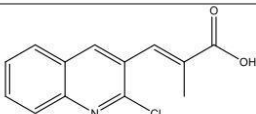
Leishmaniasis is a complex of diseases in which the cells of the mononuclear phagocytic system serve as host and replication site for the parasite as well. The parasite in turn resists lysis by the lysosomes and resides mainly in macrophages in the spleen and liver. It is important to note that the use of pentavalent antimonials is the first choice for the treatment of leishmaniasis in Brazil. However, they have a high cost and are hepatotoxic and nephrotoxic as well, which justifies the search for new therapeutic options (Ayres et al. 2007; Jain and Jain 2013).

The Morita-Baylis–Hillman reaction has proved to be effective, is low cost, and provides highly functional derivatives. Morita-Baylis–Hillman derivatives have been

studied since 1999 from a pharmacological point of view. They have a range of activities, including antifungal, anti-malarial, antineoplastic, molluscicide, antileishmanial, and antichagasic action (Lima-Junior and Vasconcellos 2012).

First, the compounds synthesized were evaluated for their effect on cell viability of J774A.1 macrophages using the MTT assay. The results showed that only the derivatives 2G, 4G, 5G, 7G, 9G, 10G, 13G, and 15G were not cytotoxic at up to the maximum concentration tested (100 μM). The other compounds (1G, 3G, 6G, 8G, 11G, 12G, 14G, and 16G) were cytotoxic when compared to the control (0.1% DMSO). When cytotoxicity was determined at a concentration of 10 μM, only 9G, 11G, 14G, and 16G showed a significant cytotoxic effect against macrophages (Table 1). As expected, 0.1% DMSO had no deleterious

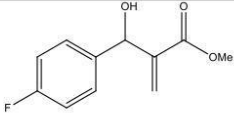
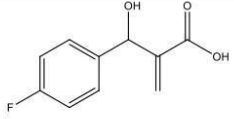
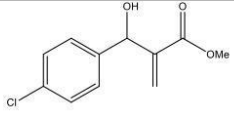
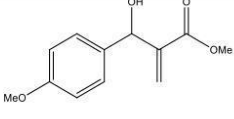
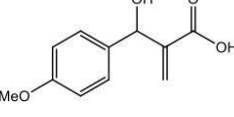
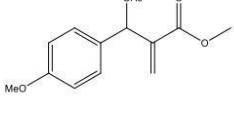
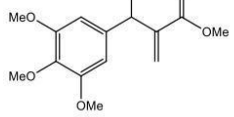
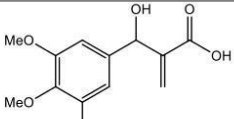
**Table 2** Effect of the test derivatives on the viability of *L. chagasi* promastigotes after 48 h of treatment

Derivative	Structure	IC <sub>50</sub> (μM) <sup>a</sup>	Maximum effect (%) <sup>b</sup>
Pentamidine		2.0 ± 1.0	97.5 ± 1.2***
Glucantime		2.0 ± 0.5	51.4 ± 0.3***
1G		0.6 ± 0.3	61.3 ± 2.6***
2G		> 100	NA
3G		> 100	NA
4G		> 100	NA
5G		> 100	NA

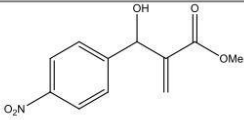
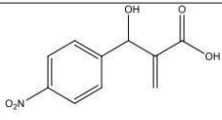
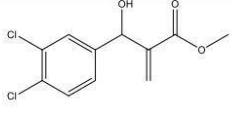
effect when compared to the negative control (RPMI culture medium). A similar assay was used by Silva et al. 2011 in evaluating the cytotoxicity of MBHA in peritoneal murine macrophages.

After determination of cytotoxicity in macrophages, the viability of promastigote forms treated with the derivatives and controls was evaluated by the MTT reduction assay. The results showed that the 1G, 6G, 8G, 10G, 11G, 13G,

Table 2 (continued)

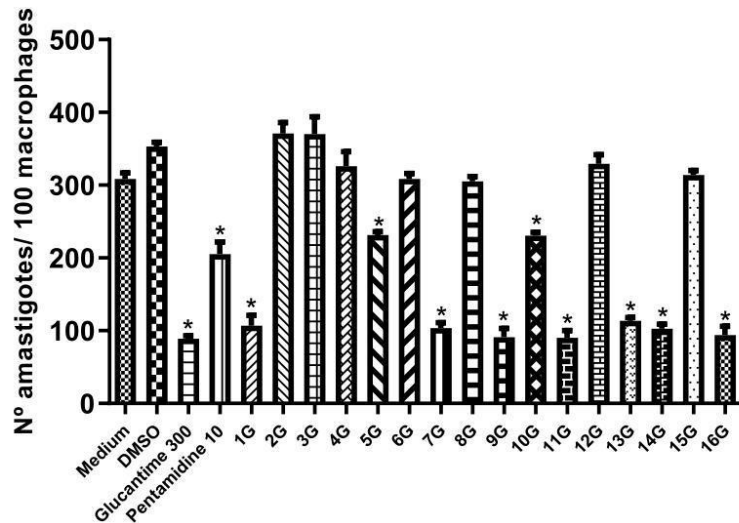
6G		$66.3 \pm 9.0$	$62.3 \pm 2.9^{***}$
7G		> 100	NA
8G		$0.6 \pm 0.3$	$67.0 \pm 4.1^{***}$
9G		> 100	NA
10G		> 100	$25.9 \pm 6.2^{***}$
11G		$58.3 \pm 3.4$	$88.1 \pm 4.4^{***}$
12G		> 100	NA
13G		> 100	$16.9 \pm 3.4^{**}$

**Table 2** (continued)

14G		> 100	22.5 ± 1.8*
15G		> 100	22.2 ± 1.5***
16G		4.3 ± 0.3	77.4 ± 1.3***

The results refer to as follows: <sup>a</sup>concentration required to kill 50% of the promastigote forms (IC<sub>50</sub>) determined by concentration–response curves and expressed as mean ± standard error of the mean; <sup>b</sup>maximum effect (ME) which is expressed as mean maximum toxicity ± standard error of mean for triplicate values of a representative experiment. ME values were considered significant when \*\*\**p* < 0.001, \*\**p* < 0.01, or \**p* < 0.05 compared to the 0.1% DMSO group. NA, substance had no significant lethal activity for *L. chagasi* promastigotes at the concentrations tested compared to the DMSO group

**Fig. 3** Leishmanicidal effect of the derivatives (10 μM) against the amastigote forms of *Leishmania chagasi*. The results refer to the mean ± standard error of the mean of triplicates of a representative experiment. The values were considered significant when \**p* < 0.05, when compared to the 0.1% DMSO group



14G, 15G, and 16G derivatives had a significant cytotoxic effect compared to the control (0.1% DMSO) (Table 2).

The direct leishmanicidal activity of MBHA has been previously described. Barbosa et al. (2011) evaluated the in vitro leishmanicidal activity of MBHA compounds in promastigotes of *L. chagasi* and *L. amazonensis*, using the molecular hybridization strategy, but without evaluating

cytotoxicity in macrophages. Additionally, it was previously observed that others MBHA had an antileishmanial effect against promastigote forms of *L. chagasi* after 72 h of treatment (Junior et al. 2010).

After cytotoxicity evaluation in macrophages and promastigote forms, the derivatives were evaluated for leishmanicidal activity in amastigote forms of *L. chagasi* at

a concentration of 10  $\mu$ M. The results obtained demonstrated that the test compounds 1G, 5G, 7G, 9G, 11G, 10G, 13G, 14G, and 16G caused a significant reduction in the number of amastigotes in 100 macrophages. On the other hand, the derivatives 2G, 3G, 4G, 6G, 8G, 12G, and 15G did not display leishmanicidal activity against intracellular parasites (Fig. 3).

Sandes et al. 2014 evaluated the effect of an MBHA on epimastigote forms of *Trypanosoma cruzi*. The group found that the 3-hydroxy-2-methylene-3-(4-nitrophenyl)propanenitrile adduct induced parasite cell death by necrosis, in a mitochondria-dependent manner. A range of therapeutic targets for the treatment of leishmaniasis has been emerging (Sundar and Singh 2018; Raj et al. 2020). The exact mechanism of action MBHA in *Leishmania* targets remains to be elucidated. However, it is possible that MBHA acts inhibiting *Leishmania* proteases (da Silva et al. 2016a, b), which are virulence factors related to the pathogenesis of this protozoan (Machado et al. 2019).

The compounds 1G, 11G, 13G, 14G, and 16G present antileishmanial activity against both amastigotes and promastigotes forms. However, 11G, 14G, and 15G derivatives showed significant cytotoxicity against macrophages, being 1G and 13G derivatives safer for mammalian cells based on this preliminary assay. Thus, in molecular prospecting for leishmanicidal compounds, this study demonstrates that derivative 1G is the most promising for drug development, since the compound was highly active against promastigotes, with  $IC_{50}$  lower than standard drugs and 13G derivative, and amastigotes of *L. chagasi*. In addition, it showed low toxicity against macrophages.

Considering that MBHA compounds are easy to synthesize and readily available, their use becomes an advantage when compared to the currently available drugs, since leishmaniasis is a neglected diseases and affects less fortunate populations (WHO 2010, 2015).

## Conclusion

On the basis of the results obtained, it can be concluded that some MBHA compounds, their O-acetylates, carboxylic acid derivatives, and acid and ester derivatives of 2-methylphenylpropanoids possess leishmanicidal activity in vitro against promastigotes and amastigotes of *L. chagasi*. Derivative 1G, which was active against promastigotes and amastigotes, showed low toxicity against the macrophage cell line J774A.1. Thus, it is a strong candidate for further pharmacological studies aimed at the treatment of leishmaniasis.

**Acknowledgements** Dr. A. Leyva (USA) helped with English editing of the manuscript.

**Funding** The authors thank the Universidade Federal de Alagoas (UFAL), the foundations Coordenação de Aperfeiçoamento de Pessoal de Nível Superior (CAPES) and Conselho Nacional de Desenvolvimento Científico e Tecnológico (CNPq), and the Instituto Nacional de Ciência e Tecnologia em Fármacos e Medicamentos (INCT-INOVAR) for funding this research.

## Declarations

**Conflict of interest** The authors declare no competing interests.

## References

- Abdel-Mageed WM, Backheet EY, Khalifa AA et al (2012) Antiparasitic antioxidant phenylpropanoids and iridoid glycosides from *Tecoma mollis*. *Fitoterapia* 83:500–507. <https://doi.org/10.1016/j.fitote.2011.12.025>
- Abreu LS, do Nascimento YM, do Espírito-Santo RF et al (2020) Phenylpropanoids from *Croton velutinus* with cytotoxic, trypanocidal and anti-inflammatory activities. *Fitoterapia* 145:104632. <https://doi.org/10.1016/j.fitote.2020.104632>
- Alvar J, Vélez ID, Bern C et al (2012) Leishmaniasis worldwide and global estimates of its incidence. *PLoS ONE* 7:e35671. <https://doi.org/10.1371/journal.pone.0035671>
- Amarante GW, Cavallaro M, Coelho F (2010) Highly diastereoselective total synthesis of the anti-tumoral agent ( $\pm$ )-Spisulosine (ES285) from a Morita-Baylis-Hillman adduct. *Tetrahedron Lett* 51:2597–2599. <https://doi.org/10.1016/j.tetlet.2010.02.169>
- Ayres DC, Marcucci MC, Giorgio S (2007) Effects of Brazilian propolis on *Leishmania amazonensis*. *Mem Inst Oswaldo Cruz* 102:215–220. <https://doi.org/10.1590/S0074-02762007005000020>
- Barbosa TP, Sousa SCO, Amorim FM et al (2011) Design, synthesis and antileishmanial in vitro activity of new series of chalcone-like compounds: a molecular hybridization approach. *Bioorganic Med Chem* 19:4250–4256. <https://doi.org/10.1016/j.bmc.2011.05.055>
- Basavaiah D, Krishnamacharyulu M, Hyma RS et al (1999) A facile one-pot conversion of acetates of the Baylis-Hillman adducts to [E]- $\alpha$ -methylcinnamic acids. *J Org Chem* 64:1197–1200. <https://doi.org/10.1021/jo981761b>
- Basavaiah D, Rao KV, Reddy RJ (2007) The Baylis-Hillman reaction: a novel source of attraction, opportunities, and challenges in synthetic chemistry. *Chem Soc Rev* 36:1581–1588. <https://doi.org/10.1039/b613741p>
- Basavaiah D, Naganaboina RT (2018) The Baylis-Hillman reaction: a new continent in organic chemistry - our philosophy, vision and over three decades of research. *New J Chem* 42:14036–14066
- Chauhan K, Kaur G, Kaur S (2019) Evaluation of antileishmanial efficacy of Salidroside against the SSG-sensitive and resistant strain of *Leishmania donovani*. *Parasitol Int* 72:101928. <https://doi.org/10.1016/j.parint.2019.101928>
- Da Costa-Silva TA, Grecco SS, De Sousa FS et al (2015) Immunomodulatory and antileishmanial activity of phenylpropanoid dimers isolated from *Nectandra leucantha*. *J Nat Prod* 78:653–657. <https://doi.org/10.1021/np500809a>
- da Silva WAV, Rodrigues DC, de Oliveira RG et al (2016a) Synthesis and activity of novel homodimers of Morita-Baylis-Hillman adducts against *Leishmania donovani*: a twin drug approach. *Bioorganic Med Chem Lett* 26:4523–4526. <https://doi.org/10.1016/j.bmcl.2016.07.022>



- Das B, Banerjee J, Chowdhury N, Majhi A (2006) Synthetic applications of Baylis-Hillman chemistry: an efficient and solely stereoselective synthesis of (E)- $\alpha$ -methylcinnamic acids and potent hypolipidemic agent LK-903 from unmodified Baylis-Hillman adducts. *Chem Pharm Bull* 54:1725–1727. <https://doi.org/10.1248/cpb.54.1725>
- Engelman D, Fuller LC, Solomon AW et al (2016) Opportunities for integrated control of neglected tropical diseases that affect the skin. *Trends Parasitol* 32:843–854. <https://doi.org/10.1016/j.pt.2016.08.005>
- Ghodsian S, Taghipour N, Deravi N et al (2020) Recent researches in effective antileishmanial herbal compounds: narrative review. *Parasitol Res* 119:3929–3946. <https://doi.org/10.1007/s00436-020-06787-0>
- Hussain RF, Nouri AME, Oliver RTD (1993) A new approach for measurement of cytotoxicity using colorimetric assay. *J Immunol Methods* 160:89–96. [https://doi.org/10.1016/0022-1759\(93\)90012-V](https://doi.org/10.1016/0022-1759(93)90012-V)
- Hzounda Fokou JB, Dize D, Etame Loe GM et al (2021) Anti-leishmanial and anti-trypanosomal natural products from endophytes. *Parasitol Res* 1–12. <https://doi.org/10.1007/s00436-020-07035-1>
- Jain K, Jain NK (2013) Novel therapeutic strategies for treatment of visceral leishmaniasis. *Drug Discov Today* 18:1272–1281. <https://doi.org/10.1016/j.drudis.2013.08.005>
- Junior CGL, De Assis PAC, Silva FPL et al (2010) Efficient synthesis of 16 aromatic Morita-Baylis-Hillman adducts: biological evaluation on *Leishmania amazonensis* and *Leishmania chagasi*. *Bioorg Chem* 38:279–284. <https://doi.org/10.1016/j.bioorg.2010.08.002>
- Lima-Junior CG, Vasconcelos MLAA (2012) Morita-Baylis-Hillman adducts: biological activities and potentialities to the discovery of new cheaper drugs. *Bioorganic Med Chem* 20:3954–3971. <https://doi.org/10.1016/j.bmc.2012.04.061>
- Luna-Freire KR, Scaramal JPS, Resende JALC et al (2014) An asymmetric substrate-controlled Morita-Baylis-Hillman reaction as approach for the synthesis of pyrrolizidinones and pyrrolizidines. *Tetrahedron* 70:3319–3326. <https://doi.org/10.1016/j.tet.2013.10.050>
- Luna-Freire KR, Tormena CF, Coelho F (2011) Heck reaction on morita-baylis-hillman adducts: diastereoselective synthesis of pyrrolizidinones and pyrrolizidines. *Synlett* 2011:2059–2063. <https://doi.org/10.1055/s-0030-1261161>
- Maaroufi Z, Cojean S, Loiseau PM et al (2021) In vitro antileishmanial potentialities of essential oils from *Citrus limon* and *Pistacia lentiscus* harvested in Tunisia. *Parasitol Res* 1–15. <https://doi.org/10.1007/s00436-020-06952-5>
- Machado P, Carneiro M, Sousa-Batista A et al (2019) Leishmanicidal therapy targeted to parasite proteases. *Life Sci* 219:163–181. <https://doi.org/10.1016/j.lfs.2019.01.015>
- MacHado PRL, Rosa MEA, Guimarães LH et al (2015) Treatment of disseminated leishmaniasis with liposomal amphotericin B. *Clin Infect Dis* 61:945–949. <https://doi.org/10.1093/cid/civ416>
- Mosmann T (1983) Rapid colorimetric assay for cellular growth and survival: application to proliferation and cytotoxicity assays. *J Immunol Methods* 65:55–63. [https://doi.org/10.1016/0022-1759\(83\)90303-4](https://doi.org/10.1016/0022-1759(83)90303-4)
- Neri FSM, Júnior DBC, Froes TQ et al (2020) Antileishmanial activity evaluation of thiazolidine-2,4-dione against *Leishmania infantum* and *Leishmania braziliensis*. *Parasitol Res* 119:2263–2274. <https://doi.org/10.1007/s00436-020-06706-3>
- Nunes MP, Cysne-Finkelstein L, Monteiro BC et al (2005) CD40 signaling induces reciprocal outcomes in *Leishmania*-infected macrophages; roles of host genotype and cytokine milieu. *Microbes Infect* 7:78–85. <https://doi.org/10.1016/j.micinf.2004.08.022>
- Raj S, Sasidharan S, Balaji S, Saudagar P (2020) An overview of biochemically characterized drug targets in metabolic pathways of *Leishmania* parasite. *Parasitol Res* 119:2025–2037. <https://doi.org/10.1007/S00436-020-06736-X>
- Sabbaga Amato V, Francisco Tuon F, Machado Siqueira A et al (2007) Treatment of mucosal leishmaniasis in Latin America: systematic review. *Am J Trop Med Hyg* 77:266–274
- Sandes JM, Fontes A, Regis-da-Silva CG et al (2014) Trypanosoma cruzi cell death induced by the Morita-Baylis-Hillman adduct 3-hydroxy-2-methylene-3-(4-nitrophenyl)propanenitrile. *PLoS ONE* 9:e93936. <https://doi.org/10.1371/journal.pone.0093936>
- Sheldon RA (2005) Green solvents for sustainable organic synthesis: state of the art. *Green Chem* 7:267–278. <https://doi.org/10.1039/b418069k>
- Silva FPL, De Assis PAC, Junior CGL et al (2011) Synthesis, evaluation against *Leishmania amazonensis* and cytotoxicity assays in macrophages of sixteen new congeners Morita-Baylis-Hillman adducts. *Eur J Med Chem* 46:4295–4301. <https://doi.org/10.1016/j.ejmech.2011.06.036>
- Silva WAV, Rodrigues DC, Oliveira RG et al (2016b) Synthesis and activity of novel homodimers of Morita-Baylis-Hillman adducts against *Leishmania donovani*: a twin drug approach. *Bioorg Med Chem Lett* 26:4523–4526. <https://doi.org/10.1016/j.bmcl.2016.07.022>
- Souza SCO, Rocha JC, Keesen TSL et al (2017) Synthesis of 16 new hybrids from tetrahydropyrans derivatives and Morita-Baylis-Hillman adducts: in vitro screening against *Leishmania donovani*. *Molecules* 22:2071-2071/14
- Stork G, Takahashi T, Kawamoto I, Suzuki T (1978) Total synthesis of prostaglandin F<sub>2</sub> $\alpha$  by chirality transfer from D-glucose 1,2. *J Am Chem Soc* 100:8272–8273. <https://doi.org/10.1021/ja00494a045>
- Sulistiyowaty MI, Uyen NH, Suganuma K et al (2021) Six new phenylpropanoid derivatives from chemically converted extract of alpinia galanga (L.) and their antiparasitic activities. *Molecules* 26:1756. <https://doi.org/10.3390/molecules26061756>
- Sundar S, Singh B (2018) Emerging therapeutic targets for treatment of leishmaniasis. *Expert Opin Ther Targets* 22:467–486
- WHO UNICEF/UNDP/World Bank/WHO Special Programme for Research and Training in Tropical Diseases & World Health Organization (2009). Research to support the elimination of visceral leishmaniasis: annual report 2008. World Health Organization. <https://apps.who.int/iris/handle/10665/70112>
- WHO Expert Committee on the Control of the Leishmaniases & World Health Organization (2010). Control of the leishmaniases: report of a meeting of the WHO Expert Committee on the Control of Leishmaniases, Geneva, 22–26 March 2010. World Health Organization. <https://apps.who.int/iris/handle/10665/44412>
- WHO/Department of control of neglected tropical diseases Sustaining the drive to overcome the global impact of neglected tropical diseases: Second WHO report on neglected tropical diseases. 2013. [https://www.who.int/neglected\\_diseases/9789241564540/en/](https://www.who.int/neglected_diseases/9789241564540/en/)
- WHO Investing to overcome the global impact of neglected tropical diseases: third WHO report on neglected diseases 2015. World Health Organization. <https://apps.who.int/iris/handle/10665/152781>
- Xavier FJS, Rodrigues KAF, Oliveira RG et al (2016) Synthesis and in vitro anti *Leishmania amazonensis* biological screening of Morita-Baylis-Hillman adducts prepared from eugenol, thymol and carvacrol. *Molecules* 21:1483/1-1483/12

**Publisher's note** Springer Nature remains neutral with regard to jurisdictional claims in published maps and institutional affiliations.

## REFERÊNCIAS

- AKHOUNDI, M. *et al.* A Historical Overview of the Classification, Evolution, and Dispersion of Leishmania Parasites and Sandflies. **PLoS neglected tropical diseases**, [S. l.], v. 10, n. 3, p. e0004349, 2016. Disponível em: <http://www.ncbi.nlm.nih.gov/pubmed/26937644> <http://www.pubmedcentral.nih.gov/articlerender.fcgi?artid=PMC4777430>. Acesso em 10 de junho de 2021.
- ALEXANDER, G.M. *et al.* Changes in plasma cytokines and their soluble receptors in complex regional pain syndrome. *J. Pain.*, **Philadelphia**, v. 13, n. 1, p. 10-20, 2012.
- ALVAR, J. *et al.* Canine leishmaniasis. **Advances in Parasitology**, [S. l.], v. 57, n. 04, p. 1–88, 2004.
- ALVAR, J. *et al.* Leishmaniasis worldwide and global estimates of its incidence. **PLoS ONE**, [S. l.], v. 7, n. 5, 2012. ISSN: 19326203. ISBN: 1932-6203 (Electronic)r1932-6203 (Linking). DOI: 10.1371/journal.pone.0035671.
- ANVERSA, L. *et al.* Human leishmaniasis in Brazil: a general review. **Revista da Associação Médica Brasileira**, São Paulo, v. 64 n. 3, Mar. 2018.
- BANETH, G; AROCH, I. Canine leishmaniasis: A diagnostic and clinical challenge. **The Veterinary Journal**, [S. l.], v. 175, n. 1, p. 14–15, 2008. ISSN: 10900233. ISBN: 1707666326. DOI: 10.1016/j.tvjl.2006.11.011. Disponível em: <http://linkinghub.elsevier.com/retrieve/pii/S1090023306002553>. Acesso em: 10 de junho de 2021.
- BASSELIN, M. *et al.* Effects of pentamidine on polyamine level and biosynthesis in wild-type pentamidine treated and pentamidine-resistant Leishmania. *Exp Parasitol.*, v. 85, p.274-282, 1997.
- BATES, P. A. Revising Leishmania's life cycle. **Nature microbiology**, v. 3, n. 5, p. 529-530, 2018.
- BELO, V. S. *et al.* Factors associated with visceral leishmaniasis in the americas: a systematic review and meta-analysis. **PLoS neglected tropical diseases**, [S. l.], v. 7, n. 4, p. e2182, 2013. ISSN: 1935-2735 (Electronic). DOI: 10.1371/journal.pntd.0002182.
- BRASIL. Ministério da Saúde. CONITEC. Comissão Nacional de Incorporação de Tecnologias no SUS. Miltefosina para o tratamento da Leishmaniose Tegumentar. 2018. Relatório de recomendação nº 365 de outubro de 2018. Disponível em [http://conitec.gov.br/images/Relatorios/2018/Relatorio\\_Miltefosina\\_LeishmanioseTegumentar.pdf](http://conitec.gov.br/images/Relatorios/2018/Relatorio_Miltefosina_LeishmanioseTegumentar.pdf). Acesso: 01 de junho de 2021.
- BRASIL. **Manual de Vigilância da Leishmaniose Tegumentar Americana**. Ministério da Saúde, Secretaria de Vigilância em Saúde. 2. ed. Brasília; 2017. 191pp.

BRASIL. **Manual de vigilância da leishmaniose visceral**. Departamento de Vigilância Epidemiológica do Ministério da Saúde. 2014.

BRASIL. **Relação Nacional de Medicamentos Essenciais: RENAME**.

Departamento de Assistência Farmacêutica e Insumos Estratégicos do Ministério da Saúde. 2020.

BURZA, S., CROFT, S. L., & BOELAERT, M. Leishmaniasis. **The Lancet**. 392:951-970, 2018.

CARVALHO, L. P.; PASSOS, S. T.; JESUS, A. R. Imunopatogênese da leishmaniose tegumentar. **Gaz. Méd. Bahia**, v. 75, n., p.57-65, jan-jun 2005.

CDC – Centers for disease control and prevention. Disponível em: <https://phil.cdc.gov/Details.aspx?pid=10277>. Acesso em 15 de julho de 2021.

CHIN, C. D. *et al.* Microfluidics-based diagnostics of infectious diseases in the developing world. **Nature Medicine**, [S. l.], v. 17, n. 8, p. 1015–1019, 2011. ISSN: 10788956. DOI: 10.1038/nm.2408. Disponível em: <http://dx.doi.org/10.1038/nm.2408>. Acesso em 05 de maio de 2021.

CROFT, S. L.; SUNDAR, S.; FAIRLAMB, A. H. Drug resistance in leishmaniasis. **Clin. Microbiol.**, 119(1): 111-26, 2006.

DE ALMEIDA, M. C. *et al.* Leishmanial Infection: Analysis of its First Steps. A Review. **Memorias do Instituto Oswaldo Cruz**, v.98 (7): p.861-70, 2003.

DE ARAUJO, V. E. M. *et al.* Relative risk of visceral leishmaniasis in Brazil: a spatial analysis in urban area. **PLoS neglected tropical diseases**, [S. l.], v. 7, n. 11, p. e2540, 2013. ISSN: 1935-2735 (Electronic). DOI: 10.1371/journal.pntd.0002540.

EDMONDSON, R. *et al.* Three-dimensional cell culture systems and their applications in drug discovery and cell-based biosensors. **Assay and Drug Development Technologies**, [S. l.], v. 12, n. 4, p. 207–218, 2014. ISSN: 15578127. DOI: 10.1089/adt.2014.573.

FOLEY, G. Reflections on interdisciplinarity and teaching chemical engineering on an interdisciplinary degree programme in biotechnology. **Education for Chemical Engineers**, [S. l.], v. 14, p. 35–42, 2016. ISSN: 17497728. DOI: 10.1016/j.ece.2015.11.002. Disponível em: <http://dx.doi.org/10.1016/j.ece.2015.11.002>. Acesso em 20 de agosto de 2021.

FRÉZARD, F., DEMICHELI, C., RIBEIRO, R. R. Pentavalent antimonials: new perspectives for old drugs. **Molecules**, v. 14 (7), p. 2317-36, 2009.

FUNABASHI, M. *et al.* A metabolic pathway for bile acid dehydroxylation by the gut microbiome. **Nature**. 582(7813):566-570, 2020.

GOTO, H.; LINDOSO, J. A. Current diagnosis and treatment of cutaneous and mucocutaneous leishmaniasis. **Expert Rev Anti Infect Ther**, [S. l.], v. 8, n. 4, p. 419–433, 2010. ISSN: 1478-7210. ISBN: 1744-8336 (Electronic)r1478-7210

(Linking). DOI: 10.1586/eri.10.19. Disponível em: [http://www.ncbi.nlm.nih.gov/entrez/query.fcgi?cmd=Retrieve&db=PubMed&dopt=Citation&list\\_uids=20377337](http://www.ncbi.nlm.nih.gov/entrez/query.fcgi?cmd=Retrieve&db=PubMed&dopt=Citation&list_uids=20377337). Acesso em 20 de abril de 2020.

HAFIZ, S.; KYRIAKOPOULOS, C. Pentamidine. In: **StatPearls**. Treasure Island (FL): StatPearls Publishing, 2021.

HAMILL, R. J. Amphotericin B formulations: A comparative review of efficacy and toxicity. **Drugs**, v. 73, n. 9, p. 919–934, 2013.

KLEMPNER, R. L. *et al.* A. Ergosterol, an orphan fungal microbe-associated molecular pattern (MAMP). **Mol Plant Pathol**. 15(7):747-61, 2014.

KRAUSPENHAR, C. *et al.* Leishmaniose visceral em um canino de Cruz Alta, Rio Grande do Sul, Brasil. **Ciência Rural**, p- 37, 2007.

LEITE, R. S. *et al.* PCR diagnosis of visceral leishmaniasis in asymptomatic dogs using conjunctival swab samples. **Veterinary Parasitology**, [S. l.], v. 170, n. 3–4, p. 201–206, 2010. ISSN: 03044017. ISBN: 1873-2550 (Electronic)r0304-4017 (Linking). DOI: 10.1016/j.vetpar.2010.02.020. Disponível em: <http://dx.doi.org/10.1016/j.vetpar.2010.02.020>. Acesso em 20 de abril de 2020.

LEMKE, A.; KIDERLEN, A. F.; KAYSER, O. Amphotericin B. Appl. **Microbiol. Biotechnol.**, v. 68, n. 2, p. 151-62, 2005.

LUKEŠ, J. *et al.* Evolution of parasitism in kinetoplastid flagellates. **Molecular and Biochemical Parasitology**. Jul, 195(2): 115-22, 2014.

MADUREIRA, A. S. **A Biotecnologia e o Sistema Internacional de Patentes: a Proteção do Direito à Saúde e as doenças negligenciadas**. 2011. Dissertação (mestrado) - Universidade Federal de Santa Catarina, Centro de Ciências Jurídicas. Programa de Pós-Graduação em Direito, Florianópolis, 2011.

MARQUES, G. R.; FORATTINI, O. P. Aedes albopictus em bromélias de solo em Ilhabela, litoral do Estado de São Paulo. **Revista de Saúde Pública**, São Paulo, v.39, n.4, p.548-552, ago. 2005.

MCCALL, J. *et al.* Cranberry impairs selected behaviors essential for virulence in Proteus mirabilis HI4320. **NRS Research Press**, v.59, p.430-436, 2013.

MCGWIRE, B. S.; SATOSKAR, A. R. Leishmaniasis: clinical syndromes and treatment. **International Journal of Medicine**, v. 107, p. 7-14, 2014.

MOHAMMADIHA, A. *et al.* Comparison of real-time PCR and conventional PCR with two DNA targets for detection of Leishmania (Leishmania) infantum infection in human and dog blood samples. **Experimental Parasitology**, [S. l.], v. 133, n. 1, p. 89–94, 2013. ISSN: 00144894. DOI: 10.1016/j.exppara.2012.10.017. Disponível em: COLOCAR. Acesso em 20 de abril de 2020.

MOTAZEDIAN, M. *et al.* A urine-based polymerase chain reaction method for the

diagnosis of visceral leishmaniasis in immunocompetent patients. **Diagnostic Microbiology and Infectious Disease**, [S. l.], v. 60, n. 2, p. 151–154, 2008. ISSN: 07328893. DOI: 10.1016/j.diagmicrobio.2007.09.001.

MUKHERJEE, S.; DAS, P.; SEN, R. Towards commercial production of microbial surfactants. **Trends in Biotechnology**, v. 24, p 509-515, 2006.

MULE, S. N. *et al.* Protein Glycosylation in Leishmania Spp. **Mol. Omics** 16 (5), 407–424. DOI: 10.1039/D0MO00043D.

NOLI, C; SARIDOMICHELAKIS, M. N. An update on the diagnosis and treatment of canine leishmaniosis caused by *Leishmania infantum* (syn. *L. chagasi*). **Veterinary Journal (London, England : 1997)**, [S. l.], v. 202, n. 3, p. 425–35, 2014. ISSN: 1532-2971. DOI: 10.1016/j.tvjl.2014.09.002. Disponível em: <http://www.sciencedirect.com/science/article/pii/S1090023314003712>  
<http://linkinghub.elsevier.com/retrieve/pii/S1090023314003712>  
<http://www.ncbi.nlm.nih.gov/pubmed/25266647>. Acesso em: 20 de abril de 2020.

PAHO. Pan American Health Organization. **Manual of procedures for surveillance and control of leishmaniasis in the Americas**. OPS: Washington-DC, 2019. 187p.

PATEL, M. V. *et al.* Cavity-induced microstreaming for simultaneous on-chip pumping and size-based separation of cells and particles. **Lab on a Chip**, [S. l.], v. 14, n. 19, p. 3860–3872, 2014. ISSN: 14730189. DOI: 10.1039/c4lc00447g. Disponível em: <http://dx.doi.org/10.1039/C4LC00447G>. Acesso em 20 de abril de 2020.

PLANO, D. *et al.* Selenocyanates and diselenides: a new class of potent antileishmanial agents. **Eur J MedChem**, v.46, p. 3315, 2011.

PORCHEDDU, A.; GIACOMELLI, G.; DE-LUCA, L. New pentamidine analogues in medicinal chemistry. **Curr. Med. Chem.**, v. 19, 5819-5836, 2012.

RATH, S. *et al.* Antimoniais empregados no tratamento da leishmaniose: estado da arte. **Química Nova**. v 26(4):550-555, 2003.

READY, Paul D. Epidemiology of visceral leishmaniasis. **Clinical Epidemiology** 2014. ISSN: 11791349. ISBN: 1179-1349 (Electronic) r1179-1349 (Linking). DOI: 10.2147/CLEP.S44267.

REBOUD, J. *et al.* Shaping acoustic fields as a toolset for microfluidic manipulations in diagnostic technologies. **Proceedings of the National Academy of Sciences of the United States of America**, [S. l.], v. 109, n. 38, p. 15162–15167, 2012. ISSN: 00278424. DOI: 10.1073/pnas.1206055109.

REIS, C. *et al.* Biotecnologia Para Saúde Humana: Tecnologias, Aplicações e Inserção na indústria farmacêutica. **BNDES Setorial**, [S. l.], v. 29, p. 359–392, 2009.

RIBEIRO, V. M. *et al.* Control of visceral leishmaniasis in Brazil: recommendations from Brasileish. **Parasites & Vectors**, [S. l.], v. 6, n. 1, p. 8, 2013. ISSN: 1756-3305. ISBN: 1756-3305 (Electronic)r1756-3305 (Linking). DOI: 10.1186/1756-3305-6-8.

Disponível em: <http://parasitesandvectors.biomedcentral.com/articles/10.1186/1756-3305-6-8>. Acesso em 15 de outubro de 2020.

ROBLEDO, J. A. F. **Parásitos del mejillón *Mytilus galloprovincialis* L.M.K. cultivado experimentalmente em la Ría de Vigo**; epizootiología, histopatología y mecanismos de defensa. Espanha, 1994. Tese (Doutorado), Universidade de Santiago de Compostela, 1994.

ROCHA, L. S. et al. Survey of natural infection by *Leishmania* in sand fly species collected in southeastern Brazil. **Transactions of the Royal Society of Tropical Medicine and Hygiene**, 104(7): 461-466, 2010.

SACKMANN, E. K.; FULTON, A. L.; BEEBE, D. J. The present and future role of microfluidics in biomedical research. **Nature**, [S. l.], v. 507, n. 7491, p. 181–189, 2014. ISSN: 14764687. DOI: 10.1038/nature13118. Disponível em: <http://dx.doi.org/10.1038/nature13118>. Acesso em: 15 de outubro de 2020.

SAKKAS, H.; GARTZONIKA, C.; LEVIDIOTOU, S. Laboratory diagnosis of human Visceral Leishmaniasis. **Journal of Vector Borne Diseases**, v. 53, n. 1, p. 8–16, 2016.

SANAR SAÚDE. Leishmaniose - Resumo Completo: tudo que o veterinário precisa saber. Disponível em: <https://www.sanarsaude.com/portal/residencias/artigos-noticias/leishmaniose-resumo-completo-tudo-que-o-veterinario-precisa-saber>. Acesso em: 08 nov. 2020.

SANGSHETTI, J. N. et al. Antileishmanial drug discovery: comprehensive review of the last 10 years. **RSC Advances** 5: 32376-32415, 2015.

SANTOS, H. D. A. 3D-Printed Acoustofluidic Devices for Raman Spectroscopy of Cells. **Advanced Engineering materials**. v. 23, n. 10, out. de 2021.

SCOTT, P; NOVAIS, F. O. Cutaneous leishmaniasis: immune responses in protection and pathogenesis. **Nature Reviews Immunology**. 16(9), 581–592, 2016.

SERENO, D. et al. Axenically grown amastigotes of *Leishmania infantum* used as an in vitro model to investigate the pentavalent antimony mode of action. **Antimicrob Agents Chemother**, v.42, n.12, Dec, p.3097-102. 1998.

SHOKRI, A; FAKHAR, M; TESHNIZI, S. H. Canine visceral leishmaniasis in Iran: A systematic review and meta-analysis. **Acta Tropica**, [S. l.], v. 165, p. 76–89, 2017. ISSN: 0001706X. DOI: 10.1016/j.actatropica.2016.08.020. Disponível em: <http://linkinghub.elsevier.com/retrieve/pii/S0001706X16306404>.. Acesso em 15 de outubro de 2020.

SILVEIRA, F. T. (2019). What Makes Mucosal and Anergic Diffuse Cutaneous Leishmaniasis So Clinically and Immunopathologically Different? A Review in Brazil. *Trans. R. Soc. Trop. Med. Hyg.* 113 (9), 505–516, 2019.

SPANAKOS, G. et al. Development of a PCR-based method for diagnosis of

Leishmania in blood samples. [S. l.], p. 415–420, 2002. DOI: 10.1006/mcpr.2002.0436.

SRIVASTAVA, P. *et al.* Diagnosis of visceral leishmaniasis. **Transactions of the Royal Society of Tropical Medicine and Hygiene**. 2011. ISSN: 00359203. ISBN: 1878-3503 (Electronic)r0035-9203 (Linking). DOI: 10.1016/j.trstmh.2010.09.006.

SRIVASTAVA, S. *et al.* Possibilities and challenges for developing a successful vaccine for leishmaniasis. **Parasites & vectors**, [S. l.], v. 9, n. 1, p. 277, 2016. ISSN: 1756-3305. ISBN: 1756-3305. DOI: 10.1186/s13071-016-1553-y.

STEVERDING, D. The history of leishmaniasis. **Parasites & Vectors**, v. 10, n. 1, p. 82. 2017.

SUNDAR S; CHAKRAVARTY J. Leishmaniasis: an update of current pharmacotherapy. **Expert Opin Pharmacother**. 2013 Jan [cited 2019 Jul 16];14(1):53-63. Disponível em: <https://www.tandfonline.com/doi/full/10.1517/14656566.2013.755515>. Acesso em 15 de outubro de 2020.

TOMIOTTO-PELLISSIER, F. *et al.* Macrophage Polarization in Leishmaniasis: Broadening Horizons. **Frontiers in Immunology**. v. 9, n. 2529, p. 1-18, 2018.

TRONCARELLI, M. Z. *et al.* Leishmania spp. and/or Trypanosoma cruzi diagnosis in dogs from endemic and nonendemic areas for canine visceral leishmaniasis. **Veterinary Parasitology**, v. 164, n. 2-4, p. 118-123, 2009.

VERMA, G. K. *et al.* A rare case of diffuse cutaneous leishmaniasis in an immunocompetent patient from sub-Himalayan India. **Tropical Doctor**, 2012: 42(4), 237–239, 2012.

VICKERMAN, V. *et al.* Design, fabrication and implementation of a novel multi-parameter control microfluidic platform for three-dimensional cell culture and real-time imaging. **Lab on a Chip**, [S. l.], v. 8, n. 9, p. 1468–1477, 2008. ISSN: 14730189. DOI: 10.1039/b802395f.

WESER, R. *et al.* The complexity of surface acoustic wave fields used for microfluidic applications. **Ultrasonics**, [S. l.], v. 106, n. March 2019, p. 106160, 2020. ISSN: 0041624X. DOI: 10.1016/j.ultras.2020.106160. Disponível em: <https://doi.org/10.1016/j.ultras.2020.106160>. Acesso em 15 de outubro de 2020.

WHO. Status of endemicity of cutaneous and visceral leishmaniasis, worldwide. World Health Organization. 2021. Disponível em: [https://www.who.int/health-topics/leishmaniasis#tab=tab\\_1](https://www.who.int/health-topics/leishmaniasis#tab=tab_1). Acesso 50/2001 em 20 de janeiro de 2022.

WYLLIE, S., CUNNINGHAM, M. L., FAIRLAMB, A. H. Dual action of antimonial drugs on thiol redox metabolism in the human pathogen *Leishmania donovani*. **J Biol Chem**, v. 279 (38), p. 39925-32, 2004.

XIE, Y. *et al.* Acoustic Cell Separation Based on Density and Mechanical Properties.

**Journal of Biomechanical Engineering**, [S. l.], v. 142, n. 3, p. 1–9, 2020. ISSN: 15288951. DOI: 10.1115/1.4046180.

XIONG, B. *et al.* Recent developments in microfluidics for cell studies. **Advanced Materials**, [S. l.], v. 26, n. 31, p. 5525–5532, 2014. ISSN: 15214095. DOI: 10.1002/adma.201305348.

ZHANG, P. *et al.* Acoustic Microfluidics. **Annual Review of Analytical Chemistry**, [S. l.], v. 13, p. 17–43, 2020. ISSN: 19361335. DOI: 10.1146/annurev-anchem-090919-102205.